

Analysis of High Performance Controlled Permanent Magnet Brushless DC Motor Drives without Position Sensor

By

Protik Chandra Biswas

A thesis submitted to the Department of Electrical and Electronic Engineering for partial fulfillment of the requirements for the degree of Master of Science in Electrical and Electronic Engineering

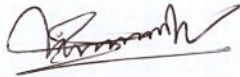


Khulna University of Engineering & Technology
Khulna-9203, Bangladesh

July 2017

Declaration

This is to certify that the thesis work entitled "*Analysis of High Performance Controlled Permanent Magnet Brushless DC Motor Drives without Position Sensor*" has been carried out by *Protik Chandra Biswas* in the Department of *Electrical and Electronic Engineering*, Khulna University of Engineering & Technology, Khulna-9203, Bangladesh. The above thesis work or any part of this work has not been submitted anywhere for the award of any degree or diploma.



Signature of Supervisor
(Prof. Dr. Bashudeb Chandra Ghosh)

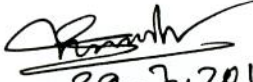
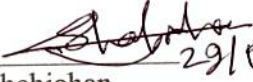
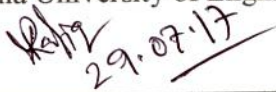




Signature of Candidate
(Protik Chandra Biswas)

Approval

This is to certify that the thesis work submitted by *Protik Chandra Biswas* entitled "*Analysis of High Performance Controlled Permanent Magnet Brushless DC Motor Drives without Position Sensor*" has been approved by the board of examiners for the partial fulfillment of the requirements for the degree of Master of Science in Electrical and Electronic Engineering in the Department of Electrical and Electronic Engineering, Khulna University of Engineering & Technology, Khulna-9203, Bangladesh in July, 2017.

BOARD OF EXAMINERS

1. 
29.7.2017
Prof. Dr. Bashudeb Chandra Ghosh
Department of Electrical and Electronic Engineering
Khulna University of Engineering & Technology, Khulna-9203
Chairman
(Supervisor)
2. 
29/07/17
Prof. Dr. Md. Shahjahan
Head
Department of Electrical and Electronic Engineering
Khulna University of Engineering & Technology, Khulna-9203
Member
3. 
29.07.17
Prof. Dr. Md. Abdur Rafiq
Department of Electrical and Electronic Engineering
Khulna University of Engineering & Technology, Khulna-9203
Member
4. 
Dr. Md. Habibullah
Assistant Professor
Department of Electrical and Electronic Engineering
Khulna University of Engineering & Technology, Khulna-9203
Member
5. 
Prof. Dr. Md. Ashraful Hoque
Department of Electrical and Electronic Engineering
Islamic University of Technology (IUT)
Member
(External)

DEDICATED TO MY BELOVED PARENTS
&
HONORABLE SUPERVISOR

Acknowledgment

At first, I would like to prostrate in worship to Almighty God for helping me at every stages of my life, especially giving me the mercy, patience and ability to complete my M.Sc. Engineering program successfully.

I would like to express my gratitude, appreciation and thanks to my always inspiring, enthusiastic & very supportive supervisor, Prof. Dr. Bashudeb Chandra Ghosh for his constructive suggestion, scholastic guidance, constant inspiration, valuable advices and kind co-operation to carry on the work of “Analysis of High Performance Controlled Permanent Magnet Brushless DC Motor Drives without Position Sensor”. Special thanks go to Dr. Md. Habibullah for providing his continuous help, support, encouragement, and for providing valuable suggestions.

I would like to thank Prof. Dr. Md. Abdur Rafiq for his constant inspiration towards this work. I would also like to thank Prof. Dr. Md. Shahjahan, Head of the Department of Electrical and Electronic Engineering for providing me all possible facilities regarding this research work.

Finally, I would like to express my gratitude to my mother, who provides the advice and mental support. The thesis would not be possible without the help of all of them.

Khulna, July 2017

Thanks to all
Protik Chandra Biswas

Abstract

Permanent Magnet Brushless DC (PMBLDC) motor is a new generation of converter fed machines (CFMs) becoming more and more popular. PMBLDC motors are extensively used as industrial motors due to its fast dynamic response, high power density, large torque to inertia ratio, high efficiency with increased reliability, less noise, long life, silent operation, compact form, low maintenance and better controllability. For innumerable applications, PMBLDC motors are used as replacement for AC motors.

PMBLDC motor is a trapezoidal shaped back EMF permanent magnet synchronous motor with solid state commutation system. The absence of a commutator and brushes or slip rings in the PMBLDC motors reduces maintenance needs and raises mechanical reliability. In solid state commutation system, rotor position information must be needed for proper commutation sequence with proper control algorithms. Motor performance degrades due to improper control action.

In this study, an adaptive PI speed controller based field oriented vector controlled current fed delta modulated PMBLDC motor drive is designed. An adaptive PI controller is proposed based on motor speed error. Scalar control of this PMBLDC motor is also performed at direct axis current component is equal to 1.0 and at direct axis current component equal to quadrature axis current component. The performance of these control drives is compared under different conditions.

In this thesis, a novel approach to enhance the torque handling capacity of a PMBLDC motor is invented. The novelty is that, torque handling capacity of a PMBLDC motor can be increased up to 25% from the conventional 120° conduction square wave current fed drive by only changing the pattern of reference current of a field oriented vector controlled PMBLDC motor drive. Torque handling capacity has to be enhanced without exceeding the maximum current rating of the PMBLDC motor. The performances of trapezoidal, square and sinusoidal current fed field oriented vector controlled PMBLDC motor drives are compared on the basis of response time, load torque handling capacity, dynamic speed and load torque changing condition, settling time of the system and torque pulsation.

In conventional PMBLDC motor, for proper commutation of the phase currents rotor position information must be obtained from the position sensors. But there are some vital disadvantages of position sensor including high cost, installation difficulty of mechanics, and poor reliability. Moreover, misalignments in position sensors, running in extreme ambient conditions, or electromagnetic interference introduce error in the position information. Instead of rotor position or speed sensor, two novel algorithms are proposed in this thesis to estimate the rotor position and speed to perform the operation of position sensorless field oriented vector control of PMBLDC motor. For algorithm 1, both rotor position and speed of the motor are determined from the estimated flux linkage. For algorithm 2, only rotor position of the PMBLDC motor is determined from the estimated flux and the speed of the motor is detected by the estimated developed electromagnetic torque and power equation. The performance of flux estimation algorithm, rotor position estimator, speed estimator is depicted by the comparative study between the actual and estimated flux, rotor position and speed respectively.

The performance of the proposed algorithms for sensorless operation is also justified through the sensorless trapezoidal current fed field oriented PMBLDC motor drive. In this drive, both the advantages of position sensorless operation and enhanced torque handling capacity are incorporated due to establish a novel high performance control drive for PMBLDC motor.

A novel position sensorless two phase conduction direct torque controlled PMBLDC motor drive is also proposed in this study. Without considering flux control, two-phase conduction direct torque control (DTC) of a PMBLDC motor on the basis of electromagnetic torque, rotor position and speed estimation is pictured in the proposed drive system. The performance of the proposed position sensorless direct torque controlled PMBLDC motor drive is compared with the performance of conventional position sensed two phase conduction direct torque controlled PMBLDC motor drive in terms of starting, dynamic speed and load torque changing characteristics.

CONTENTS

	Page
Title Page	i
Declaration	ii
Certificate of Research	viii
Acknowledgement	v
Abstract	vi
Contents	viii
List of Tables	x
List of Figures	xi
List of Abbreviations	xviii
Nomenclature	Xix
CHAPTER I Introduction	
1.1 Fundamentals of the Study	2
1.2 Literature Review	3
1.3 Scope of the Present Study	8
1.4 Objectives	9
1.5 Dissertation Organization	10
CHAPTER II Overview and Mathematical Modeling of PMBLDC Motor	
2.1 Introduction	13
2.2 Construction of PMBLDC Motor	14
2.3 Operating Principle of PMBLDC Motor	17
2.4 PMBLDC Drives Operation with Inverter	18
2.5 Comparison of Various Motor Types	20
2.6 Mathematical Model of PMBLDC Motor	22
2.7 Conclusion	27
CHAPTER III Field Oriented Control of PMBLDC Motor	
3.1 Introduction	29
3.2 Scalar Control Methods	29
3.3 Vector Control Methods	30
3.4 Proposed Field Oriented Control System	34
3.5 Results and Discussion	38
3.6 Conclusion	47

CHAPTER IV	Novel Approach to Enhance Torque Handling Capacity of PMBLDC Motor Drives	
	4.1 Introduction	49
	4.2 Approach to Enhance Torque Handling Capacity	49
	4.3 Proposed Control Scheme	52
	4.4 Simulation Results and Discussion	55
	4.5 Conclusion	65
CHAPTER V	Field Oriented Control of PMBLDC Motor without Position Sensor	
	5.1 Introduction	67
	5.2 Field Oriented Control Drive without Position Sensor	68
	5.3 Flux Estimation Algorithm	69
	5.4 Rotor Position Estimation	72
	5.5 PMBLDC Motor Speed Estimation	73
	5.6 Simulation Results and Discussion	74
	5.7 Conclusion	95
CHAPTER VI	High Performance Controlled PMBLDC Motor Drives	96
	6.1 Introduction	97
	6.2 Proposed Control Scheme	98
	6.3 Simulation Results and Discussion	100
	6.4 Conclusion	121
CHAPTER VII	Direct Torque Control of PMBLDC Motor without Position Sensor	122
	7.1 Introduction	123
	7.2 Conventional DTC Drive Using Two Phase Conduction Mode	124
	7.3 Novel Position Sensorless DTC Drive Using Two Phase Conduction Mode	128
	7.4 Simulation Results and Discussion	130
	7.5 Conclusion	148
CHAPTER VIII	Conclusion	149
	8.1 Conclusion	150
	8.2 Recommendation for Future Work	152
	References	153
	Appendix	158

LIST OF TABLES

Table No.	Description	Page
2.1	Comparison of PMBLDC Motor with Brushed DC Motor	20
2.2	Comparison of PMBLDC Motor with AC Induction Motor	21
4.1	3-phase square wave reference current corresponding to rotor position	54
5.1	Rotor position corresponding to three phase flux linkage	72
5.2	Estimated speed corresponding to three phase flux linkage	73
7.1	Two-phase voltage vector selection for PMBLDC motor	126
App. 1	PMBLDC Motor Specifications	158

LIST OF FIGURES

Figure No.	Description	Page
2.1	Classification of permanent magnet machine	13
2.2	Stator of a PMBLDC motor	15
2.3	Rotor magnet cross sections	16
2.4	PMBLDC motor transverse section	16
2.5	Pictorial view of operating principle of PMBLDC motor	17
2.6	Basic block diagram of PMBLDC motor drive	18
2.7	PMBLDC drives operation with inverter	18
2.8	Back EMF and current waveform according to Hall position sensors signals of PMBLDC motor drive	20
2.9	Trapezoidal shaped back EMF of PMBLDC motor	22
2.10	PMBLDC motor three phase rotor flux φ_a , φ_b and φ_c as function of rotor position	24
3.1	Decomposition of stator current for field oriented control	30
3.2	Clarke transformation	32
3.3	Inverse Clarke transformation	32
3.4	Park transformation	33
3.5	Block diagram of field oriented vector controlled current fed PMBLDC motor drive by using adaptive PI speed controller	34
3.6	Starting characteristics of PMBLDC motor drives for both vector and scalar field control	38
3.7	3-Phase starting current of PMBLDC for vector and scalar control	39
3.8	(a) 3-phase back EMF at starting, (b) steady state back EMF at rated speed, (c) rotor position of vector control PMBLDC motor drive	40
3.9	Flux orientation representation in the stationary $\alpha\beta$ – axes reference frame for both vector and scalar controlled PMBLDC motor drive	41
3.10	Comparison between speed responses of PMBLDC motor vector and scalar controlled drive at dynamic speed changing condition	42
3.11	3-phase current of vector controlled drive for variable speed condition considering transient current at the interface of speed changes	42
3.12	3-phase back EMF at dynamic speed changing condition for Vector controlled PMBLDC motor drives	43
3.13	Speed characteristics of PMBLDC motor drives for sudden load torque change at 1.5 second from initial load torque 0.4 Nm to rated load torque 1.55 Nm both for field oriented vector and scalar control	44

Figure No.	Description	Page
3.14	3-phase current of vector controlled PMBLDC motor drives for sudden load torque change at 1.5 second	44
3.15	Starting characteristics of PMBLDC motor drives for vector control with moment of inertia at 0.0048 kg-m ² (rated value) and 0.006 kg-m ² (125% of rated value)	46
3.16	Speed characteristics of PMBLDC motor drives for increasing 25% of its moment of inertia from the motor rated moment of inertia 0.0048 kg-m ² at 1.5 second both for field oriented vector and scalar control	46
3.17	3-phase stator current of vector controlled PMBLDC motor drives for increasing 25% of motor moment of inertia from the rated value 0.0048 kg-m ²	47
4.1	Typical trapezoidal back EMF and square current waveforms of 3-phase PMBLDC motor	50
4.2	Typical trapezoidal back EMF and sinusoidal current waveforms of 3-phase PMBLDC motor	51
4.3	Typical trapezoidal back EMF and trapezoidal current waveforms of 3-phase PMBLDC motor	51
4.4	Overall block diagram of trapezoidal or square or sinusoidal current fed field oriented vector controlled PMBLDC motor drives by using adaptive PI speed controller	52
4.5	Starting characteristics of PMBLDC motor drives for trapezoidal, square and sinusoidal reference current fed field oriented control	55
4.6	3-Phase starting stator current of PMBLDC motor for trapezoidal, square and sinusoidal current fed field oriented control drive	56
4.7	(a) 3-phase back EMF at starting and (b) rotor position of trapezoidal current fed field oriented controlled PMBLDC motor drive	57
4.8	Per phase back EMF and corresponding phase current for Trapezoidal, Square and Sinusoidal current fed field oriented control drives	58
4.9	Torque developed for Trapezoidal, Square and Sinusoidal current fed field oriented controlled drives	59
4.10	Flux linkage trajectories in the stationary $\alpha\beta$ axes reference frame for trapezoidal, square and sinusoidal current fed vector controlled PMBLDC motor drives	60
4.11	Comparison between speed responses of PMBLDC motor for trapezoidal, square and sinusoidal current fed vector controlled drives at dynamic speed changing condition	61
4.12	3-phase current of PMBLDC motor for trapezoidal, square and sinusoidal current fed field oriented controlled drive for variable speed condition considering transient current at the interface of speed changes	62

Figure No.	Description	Page
4.13	3-phase back EMF at dynamic speed changing condition for trapezoidal current fed vector controlled PMBLDC motor drive	63
4.14	Speed characteristics of PMBLDC motor for sudden load torque change at 1.0 second from initial load torque 0.4 Nm to rated load torque 2.0 Nm for trapezoidal, square and sinusoidal current fed field oriented control drives	64
4.15	3-phase stator current of trapezoidal current fed field oriented controlled PMBLDC motor drives for sudden load torque change at 1.0 second	64
5.1	Block diagram of field oriented vector controlled PMBLDC motor drive without rotor position or speed sensor (Algorithm 1)	68
5.2	Block diagram of field oriented controlled PMBLDC motor drive without rotor position or speed sensor (Algorithm 2)	69
5.3	Flowchart for flux estimation	70
5.4	3-phase back EMF and per unit estimated flux linkage according to the back EMF	71
5.5	Starting characteristics of PMBLDC motor drives for field oriented control without position sensor	75
5.6	3-Phase stator current of PMBLDC motor for field oriented current fed drive without position sensor	76
5.7	3-phase back EMF of field oriented controlled PMBLDC motor drive without position sensor	77
5.8	Per phase back EMF and corresponding phase current for field oriented controlled current fed drives without position sensor	78
5.9	Comparison of per phase actual back EMF with calculated back EMF for field oriented current fed drives without position sensor	79
5.10	Actual and estimated rotor flux for field oriented control drives without position sensor	81
5.11	Comparison of actual rotor position with estimated rotor position for field oriented control drives without position sensor	82
5.12	Actual and estimated developed torque according to load torque for sensorless field oriented vector controlled PMBLDC motor drives	83
5.13	Stator flux linkage trajectories in the stationary $\alpha\beta$ axes reference frame for sensorless field oriented vector controlled PMBLDC motor drives	84
5.14	Comparison between speed responses of PMBLDC motor for sensorless field oriented vector controlled drives at dynamic speed changing condition	86
5.15	3-phase current of PMBLDC motor for sensorless field oriented control drive for variable speed condition considering transient current at the interface of speed changes	87
5.16	3-phase back EMF at dynamic speed changing condition for field oriented vector controlled PMBLDC motor drive without position sensor	88

Figure No.	Description	Page
5.17	Actual and estimated rotor flux in per unit value at dynamic speed changing condition for field oriented vector controlled PMBLDC motor drive without position sensor	89
5.18	Actual and estimated rotor position at dynamic speed changing condition for field oriented control drive without position sensor	90
5.19	Actual and estimated rotor developed torque according to the response of load torque at dynamic speed changing condition for current fed field oriented controlled PMBLDC motor drives without position sensor	91
5.20	Speed characteristics of PMBLDC motor for sudden load torque change at 1.5 second from initial load torque 0.4 Nm to load torque 1.55 Nm for sensorless field oriented control drives	93
5.21	3-phase stator current of sensorless field oriented vector controlled PMBLDC motor drives for sudden load torque change at 1.5 second	93
5.22	Comparison of actual and estimated rotor position of sensorless field oriented vector controlled PMBLDC motor drives for sudden load torque change at 1.5 second	94
5.23	Actual and estimated rotor developed torque according to the response of dynamic load torque change for field oriented vector controlled PMBLDC motor drives without position sensor	95
6.1	Block diagram of high performance trapezoidal current fed field oriented PMBLDC motor drive without rotor position or speed sensor (Based on Algorithm 1)	98
6.2	Block diagram of high performance trapezoidal current fed field oriented PMBLDC motor drive without rotor position or speed sensor (Based on Algorithm 2)	99
6.3	Starting characteristics of PMBLDC motor drives for trapezoidal current fed field oriented control without position sensor	101
6.4	3-Phase stator current of PMBLDC motor for high performance trapezoidal current fed field oriented control drive without position sensor	102
6.5	3-phase back EMF of trapezoidal current fed field oriented controlled PMBLDC motor drive without position sensor	103
6.6	Per phase back EMF and corresponding phase current for trapezoidal current fed field oriented control drives without position sensor	104
6.7	Comparison of per phase actual back EMF with calculated back EMF for proposed algorithm 1 and algorithm 2 of trapezoidal current fed FOC drives without position sensor	105
6.8	Actual and estimated rotor flux for trapezoidal current fed field oriented control drives without position sensor	106
6.9	Actual and estimated rotor position for trapezoidal current fed field oriented control drives without position sensor	107

Figure No.	Description	Page
6.10	Actual and estimated developed torque according to load torque for sensorless trapezoidal current fed field oriented controlled drives	108
6.11	Stator flux linkage trajectories in the stationary $\alpha\beta$ axes reference frame for sensorless trapezoidal current fed vector controlled PMBLDC motor drive	109
6.12	Comparison between speed responses of PMBLDC motor for sensorless trapezoidal current fed vector controlled drives at dynamic speed changing condition	111
6.13	3-phase current of PMBLDC motor for sensorless trapezoidal current fed field oriented controlled drive for variable speed condition considering transient current at the interface of speed changes	112
6.14	3-phase back EMF at dynamic speed changing condition for trapezoidal current fed vector controlled PMBLDC motor drive without position sensor	113
6.15	Actual and estimated rotor flux in per unit value at dynamic speed changing condition for trapezoidal current fed field oriented PMBLDC motor drive without position sensor	114
6.16	Actual and estimated rotor position at dynamic speed changing condition for trapezoidal current fed field oriented PMBLDC motor drive without position sensor	115
6.17	Actual and estimated developed electromagnetic torque according to the response of load torque at dynamic speed changing condition for trapezoidal current fed vector controlled PMBLDC motor drives without position sensor	116
6.18	Speed characteristics of PMBLDC motor for sudden load torque change at 1.5 second from initial load torque 0.4 Nm to rated load torque 2.0 Nm for sensorless trapezoidal current fed field oriented control drives	118
6.19	3-phase stator current of sensorless trapezoidal current fed field oriented PMBLDC motor drives for sudden load torque change at 1.5 second	118
6.20	Comparison of actual and estimated rotor position of sensorless trapezoidal current fed field oriented PMBLDC motor drives for sudden load torque change at 1.5 second	119
6.21	Actual and estimated developed electromagnetic torque according to the response of dynamic load torque change for trapezoidal current fed field oriented PMBLDC motor drives without position sensor	120
7.1	Actual (solid-line) and ideal (dashed-line) stator flux linkage trajectories, representation of two-phase voltage space vectors, and placement of the three hall-effect sensors in the stationary $\alpha\beta$ -axes reference frame	125
7.2	Two-phase switching states of the inverter voltage space vectors for a PMBLDC motor	126
7.3	Block diagram of conventional two phase conduction direct torque controlled PMBLDC motor drive	127

Figure No.	Description	Page
7.4	Block diagram of two phase conduction direct torque controlled PMBLDC motor drive without rotor position or speed sensor	128
7.5	Starting characteristics of PMBLDC motor drives for two phase conduction direct torque control	131
7.6	3-phase back EMF of two phase conduction direct torque controlled PMBLDC motor drive	132
7.7	Comparison of per phase actual back EMF with calculated back EMF for two phase conduction DTC drive without position sensor	133
7.8	Per phase rotor flux for two phase conduction direct torque controlled PMBLDC motor drives with and without position sensor	134
7.9	Rotor position for two phase conduction direct torque controlled PMBLDC motor drives	135
7.10	Actual and estimated developed torque according to load torque for proposed position sensorless two phase conduction DTC PMBLDC motor drive	136
7.11	Developed electromagnetic torque according to load torque for conventional sensed two phase conduction DTC PMBLDC motor drive	137
7.12	Stator flux linkage trajectories in the stationary $\alpha\beta$ axes reference frame for two phase conduction direct torque controlled PMBLDC motor drives	138
7.13	Comparison between speed responses of PMBLDC motor for proposed position sensorless DTC drive and conventional position sensed DTC drive at dynamic speed changing condition	140
7.14	3-phase back EMF at dynamic speed changing condition for two phase conduction direct torque controlled PMBLDC motor drives	141
7.15	Per phase actual and estimated rotor flux (in PU) at dynamic speed changing condition for proposed position sensorless two phase conduction DTC drive of PMBLDC motor	142
7.16	Actual and estimated rotor position at dynamic speed changing condition for proposed position sensorless two phase conduction DTC drive of PMBLDC motor	142
7.17	Actual and estimated rotor developed torque according to the response of load torque at dynamic speed changing condition for proposed position sensorless two phase conduction DTC PMBLDC motor drive	144
7.18	Developed electromagnetic torque according to the response of load torque at dynamic speed changing condition for conventional position sensed two phase conduction DTC drive of PMBLDC motor	144
7.19	Speed characteristics of PMBLDC motor for sudden load torque change at 1.5 second from initial load torque 0.4 Nm to load torque 1.55 Nm for proposed and conventional DTC drives	146

Figure No.	Description	Page
7.20	Comparison of actual and estimated rotor position of proposed position sensorless two phase conduction DTC drive for sudden load torque change at 1.5 second	146
7.21	Actual and estimated developed torque according to the response of dynamic load torque change for proposed two phase conduction direct torque controlled PMBLDC motor drive without position sensor	147
7.22	Developed torque according to the response of dynamic load torque change for conventional position sensed direct torque controlled PMBLDC motor drive	147

LIST OF ABBREVIATIONS

ANN	Artificial Neural Network
CFM	Converter Fed Machine
DTC	Direct Torque Control
EMF	Electromotive Force
FOC	Field Oriented Control
IGBT	Insulated Gate Bipolar Transistor
MTPA	Maximum Torque Per Ampere
PMBLDC	Permanent Magnet Brushless DC
PMSM	Permanent Magnet Synchronous Motor
PM	Permanent Magnet
PMBLAC	Permanent Magnet Brushless AC
PI	Proportional-Integral
PMAC	Permanent Magnet AC
PMDC	Permanent Magnet DC
PWM	Pulse Width Modulation
PAM	Pulse Amplitude Modulation
RPM	Revolution Per Minute

NOMENCLATURE

a, b, c	Three phase stationary reference frame
$d-q$	Orthogonal synchronously rotating reference frame
$\alpha-\beta$	Orthogonal stationary reference frame
I_{dc}	Input DC link current
V_{dc}	DC link supply voltage
ω_m	Angular speed of the motor
θ_r	Electrical rotor position
ω_r	Electrical angular speed of the motor
$\varphi_a, \varphi_b, \varphi_c$	Three phase rotor flux
λ_m	Rotor flux linkages constant
e_a, e_b, e_c	Three phase back EMF
V_{as}, V_{bs}, V_{cs}	Stator phase voltages of phase a, b and c respectively
i_{as}, i_{bs}, i_{cs}	Stator phase currents of phase a, b and c respectively
R_s	Per phase stator resistance
L_s	Per phase self-inductance
M	Mutual inductance between two phases
V_{a0}, V_{b0}, V_{c0}	Three phase stator voltage referred to the zero reference potential at the mid-point of dc link
V_{n0}	Neutral voltage referred to the zero reference potential at the mid-point of dc link
T_e	Developed electromagnetic torque
T_l	Load torque
J_m	Moment of inertia of motor
J_l	Moment of inertia of load
B	Rotational damping co-efficient
P	Number of pole
i_{ds}	Direct axis (d -axis) stator current component
i_{qs}	Quadrature axis (q -axis) stator current component
L_d, L_q	Self-inductance along $d-q$ axes
$i_{\alpha s}$	Stator current component along α -axis
$i_{\beta s}$	Stator current component along β -axis
$\omega_{m(error)}$	Speed error

$\omega_{m(ref)}$	Angular reference speed
T_{ref}	Reference torque
K_t	Motor torque constant
K_p	Proportional gain constant
K_I	Integral gain constant
K_{p0}	Initial proportional gain constant
K_{I0}	Initial integral gain constant
K_1	Proportional gain constant tuner
K_2	Integral gain constant tuner
$i_{qs(ref)}$	Quadrature axis (q -axis) stator reference current
$i_{ds(ref)}$	Direct axis (d -axis) stator reference current
$i_{as(ref)}$	Stator reference current along α -axis
$i_{\beta s(ref)}$	Stator reference current along β -axis
$i_{as(ref)}, i_{bs(ref)},$	Stator reference currents of phase a , b and c
$i_{cs(ref)}$	
h_b	Hysteresis band around reference current
i_d	Direct axis (d -axis) current component
i_q	Quadrature axis (q -axis) current component
I_{max}	Per phase maximum peak value of current
$i_s(ref)$	Maximum peak value of per phase stator reference current
i	Iteration number
e_{ac}, e_{bc}, e_{cc}	Three phase back EMF at constant back EMF region
T_{em}	Estimated developed electromagnetic torque
$\varphi_{\alpha r}$	Rotor flux linkages along α -axis
$\varphi_{\beta r}$	Rotor flux linkages along β -axis
e_{α}	Motor back-EMF along α -axis
e_{β}	Motor back-EMF along β -axis
$V_{\alpha s}$	Stator voltage component along α -axis
$V_{\beta s}$	Stator voltage component along β -axis
$\varphi_{\alpha s}$	Stator flux linkages along α -axis
$\varphi_{\beta s}$	Stator flux linkages along β -axis
τ	Torque error within the hysteresis bandwidth
$V_1, V_2, V_3, V_4, V_5, V_6$	Six non-zero voltage vectors

φ_{error}	Flux error
$T_{em(ref)}$	Reference torque
$T_{em(error)}$	Torque error

Chapter I

Introduction

Chapter Outlines:

- 1.1 Fundamentals of the Study**
 - 1.2 Literature Review**
 - 1.3 Scope of the Present Study**
 - 1.4 Objectives**
 - 1.5 Dissertation Organization**
-

1.1 Fundamentals of the Study

During the last several decades, electrical AC machines have been considered mainly as work horse of industry. AC machines have been designed considering the fact that they will be directly connected to the electrical network. Induction and DC-excited synchronous machines are well-known conventional AC machines. The stator windings of AC machines are sinusoidally distributed in slots around the air gap so as to connect directly with the sinusoidal excitation. Starting from the 80th of the last century, the emergence of power electronic converters has removed the need for such a concept as the basis for AC machine application. Converter fed machines (CFMs) become more popular. A typical example of CFMs is the Permanent Magnet Brushless DC motor [1].

Permanent Magnet Brushless DC (PMBLDC) motor is a trapezoidal shaped back EMF permanent magnet synchronous motor with solid state commutation system. Permanent Magnet Brushless DC motors are extensively used as industrial motors due to their advantages as given below [2]-[5].

- ❖ fast dynamic response
- ❖ high power density
- ❖ high power factor
- ❖ large torque to inertia ratio
- ❖ higher efficiency with increased reliability
- ❖ higher speed ranges
- ❖ noiseless operation
- ❖ long operating life
- ❖ silent operation
- ❖ compact form
- ❖ low maintenance due to low friction
- ❖ better controllability [40]

Therefore, for innumerable applications, PMBLDC motors are used as a replacement for AC motors and these motors also reduce the overall system weight. Its market is rapidly growing. In comparison to induction motor, PMBLDC motors possess some distinct advantages such as higher power density, higher efficiency, and simpler controllability. Hence PMBLDC motors are becoming more and more attractive solution than induction motors for many industrial applications, such as compressors, electrical vehicles, and DVD players etc. [6].

Compared to permanent magnet synchronous machines (PMSMs), PMBLDC motor has the advantage of high-speed adjusting performance and high power density. It is less expensive due to the concentrated windings which shorten the end windings compared to three-phase feeding PMSM [7]. For the commutation of PMBLDC motor, three hall-effect sensors are usually used as position sensors to detect the current commutation points that occur at every 60 electrical degrees. Therefore, a relatively low cost drive is achieved when compared to a PMSM drive. Because expensive high resolution position sensors, such as optical encoder have to be used for PMSM drive. While PMSM drives require a precision rotor position sensor, such as encoder, PMBLDC drives only require discrete position sensors, such as Hall devices. Therefore, in general, PMBLDC drives are relatively low cost compared to PMSM [45]. By virtue of cost, for efficiency and higher power density of PMBLDC motors are well suited for automotive fan and fuel pump applications [8].

In recent years, PMBLDC motor is receiving more interest for automotive applications. This is due to the higher reliability, longevity, lower maintenance, and quieter operation of PMBLDC as compared to brushed dc motor. For continuing improvements in power semiconductors and controller ICs as well as the permanent magnet brushless motor production, PMBLDC motors become reliable cost-effective solutions for a broad range of adjustable speed applications. As matter of fact, PMBLDC motors are being currently used in power steering, engine cooling fan, fuel or water pump, air-conditioning compressor, ventilating, and air-conditioning blower motors [9].

During the last decades, for home appliances energy saving has been one of the important issues. Compressor is the device which consumes most of the electrical energy in air conditioners and refrigerators. PMBLDC motor holds high efficiency over the entire operating range and is easily controlled because the torque of the motor is proportional to the input voltage. For these reasons, the PMBLDC motor is expanding its application in compressor markets [10]. Small power (up to 1 Nm torque) and small starting torque applications (blowers, pumps), single phase PMBLDC motor presents a growing interest particularly in the residential and automotive industry [11].

1.2 Literature Review

Permanent Magnet AC (PMAC) and Permanent Magnet DC (PMDC) machines are two types of permanent magnet electric machines [12]. Depending on the type of back EMF, PMAC machines can be classified into two types. The first type of motor is referred to as Permanent Magnet Synchronous Motors (PMSM). These produce sinusoidal back EMF and should be supplied with sinusoidal current. The second type of PMAC motor is called Permanent Magnet Brushless DC (PMBLDC) motors because of its trapezoidal shaped back EMF and rectangular shaped currents are to be fed to these motors [45]. The PMDC machines are similar with the DC commutator machines. The only difference is that permanent magnets are used instead of the electromagnetic field windings. Besides in case of PMBLDC motor, the field is generated by the permanent magnets placed on the rotor, the brushes and the commutator do not exist in this machine type. The absence of a commutator and brushes or slip rings in the PMBLDC motors reduces maintenance needs and raises mechanical reliability. For this reason the PMBLDC motor is simpler and more attractive to use instead of brushed DC motor [13]-[14]. The commutation of PMBLDC motor is done electronically, hence it is simple to control the torque and RPM of the motor even at much higher speed [15].

The transformation of machine equations to the well-known d, q reference frame is not appropriate for modeling and simulation of PMBLDC motor drives because of the trapezoidal back EMF and the consequent no sinusoidal variation of the motor inductances with rotor angle. For non-sinusoidal flux distribution, it is prudent to drive a model of the PMBLDC motor in natural or phase variables [16]. Detail mathematical modeling for PMBLDC motor on the basis of phase variables is pictured in [17]. Modeling of trapezoidal shaped back EMF using rotor position information is also performed. Fuzzy logic controller based square current fed PWM current control scheme is used for PMBLDC motor speed control drive.

A space vector PWM based PMBLDC motor modeling and simulation are provided in [18]. Both continuous and discrete time models are considered in this study. Torque is calculated on the basis of back EMF, phase currents and speed. Switching to proper space vector is done using torque error and position of the field. Fuzzy Logic based PI controller adjustment system is used in this control system. A mathematical model of a PMBLDC motor has been proposed in [19] with a trapezoidal back EMF function for sensorless operation. A standard mathematical model of a PMBLDC motor in the a, b, c reference frame which is suitable for simulation of the six-step control strategy, and a mathematical model of a PMBLDC motor in the d, q reference frame suitable for standard and modified field oriented control strategies are presented in [20].

An approach of field oriented control (FOC) of a PMBLDC motor to produce a significantly reduced torque ripple is also proposed in [20]. A simple predicted current control scheme for PMBLDC motor to reduce the torque ripple in the commutation and conduction region is used in [21] to keep the constant torque during the conduction and commutation region. In this proposed control system, the inverse function of back EMF is used to consider the back EMF characteristic in the conduction region. Brief comparative study of three different control schemes i.e. sinusoidal field oriented control, field oriented control and hysteresis control of a PMBLDC motor primarily on the aspect of output torque ripple is given in [22].

The most popular way to control PMBLDC motors is by PWM current control in which a two phase feeding scheme is considered with variety of PWM modes such as soft switching, hard switching etc. Three hall-effect sensors are usually used as position sensors to detect the current commutation points that occur at every 60 electrical degrees [46]. Generally current control is used in PMBLDC motor drives by assuming that torque is proportional to the phase current. In practice there is nonlinear relationship between phase current and torque. To minimize torque pulsation, various current control strategies are used by employing pre-optimized waveforms for the reference current. An optimal current excitation scheme which resulted ripple-free torque is proposed in [23]. Since this control strategy is on the basis of $d-q$ axes transformation, it could not respond to rapid torque changes.

In a conventional commutation method current amplitude is kept constant, but in [24] current amplitude is adapted to the rotor position to reduce the torque ripple in PMBLDC motor drives. For this purpose, an optimum reference current is computed based on the phase back-EMF waveform. Comparison of the PWM control and the PAM control for high-speed PMBLDC motor is introduced in [25]. PMBLDC motor can be driven by either pulse width modulation (PWM) techniques with a constant DC-link voltage or pulse amplitude modulation (PAM) techniques with an adjustable DC-link voltage. This paper messaged that for high speed operation PAM control is superior to the PWM control.

PMBLDC motor is usually driven by a three-phase full-bridge inverter employing a two-phase conduction method [26]-[27]. For proper commutation of the phase currents, the conventional PMBLDC motor, rotor position must be obtained by the position sensors [28]. In order to obtain an accurate and ripple free instantaneous torque of the PMBLDC motor, the commutation logic of the inverter transistors is provided by the position sensors, such as Hall sensors. It is well known that the PMBLDC motor requires six discrete rotor positions for commutation, and three

hall sensors are always used to generate the position signals [29]. Hall sensors used as rotor position encoder are advantageous for simple control algorithm and mature application [30]. But there are some constraints to the position sensors including high cost, installation difficulty of mechanics, misalignment in sensors, running in extreme ambient conditions, electromagnetic interference introduce error in the position information and poor reliability [28], [30], [31]. Moreover, the high placement accuracy of Hall sensors is hard to achieve, which will increase the motor power loss at the steady state in the high speed region. When the motor is commutating with the ideal commutation instants, the motor can work at maximum efficiency [27]. So the development of sensorless PMSM motor drives has been a hot research issue in recent years.

The PMSM motor is inherently electronically controlled and requires rotor position information for proper commutations of current. However, the problems of the cost and reliability of rotor position sensors have motivated research in the area of position sensorless PMSM motor drives. Solving this problem effectively will open the way for full penetration of this motor drive into all low cost, high reliability, and large volume applications [32]. Recently sensorless operation of PMSM motor using the back EMF information, such as back-EMF zero crossing, has widely been used and is adequate for small or low-cost application such as the hard disk drive (HDD) [33].

In the last two decades, many sensorless motor drives have been proposed to eliminate the costly and fragile position sensor for PMSM motors with trapezoidal back-EMF. Sensorless control based on a hysteresis comparator of terminal voltage and a potential start-up method with a high starting torque for an automotive fuel pump application is presented in paper [34]. Maximum commutation phase lag is significantly reduced by adjusting both the resistance ratio and the output voltage level of the hysteresis comparator. Commutation signal is nearly in phase with the back EMF in [34].

By the zero crossing point (ZCP) of back EMFs with 30° phase shift [26] or the ZCPs detection of the three-phase line-to-line voltages without 30° phase shift, commutation instants are estimated [35]–[36]. A simple technique to detect back EMF zero crossings for a PMSM motor using the line voltages is proposed in [35]. Only three motor terminal voltages need to be measured thus eliminating the need for motor neutral voltage in this proposed technique. For current commutation, virtual Hall signals are developed in [36] by a novel sensorless method using line-to-line voltages that are calculated from the measured terminal voltages. Cost saving is achieved by reducing the number of inverter power switches and also by elimination of the position Hall-effect sensors. The motor neutral voltage is required to get the ZCP of phase back EMFs [26], but the neutral line of the motor is usually not extracted. To obtain the virtual neutral voltage, a resistance network composed by three resistors is used [37]. With sensorless control method based on the virtual neutral voltage, a hybrid drive method combining PWM and PAM techniques is also reported in [37].

In [38], an offline finite element method assisted position and speed observer for PMBLDC motor drive is investigated. The zero crossing of the line-to-line PM flux linkage occurs right in the middle of two commutation points and is used in [38] as a basis for the position and speed observer. The line-to-line PM flux linkage can be estimated from measured phase currents and measured line-to-line voltages.

Rotor position information can also be extracted from zero sequence voltage signals [13]. Paper [39] presents a new 12-step sensorless drive for brushless dc motor based on back EMF differences, which are estimated from the disturbance observer structure. The rotor-position signals are constructed in [40] by the two-phase terminal voltages without using the neutral voltage signal of the motor, which can be used for commutation. Initial rotor position is estimated in [41] based on the stator inductance variation due to the influences of the saturation of the stator iron and the flux due to the position of the rotor magnets. This paper only presents a method for determining the initial rotor position of a brushless dc machine at standstill without a position sensor. Integration of third harmonic back EMF and the phase-locked loop technique are used in [42] and provides controllable advanced commutation to the PMBLDC motor.

Direct Torque Control (DTC) strategies allow a direct control of the electromagnetic torque and the stator flux through the application of suitable combinations of the inverter control signals. DTC strategies have been extensively implemented in induction machine drives. In 1986, DTC strategy has been first invented by Takahashi and Noguchi for induction motor drives [43]. The most recent and highly performed DTC strategy has been proposed by Zhu and Leong [44]. Such strategy exhibits a vector selection table simply reduced to the torque control with a two-phase conduction mode during sequences and three phase conduction mode during sector-to-sector commutations.

The paper [45] considers the application of direct torque control, to a three-phase PMBLDC drive operating in the 120° conduction mode (i.e. two phases conducting) to achieve instantaneous torque control and reduced torque ripple. Application of DTC scheme is extended to PMBLDC motor drives to minimize the torque ripples and torque response time as compared to conventional PWM current controlled PMBLDC motor drives [45]. Difference between the implementation of DTC to PMBLAC and PMBLDC drives is also depicted in [45]. The main difference is in the estimation of torque and the representation of the inverter voltage vectors. It has been shown that DTC is capable of instantaneous torque control and thereby, of reducing torque pulsations [45].

In paper [45], the voltage space vectors in a two-phase conduction mode are defined and a stationary reference frame electromagnetic torque equation is derived for PMBLDC motor. It is claimed that the electromagnetic torque and the stator flux linkage amplitude of the DTC of PMBLDC motor under two phase conduction mode can be controlled simultaneously. In paper [46], the DTC of a BLDC motor drive operating in two-phase conduction mode, proposed in [45], is further studied and simplified to just a torque controlled drive by intentionally keeping the stator flux linkage amplitude almost constant by eliminating the flux control in the constant torque region. Since the flux control is removed, fewer algorithms are required for the proposed control scheme.

The DTC for BLDC motor drive using two phase conduction mode in the constant torque region with rotor position estimation has been implemented in [46]-[47]. Unlike conventional six-step PWM current control, by properly selecting the inverter voltage space vectors in the two-phase conduction mode from a simple look-up table at a predefined sampling time, a much faster torque response is achieved compared to conventional PWM current control. The position sensorless direct torque and indirect flux control of PMBLDC motor with non-sinusoidal back-EMF has been extensively investigated in [48] using three-phase conduction scheme with six-switch inverter and so the motor could operate in the field weakening region by properly selecting the d -axis current reference in the proposed DTC scheme.

Indeed, referring to Masmoudi et al. [1], the proposed novel DTC strategy makes it possible the improvement of the drive reliability for balancing of the switching frequencies of the inverter upper and lower IGBTs and significantly reduces the average value of the motor common mode voltage. This has been carried out through the application of appropriate null voltage vectors to decrease the electromagnetic torque. Furthermore, in [1] the torque ripple has been notably damped during sector-to-sector commutations because of the substitution of the two-level torque controller by a three-level one which makes it much appropriate the three-phase conduction mode adopted during sector-to-sector commutations.

Ref. [2] demonstrates the application of four-switch two-phase conduction DTC scheme for PMBLDC motor drives in the constant torque region. A look-up table for the two-phase voltage selection has been proposed to provide faster torque response. In addition, a novel switching pattern incorporating with the voltage vector look-up table has been developed for the two-phase four-switch DTC of a PMBLDC motor for effective torque control. Pre-stored back EMF versus electrical rotor position look-up tables are used in the torque estimation to eliminate the low-frequency torque oscillations caused by the non-ideal trapezoidal shaped back EFM. Compared to the three-phase DTC technique, this approach [2] eliminates the flux control and only torque is considered in the overall control system.

1.4 Scope of the Present Study

Comprising with above mentioned many special features, characteristics and applications of PMBLDC motor, it has been found very prominent field of research. PMBLDC motor drive is largely maintenance free, which ensures the most efficient operation. From the research over PMBLDC motor until now, it shows that, in future market PMBLDC motor drive could become an emerging competitor for the induction motor and PMSM drive in many industrial applications. So now there is a great challenge to improve the performance of PMBLDC motor drive with accurate speed tracking and sufficient torque output during transient as well as steady state condition such that it can meet the expectation of future market demand.

High performance PMBLDC motor drives are very much popular in modern industries. There are various control laws to implement these high performance drives. The PMBLDC motor drive technologies are now in immature state. However, a good number of researchers have been working in this field to improve the control methodologies. The main methodologies of high performance control are the field orientated control and direct torque control.

Since PMBLDC motor does not use brushes for commutation. It is electronically commutated. For electronic commutation, rotor position information must be needed for stator current commutation. Generally position sensors such as Hall-effect sensors or optical encodes are employed to provide rotor position information for commutation. But considering the high cost, poor reliability and installation difficulty of high resolution position sensor, it is the right time to think about a position sensorless PMBLDC motor drive for industrial applications. The development of the PMBLDC motor sensorless operation has been a hot issue in recent years.

The main purpose of my research is to establish the sensorless high performance field oriented controlled and direct torque controlled PMBLDC motor drives without (i) zero crossing point detection, (ii) the integration of the silent phase's back EMF to get the commutation instants, (iii) utilizing the third harmonic of the back EMF to determine the commutation instants, and (iv) utilizing phase current flowing through a freewheeling diode in silent phase. Sufficient torque output is an important issue for a motor to evaluate its performance for industrial application. Therefore, a novel approach for enhancing torque handling capacity is also proposed for the sensorless high performance field oriented vector controlled PMBLDC motor drive.

1.3 Objectives

The main objectives of the proposed research work are_

- ❖ To compare the performance of adaptive PI controller based field oriented vector controlled current fed delta modulated PMBLDC motor drive with the scalar control drives at direct axis current component is equal to 1.0 and at direct axis current component equal to quadrature axis current component.
- ❖ To propose a novel approach to enhance the torque handling capacity of a PMBLDC motor drive without exceeding the maximum current rating of the motor, by only changing the reference current of PWM modulator.
- ❖ Instead of using rotor position or speed sensor, two novel algorithms are proposed to estimate the rotor position and speed to perform the operation of position sensorless field oriented vector control of PMBLDC motor. The performance of these proposed algorithms for position sensorless operation of field oriented vector controlled PMBLDC motor drive are compared.
- ❖ To develop a high performance PMBLDC motor drive to increase the torque handling capacity of a PMBLDC motor drive without exceeding the maximum current rating of the motor and without high cost and high resolution speed sensor or rotor position encoder.
- ❖ To propose a novel position sensorless two phase conduction direct torque controlled PMBLDC motor drive keeping stator flux linkage amplitude almost constant and to compare the performance of this proposed drive with the conventional position sensed direct torque controlled PMBLDC motor drive.

1.4 Dissertation Organization

The work presented in this thesis is organized in eight chapters. These eight chapters are structured as follows:

Chapter I is entitled "**Introduction**". This chapter includes the motivation and the objectives of this research work. Brief literature review in field of PMBLDC motor drives is also introduced.

Chapter II is entitled "**Overview and Mathematical Modeling of PMBLDC Motor**". This chapter describes the basic operating principle and construction of PMBLDC motor. Comparison of PMBLDC motor with brushed DC motor and AC motors are presented. It includes mathematical model of PMBLDC motor on the basis of phase variables.

Chapter III is entitled "**Field Oriented Control of PMBLDC Motor**". It describes scalar control and field oriented vector control strategies for machine drives. A field oriented control drive for PMBLDC motor is proposed in this chapter. The performance of this proposed drive is compared with the scalar controlled PMBLDC motor drive at direct axis current component equal to 1.0 and at direct axis current component equal to quadrature axis current component through the simulation results.

Chapter IV is entitled "**Novel Approach to Enhance Torque Handling Capacity of PMBLDC Motor Drives**". A novel approach to enhance the torque handling capacity of a PMBLDC motor without exceeding the maximum rated current of the motor is proposed in this chapter. Simulation results are depicted to show that 25% torque handling capacity can be increased than the conventional PMBLDC motor drives.

Chapter V is entitled "**Field Oriented Control of PMBLDC Motor without Position Sensor**". It includes position sensorless operation for field oriented vector controlled PMBLDC motor drive. Novel rotor flux estimation and rotor position estimation algorithms are proposed for position sensorless operation. Two different approaches to estimate the speed of PMBLDC motor are also presented in this chapter for speed sensorless operation. A comparison between actual and estimated quantities is discussed through the simulation results for evaluating the performance of proposed flux estimator, rotor position estimator and speed estimator.

Chapter VI is entitled "**High Performance Controlled PMBLDC Motor Drives**". In this chapter approach to enhance the torque handling capacity, approach for position sensorless operation and approach for field oriented control are incorporated in a single PMBLDC motor drive to make a high performance system. All advantages of these three strategies are present in this high performance PMBLDC motor drive.

Chapter VII is entitled "**Direct Torque Control of PMBLDC Motor without Position Sensor**". A novel two phase conduction direct torque controlled PMBLDC motor drive without position sensor is proposed. This proposed direct torque control drive is compared with a conventional position sensed two phase conduction direct torque controlled PMBLDC motor drive. Both of these drives, flux control is ignored by keeping stator flux linkage amplitude almost constant in the constant torque region due to achieve faster torque response.

Chapter VIII is entitled "**Conclusion**". An appropriate conclusion and recommendations for future work are drawn here.

Chapter II

Overview and Mathematical Modeling of PMBLDC Motor

Chapter Outlines:

- 2.1 Introduction**
 - 2.2 Construction of PMBLDC Motor**
 - 2.3 Operating Principle of PMBLDC Motor**
 - 2.4 PMBLDC Drives Operation with Inverter**
 - 2.5 Comparison of Various Motor Types**
 - 2.6 Mathematical Model of PMBLDC Motor**
 - 2.7 Conclusion**
-

2.1 Introduction

Permanent magnet machines are classified as permanent magnet AC (PMAC) and permanent magnet DC (PMDC) machines. Classification of permanent magnet machine is shown in Fig. 2.1. The PMDC machines are similar with the DC commutator machines; the only difference is that permanent magnets are used instead of the electromagnetic field windings. Besides in case of PMAC motor, the field is generated by the permanent magnets placed on the rotor, the brushes and the commutator does not exist in this machine type. For this reason the PMBLDC motor is simpler and more attractive to use instead of PMDC [12]. Depending on the type of back EMF, PMAC machines can be classified into two types. The first type of PMAC motor is called Permanent Magnet Brushless DC (PMBLDC) motors because of its trapezoidal shaped back EMF and rectangular shaped currents are to be fed to these motors. The second type of motor is referred to as Permanent Magnet Synchronous Motors (PMSM). These produce sinusoidal back EMF and should be supplied with sinusoidal current. Based on the rotor configuration the PM synchronous machine can be further classified as Surface Mounted Permanent Magnet Synchronous Motor (SMPMSM) and Interior Permanent Magnet Synchronous Motor (IPMSM).

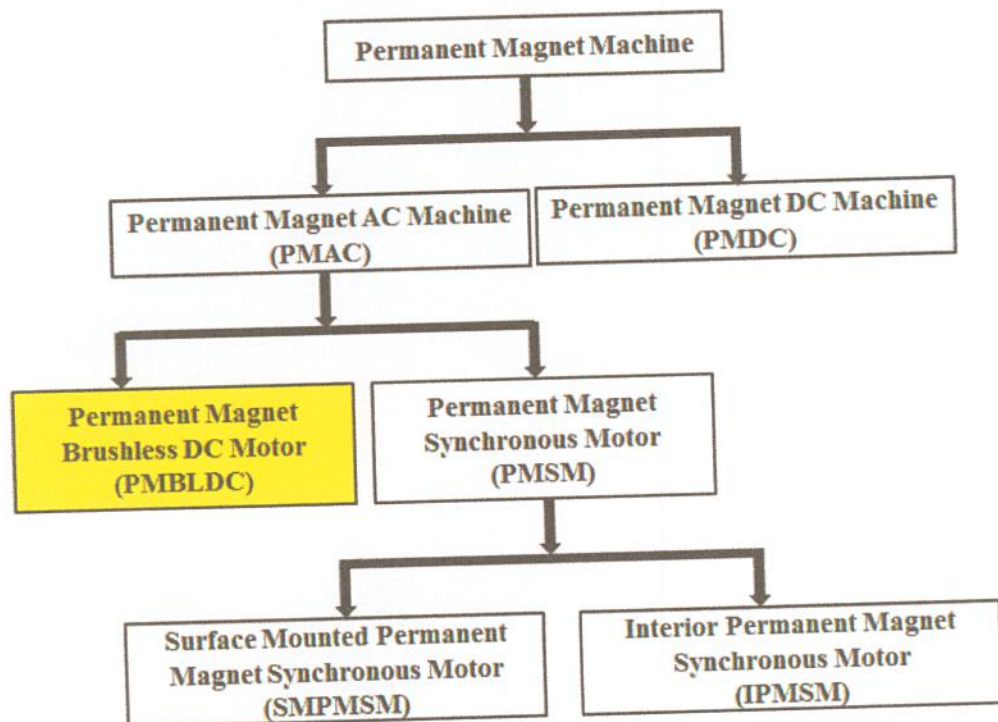


Fig. 2.1: Classification of permanent magnet machine

In a permanent magnet machine, the DC field winding of the rotor is replaced by a permanent magnet to produce the air-gap magnetic field. Having the magnets on the rotor, some electrical losses due to field winding of the machine get reduced and the absence of the field losses improves the thermal characteristics of the PM machines hence its efficiency. Also lack of mechanical components such as brushes and slip rings makes the motor lighter, high power to weight ratio which assure a higher efficiency and reliability. PM machines also have some disadvantages. At high temperature, the permanent magnet gets demagnetized. It has difficulties to manufacture and high cost of PM material.

A permanent magnet brushless dc motor is a dc motor turned inside out, so that the field is on the rotor and the armature is on the stator. The brushless dc motor is actually a permanent magnet ac motor whose torque-current characteristics mimic the dc motor. Instead of commutating the armature current using brushes, electronic commutation is used. This eliminates the problems associated with the brush and the commutator arrangement, for example, sparking and wearing out of the commutator-brush arrangement, thereby, making a PMBLDC more rugged as compared to a DC motor. Having the armature on the stator makes it easy to conduct heat away from the windings, and if desired, having cooling arrangement for the armature windings is much easier as compared to a dc motor. PMBLDC is a modified PMSM motor with the modification being that the back EMF is trapezoidal instead of being sinusoidal as in the case of PMSM.

2.2 Construction of PMBLDC Motor

As the name implies, PMBLDC motors do not use brushes for commutation; instead, they are electronically commutated. PMBLDC motors are a type of synchronous motor. This means the magnetic field generated by the stator and the magnetic field generated by the rotor rotates at the same frequency. PMBLDC motors do not experience the "slip" that is normally seen in induction motors. PMBLDC motors come in single-phase, 2-phase and 3-phase configurations. Corresponding to its type, the stator has the same number of windings. Out of these, 3-phase motors are the most popular and widely used. This thesis focuses on 3-phase PMBLDC motors.

2.2.1 Stator

The stator of a PMBLDC motor consists of stacked steel laminations with windings placed in the slots that are axially cut along the inner periphery as shown in Fig. 2.2. The stator is balanced phase wound. Traditionally, the stator resembles that of an induction motor. However the windings are distributed in a different manner. Most PMBLDC motors have three stator windings connected in star fashion. Each of these windings is constructed with numerous coils interconnected to form a winding. One or more coils are placed in the slots and they are interconnected to make a winding. Each of these windings is distributed over the stator periphery to form an even numbers of poles. There are two types of stator windings variants such as trapezoidal and sinusoidal. This differentiation is made on the basis of the interconnection of coils in the stator windings to give the different types of back EMF. As their names indicate, the trapezoidal motor gives a back EMF in trapezoidal fashion and the sinusoidal motor's back EMF

is sinusoidal. In addition to the back EMF, the phase current also has trapezoidal and sinusoidal variations in the respective types of motor. This makes the torque output by a sinusoidal motor smoother than that of a trapezoidal motor. However, this comes with an extra cost, as the sinusoidal motors take extra winding interconnections because of the coils distribution on the stator periphery, thereby increasing the copper intake by the stator windings.

Depending upon the control power supply capability, the motor with the correct voltage rating of the stator can be chosen. Forty-eight volts, or less voltage rated motors are used in automotive, robotics, small arm movements and so on. Motors with 100 volts or higher ratings, are used in appliances, automation and in industrial applications.

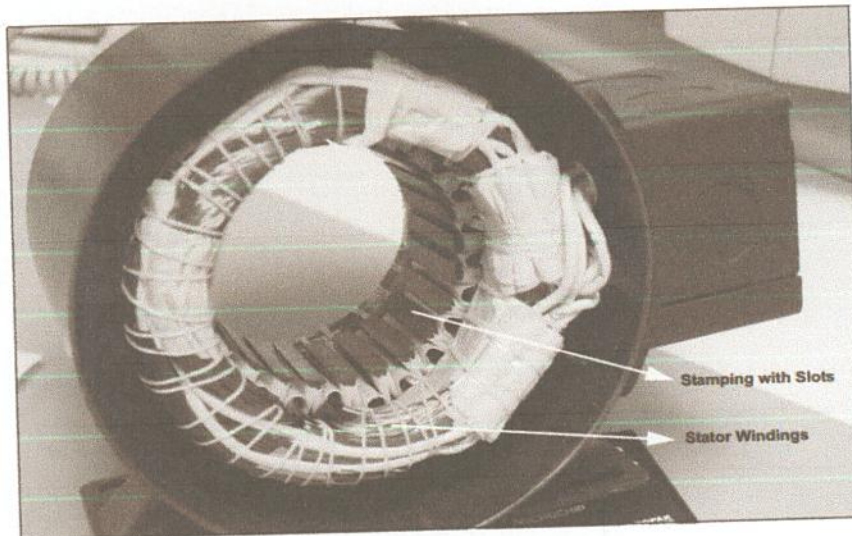


Fig. 2.2: Stator of a PMBLDC motor

2.2.2 Rotor

The rotor is made of permanent magnet and can vary from two to eight pole pairs with alternate North (N) and South (S) poles. Based on the required magnetic field density in the rotor, the proper magnetic material is chosen to make the rotor. Ferrite magnets are traditionally used to make permanent magnets. As the technology advances, rare earth alloy magnets are gaining popularity. The ferrite magnets are less expensive but they have the disadvantage of low flux density for a given volume. In contrast, the alloy material has high magnetic density per volume and enables the rotor to compress further for the same torque. Also, these alloy magnets improve the size-to-weight ratio and give higher torque for the same size motor using ferrite magnets. Neodymium (Nd), Samarium Cobalt (SmCo) and the alloy of Neodymium, Ferrite and Boron (NdFeB) are some examples of rare earth alloy magnets. Continuous research is going on to improve the flux density to compress the rotor further. Fig. 2.3 shows cross sections of different arrangements of magnets in a rotor.

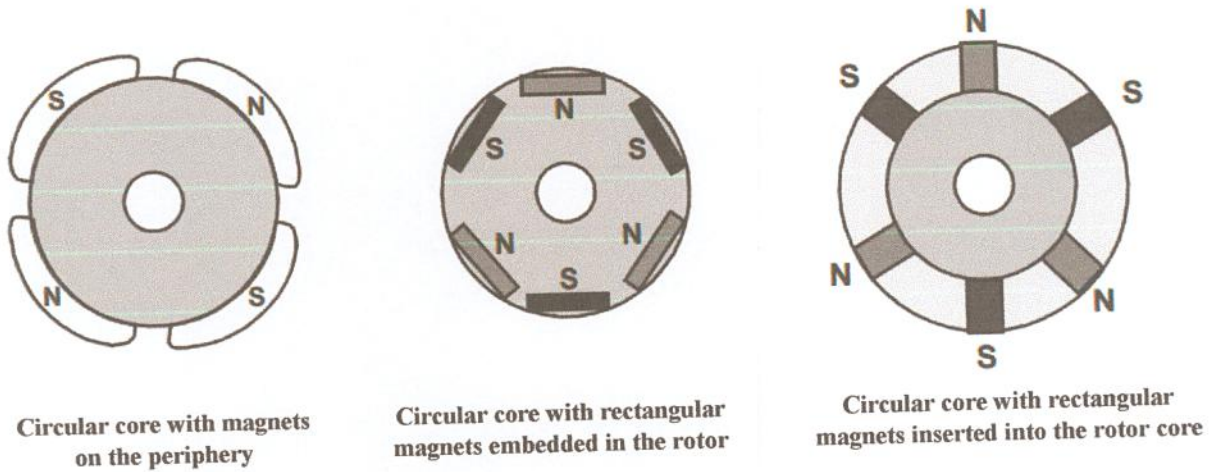


Fig. 2.3: Rotor magnet cross sections

2.2.3 Rotor Position Sensors

Unlike a brushed DC motor, the commutation of a PMSM motor is controlled electronically. To rotate the PMSM motor, the stator windings should be energized in a sequence. It is important to know the rotor position in order to understand which winding will be energized following the energizing sequence. Rotor position is sensed using Hall effect sensors embedded into the stator. Most BLDC motors have three Hall sensors embedded into the stator on the non-driving end of the motor. Whenever the rotor magnetic poles pass near the Hall sensors, they give a high or low signal, indicating the N or S pole is passing near the sensors. Based on the combination of these three Hall sensor signals, the exact sequence of commutation can be determined.

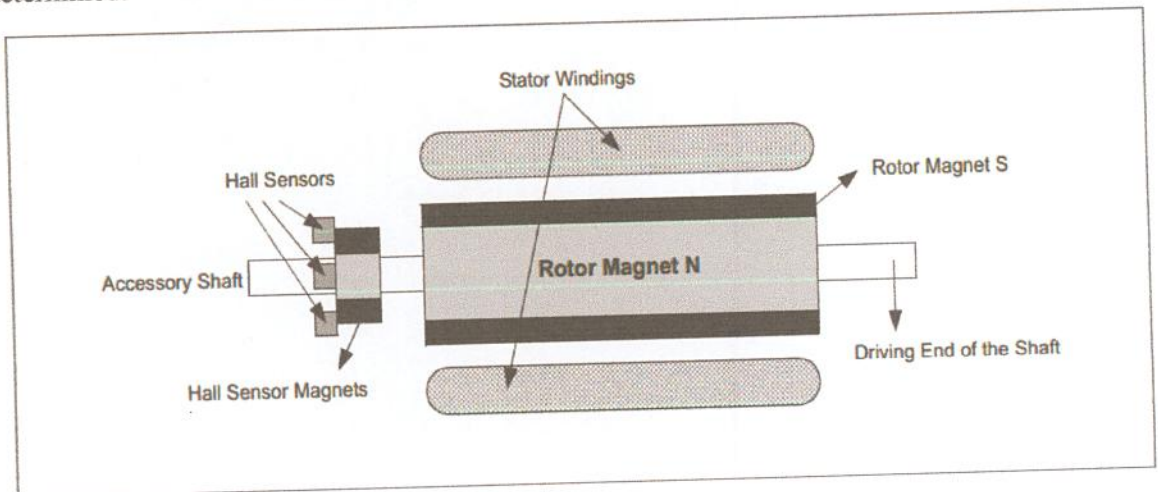


Fig. 2.4: PMSM motor transverse section

Fig. 2.4 shows a transverse section of a PMBLDC motor with a rotor that has alternate N and S permanent magnets. Hall sensors are embedded into the stationary part of the motor. Embedding the Hall sensors into the stator is a complex process because any misalignment in these Hall sensors, with respect to the rotor magnets, will generate an error in determination of the rotor position. To simplify the process of mounting the Hall sensors onto the stator, some motors may have the Hall sensor magnets on the rotor, in addition to the main rotor magnets. These are a scaled down replica version of the rotor. Therefore, whenever the rotor rotates, the Hall sensor magnets give the same effect as the main magnets. The Hall sensors are normally mounted on a PC board and fixed to the enclosure cap on the non-driving end. This enables users to adjust the complete assembly of Hall sensors, to align with the rotor magnets, in order to achieve the best performance. Based on the physical position of the Hall sensors, there are two versions of output. The Hall sensors may be at 60° or 120° phase shift to each other. Based on this, the motor manufacturer defines the commutation sequence, which should be followed when controlling the motor. The position of the rotor can also be sensed by using an optical position sensors and its associated logic. Optical position sensors consist of phototransistors (sensitive to light), revolving shutters, and a light source. The output of an optical position sensor is usually a logical signal.

2.3 Operating Principle of PMBLDC Motor

PMBLDC motor operation is based on the attraction or repulsion between magnetic poles. Using the three-phase motor shown in Fig. 2.5, the process starts when current flows through one of the three stator windings and generates a magnetic pole that attracts the closest permanent magnet of the opposite pole. The rotor will move if the current shifts to an adjacent winding. Sequentially charging each winding will cause the rotor to follow in a rotating field. The torque depends on the current amplitude and the number of turns on the stator windings, the strength and the size of the permanent magnets, the air gap between the rotor and the windings, and the length of the rotating arm.

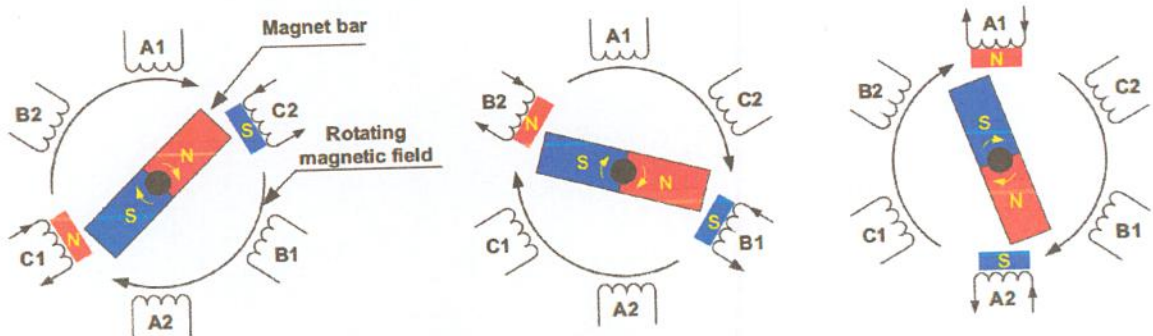


Fig. 2.5: Pictorial view of operating principle of PMBLDC motor

PMBLDC motor is defined as a permanent synchronous machine with rotor position feedback. The basic block diagram PMBLDC motor drive is shown Fig. 2.6. This motor drive consists of four main parts power converter, rotor position sensors, control algorithm and PMBLDC motor.

The power converter transforms power from the source to the PMBLDC motor which in turn converts electrical energy to mechanical energy. One of the salient features of the PMBLDC motor is the rotor position sensors, based on the rotor position and command signals which may be a torque command, voltage command, speed command and so on the control algorithms determine the gate signal to each semiconductor switch in the power electronic converter.

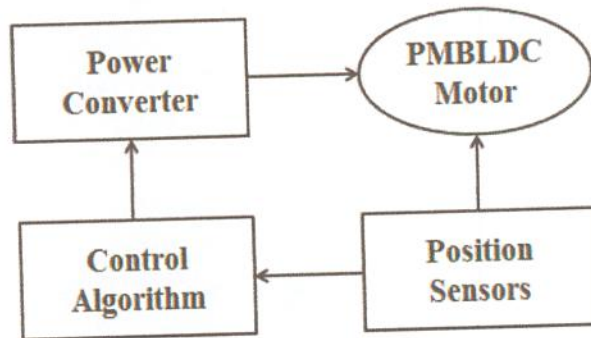


Fig. 2.6: Basic block diagram of PMBLDC motor drive

2.4 PMBLDC Drives Operation with Inverter

Basically PMBLDC motor is an electronic motor and requires a three-phase inverter as shown in Fig. 2.7. In self-control mode the inverter acts like an electronic commutator that receives the switching logical pulse from the absolute position sensors. So the drive is known as an electronic commutated motor drive. Basically the inverter can operate in the following two modes.

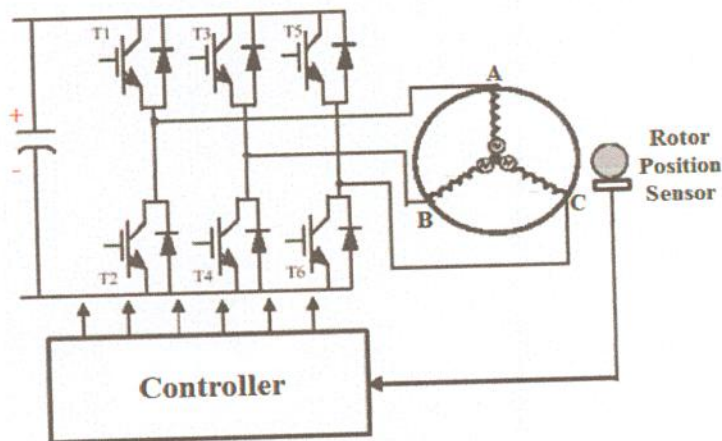


Fig. 2.7: PMBLDC drives operation with inverter

2.4.1 $\frac{2\pi}{3}$ Angle Switch ON Mode

Inverter operation in this mode with the help of the wave form is shown in Fig. 2.8. The six switches of the inverter (T1-T6) operate in such way so as to place the input dc current I_{dc} symmetrical for $\frac{2\pi}{3}$ angle at the center of each phase voltage wave. It can be seen that any instant, two switches are ON, one in the upper group and another is lower group. For example at any instant time t_1 , switch T1 and T6 are ON when the supply voltage V_{dc} and current I_{dc} are placed across the line ab (phase A and phase B in series) so that I_{dc} is positive in phase a . But negative in phase b then after $\frac{\pi}{3}$ interval (the middle of phase A). T6 is turned OFF and T2 is turned ON but T1 continues conduction of the full $\frac{2\pi}{3}$ angle. This switching commutates $-I_{dc}$ from phase b to phase c while phase a carry $+I_{dc}$. The conduction pattern changes every $\frac{\pi}{3}$ angle indication switching modes in full cycle. The absolute position sensor dictates the switching or commutation of devices at the precise instants of wave. The inverter basically operates as a rotor position sensitive electronic commutator.

2.4.2 Voltage and Current Control PWM Mode

In the previous mode the inverter switches were controlled to give commutator function only when the devices were sequentially ON, OFF $\frac{2\pi}{3}$ - angle duration. In addition to the commutator function. It is possible to control the switches in PWM chopping mode for controlling voltage and current continuously at the machine terminal. There are essentially two chopping modes, current controlled operation of the inverter. There are essentially two chopping modes such as feedback mode and freewheeling mode. In both these modes devices are turned on and off on duty cycle basis to control the machine average current I_{AV} and the machine average voltage V_{AV} .

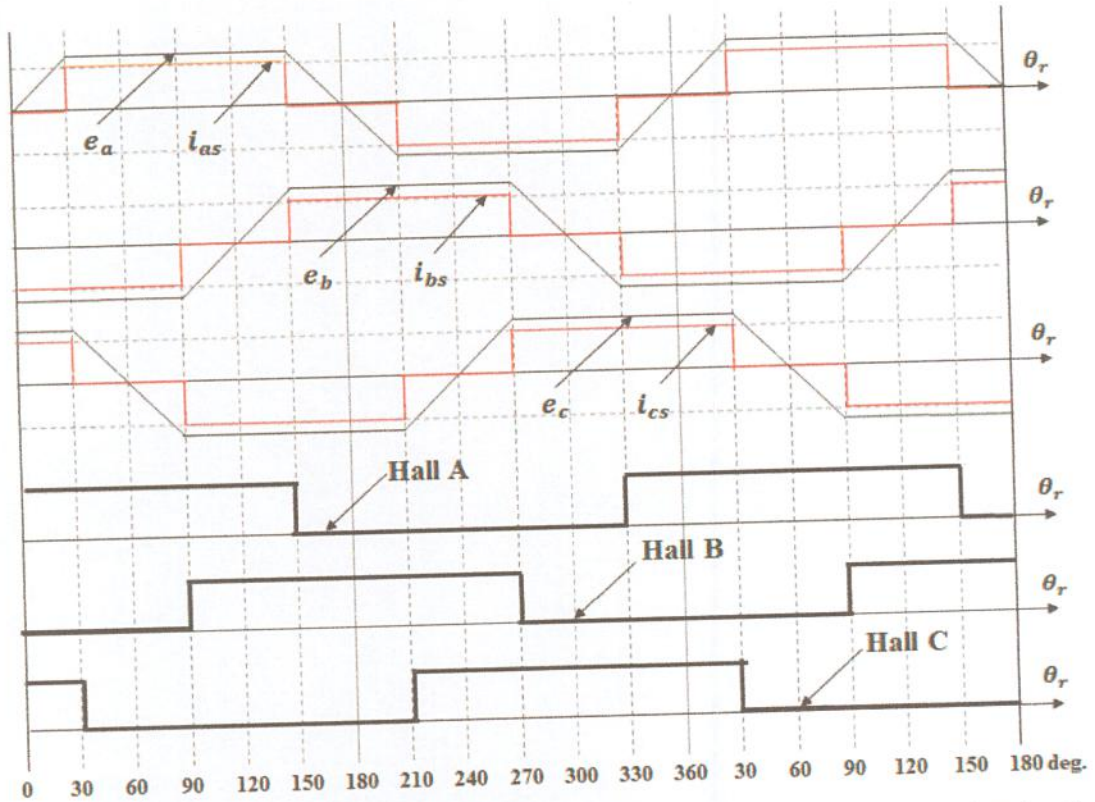


Fig. 2.8: Back EMF and current waveform according to Hall position sensors signals of PMBLDC motor drive

2.5 Comparison of Various Motor Types

The PMBLDC motor has several advantages over other motors. Table 2.1 and Table 2.2 summarize the advantages of the PMBLDC motor when compared against a brushed DC motor and an AC induction motor.

Table 2.1: Comparison of PMBLDC Motor with Brushed DC Motor

Feature	PMBLDC Motor	Brushed DC Motor	Actual Advantage
Commutation	Electronic commutation based on rotor position information	Mechanical brushes and commutator	Electronic switches replace the mechanical devices
Efficiency	High	Moderate	Voltage drop on electronic device is smaller than that on brushes
Maintenance	Little/None	Periodic	No brushes/commutator maintenance

Feature	PMBLDC Motor	Brushed DC Motor	Actual Advantage
Thermal Performance	Better	Poor	Only the armature windings generate heat, which is the stator and is connected to the outside case of the PMBLDC; The case dissipates heat better than a rotor located inside of brushed DC motor
Output Power/ Frame Size (Ratio)	High	Moderate/Low	Modern permanent magnet and no rotor losses
Speed/Torque Characteristics	Flat	Moderately flat	No brush friction to reduce useful torque
Dynamic Response	Fast	Slow	Lower rotor inertia because of permanent magnets
Speed Range	High	Low	No mechanical limitation imposed by brushes or commutator
Electric Noise	Low	High	No arcs from brushes to generate noise, causing EMI problems
Lifetime	Long	Short	No brushes and commutator

Table 2.2: Comparison of PMBLDC Motor with AC Induction Motor

Feature	PMBLDC Motor	AC Induction Motor	Actual Advantage
Speed/Torque Characteristics	Flat	Nonlinear; lower torque at lower speeds	Permanent magnet design with rotor position feedback gives PMBLDC higher starting and low speed torque
Output Power/ Frame Size (Ratio)	High	Moderate	Both stator and rotor have windings for induction motor
Dynamic Response	Fast	Low	Lower rotor inertia because of permanent magnet
Slip Between Stator And Rotor Frequency	No	Yes; rotor runs at a lower frequency than stator by slip frequency and slip increases with load on the motor	PMBLDC is a synchronous motor, induction motor is an asynchronous motor

The primary disadvantage of PMBLDC is cost, though this is no inherent reason due to the motor itself. The construction of a PMBLDC motor is actually simpler than that of brushed DC motor or AC induction motor. The higher cost of PMBLDC motor is caused by the additional driver circuit for PMBLDC motor. However if the application requires adjustable speed, accurate position control, or requires a driver circuit, then PMBLDC motor is not only advantageous but also less expensive overall.

2.6 Mathematical Model of PMBLDC Motor

The flux distribution in PMBLDC motor is trapezoidal and therefore the $d-q$ axes rotor reference frame model is not applicable. For this non-sinusoidal flux distribution, it is suitable to drive a model of PMBLDC motor on the basis of phase variables. The permanent magnet creates a trapezoidal field. Therefore the phase back EMF in the PMBLDC motor is trapezoidal in nature and is the function of the speed ω_m and rotor position θ_r as shown in Fig. 2.9. From Fig. 2.9, the phase back EMF's can be expressed as given in Eq. (2.1).

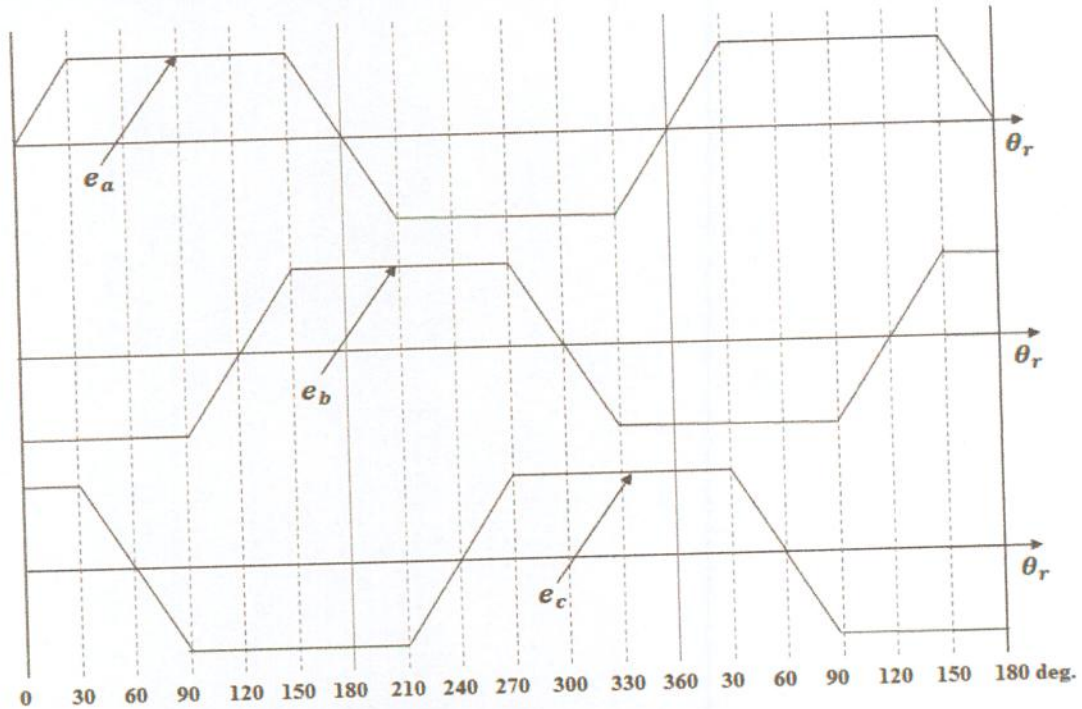


Fig. 2.9: Trapezoidal shaped back EMF of PMBLDC motor

$$\begin{bmatrix} e_a \\ e_b \\ e_c \end{bmatrix} = \omega_m \lambda_m \begin{bmatrix} \varphi_a(\theta_r) \\ \varphi_b(\theta_r) \\ \varphi_c(\theta_r) \end{bmatrix} \quad (2.1)$$

Where, λ_m is the flux linkage, ω_m is angular rotor speed in radian per second, θ_r is the rotor position in radian and $\varphi_a(\theta_r)$, $\varphi_b(\theta_r)$ and $\varphi_c(\theta_r)$ are three phase rotor flux function of rotor position having the same shape of 3-phase back EMF e_a , e_b and e_c with a maximum value of ± 1 . The flux function $\varphi_a(\theta_r)$, $\varphi_b(\theta_r)$ and $\varphi_c(\theta_r)$ are described in Eq. (2.2-2.4) and shown in Fig. 2.10.

$$\varphi_a(\theta_r) = \begin{cases} \theta_r \frac{6}{\pi}, & 0 \leq \theta_r < \frac{\pi}{6} \\ 1, & \frac{\pi}{6} \leq \theta_r < \frac{5\pi}{6} \\ (\pi - \theta_r) \frac{6}{\pi}, & \frac{5\pi}{6} \leq \theta_r < \frac{7\pi}{6} \\ -1, & \frac{7\pi}{6} \leq \theta_r < \frac{11\pi}{6} \\ (\theta_r - 2\pi) \frac{6}{\pi}, & \frac{11\pi}{6} \leq \theta_r < 2\pi \end{cases} \quad (2.2)$$

$$\varphi_b(\theta_r) = \begin{cases} -1, & 0 \leq \theta_r < \frac{\pi}{2} \\ \left(-\frac{2\pi}{3} + \theta_r\right) \frac{6}{\pi}, & \frac{\pi}{2} \leq \theta_r < \frac{5\pi}{6} \\ 1, & \frac{5\pi}{6} \leq \theta_r < \frac{3\pi}{2} \\ \left(-\frac{5\pi}{3} + \theta_r\right) \frac{6}{\pi}, & \frac{3\pi}{2} \leq \theta_r < \frac{11\pi}{6} \\ -1, & \frac{11\pi}{6} \leq \theta_r < 2\pi \end{cases} \quad (2.3)$$

$$\varphi_c(\theta_r) = \begin{cases} 1, & 0 \leq \theta_r < \frac{\pi}{6} \\ \left(\frac{\pi}{3} - \theta_r\right) \frac{6}{\pi}, & \frac{\pi}{6} \leq \theta_r < \frac{\pi}{2} \\ -1, & \frac{\pi}{2} \leq \theta_r < \frac{7\pi}{2} \\ \left(-\frac{4\pi}{3} + \theta_r\right) \frac{6}{\pi}, & \frac{7\pi}{2} \leq \theta_r < \frac{3\pi}{2} \\ 1, & \frac{3\pi}{2} \leq \theta_r < 2\pi \end{cases} \quad (2.4)$$

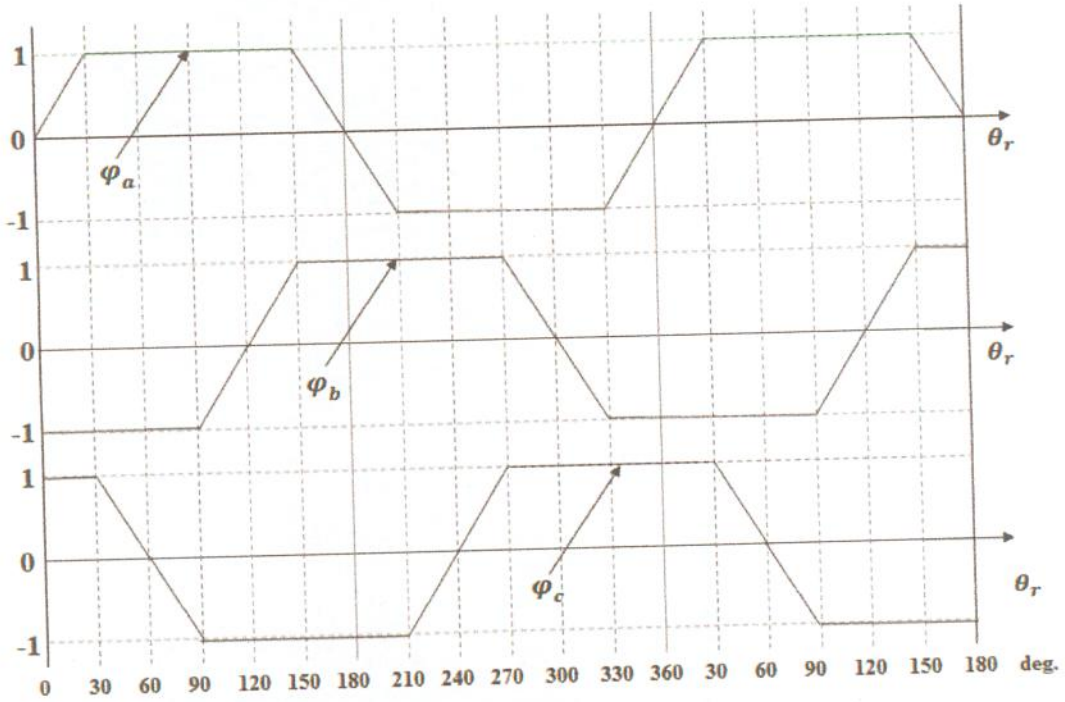


Fig. 2.10: PMBLDC motor three phase rotor flux φ_a , φ_b and φ_c as function of rotor position

Classical modeling equations are used to model the PMBLDC motor and hence the motor model is highly flexible. These equations are based on the dynamic equivalent circuit of PMBLDC motor. Resistance of all the phase windings are assumed to be equal to R_s . By considering ideal non-salient rotor with uniform reluctance reduces the three phase voltage equation to the form as shown in Eq. (2.5). Rotor induced currents can be neglected due to the high resistivity of both magnets and stainless steel. No damper winding are modeled.

$$\begin{bmatrix} V_{as} \\ V_{bs} \\ V_{cs} \end{bmatrix} = \begin{bmatrix} R_s & 0 & 0 \\ 0 & R_s & 0 \\ 0 & 0 & R_s \end{bmatrix} \begin{bmatrix} i_{as} \\ i_{bs} \\ i_{cs} \end{bmatrix} + \frac{d}{dt} \begin{bmatrix} L_{aa} & L_{ab} & L_{ac} \\ L_{ba} & L_{bb} & L_{bc} \\ L_{ca} & L_{cb} & L_{cc} \end{bmatrix} \begin{bmatrix} i_{as} \\ i_{bs} \\ i_{cs} \end{bmatrix} + \begin{bmatrix} e_a \\ e_b \\ e_c \end{bmatrix} \quad (2.5)$$

Where,

V_{as}, V_{bs}, V_{cs} are the phase voltages of stator winding,

i_{as}, i_{bs}, i_{cs} are the stator phase currents,

R_s is the stator resistance per phase,

L_{aa}, L_{bb} and L_{cc} are the self-inductance of phase a, b and c respectively,

L_{ab}, L_{bc} and L_{ac} are mutual inductance between phases a, b and c.

It has been assumed that if there is no change in rotor reluctance with angle because of considering non-salient rotor and then _

$$L_{aa} = L_{bb} = L_{cc} = L_s \quad (2.6)$$

$$L_{ab} = L_{ba} = L_{bc} = L_{cb} = L_{ac} = L_{ca} = M \quad (2.7)$$

By Substituting Eq. (2.6) and Eq. (2.7) in Eq. (2.5) gives _

$$\begin{bmatrix} V_{as} \\ V_{bs} \\ V_{cs} \end{bmatrix} = \begin{bmatrix} R_s & 0 & 0 \\ 0 & R_s & 0 \\ 0 & 0 & R_s \end{bmatrix} \begin{bmatrix} i_{as} \\ i_{bs} \\ i_{cs} \end{bmatrix} + \frac{d}{dt} \begin{bmatrix} L_s & M & M \\ M & L_s & M \\ M & M & L_s \end{bmatrix} \begin{bmatrix} i_{as} \\ i_{bs} \\ i_{cs} \end{bmatrix} + \begin{bmatrix} e_a \\ e_b \\ e_c \end{bmatrix} \quad (2.8)$$

Where phase voltages V_{as} , V_{bs} and V_{cs} are designed as _

$$V_{as} = V_{a0} - V_{n0} \quad (2.9)$$

$$V_{bs} = V_{b0} - V_{n0} \quad (2.10)$$

$$V_{cs} = V_{c0} - V_{n0} \quad (2.11)$$

Where V_{a0} , V_{b0} , V_{c0} and V_{n0} are three phase and neutral voltages referred to the zero reference potential at the mid- point of dc link.

The phase currents of stator are considered to be balanced for no neutral connection _

$$i_{as} + i_{bs} + i_{cs} = 0 \quad (2.12)$$

$$Mi_{bs} + Mi_{cs} = - Mi_{as} \quad (2.13)$$

Then Eq. (2.13) is used to simplify inductances matrix. Therefore Eq. (2.8) becomes _

$$\begin{bmatrix} V_{as} \\ V_{bs} \\ V_{cs} \end{bmatrix} = \begin{bmatrix} R_s & 0 & 0 \\ 0 & R_s & 0 \\ 0 & 0 & R_s \end{bmatrix} \begin{bmatrix} i_{as} \\ i_{bs} \\ i_{cs} \end{bmatrix} + \frac{d}{dt} \begin{bmatrix} L_s - M & 0 & 0 \\ 0 & L_s - M & 0 \\ 0 & 0 & L_s - M \end{bmatrix} \begin{bmatrix} i_{as} \\ i_{bs} \\ i_{cs} \end{bmatrix} + \begin{bmatrix} e_a \\ e_b \\ e_c \end{bmatrix} \quad (2.14)$$

It is significant to observe that the phase voltage equation in Eq. (2.14) is identical to armature voltage equation of DC machine. That is one of reasons for naming this motor as Permanent Magnet Brushless DC motor. Eq. (2.14) in state space form is _

$$\dot{x} = Ax + Bu + Ce \quad (2.15)$$

$$\text{Where, } x = [i_{as} \ i_{bs} \ i_{cs}]^t \quad (2.16)$$

$$u = [V_{as} \ V_{bs} \ V_{cs}]^t \quad (2.17)$$

$$e = [e_a \ e_b \ e_c]^t \quad (2.18)$$

$$A = \begin{bmatrix} -\frac{R_s}{L_s-M} & 0 & 0 \\ 0 & -\frac{R_s}{L_s-M} & 0 \\ 0 & 0 & -\frac{R_s}{L_s-M} \end{bmatrix} \quad (2.19)$$

$$B = \begin{bmatrix} \frac{1}{L_s-M} & 0 & 0 \\ 0 & \frac{1}{L_s-M} & 0 \\ 0 & 0 & \frac{1}{L_s-M} \end{bmatrix} \quad (2.20)$$

$$C = \begin{bmatrix} -\frac{1}{L_s-M} & 0 & 0 \\ 0 & -\frac{1}{L_s-M} & 0 \\ 0 & 0 & -\frac{1}{L_s-M} \end{bmatrix} \quad (2.21)$$

The system consists of two other mechanical variables as described now. The electromagnetic torque developed is given by Eq. (2.22).

$$T_e = [e_a i_{as} + e_b i_{bs} + e_c i_{cs}] / \omega_m \quad (Nm) \quad (2.22)$$

If the system moment of inertia J , friction coefficient B is constant and load torque is T_l , then the system motion equation is_

$$J \frac{d\omega_m}{dt} + B\omega_m = (T_e - T_l) \quad (2.23)$$

$$J = J_m + J_l \quad (2.24)$$

Where, J_m and J_l are the moment of inertia of motor and load respectively. Electrical rotor position θ_r is related with mechanical rotor speed ω_m by Eq. (2.25). Here, P is number of poles. The rotor position θ_r repeats every 2π radians. Where ω_r is electrical angular speed of the PMBLDC motor.

$$\omega_r = \frac{d\theta_r}{dt} = \frac{P}{2} \omega_m \quad (2.25)$$

The potential of the neutral point with respect to the zero potential (V_{n0}) is required to be considered in order to avoid imbalance in the applied voltage and simulate the performance of the drive. This is obtained by substituting Eq. (2.12) in the phase voltage Eq. (2.14) and adding then give as _

$$\begin{aligned} V_{a0} + V_{b0} + V_{c0} - 3V_{n0} \\ = R_s(i_{as} + i_{bs} + i_{cs}) + (L_s - M) \left(\frac{di_{as}}{dt} + \frac{di_{bs}}{dt} + \frac{di_{cs}}{dt} \right) + (e_a + e_b + e_c) \end{aligned} \quad (2.26)$$

Substituting Eq. (2.12) in Eq. (2.26) and then V_{n0} can be calculated.

$$V_{n0} = \frac{\{(V_{a0} + V_{b0} + V_{c0}) - (e_a + e_b + e_c)\}}{3} \quad (2.27)$$

2.7 Conclusion

The brushless motors are generally controlled using a three phase power semiconductor bridge. The motor requires a rotor position sensor for starting and for providing proper commutation sequence to turn on the power devices in the inverter bridge. Based on the rotor position, the power devices are commutated sequentially every 60 degrees. Instead of commutating the armature current using brushes, electronic commutation is used for this reason it is an electronic motor. This eliminates the problems associated with the brush and the commutator arrangement, for example, sparking and wearing out of the commutator brush arrangement, thereby, making a PMBLDC more rugged as compared to a dc motor.

Chapter III

Field Oriented Control of PMBLDC Motor

Chapter Outlines:

3.1 Introduction

3.2 Scalar Control Methods

3.3 Vector Control Methods

3.4 Proposed Field Oriented Control System

3.5 Results and Discussion

3.6 Conclusion

3.1 Introduction

Permanent Magnet Brushless DC (PMBLDC) Motors are high power density motors with a huge scope to be used as an industrial motor in future. But the motor performance degrades due to improper control actions. Control methods for electric motors can be divided into two main categories depending of what quantities they control. The scalar control algorithm controls only magnitudes, whereas the vector control algorithms control both magnitude and angles. The preferred method for controlling a PMBLDC motor is vector control. Vector control can be divided into two main types, Field Oriented Control (FOC) and Direct Torque Control (DTC). The FOC aims to control the current vector and DTC aims to control the torque producing flux vector.

In this chapter field oriented control of a PMBLDC motor drive is presented. Scalar control of this PMBLDC motor is also performed at direct axis current component is equal to 1.0 and at direct axis current component equal to quadrature axis current component. Since the motor has a trapezoidal field pattern rather than sinusoidal it is desirable to study the motor behavior with field oriented control and compare that with scalar control. The performances of these control systems are compared under different transient conditions.

Current fed field oriented control for PMBLDC motor drive is introduced for this motor control. An adaptive PI controller based on motor speed error is proposed in this chapter to have a simplified drive system. A hysteresis type current controller is also proposed and implemented. The drive system is simulated in a C++ environment in discrete form. Transient response and loading capability of the motor are studied with two different conditions of scalar control with flux component of currents.

3.2 Scalar Control Methods

The simplest method to control a PMBLDC motor is scalar control, where the relationship between voltage or current and frequency are kept constant through the motors speed range. The frequency is set according to the wanted synchronous speed and the magnitude of the voltage/current is adjusted to keep the ratio between them constant. No control over angles is utilized, hence the name scalar control. This makes the method easy to implement and with low demands on computation power of the control hardware. But its simplicity also comes with some disadvantages. One of them are instability of the drive system after exceeding a certain applied frequency, to overcome this the rotor has to be constructed with damper windings to assure synchronization of the rotor to the electrical frequency. This will limit the number of design choices for the rotor, e.g. the magnets has to be located on the inside of the damper bars. Most PMBLDC motors are therefore constructed without damper windings, and they are not suitable for traditional scalar control. Another drawback is the systems low dynamic performance, which limits the use of this control method for some applications such as fan and pump-drives. For applications that demands high dynamic performance, vector control is recommended [49].

3.3 Vector Control

With control of both magnitude and the angle of the flux it is possible to achieve higher dynamic performance of the drive system than scalar control can offer. Two different types of strategies exist for vector control, Field Oriented Control and Direct Torque Control. Direct Torque Control will be discussed in Chapter VII of this thesis report.

3.3.1 Field Oriented Control

In field oriented control, the direct and quadrature axis current i_{ds} and i_{qs} are controlled to achieve the requested torque. It is possible to achieve a Maximum Torque Per Ampere (MTPA) ratio to minimize the current needed for a specific torque by controlling i_{ds} and i_{qs} independently which maximizes the motors efficiency. For a non-salient machine i.e. $L_d = L_q$, this control is easy to implement. A motor without saliency cannot produce any reluctance torque. Therefore i_{ds} has no effect on torque production, and it needs to be zero at all times to reach MTPA. The torque curves will be linear in the d - q plane and the MTPA trajectory will be along the quadrature-axis. For a salient machine, i.e. $L_d \neq L_q$, this control is a bit more difficult to implement since the motor produces both electromechanical and reluctance torque. That's why the torque as a function of current in the d - q plane is no longer linear. To reach MTPA, the minimum distance from the origin to the curve of requested torque has to be calculated [49].

One of the critical parameters for FOC is the need of correct information of the rotor position. The most common way to do this is Indirect FOC, where a mechanical sensor coupled to the motors shaft is used for positioning. Another type is Direct FOC where the position is estimated from the flux or back EMF vector [50].

Field oriented control is mainly a mathematical technique utilized for achieving a separate control of the field producing and the torque producing portions of the stator currents in a three-phase motor. Stator current is decomposed into magnetizing current i_{ds} responsible for producing a magnetic field and quadrature current i_{qs} which controls developed torque as shown in Fig. 3.1 [51].

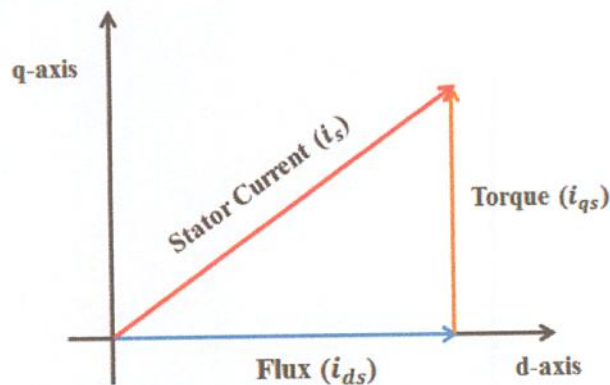


Fig. 3.1: Decomposition of stator current for field oriented control.

In DC motors, the flux and torque producing currents are orthogonal and can be controlled independently. The magneto motive forces, developed by these currents are also held orthogonal. The torque developed is given by the Eq. (3.1).

$$T_e = k_a \times \varphi(I_f) \times I_a \quad (3.1)$$

Where, $\varphi(I_f)$ is flux function of field current and I_a is armature current. Hence the flux is only dependent on the field winding current. If the flux is held constant, then the torque can be controlled by the armature current. For this reason DC machines are said to have decoupled or have independent control of torque and flux.

In PMLDLC machines, the stator and rotor fields are not orthogonal to each other. The only current that can be controlled is the stator current. Field Oriented Control is the technique used to achieve the decoupled control of torque and flux by transforming the stator current quantities (phase currents) from stationary reference frame to torque and flux producing currents components in rotating reference frame. Advantages of FOC_

- ❖ Transformation of a complex and coupled AC model into a simple linear system
- ❖ Independent control of torque and flux, similar to a DC motor
- ❖ Fast dynamic response and good transient and steady state performance
- ❖ High torque and low current at startup
- ❖ High Efficiency
- ❖ Wide speed range through field weakening

FOC technique involves three reference frames and needs transformations from one to the other.

- ❖ Stator reference frame (a, b, c) in which the a, b, c are co-planar, at 120 degrees to each other.
- ❖ An orthogonal reference frame ($\alpha\text{-}\beta$) in the same plane as the stator reference frame in which the angle between the two axes is 90 degrees instead of 120 degrees. The a axis is aligned with α axis in the second frame.
- ❖ Rotor reference frame ($d\text{-}q$), in which the d axis is along the N and S poles or along the flux vector of the rotor and the q axis is at 90 degrees to the d axis.

3.3.2 Reference Frame Transformations

Clarke and Park transformations are mainly used in vector control architectures. This section explains the Park, Inverse Park and Clarke, Inverse Clarke transformations.

❖ Clarke Transformation

The three-phase quantities are translated from the three-phase reference frame to the two-axis orthogonal stationary reference frame using Clarke transformation as shown in Fig. 3.2. The Clarke transformation is expressed by the following equations_

$$i_{\alpha s} = \frac{2}{3}(i_{as}) - \frac{1}{3}(i_{bs} - i_{cs}) \quad (3.2)$$

$$i_{\beta s} = \frac{2}{\sqrt{3}}(i_{bs} - i_{cs}) \quad (3.3)$$

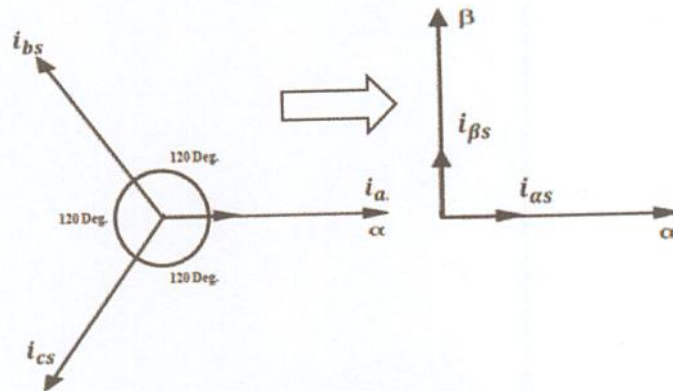


Fig. 3.2: Clarke transformation

❖ Inverse Clarke Transformation

The transformation from a two-axis orthogonal stationary reference frame to a three-phase stationary reference frame is accomplished using Inverse Clarke transformation as shown in Fig. 3.3. The Inverse Clarke transformation is expressed by the following equations_

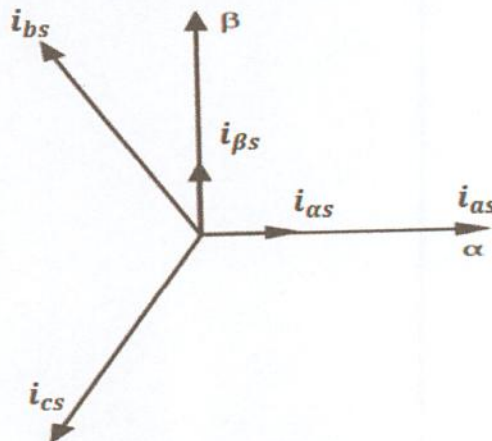


Fig. 3.3: Inverse Clarke transformation

$$i_{as} = i_{\alpha s} \quad (3.4)$$

$$i_{bs} = -\frac{1}{2}i_{\alpha s} + \frac{\sqrt{3}}{2}i_{\beta s} \quad (3.5)$$

$$i_{cs} = -\frac{1}{2}i_{\alpha s} - \frac{\sqrt{3}}{2}i_{\beta s} \quad (3.6)$$

❖ Park Transformation

The two-axis orthogonal stationary reference frame quantities are transformed into rotating reference frame quantities using Park transformation as shown in Fig. 3.4. The Park transformation is expressed by the following equations_

$$i_{ds} = i_{\alpha s} \cos(\theta) + i_{\beta s} \sin(\theta) \quad (3.7)$$

$$i_{qs} = i_{\beta s} \cos(\theta) - i_{\alpha s} \sin(\theta) \quad (3.8)$$

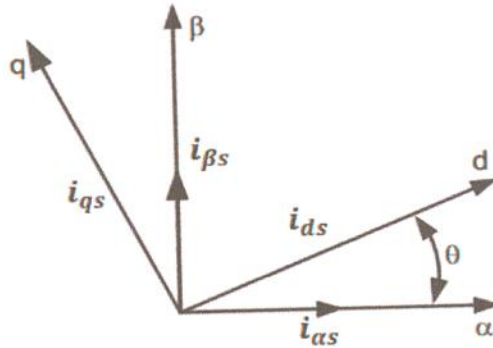


Fig. 3.4: Park transformation

❖ Inverse Park Transformation

The quantities in rotating reference frame are transformed to two-axis orthogonal stationary reference frame using Inverse Park transformation. The Inverse Park transformation is expressed by the following equations_

$$i_{\alpha s} = i_{ds} \cos(\theta) - i_{qs} \sin(\theta) \quad (3.9)$$

$$i_{\beta s} = i_{ds} \sin(\theta) + i_{qs} \cos(\theta) \quad (3.10)$$

3.4 Proposed Field Oriented Control System

Field oriented current fed drive for PMBLDC motor control is proposed. The performance of vector controlled drive is compared with a traditional scalar control drive. The proposed control drive mainly consists of an adaptive PI controller, field oriented reference current generator, delta modulated PWM current controller, IGBT voltage source inverter, position sensor, current sensors and PMBLDC motor as shown in Fig. 3.5.

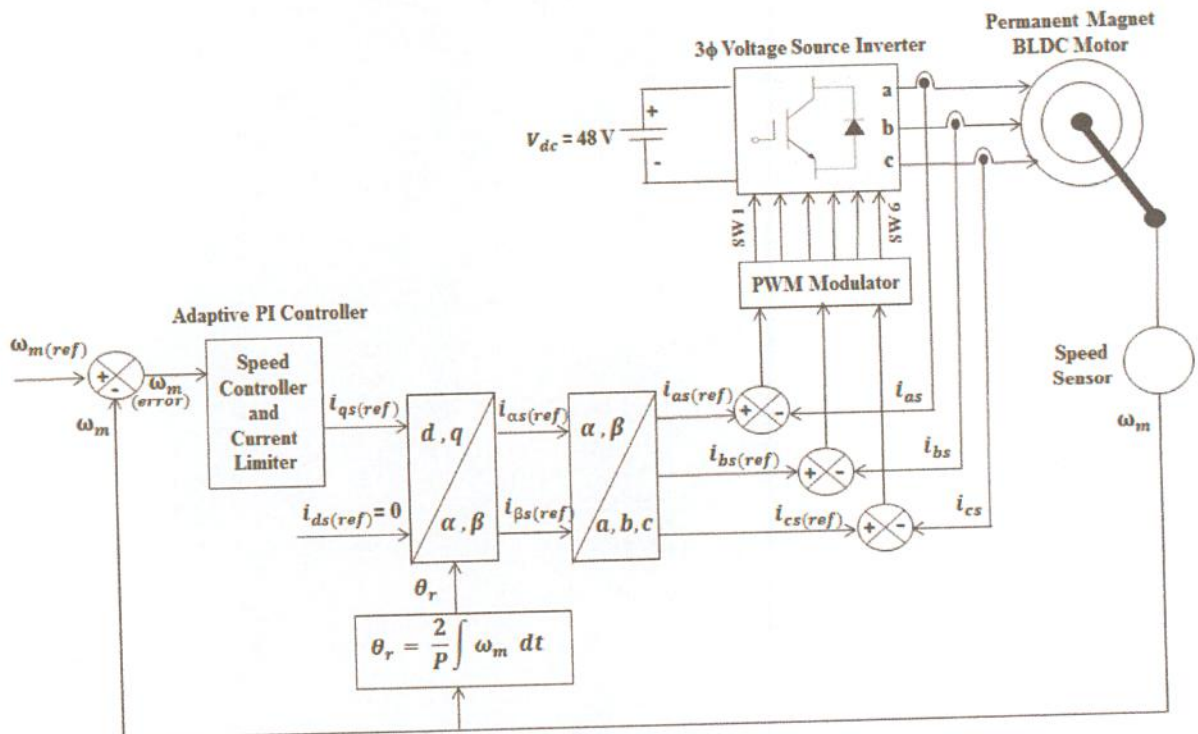


Fig. 3.5: Block diagram of field oriented vector controlled current fed PMBLDC motor drive by using adaptive PI speed controller

3.4.1 Adaptive PI controller Design

In industry PI controller is widely used due to its simple structure and easy to design. In a system PI controller attempts to correct the error between actual system variable and desired set point. There are proportional and integral modes of calculation in PI controller. PI controller is implemented as

$$e_o(t) = K_p e_i(t) + K_I \int_0^t e_i(\tau) d\tau \quad (3.11)$$

Where, $e_i(t)$ = Desired reference value - Actual value, K_p and K_I are the proportional and integral gains of the PI controller respectively. The actual speed of the PMBLDC motor is compared with its reference speed and the speed error is processed through PI controller to estimate reference torque by Eq. (3.13).

$$\text{Speed error, } \omega_{m(\text{error})}(t) = e(t) = \omega_{m(\text{ref})}(t) - \omega_m(t) \quad (3.12)$$

$$T_{\text{ref}}(t) = T_{\text{ref}}(t-1) + K_p[e(t) - e(t-1)] + K_I e(t) \quad (3.13)$$

From simulation studies it has been observed that the speed error reduces the effectiveness of the PI controller & becomes slower due to the nonadjustable nature of gain constants. In this control systems K_p and K_I gain constants are made adjustable with speed by using Eq. (3.14-3.15). Where, K_{p0} and K_{I0} are initial gain constants of the system, K_1 and K_2 are the constant of the tuner of the proportional and integral gain constants with speed respectively. Thus an adaptive PI controller is designed. So that speed overshoot in system have to be prevented and settling time to gain reference speed can be minimized.

$$K_p = K_{p0} + K_1 * \omega_m \quad (3.14)$$

$$K_I = K_{I0} + K_2 * \omega_m \quad (3.15)$$

The output of this adaptive PI speed controller is the reference torque of the system. A limit has to be put on the speed controller output depending on the permissible maximum winding currents. The reference quadrature axis current i_{qs} is determined from the value of reference torque T_{ref} by using Eq. (3.16). Where K_t is the torque constant of the PMBLDC motor.

$$i_{qs(\text{ref})} = T_{\text{ref}} / K_t \quad (3.16)$$

3.4.2 Field oriented control of PMBLDC motor drive

In this proposed control system, three phase reference current is generated by considering direct axis current $i_{ds(ref)} = 0$ and by calculated the value of quadrature axis current $i_{qs(ref)}$ according to the requested load torque through the adaptive PI controller. The field oriented control system requires the synchronous d axis current of stator coils forced to zero. For this control system transformation to different frames is necessary. At first the currents in rotating $d-q$ reference frame are transformed to two-axis orthogonal stationary $\alpha-\beta$ reference frame by using Inverse Park transformation as shown in Eq. (3.17-3.18). Where θ_r is electrical rotor position of the PMBLDC motor.

Inverse Park Transformation

$$i_{\alpha s(ref)} = i_{ds(ref)} \cos(\theta_r) - i_{qs(ref)} \sin(\theta_r) \quad (3.17)$$

$$i_{\beta s(ref)} = i_{ds(ref)} \sin(\theta_r) + i_{qs(ref)} \cos(\theta_r) \quad (3.18)$$

Now the currents of two-axis orthogonal stationary $\alpha-\beta$ reference frame have to convert three-phase stationary a, b, c reference frame through Inverse Clarke transformation mentioned in Eq. (3.19-3.21).

Inverse Clarke Transformation

$$i_{as(ref)} = i_{\alpha s(ref)} \quad (3.19)$$

$$i_{bs(ref)} = -\frac{1}{2}i_{\alpha s(ref)} + \frac{\sqrt{3}}{2}i_{\beta s(ref)} \quad (3.20)$$

$$i_{cs(ref)} = -\frac{1}{2}i_{\alpha s(ref)} - \frac{\sqrt{3}}{2}i_{\beta s(ref)} \quad (3.21)$$

3.4.3 PWM current controller

Delta modulated current control PWM is used for the switching of voltage source inverter. This hysteresis-band PWM is basically an instantaneous feedback current control method of PWM where the actual current continually tracks the reference current. When the current exceeds upper band limit, then the upper switch has to be off and lower switch has to be on. Similarly when the current exceeds lower band limit, upper switch is on and lower switch is off.

The switching logic which is used in this control drive given below

$$\text{If } i_{as} < (i_{as(ref)} - h_b)$$

Then switch 1 is ON and switch 4 is OFF ($S_A = 1$)

$$\text{If } i_{as} < (i_{as(ref)} + h_b)$$

Then switch 1 is OFF and switch 4 is ON ($S_A = 0$)

$$\text{If } i_{bs} < (i_{bs(ref)} - h_b)$$

Then switch 3 is ON and switch 6 is OFF ($S_B = 1$)

$$\text{If } i_{bs} < (i_{bs(ref)} + h_b)$$

Then switch 3 is OFF and switch 6 is ON ($S_B = 0$)

$$\text{If } i_{cs} < (i_{cs(ref)} - h_b)$$

Then switch 5 is ON and switch 2 is OFF ($S_C = 1$)

$$\text{If } i_{cs} < (i_{cs(ref)} + h_b)$$

Then switch 5 is OFF and switch 2 is ON ($S_C = 0$)

Where, h_b is the hysteresis band around reference current. The inverter output voltages according to the above switching conditions are given below

$$V_{as} = \frac{1}{3}[2S_A - S_B - S_C] \quad (3.22)$$

$$V_{bs} = \frac{1}{3}[-S_A + 2S_B - S_C] \quad (3.23)$$

$$V_{cs} = \frac{1}{3}[-S_A - S_B + 2S_C] \quad (3.24)$$

3.5 Results and Discussion

The drive system was simulated in a digital computer with software written in C++ environment in discrete form. The specifications of the simulated PMSM motor are described in Appendix. The sampling time used for this simulation is 0.0000025 second.

3.5.1 Starting characteristics

Starting speed characteristics i.e. time taken by the motor to reach its rated speed (150 rad/s) with its initial torque (0.4 Nm) for both vector and scalar control of PMSM motor drives is shown in Fig. 3.6. From this graph, it is seen that, PMSM vector control drive takes 0.55 seconds to gain rated speed. For scalar control with $i_d=1.0$ and $i_d=i_q$, motor takes 0.63 and 0.96 seconds respectively. So vector control is suitable to gain rated speed as fast as possible than scalar control.

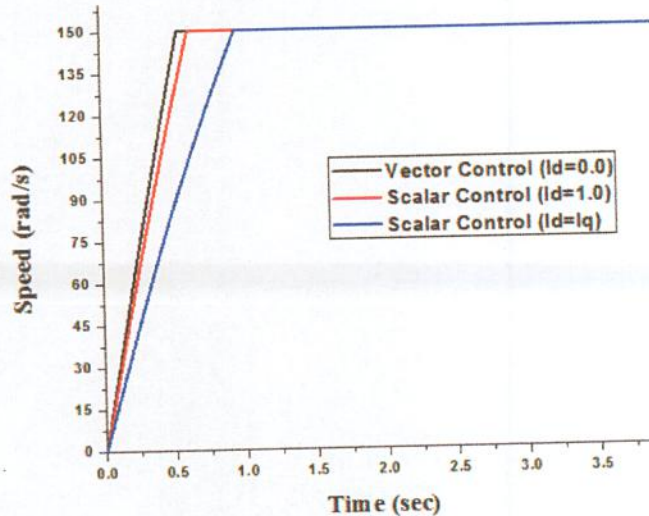
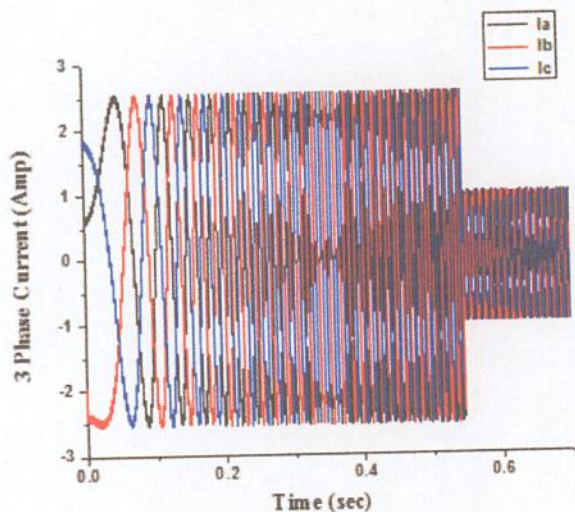
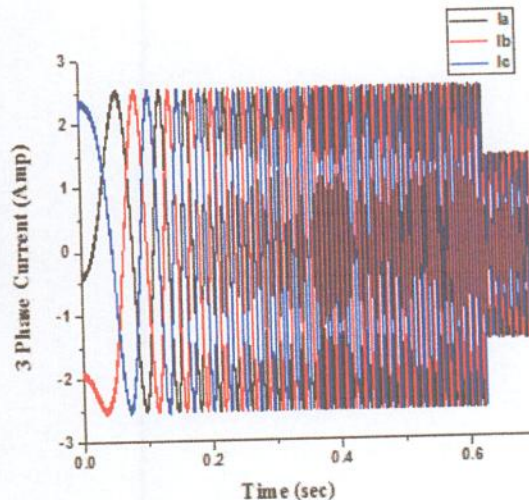


Fig. 3.6: Starting characteristics of PMSM motor drives for both vector and scalar field control

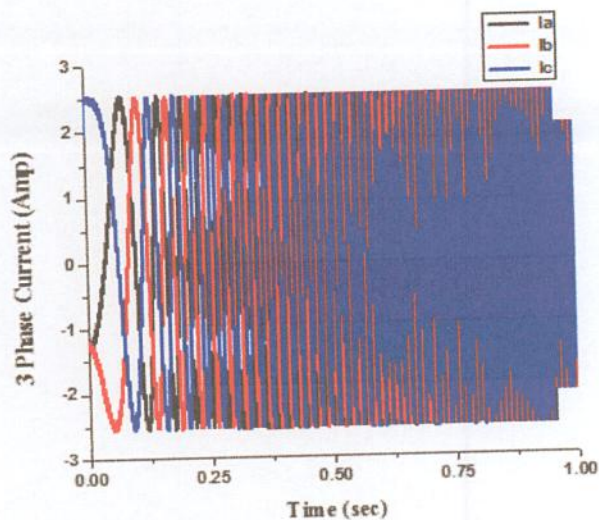
Phase current of PMSM motor at the time of starting for vector control and scalar control are depicted in Fig. 3.7. It shows that the amplitude of 3-phase current is 2.5 Amp (rated current of the motor) at the transient time of starting for both vector and scalar control drives. Starting current is limited through the current limiter block as shown in Fig. 3.5. Fig. 3.7 also describes that after gaining rated speed i.e. at steady state motor takes maximum 1 Amp current for $i_d = 0.0$ (vector control), maximum 1.5 Amp current for $i_d = 1.0$ (scalar control), maximum 2.0 Amp current for $i_d=i_q$ (scalar control) for initial load torque 0.4 Nm. So that PMSM motor takes less current at stable condition for vector control drive than scalar control drives.



(a) Vector control ($i_d = 0.0$)



(b) Scalar control ($i_d = 1.0$)



(c) Scalar control ($i_d = i_q$)

Fig. 3.7: 3-Phase starting current of PMSM for vector and scalar control

3-phase back EMF, rotor position curve at the time of starting for vector control PMSM drive is shown in Fig. 3.8. In Fig. 3.9, stator flux linkage trajectories i.e. flux orientation representation in the stationary $\alpha\beta$ axes reference frame for both vector and scalar controlled PMSM motor drives are pictured.

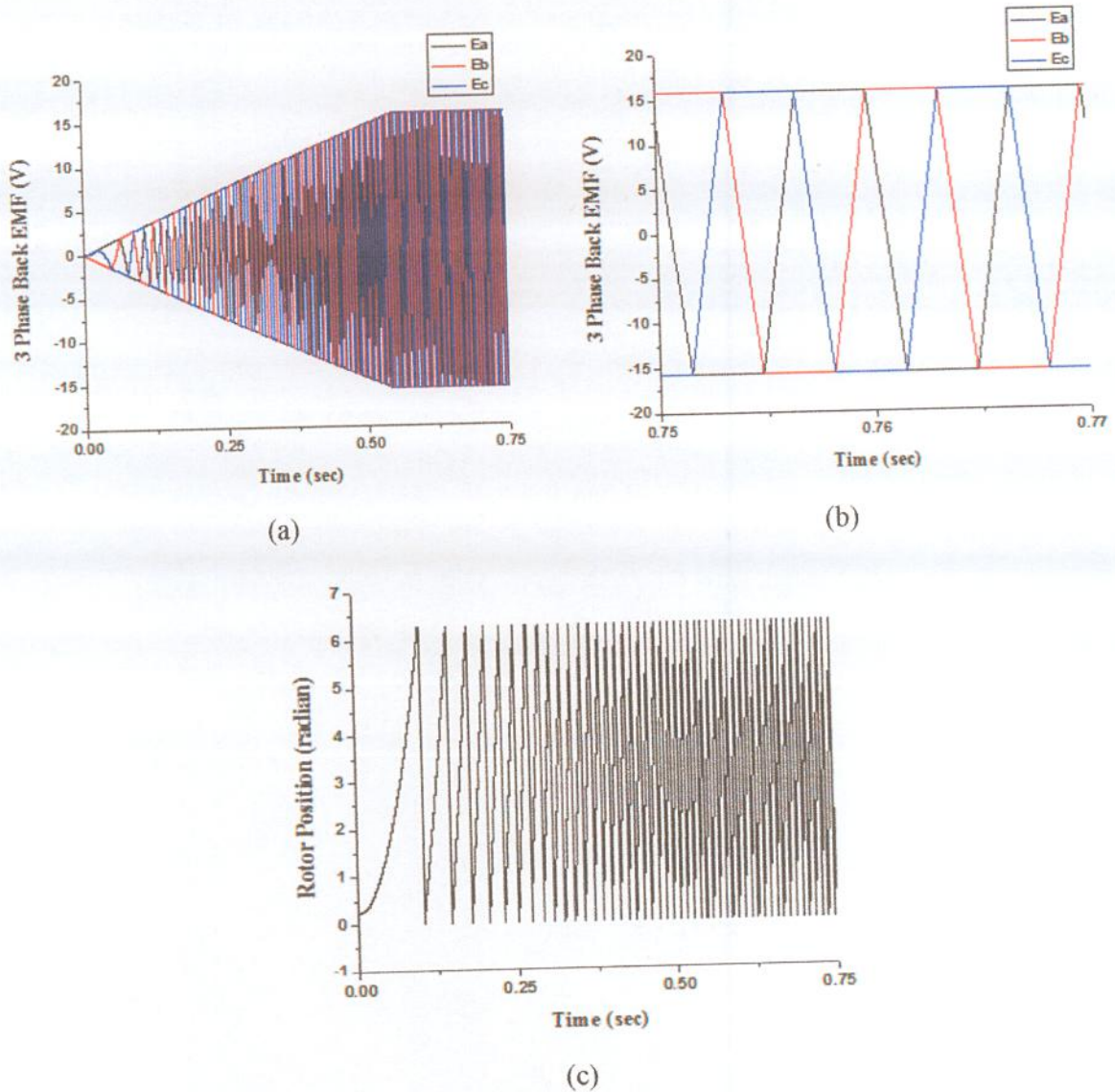
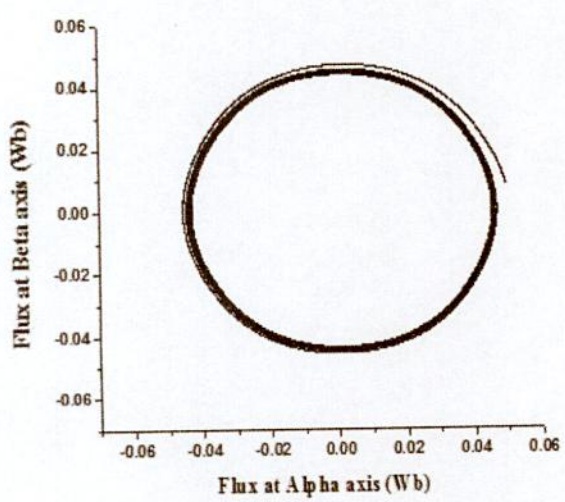
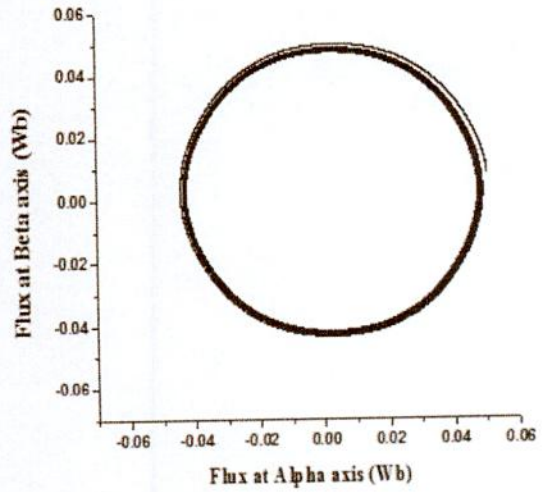


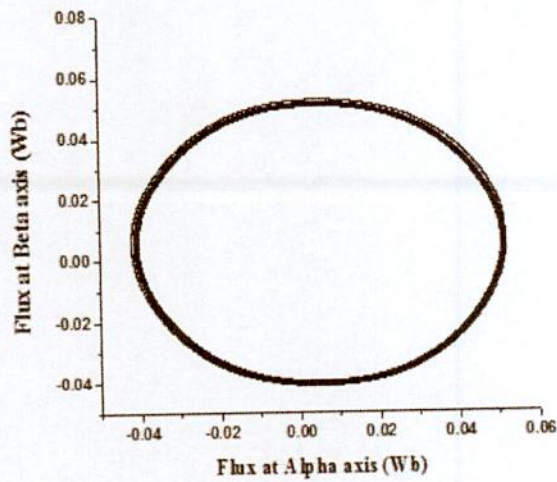
Fig. 3.8: (a) 3-phase back EMF at starting, (b) steady state back EMF at rated speed and (c) rotor position of vector control PMSM motor drive



(a) Vector control ($i_d = 0.0$)



(b) Scalar control ($i_d = 1.0$)



(c) Scalar control ($i_d = i_q$)

Fig. 3.9: Flux orientation representation in the stationary $\alpha\beta$ – axes reference frame for both vector and scalar controlled PMBLDC motor drive

3.5.2 Variable speed characteristic

To measure the dynamic performance of the vector and scalar controlled PMBLDC motor drive, variable speed command is given. Motor runs at speed 100 rad/s. At 1.0 second the speed command is changed to 75 rad/s and finally at 1.5 second speed command is changed to 150 rad/s. From Fig. 3.10, motor speed follows the reference speed sharply for vector controlled PMBLDC motor drives than scalar controlled. Scalar control for the case of $i_d=i_q$, there is noticeable difference between reference speed and actual motor speed. From 3-phase current curve for variable speed condition for vector control as shown in Fig. 3.11, it is seen that, at 1.0 second when the reference speed changes from 100 rad/s to 75 rad/s, there exists no high value of transient current and undershoot from reference speed for both vector and scalar control. Condition of back EMF at the time of variable speed is shown in Fig. 3.12.

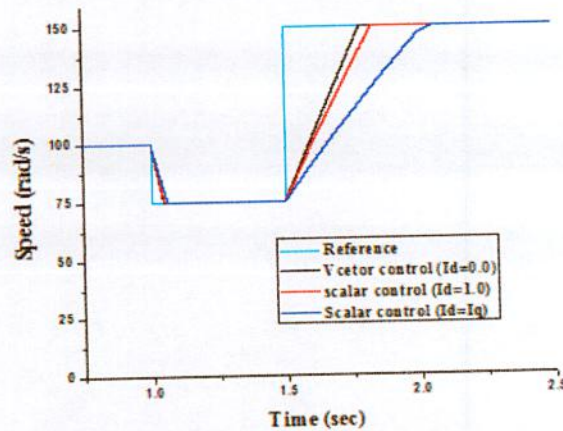


Fig. 3.10: Comparison between speed responses of PMBLDC motor vector and scalar controlled drive at dynamic speed changing condition

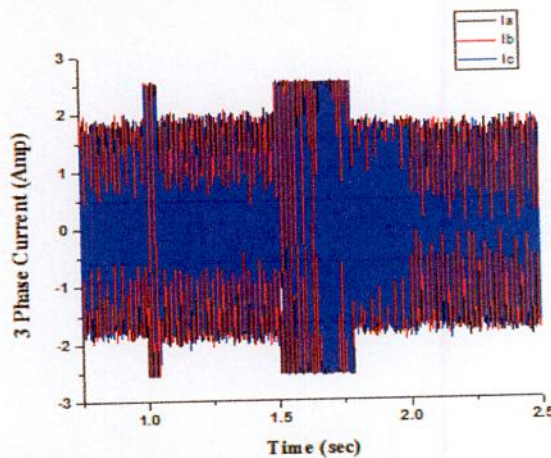


Fig. 3.11: 3-phase current of vector controlled drive for variable speed condition considering transient current at the interface of speed changes

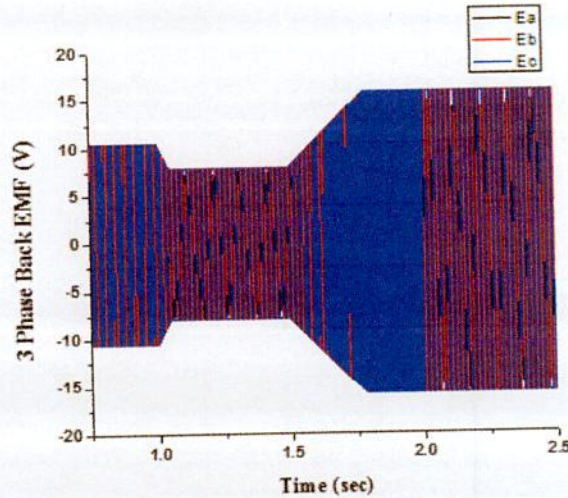


Fig. 3.12: 3-phase back EMF at dynamic speed changing condition for Vector controlled PMLDLC motor drives

3.5.3 Motor characteristics due to load torque change

Now the performance of PMLDLC motor drives for vector and scalar control are determined under the condition of load torque change. At first motor runs at 150 rad/s rated speed with initial load torque 0.4 Nm. At time 1.5 second motor is loaded with load torque 1.55 Nm. At that condition only vector controlled drive can sustain motor speed to its rated value 150 rad/s. But scalar controlled drive cannot sustain its previous speed as shown in Fig. 3.13. The speed of scalar controlled drives is gradually decreased after the loading of the motor. It verifies that the load torque handling capacity of scalar controlled PMLDLC motor drive is very poor than vector controlled drive.

The rate of gradually fall down speed of scalar drive with $i_d=i_q=1.7677$ Amp (To limit current in rated value 2.5 Amp) is very high than the rate of scalar drive $i_d=1.0$ Amp (i.e. $i_q=2.29$ Amp). So load torque handling capacity decrease with the increase of the value i_d of a scalar drive keeping the stator current within the maximum value. Maximum load torque have to be given to the scalar controlled PMLDLC motor drive without hampering the drive stability for $i_d = 1.0$ and $i_d=i_q$ are 1.4 Nm and 1.0 Nm respectively.

From graphical representation of 3-phase current for sudden load torque change as shown in Fig. 3.14, it summaries that, before stable reference speed stator current is maximum rated current of the motor. At stable reference speed stator current decreases to 1.0 Amp. But when the rated load torque is applied, the stator current is about its rated value (2.5 Amp).

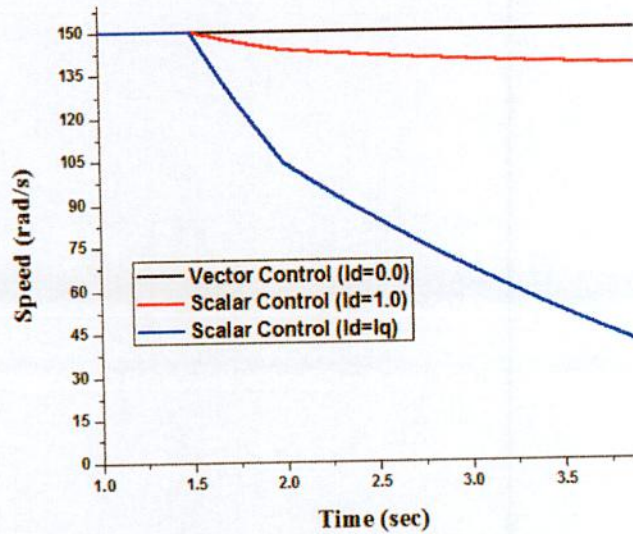


Fig. 3.13: Speed characteristics of PMBLDC motor drives for sudden load torque change at 1.5 second from initial load torque 0.4 Nm to rated load torque 1.55 Nm both for field oriented vector and scalar control

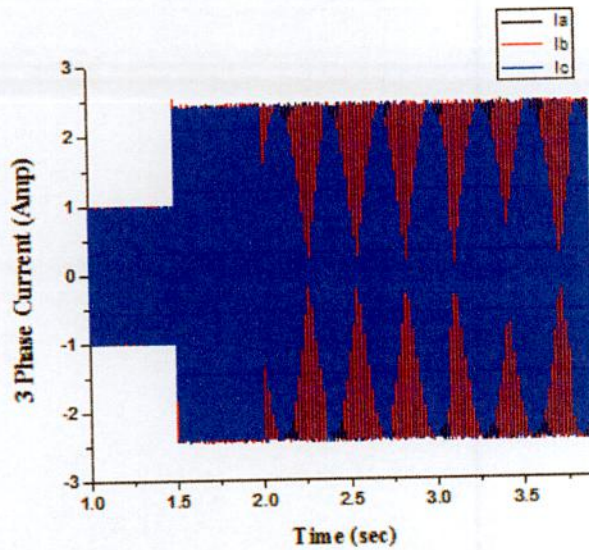


Fig. 3.14: 3-phase current of vector controlled PMBLDC motor drives for sudden load torque change at 1.5 second

3.5.4 Study of drive system performance due to the change of PMBLDC motor parameters

In this section the performance of the proposed PMBLDC motor drive is tested due to the change of PMBLDC motor parameters. There is an effect of moment of inertia on starting characteristic of proposed PMBLDC motor drive as shown in Fig. 3.15. With the rated moment of inertia ($0.0048 \text{ kg}\cdot\text{m}^2$), the vector control drive takes 0.55 seconds to gain its rated speed. When the 25% moment of inertia is increased, then the vector control drive takes 0.69 seconds to gain rated speed. Similarly, the scalar control drives with $i_d=1.0$ and $i_d=i_q$ take 0.77 seconds and 1.17 seconds respectively to gain rated speed, when the moment of inertia is increased by 25% of its rated value. Here only starting characteristic for vector controlled PMBLDC motor drive is pictured. So with the increase of moment of inertia, the time taken by the drive to reach its command speed is increased.

Now consider the steady state condition, motor runs at 150 rad/s rated speed with rated moment of inertia $0.0048 \text{ kg}\cdot\text{m}^2$. At time 1.5 second the moment of inertia of the PMBLDC motor is increased 25% (i.e. $0.006 \text{ kg}\cdot\text{m}^2$) from its rated inertia. At that condition speed characteristics of PMBLDC motor drive is shown in Fig. 3.16 for both vector and scalar control. From Fig. 3.16, it is seen that, there is no effect of change of 25% moment of inertia in speed characteristic i.e. the drive can sustain motor speed to its rated value 150 rad/s for both vector and scalar control. Similar scenario is seen for 25% decrease of moment of inertia from its rated value. 3-phase current of vector controlled PMBLDC motor drives for increasing 25% of motor moment of inertia at 1.5 second from the rated value is depicted in Fig. 3.17. It shows that, there is no effect of 25% increase of moment of inertia on 3 phase stator current. It is also found that, there is no effect of 25% increase or decrease of motor inertia on the performance of PMBLDC motor drive for both vector and scalar control. Here only the speed characteristic is depicted.

The motor parameters of damping constant, stator resistance per phase, self-inductance, and mutual inductance are changed 25% (both for increasing and decreasing) from its rated value (as shown in Table 1). But there is no effect on the performance of PMBLDC motor drive for both vector and scalar control. After the change of every PMBLDC motor parameters at time 1.5 second, similar speed characteristics are found as shown in Fig. 3.16.

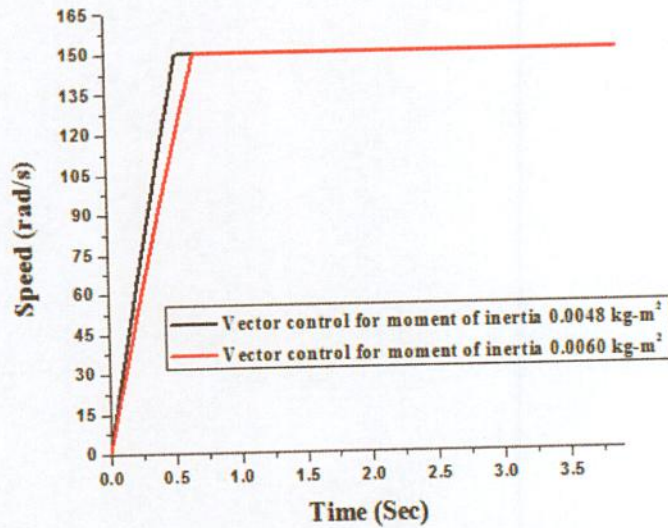


Fig. 3.15: Starting characteristics of PMBLDC motor drives for vector control with moment of inertia at 0.0048 kg-m² (rated value) and 0.006 kg-m² (125% of rated value)

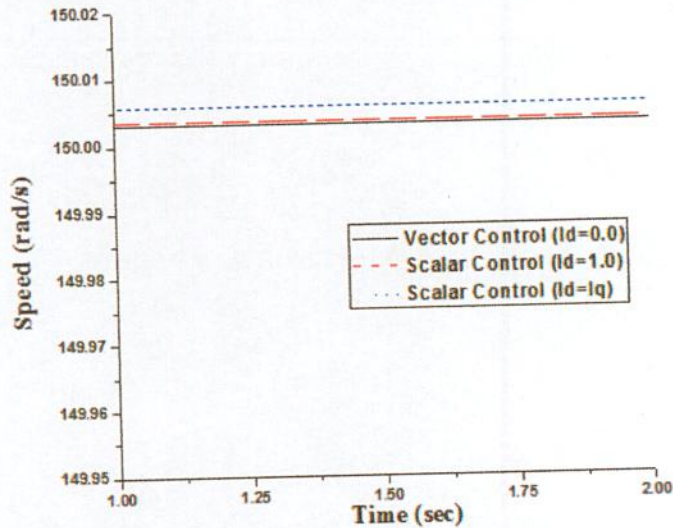


Fig. 3.16: Speed characteristics of PMBLDC motor drives for increasing 25% of its moment of inertia from the motor rated moment of inertia 0.0048 kg-m² at 1.5 second both for field oriented vector and scalar control

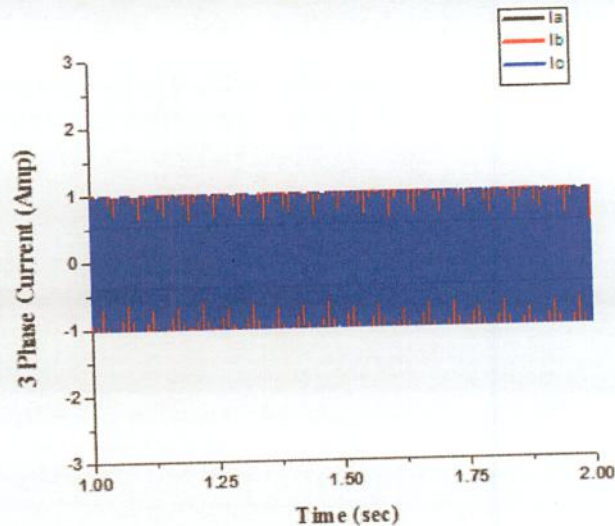


Fig. 3.17: 3-phase stator current of vector controlled PMLDLC motor drives for increasing 25% of motor moment of inertia from the rated value 0.0048 kg-m^2

3.6 Conclusion

An adaptive PI speed controller based vector controlled current fed delta modulated PMLDLC motor drives is designed in this chapter. This section mainly represents the comparison between vector i.e. field oriented control ($i_d=0.0$) of PMLDLC motor drives and scalar controlled PMLDLC motor drives. In scalar controlled drives, two cases of $i_d=1.0$ and $i_d=i_q$ are analyzed. By considering starting, dynamic speed and load torque changing characteristics, it is clear that, the performance of vector control PMLDLC drive is superior to scalar control. Vector control is suitable to gain rated speed as fast as possible than scalar control. PMLDLC motor takes less current at stable condition for vector control than scalar control. Keeping maximum rated current of the PMLDLC motor constant, the performance of scalar controlled drives degrades with the increase of the value i_d . Load torque handling capacity of scalar controlled PMLDLC motor drive is very poor than vector controlled drive. Load torque handling capacity of scalar controlled PMLDLC motor drives decreases with increasing the value of i_d in scalar control drives. Both the transient and steady state characteristics of vector control current fed PMLDLC motor drive are outstanding. Performance of the field oriented vector controlled and scalar controlled PMLDLC motor drives are tested due to the change of PMLDLC motor parameters. There is no effect of 25% increase or decrease of motor inertia on the performance of PMLDLC motor drive for both vector and scalar control. The motor parameters of damping constant, stator resistance per phase, self-inductance, and mutual inductance are changed 25% (both for increasing and decreasing) from its rated value. But there is also no effect on the performance of PMLDLC motor drive for both vector and scalar control.

Chapter IV

Novel Approach to Enhance Torque Handling Capacity of PMBLDC Motor Drives

Chapter Outlines:

4.1 Introduction

4.2 Approach to Enhance Torque Handling Capacity

4.3 Proposed Control Scheme

4.4 Simulation Results and Discussion

4.5 Conclusion

4.1 Introduction

Permanent Magnet Brushless DC (PMLDLC) Motors are trapezoidal shaped back EMF permanent magnet AC machine with high power density. Since the motor has a trapezoidal field pattern rather than sinusoidal it is desirable to study the motor behavior under different current fed conditions to analyze the developed electromagnetic torque. In this chapter three different trapezoidal, square and sinusoidal current fed field oriented vector controlled PMLDLC motor drives are presented. The novel approach of this part is that, the torque handling capacity of a PMLDLC motor can be increased up to its rated torque by only changing the pattern of reference current of a field oriented vector controlled PMLDLC motor drive. Torque handling capacity has to be enhanced without exceeding the maximum current rating of the PMLDLC motor.

In this section, field oriented control of a PMLDLC motor with three different current fed drives are presented. This part shows how the torque handling capacity of a PMLDLC motor can be increased up to its rated torque by only changing the reference current of PWM modulator. Conventionally square and sinusoidal current fed PMLDLC motor drives are implemented. In this chapter novel trapezoidal current fed drive is proposed because of the trapezoidal shaped back EMF of PMLDLC motor. The scenario of torque pulsation is also depicted individually for these three different current drives. A hysteresis type current controller is proposed and implemented to maintain the actual current flowing into the motor as close as possible to the reference current. The drive system is simulated in a C++ platform in discrete form. Transient response, loading capability of the motor and dynamic system performance of PMLDLC motor are studied for these three different current fed drives.

4.2 Approach to Enhance Torque Handling Capacity

Generally per phase torque is proportional to the product of per phase back EMF and corresponding per phase current. From Fig. 4.1, it is seen that, for square wave current fed drive of phase 'a', for rotor position 0° - 30° , the developed electromagnetic torque in phase 'a' is zero because phase current i_{as} at that time is zero. So the distributed flux at that time (0° - 30°) is unutilized for torque production. At that time same positive electromagnetic torque are developed in phase 'b' and in phase 'c' considering balanced phase system. For rotor position 30° - 60° , the developed electromagnetic torque in phase 'c' is zero and there are same positive developed torque in phase 'a' and in phase 'b'. Similarly for the shaded region in Fig. 4.1, the motor cannot developed any torque. Theoretically this 120° switch on mode is used to generate constant instantaneous total torque by considering the torque developed in each phase.

Now considering trapezoidal back EMF and trapezoidal reference current waveforms of 3-phase trapezoidal current fed drives as shown in Fig. 4.3. For rotor position 0° - 30° , there is a positive developed electromagnetic torque in phase 'a' because phase current i_{as} at that time is not zero. Similar to the square wave current fed drive, at that time same positive electromagnetic torque are developed in phase 'b' and in phase 'c'. So additional torque is found from phase 'a' which contributes to the total developed torque at the rotor position 0° - 30° for trapezoidal current fed drives. But this additional torque is not generated for square current fed drive. So trapezoidal

current fed drive can utilize the flux of that portion of shaded region in Fig. 4.1. Thus torque handling capacity for trapezoidal current fed drive is greater than the square current fed drive. From Fig. 4.3, it is seen that for 0° - 30° , instantaneous total developed torque is gradually increasing from 0° to 30° , but from 30° to 60° instantaneous total developed torque is decreasing at the same rate of increasing from 0° to 30° . This scenario is same for other rotor position spans in Fig. 4.3. So for trapezoidal current fed drive the instantaneous total developed torque is not constant, but the average torque is constant.

From the inspection of Fig. 4.2, it can be understood that, the shaded area i.e. the amount of unutilized flux of sinusoidal current fed drive for torque generation is little bit greater than the amount of unutilized flux of square current fed drive. That is the torque handling capacity of sinusoidal current fed drive is less than the torque handling capacity of square current fed drive. So trapezoidal current fed drive is superior on the respect of torque generation. Besides torque handling capacity is increased without exceeds the maximum current rating of the PMBLDC motor. From Fig. 4.1-4.3, it is seen that, for three different current system the maximum value of current is maintained constant value I_{max} . A current limiter is used with adaptive PI speed controller for the purpose to limit the current to the rated value.

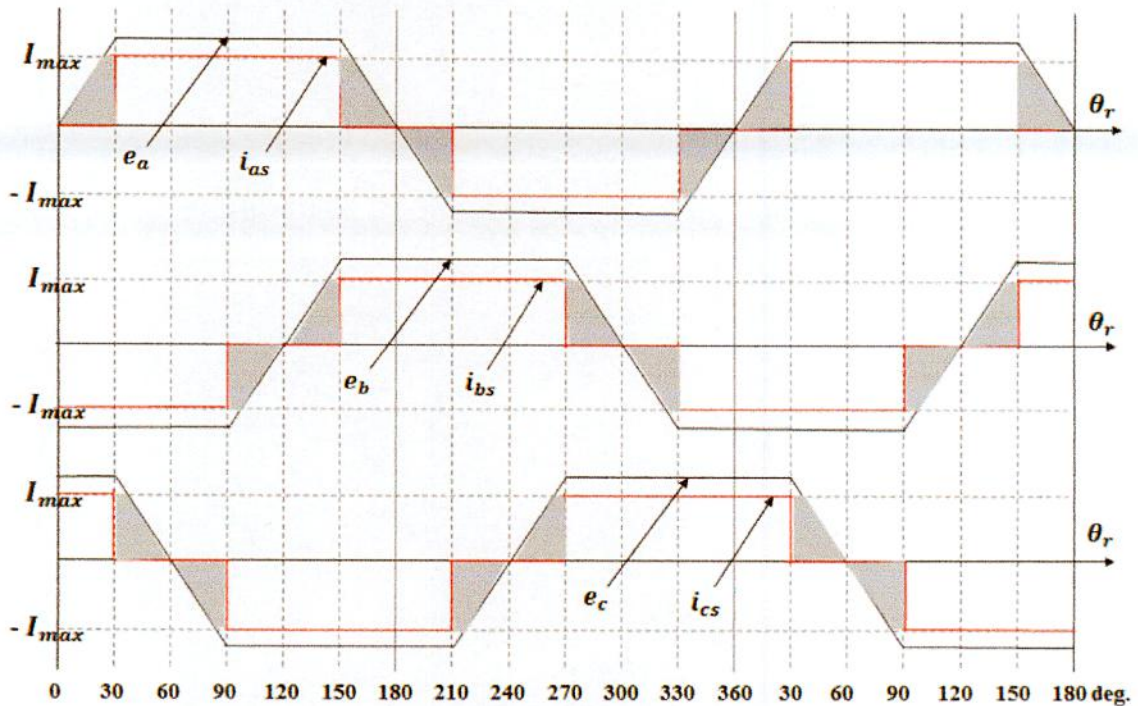


Fig. 4.1: Typical trapezoidal back EMF and square current waveforms of 3-phase PMBLDC motor

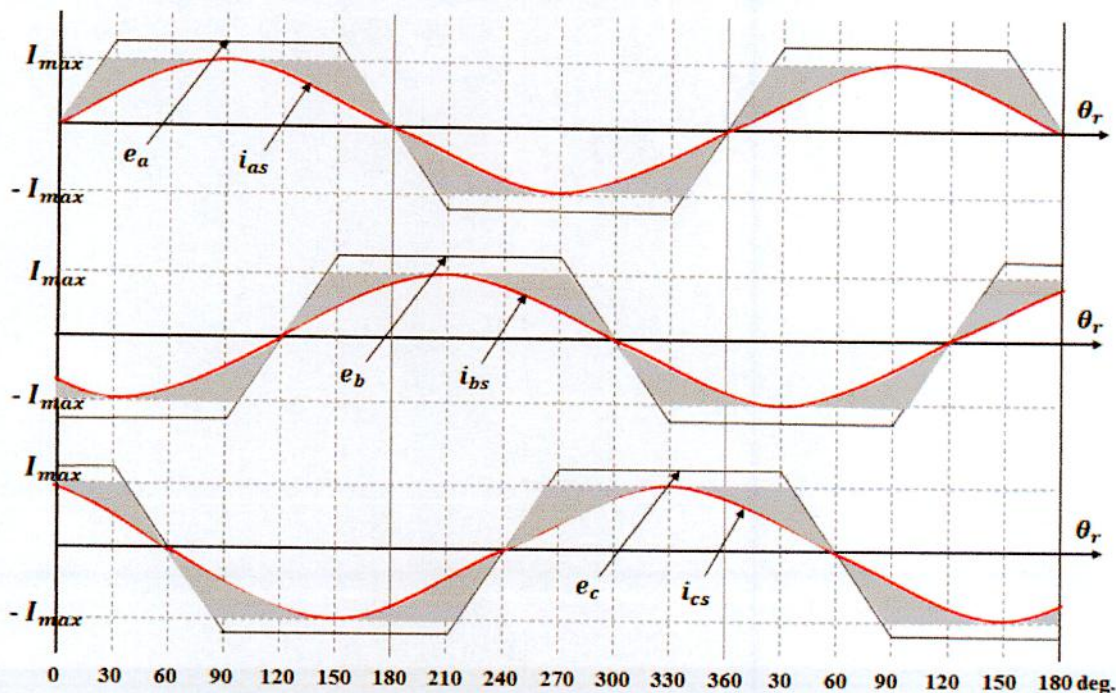


Fig. 4.2: Typical trapezoidal back EMF and sinusoidal current waveforms of 3-phase PMBLDC motor

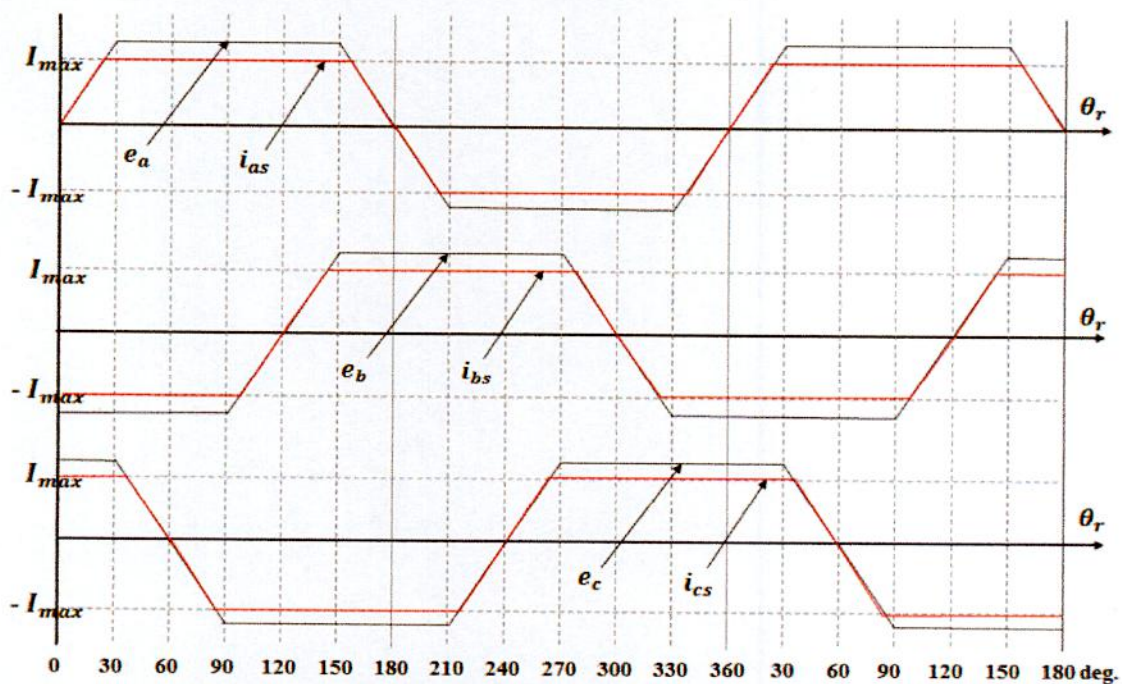


Fig. 4.3: Typical trapezoidal back EMF and trapezoidal current waveforms of 3-phase PMBLDC motor

4.3 Proposed Control Scheme

The proposed control drive mainly consists of an adaptive PI controller, field oriented reference current generator, delta modulated PWM current controller, IGBT voltage source inverter, position sensor, current sensors and PMBLDC motor as shown in block diagram in Fig. 4.4. Field oriented controlled three different trapezoidal, square and sinusoidal reference current fed drives for PMBLDC motor control is proposed in this chapter to see the scenario of torque handling capacity of these three different reference current drives. The performance of vector controlled trapezoidal current fed drive is compared with traditional square current and sinusoidal current fed vector controlled drive. Design of adaptive PI controller, delta modulated PWM current controller and current limiter has been discussed in Chapter III.

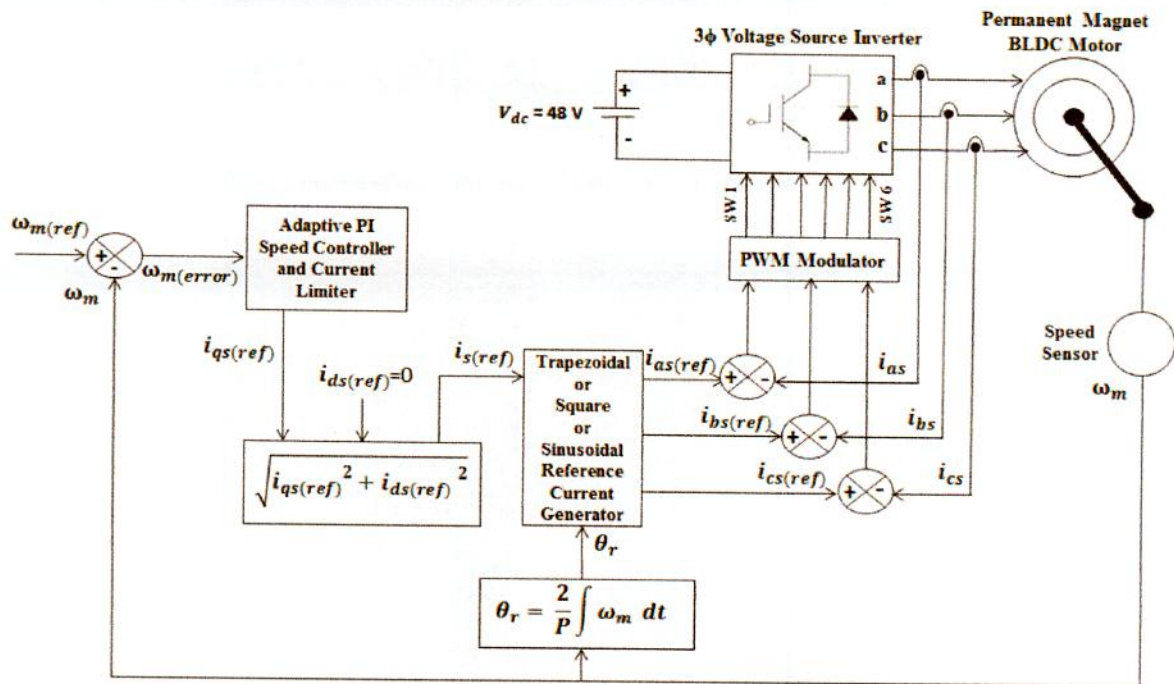


Fig. 4.4: Overall block diagram of trapezoidal or square or sinusoidal current fed field oriented vector controlled PMBLDC motor drives by using adaptive PI speed controller

4.3.1 Field Oriented Control of PMBLDC Motor Drive

In this proposed control system, maximum value of reference current $i_s(ref)$ is generated by considering direct axis current $i_{ds}(ref) = 0$ and by calculated the value of quadrature axis current $i_{qs}(ref)$ according to the requested load torque through the adaptive PI controller and current limiter. The field oriented control system requires the synchronous d axis current of stator coils forced to zero. Thus the peak of reference current $i_s(ref)$ is given by Eq. (4.1).

$$i_{s(ref)} = \sqrt{i_{qs(ref)}^2 + i_{ds(ref)}^2} \quad (4.1)$$

The reference current of each phase $i_{as(ref)}$, $i_{bs(ref)}$, $i_{cs(ref)}$ are function of rotor position θ_r . These reference currents are fed to the hysteresis band PWM current controller.

First consider the trapezoidal current fed field oriented controlled drive. By using the value of peak reference current $i_{s(ref)}$, three phase trapezoidal reference current $i_{as(ref)}$, $i_{bs(ref)}$ and $i_{cs(ref)}$ are generated as a function of rotor position θ_r . Three phase trapezoidal reference current function $i_{as(ref)}(\theta_r)$, $i_{bs(ref)}(\theta_r)$, and $i_{cs(ref)}(\theta_r)$, are described in Eq. (4.2-4.4).

$$i_{as(ref)}(\theta_r) = \begin{cases} i_{s(ref)} * \theta_r * \frac{6}{\pi}, & 0 \leq \theta_r < \frac{\pi}{6} \\ i_{s(ref)}, & \frac{\pi}{6} \leq \theta_r < \frac{5\pi}{6} \\ i_{s(ref)} * (\pi - \theta_r) * \frac{6}{\pi}, & \frac{5\pi}{6} \leq \theta_r < \frac{7\pi}{6} \\ -i_{s(ref)}, & \frac{7\pi}{6} \leq \theta_r < \frac{11\pi}{6} \\ i_{s(ref)} * (\theta_r - 2\pi) * \frac{6}{\pi}, & \frac{11\pi}{6} \leq \theta_r < 2\pi \end{cases} \quad (4.2)$$

$$i_{bs(ref)}(\theta_r) = \begin{cases} -i_{s(ref)}, & 0 \leq \theta_r < \frac{\pi}{2} \\ i_{s(ref)} * \left(-\frac{2\pi}{3} + \theta_r\right) \frac{6}{\pi}, & \frac{\pi}{2} \leq \theta_r < \frac{5\pi}{6} \\ i_{s(ref)}, & \frac{5\pi}{6} \leq \theta_r < \frac{3\pi}{2} \\ i_{s(ref)} * \left(-\frac{5\pi}{3} + \theta_r\right) \frac{6}{\pi}, & \frac{3\pi}{2} \leq \theta_r < \frac{11\pi}{6} \\ -i_{s(ref)}, & \frac{11\pi}{6} \leq \theta_r < 2\pi \end{cases} \quad (4.3)$$

$$i_{cs(ref)}(\theta_r) = \begin{cases} i_{s(ref)}, & 0 \leq \theta_r < \frac{\pi}{6} \\ i_{s(ref)} * \left(\frac{\pi}{3} - \theta_r\right) \frac{6}{\pi}, & \frac{\pi}{6} \leq \theta_r < \frac{\pi}{2} \\ -i_{s(ref)}, & \frac{\pi}{2} \leq \theta_r < \frac{7\pi}{2} \\ i_{s(ref)} * \left(-\frac{4\pi}{3} + \theta_r\right) \frac{6}{\pi}, & \frac{7\pi}{2} \leq \theta_r < \frac{3\pi}{2} \\ i_{s(ref)}, & \frac{3\pi}{2} \leq \theta_r < 2\pi \end{cases} \quad (4.4)$$

Now three phase square wave reference current $i_{as(ref)}$, $i_{bs(ref)}$, $i_{cs(ref)}$ are generated corresponding to the rotor position according to the Table 4.1 for square current fed field oriented controlled PMSM motor drive. Finally three phase sinusoidal reference current $i_{as(ref)}$, $i_{bs(ref)}$, $i_{cs(ref)}$ are generated according to Eq. (4.5-4.7) as a function of rotor position.

$$i_{as(ref)} = i_s(ref) * \sin(\theta_r) \quad (4.5)$$

$$i_{bs(ref)} = i_s(ref) * \sin\left(\theta_r - \frac{2\pi}{3}\right) \quad (4.6)$$

$$i_{cs(ref)} = i_s(ref) * \sin\left(\theta_r + \frac{2\pi}{3}\right) \quad (4.7)$$

Table 4.1: 3-phase square wave reference current corresponding to rotor position

Rotor Position θ_r	$i_{as(ref)}(\theta_r)$	$i_{bs(ref)}(\theta_r)$	$i_{cs(ref)}(\theta_r)$
$0 \leq \theta_r < \frac{\pi}{6}$	0	$-i_s(ref)$	$i_s(ref)$
$\frac{\pi}{6} \leq \theta_r < \frac{3\pi}{6}$	$i_s(ref)$	$-i_s(ref)$	0
$\frac{3\pi}{6} \leq \theta_r < \frac{5\pi}{6}$	$i_s(ref)$	0	$-i_s(ref)$
$\frac{5\pi}{6} \leq \theta_r < \frac{7\pi}{6}$	0	$i_s(ref)$	$-i_s(ref)$
$\frac{7\pi}{6} \leq \theta_r < \frac{9\pi}{6}$	$-i_s(ref)$	$i_s(ref)$	0
$\frac{9\pi}{6} \leq \theta_r < \frac{11\pi}{6}$	$-i_s(ref)$	0	$i_s(ref)$
$\frac{11\pi}{6} \leq \theta_r < 2\pi$	0	$-i_s(ref)$	$i_s(ref)$

4.4 Simulation Results and Discussion

The drive system was simulated in a digital computer with software written in C++ environment. The specifications of the simulated PMBLDC motor are described in Appendix. The sampling time used for this simulation is 0.0000025 second.

4.4.1 Starting Characteristics

The PMBLDC motor starts with an initial load torque 0.4 Nm. Starting speed characteristics i.e. time taken by the motor to reach its rated speed (150 rad/s) with its initial torque (0.4 Nm) for trapezoidal, square and sinusoidal reference current fed field oriented controlled PMBLDC motor drives is shown in Fig. 4.5. From Fig. 4.5, it is seen that, PMBLDC vector controlled trapezoidal, square and sinusoidal current fed drives take 0.39, 0.48 and 0.55 seconds respectively to gain rated speed. So trapezoidal current fed field oriented control drive is suitable to gain rated speed as fast as possible. Trapezoidal reference current fed drive takes minimum time to reach its rated speed than square and sinusoidal reference current fed drives, because the torque handling capacity of trapezoidal reference current fed PMBLDC motor drive is greater than the other two reference current fed PMBLDC motor drives.

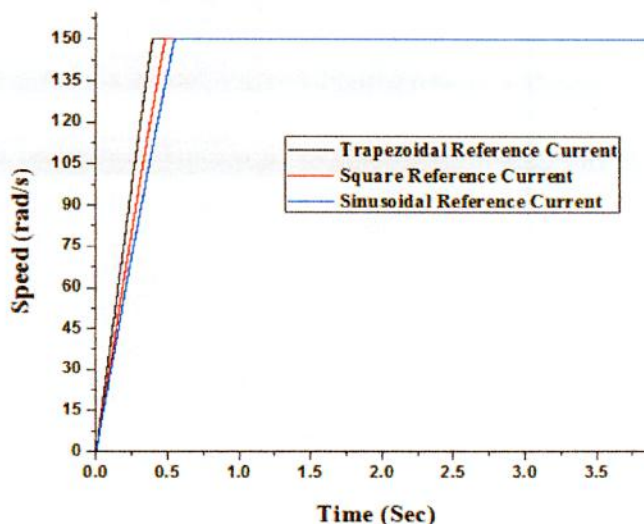
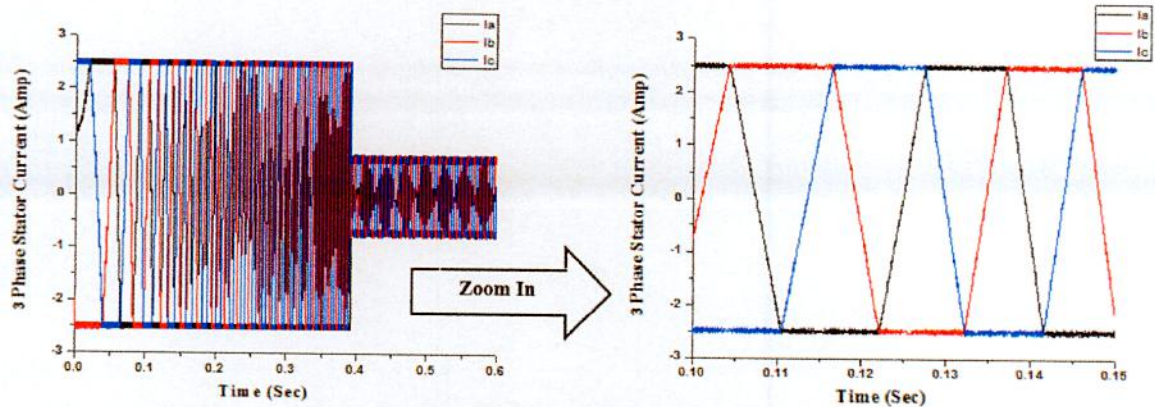
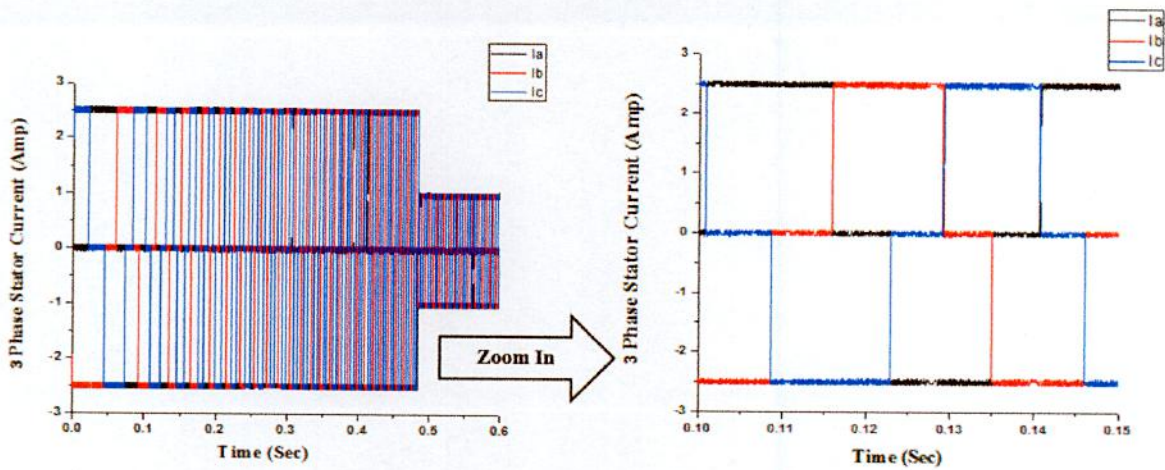


Fig. 4.5: Starting characteristics of PMBLDC motor drives for trapezoidal, square and sinusoidal reference current fed field oriented control

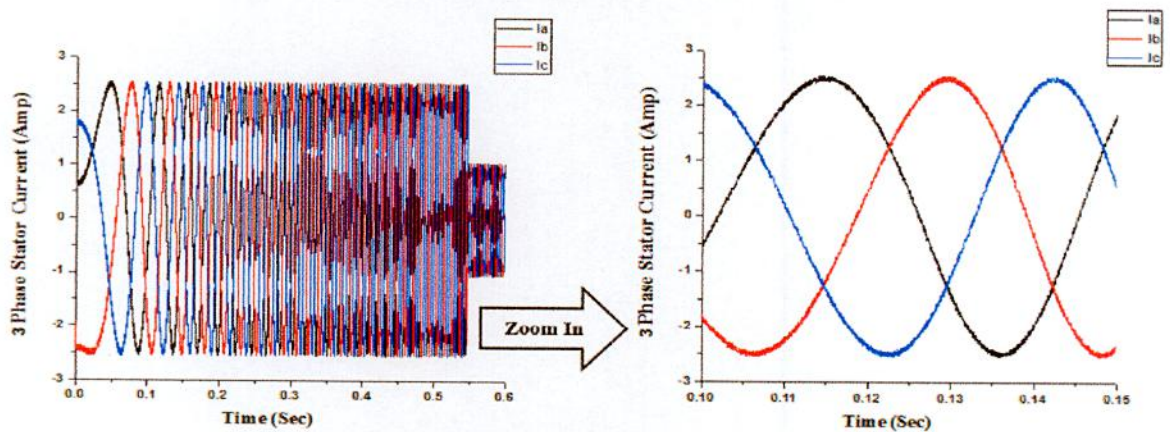
Phase currents of PMBLDC motor at the time of starting for vector controlled trapezoidal, square and sinusoidal current fed drives are depicted in Fig. 4.6. It shows that the amplitude of 3-phase current is 2.5 Amp (rated current of the motor) at the transient time of starting for these three control drives. Started current is limited through the current limiter block as shown in Fig. 4.4. Fig. 4.6 also describes that after gaining rated speed i.e. at steady state motor takes maximum 0.75 Amp current for trapezoidal current fed, maximum 1.0 Amp current for square current fed and maximum 1.12 Amp current for sinusoidal current fed drives for initial torque 0.4 Nm. So that PMBLDC motor takes less current at stable condition for trapezoidal current fed drive than square and sinusoidal drives due to the capability of more load torque handling capacity.



(a) For trapezoidal current fed field oriented control drive



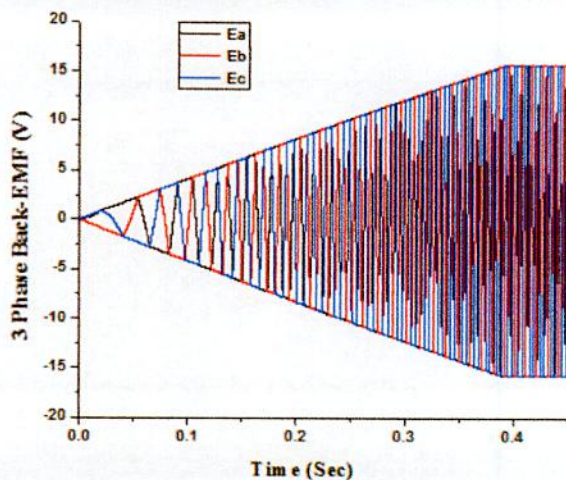
(b) For square current fed field oriented control drive



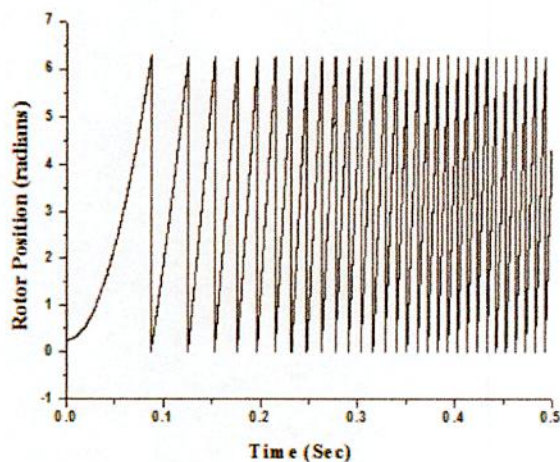
(c) For sinusoidal current fed field oriented control drive

Fig. 4.6: 3-Phase starting stator current of PMBLDC motor for trapezoidal, square and sinusoidal current fed field oriented control drive

3-phase back EMF, rotor position curve at the time of starting for vector controlled trapezoidal reference current fed PMSM drive is shown in Fig. 4.7 as for example. Now the back EMF and corresponding phase current of trapezoidal, square and sinusoidal current fed field oriented control drives for steady state condition of these drives are pictured in Fig. 4.8.

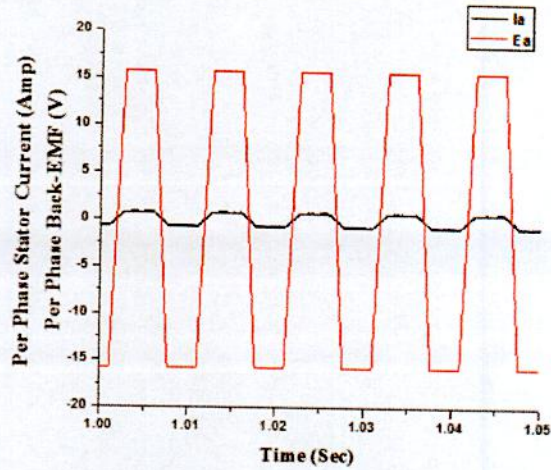


(a)

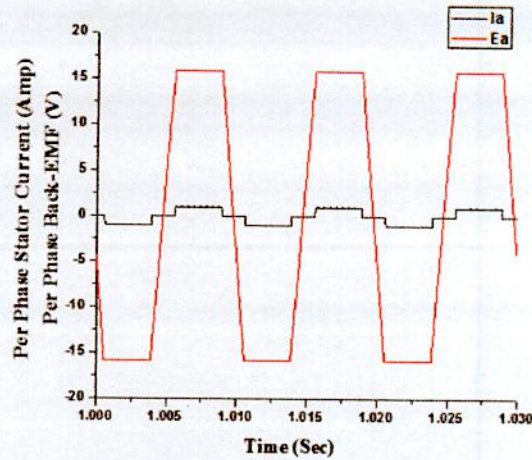


(b)

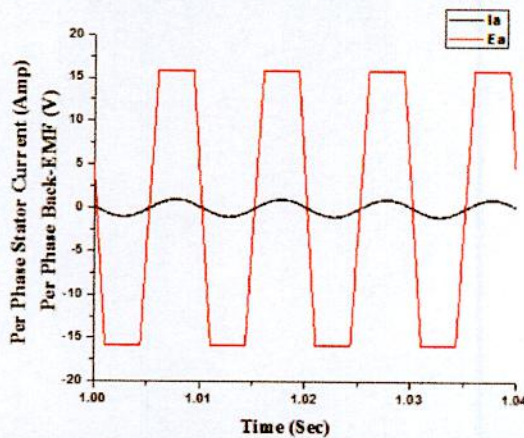
Fig. 4.7: (a) 3-phase back EMF at starting and (b) rotor position of trapezoidal current fed field oriented controlled PMSM motor drive



(a) For trapezoidal current fed PMSM motor drive



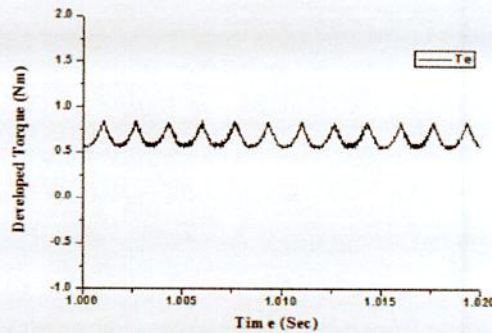
(b) For square current fed PMSM motor drive



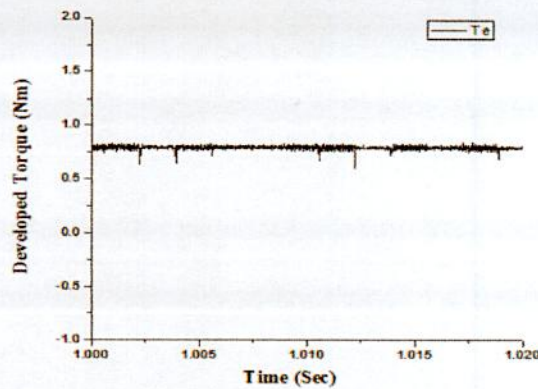
(c) For sinusoidal current fed PMSM motor drive

Fig. 4.8: Per phase back EMF and corresponding phase current for Trapezoidal, Square and Sinusoidal current fed field oriented control drives

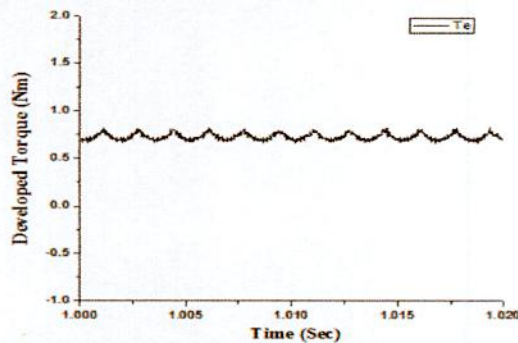
Fig. 4.9 depicts developed electromagnetic torque in PMBLDC motor for trapezoidal, square and sinusoidal current fed field oriented controlled drives. It mainly describes the torque pulsation status for three different current fed drives. Periodic small scale torque pulsation can be seen for trapezoidal and sinusoidal current fed drives. So the average torque for both trapezoidal and sinusoidal current fed drives is nearly constant. The range of torque pulsation for sinusoidal system is smaller than trapezoidal system. Though the torque pulsation for square current fed drive is very small but there exists aperiodic torque ripple.



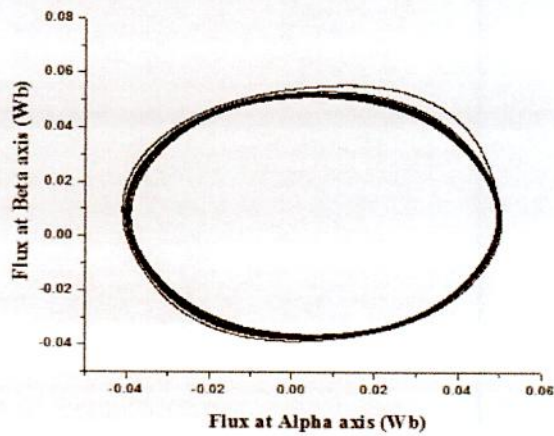
(a) Developed electromagnetic torque of trapezoidal current fed field oriented control drive



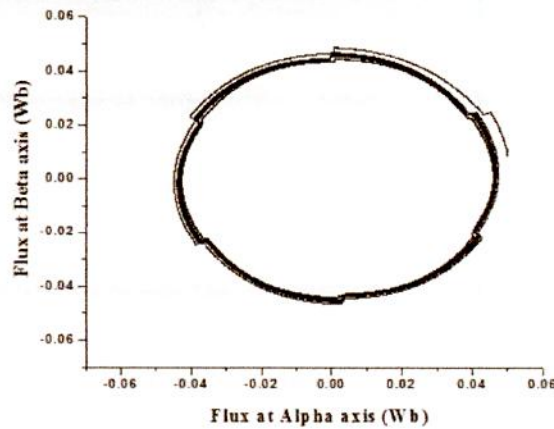
(b) Developed electromagnetic torque of square current fed field oriented control drive



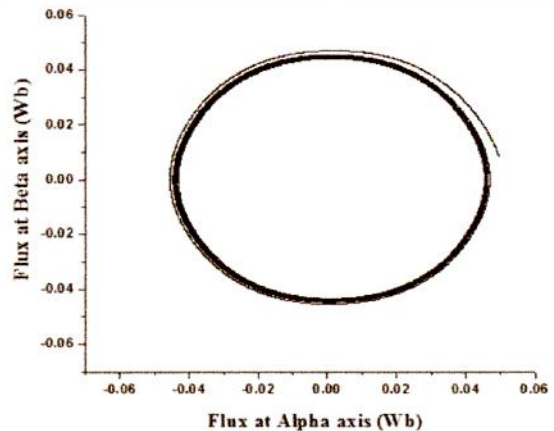
(c) Developed electromagnetic torque of sinusoidal current fed field oriented control drive
 Fig. 4.9: Torque developed for Trapezoidal, Square and Sinusoidal current fed field oriented controlled drives



(a) For trapezoidal current fed field oriented control



(b) For square current fed field oriented control



(c) For sinusoidal current fed field oriented control

Fig. 4.10: Stator flux linkage trajectories in the stationary $\alpha\beta$ axes reference frame for trapezoidal, square and sinusoidal current fed vector controlled PMLDC motor drives

In Fig. 4.10, stator flux linkage trajectories i.e. flux orientation representation in the stationary $\alpha\beta$ axes reference frame for trapezoidal, square and sinusoidal current fed vector controlled PMBLDC motor drives are pictured.

4.4.2 Variable Speed Characteristics

To measure the dynamic performance for three different current fed vector controlled PMBLDC motor drives, variable speed command is given. Motor runs at speed 100 rad/s. At 1.0 second the speed command is changed to 75 rad/s and finally at 1.5 second speed command is changed to 150 rad/s. At that time, the given load torque is 0.4 Nm. From Fig. 4.11, motor speed follows the reference speed sharply for trapezoidal current fed vector controlled PMBLDC motor drive than the square and sinusoidal current fed drives. For sinusoidal reference current fed drive, there is noticeable difference between reference speed and actual motor speed.

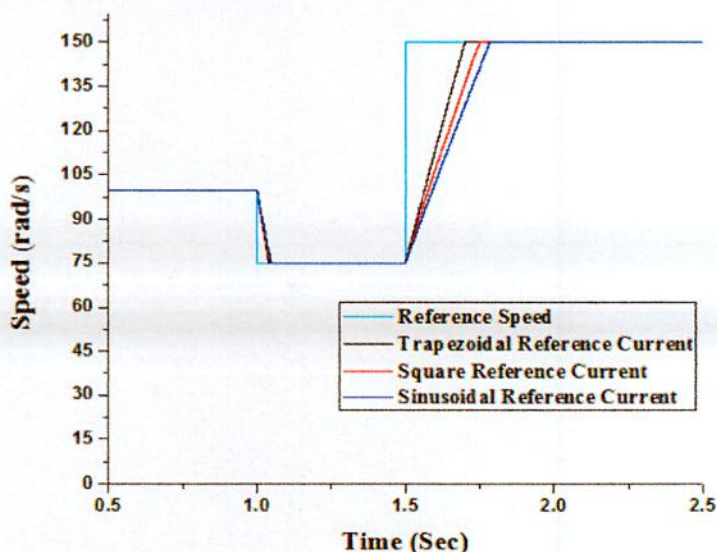
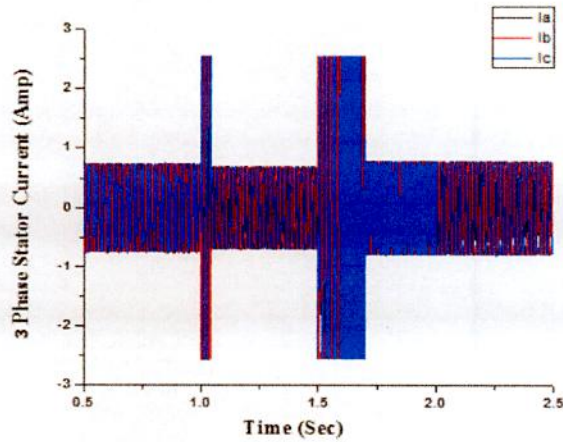
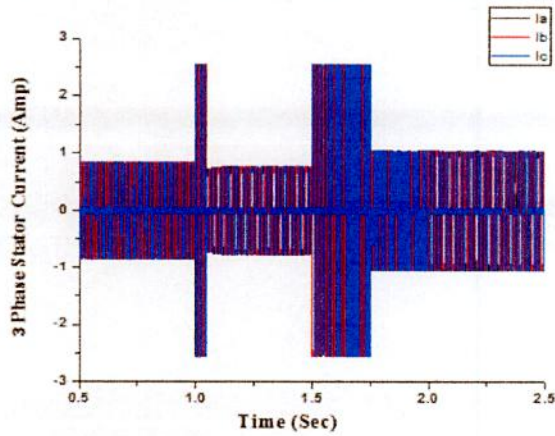


Fig. 4.11: Comparison between speed responses of PMBLDC motor for trapezoidal, square and sinusoidal current fed vector controlled drives at dynamic speed changing condition

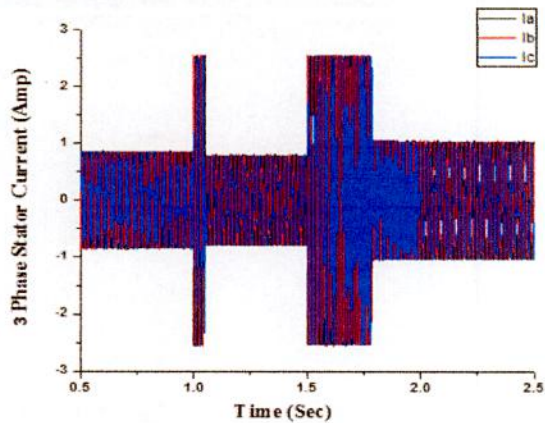
From 3-phase current curve for variable speed condition for three different current fed system as shown in Fig. 4.12, it is seen that, at 1.0 second when the reference speed changes from 100 rad/s to 75 rad/s, there exists no high value of transient current beyond the limit of rated current (2.5 Amp) and no undershoot from reference speed for these three different current fed drives. Besides there is no overshoot at 1.5 second, when the reference speed goes to 150 rad/s from 75 rad/s. Condition of back EMF at the time of variable speed for trapezoidal current fed drive is shown in Fig. 4.13.



(a) For trapezoidal current fed field oriented control



(b) For square wave current fed field oriented control



(c) For sinusoidal current fed field oriented control

Fig. 4.12: 3-phase current of PMBLDC motor for trapezoidal, square and sinusoidal current fed field oriented controlled drive for variable speed condition considering transient current at the interface of speed changes

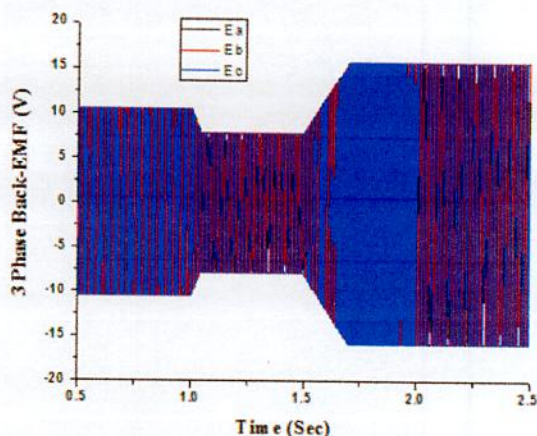


Fig. 4.13: 3-phase back EMF at dynamic speed changing condition for trapezoidal current fed vector controlled PMBLDC motor drive

4.4.3 Motor Characteristics due to Load Torque Change

Now performance of PMBLDC motor vector controlled drives are determined under the condition of load torque change. At first motor runs at 150 rad/s rated speed with initial load torque 0.4 Nm. At time 1.0 second motor is loaded with its rated load torque 2.0 Nm. At that condition only trapezoidal current fed drive can sustain motor speed to its rated value 150 rad/s. But square and sinusoidal current fed drives cannot sustain its previous speed as shown in Fig. 4.14. The speed of square and sinusoidal current fed vector controlled drives are gradually decreased after the loading of the motor. It verifies that the load torque handling capacity of square and sinusoidal current fed vector controlled PMBLDC motor drives is very poor than trapezoidal current fed vector controlled drive.

In Fig. 4.14, the rate of gradually fall down of speed of sinusoidal current fed drive (To limit current in rated value 2.5 Amp) is higher than the rate of square wave current fed drive. Maximum load torque have to be given to the vector controlled PMBLDC motor without hampering the drive stability for square and sinusoidal current fed drives are 1.60 Nm and 1.55 Nm respectively. I.e. when square current fed drive is used to control the specified PMBLDC motor (From Appendix), the maximum torque generating capacity is 1.60 Nm. For sinusoidal current drive, it is 1.55 Nm. Beyond these torque limit the motor cannot sustain its steady state characteristics.

From graphical representation of 3-phase stator current for sudden load torque change of trapezoidal current fed drive as shown in Fig. 4.15, it summaries that, at stable reference speed stator current decreases to 0.75 Amp. But when the rated load torque is applied, the stator current is about its rated value (2.5 Amp).

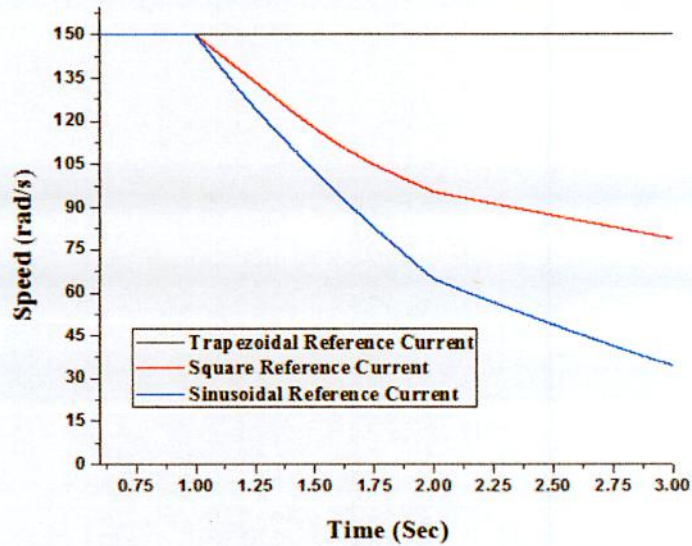


Fig. 4.14: Speed characteristics of PMBLDC motor for sudden load torque change at 1.0 second from initial load torque 0.4 Nm to rated load torque 2.0 Nm for trapezoidal, square and sinusoidal current fed field oriented control drives

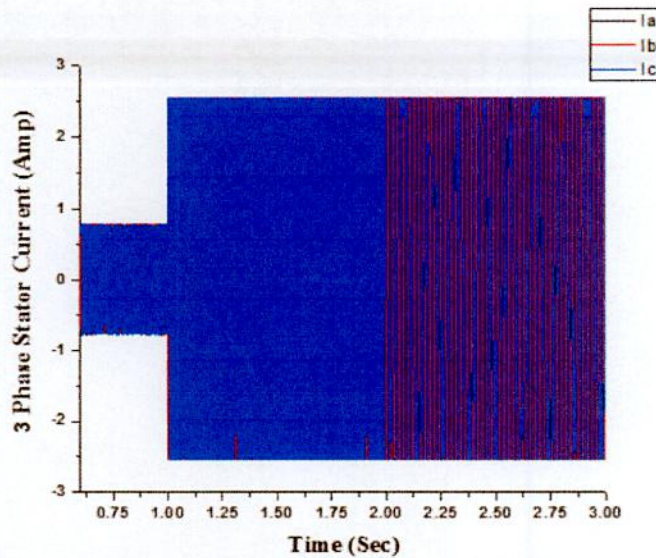


Fig. 4.15: 3-phase stator current of trapezoidal current fed field oriented controlled PMBLDC motor drives for sudden load torque change at 1.0 second

4.5 Conclusion

A novel approach to enhance the torque handling capacity of a PMBLDC motor without exceeding the rated current of the motor is proposed in this chapter. An adaptive PI speed controller based vector controlled three different trapezoidal, square and sinusoidal reference current fed delta modulated PMBLDC motor drives are designed. This chapter mainly presents how to increase the load torque handling capacity of vector controlled PMBLDC motor drives only by changing the reference current of a current fed delta modulated inverter. Individually trapezoidal, square and sinusoidal reference current fed vector controlled PMBLDC motor drives are implemented and compared among them. Trapezoidal reference current fed drive takes minimum time to reach its rated speed than square and sinusoidal reference current fed drives. PMBLDC motor takes less current at stable condition for trapezoidal current fed drive than square and sinusoidal drives due to the capability of more load torque handling capacity. There exists no high value of transient current beyond the limit of rated current (2.5 Amp) and no undershoot or overshoot from reference speed for these three different current fed drives during dynamic speed and load torque changing interfaces.

It is seen from the results that, only by using trapezoidal reference current fed drive instead of sinusoidal current fed drive, the load torque handling capacity can be increased from 1.55 Nm to 2.0 Nm. Load torque handling capacity of square current fed PMBLDC motor drive (1.60 Nm) is higher than the sinusoidal current fed drive (1.55 Nm). Novelty of the proposed trapezoidal current fed field oriented control drive is that, torque handling capacity of a PMBLDC motor can be increased up to 25% from the conventional 120° conduction square wave current fed drive by only changing the pattern of reference current. By considering starting, dynamic speed and load torque changing characteristics, it is clear that, the performance of trapezoidal current fed vector controlled drive is superior to the square and sinusoidal vector controlled drives. Torque pulsation is to be considered, which is in acceptable limit. For trapezoidal current fed drive, the developed electromagnetic torque is periodic in nature and has constant average value. Both the transient and steady state characteristics of trapezoidal current fed vector controlled PMBLDC motor drive are superior.

Chapter V

Field Oriented Control of PMBLDC Motor without Position Sensor

Chapter Outlines:

5.1 Introduction

5.2 Field Oriented Control Drive without Position Sensor

5.3 Flux Estimation Algorithm

5.4 Rotor Position Estimation

5.5 PMBLDC Motor Speed Estimation

5.6 Simulation Results and Discussion

5.7 Conclusion

5.1 Introduction

For desired operation of a PMBLDC motor, accurate rotor position information is needed. Conventionally, it is obtained by the position sensors embedded in the motor. In order to obtain an accurate and ripple free instantaneous torque from PMBLDC motor, the rotor position information is used for stator current commutation.

Normally, position sensors such as Hall-effect sensors or optical encoder are employed to provide rotor position information for commutation. But misalignments in position sensors, running in extreme ambient conditions, or electromagnetic interference introduce error in the position information. Moreover, there are some constraints to the position sensors including high cost, installation difficulty of mechanics, and poor reliability. Therefore, the development of the PMBLDC motor sensorless operation has been a hot issue in recent years.

In this section, field oriented control of a current fed PMBLDC motor drive without rotor position or speed sensors is presented. Instead of using rotor position or speed sensor, two novel algorithms will be proposed in this chapter to estimate the rotor position and speed to perform the operation of position sensorless field oriented vector control of PMBLDC motor. For algorithm 1 both rotor position and speed of the motor is determined from the estimated flux linkage. For algorithm 2 only rotor position of the PMBLDC motor is determined from the estimated flux and the speed of the motor is detected by the estimated developed electromagnetic torque and power equation.

The performances of algorithm 1 based sensorless field oriented vector controlled PMBLDC motor drive are compared with the algorithm 2 based sensorless drive under different transient and steady state conditions. The performance of these two different position sensorless field oriented vector controlled PMBLDC motor drives are also verified by comparing with the performance of sensed field oriented vector controlled PMBLDC motor drive as discussed in chapter III.

5.2 Field Oriented Control Drive without Position Sensor

Sensorless field oriented current fed PMBLDC motor drive is proposed here. Sensorless means that, rotor position encoder or speed sensors are absent in these proposed system. No Hall sensors or optical encoders are used to detect the rotor position for the purpose of stator current commutation. The proposed control drives consists of an adaptive PI controller, field oriented reference current generator, delta modulated PWM current controller, IGBT voltage source inverter, current sensors and PMBLDC motor as shown in Fig. 5.1 and Fig. 5.2. These parts of control drive are also used in the field oriented vector controlled PMBLDC motor drive with position sensor as discussed in chapter III (Fig. 3.5). Main difference is that, position sensor is absent in proposed control drives as shown in Fig. 5.1 and Fig. 5.2.

In this section, two different algorithms are used to estimate rotor position and speed of the motor, instead of using position sensors. Algorithm 1 is proposed for sensorless operation of field oriented vector controlled PMBLDC motor drive as shown in Fig. 5.1. In Fig. 5.2, Algorithm 2 is proposed for sensorless operation of field oriented vector controlled PMBLDC motor drive.

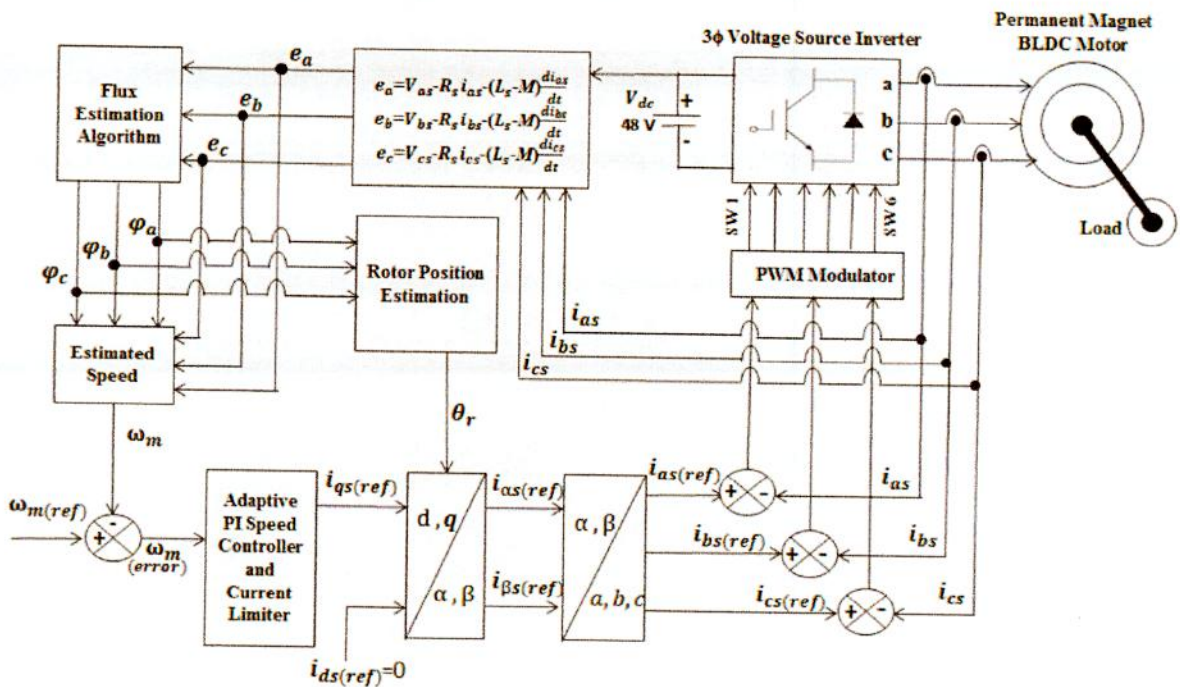


Fig. 5.1: Block diagram of field oriented vector controlled PMBLDC motor drive without rotor position or speed sensor (Algorithm 1)

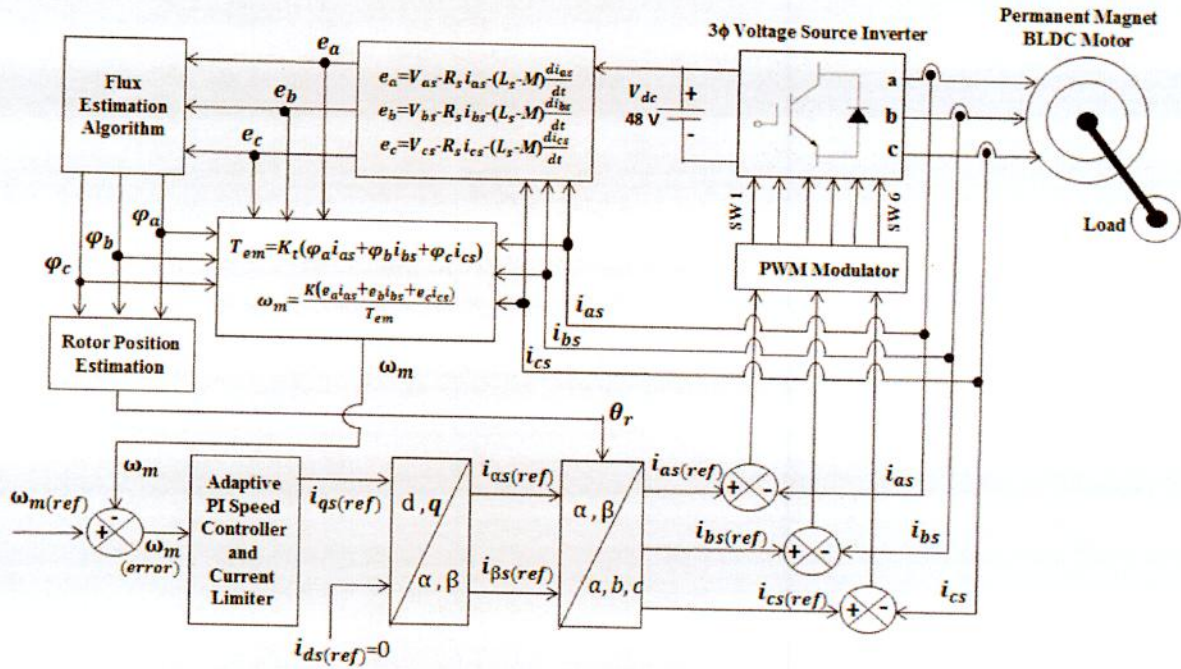


Fig. 5.2: Block diagram of field oriented controlled PMSBLDC motor drive without rotor position or speed sensor (Algorithm 2)

5.3 Flux Estimation Algorithm

A novel flux estimation algorithm is proposed in this section. Same flux estimation algorithm block is used both in Fig. 5.1 and Fig. 5.2. i.e. same novel flux estimation algorithm is used for both algorithm 1 and algorithm 2 based sensorless operation of field oriented current fed PMSBLDC motor drives. Three phase back EMF e_a , e_b , e_c have to be calculated for the flux estimation algorithm by using Eq. (5.1-5.3).

$$e_a = V_{as} - R_s i_{as} - (L_s - M) \frac{di_{as}}{dt} \quad (5.1)$$

$$e_b = V_{bs} - R_s i_{bs} - (L_s - M) \frac{di_{bs}}{dt} \quad (5.2)$$

$$e_c = V_{cs} - R_s i_{cs} - (L_s - M) \frac{di_{cs}}{dt} \quad (5.3)$$

Three phase flux linkage ϕ_a , ϕ_b , ϕ_c can be estimated by using three phase back EMF e_a , e_b , e_c according to the following algorithm as shown in Fig 5.3. Where i is the iteration number. Delta modulated current control PWM is used for the switching of voltage source inverter as discussed in chapter III (Section 3.4.3). This hysteresis-band PWM is basically an instantaneous feedback current control method of PWM where the actual current continuously tracks the reference current. Hysteresis-band used for this delta modulated PWM is 0.001. So, for field oriented

current fed PMBLDC motor drives, the actual stator phase currents oscillate around the reference current with maximum oscillation width 0.001 A. Since three phase back EMF e_a , e_b , e_c are calculated by using the stator phase currents i_{as} , i_{bs} and i_{cs} as shown in Eq. (5.1-5.3). As a result oscillation of stator phase currents incorporate in three phase calculated back EMF. For this reason a band is used in flux estimation algorithm to compare per phase back EMF with the back EMF of previous iteration. In this algorithm, main objectives are to find out the value of back EMF e_{ac} , e_{bc} and e_{cc} at constant back EMF region in trapezoidal shaped back EMF as shown in Fig. 5.4. Thus the flux linkage can be estimated in per unit value by using e_{ac} , e_{bc} and e_{cc} as given in Fig. 5.3. To understand this proposed flux estimation algorithm, graphical representation of 3-phase back EMF and per unit estimated flux linkage according to the back EMF is illustrated in Fig. 5.4.

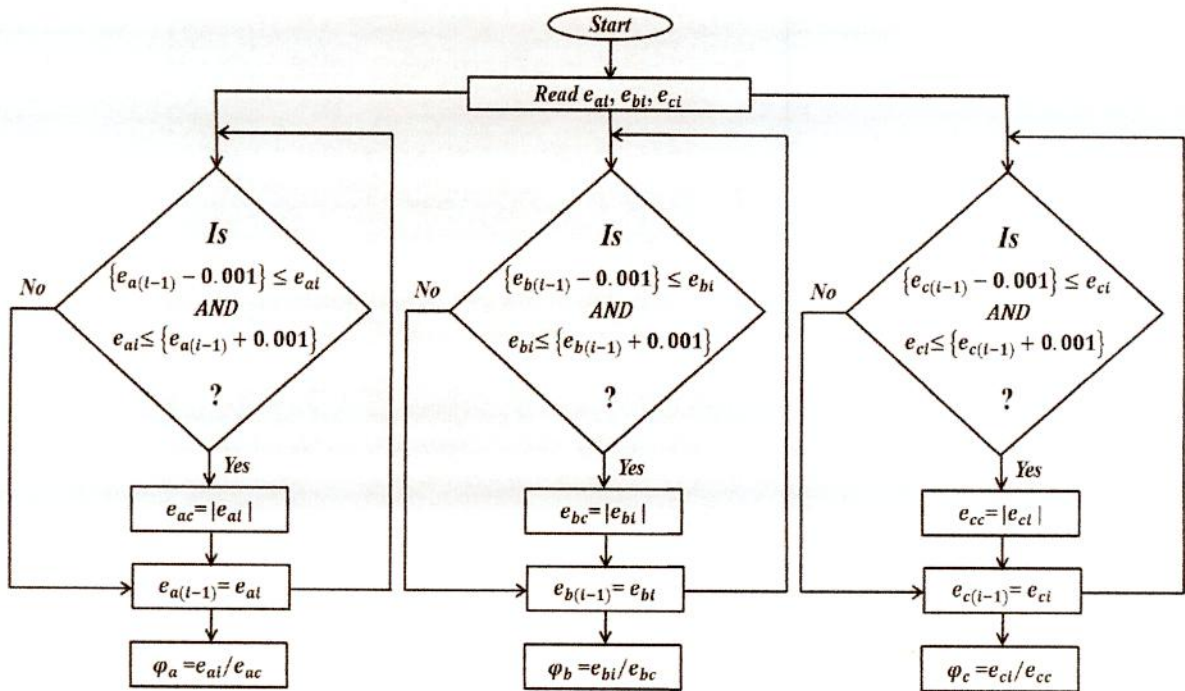


Fig. 5.3: Flowchart for flux estimation

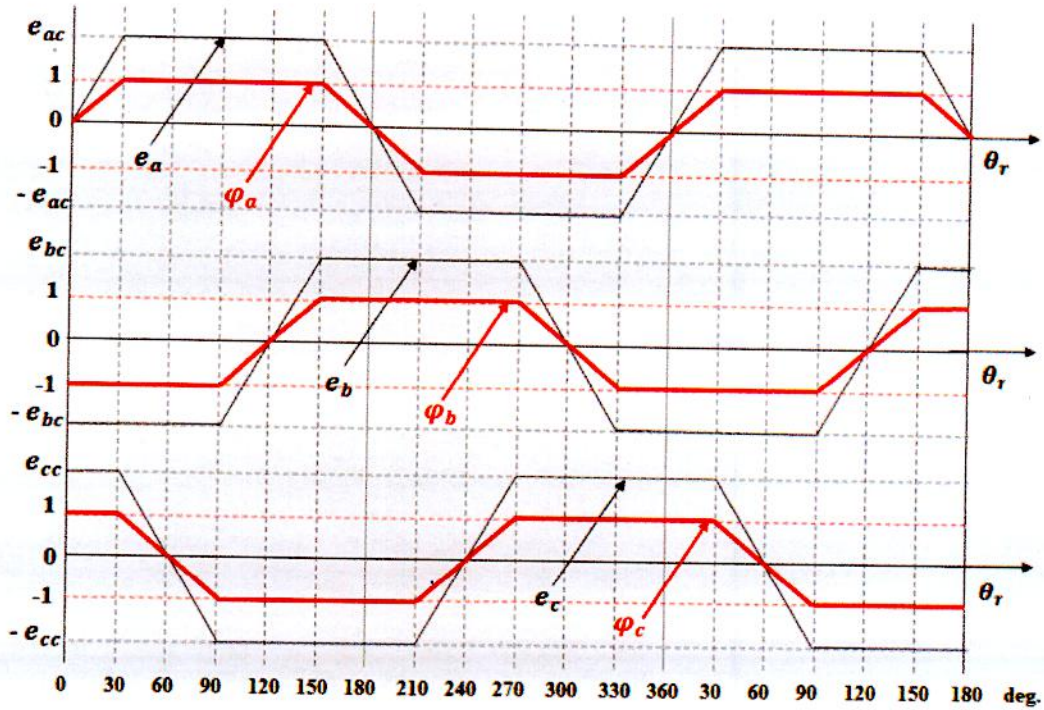


Fig. 5.4: 3-phase back EMF and per unit estimated rotor flux linkage according to the back EMF

5.4 Rotor Position Estimation

Rotor position estimation block is also same for both algorithm 1 and algorithm 2 as shown in Fig. 5.1 and Fig. 5.2. Rotor position θ_r is estimated by using estimated flux φ_a , φ_b and φ_c according to the Table 5.1. At a specific time, rotor position is determined only by using estimated flux of a single phase as tabulated in Table 5.1. This phase is selected on the basis of a simple rule. From Fig 5.4, it is seen that, at every instant flux of any two phases have constant value and flux of other phase changes with rotor position. This phase have to be chosen to determine the rotor position according to the value of flux of that phase.

Table 5.1: Rotor position corresponding to three phase flux linkage

Condition of Stator Flux Linkage			Rotor Position, θ_r (radian)
$\varphi_a \geq 0.0$	$\varphi_b \leq -1.0$	$\varphi_c \geq 1.0$	$\theta_r = (\varphi_a \times \frac{\pi}{6})$
$\varphi_a \geq 1.0$	$\varphi_b \leq -1.0$	–	$\theta_r = \frac{\pi}{3} - (\varphi_c \times \frac{\pi}{6})$
$\varphi_a \geq 1.0$	–	$\varphi_c \leq -1.0$	$\theta_r = (\varphi_b \times \frac{\pi}{6}) + \frac{2\pi}{3}$
–	$\varphi_b \geq 1.0$	$\varphi_c \leq -1.0$	$\theta_r = \pi - (\varphi_a \times \frac{\pi}{6})$
$\varphi_a \leq -1.0$	$\varphi_b \geq 1.0$	–	$\theta_r = (\varphi_c \times \frac{\pi}{6}) + \frac{4\pi}{3}$
$\varphi_a \leq -1.0$	–	$\varphi_c \geq 1.0$	$\theta_r = \frac{5\pi}{3} - (\varphi_b \times \frac{\pi}{6})$
$\varphi_a < 0$	$\varphi_b \leq -1.0$	$\varphi_c \geq 1.0$	$\theta_r = (\varphi_a \times \frac{\pi}{6}) + 2\pi$

5.5 PMBLDC Motor Speed Estimation

Generally motor speed can be determined by the differentiation of the rotor position of a motor. But this conventional approach is not applicable for estimated rotor position of a PMBLDC motor for delta modulated PWM current fed field oriented control drives. Because there exists oscillation in estimated rotor position which is incorporated from delta modulated stator phase currents as discussed in section 5.3. So new approach to determine motor speed have to be found out.

5.5.1 PMBLDC Motor Speed Estimation for Algorithm 1

PMBLDC motor speed can be estimated by using the estimated flux linkage $\varphi_a, \varphi_b, \varphi_c$ and calculated three phase back EMF e_a, e_b, e_c according to the Table 5.2. Flux of one phase and the calculated back EMF of that phase are used to determine the motor speed. Similar to the rotor position estimation, the phase has to be selected to determine the motor speed according to a rule that, the value of flux of selected phase changes with rotor position and other two phases have constant value of flux.

Table 5.2: Estimated speed corresponding to three phase flux linkage

Condition of Stator Flux Linkage			Motor Speed, ω_m (radian/s)
$\varphi_a \geq 0.0$	$\varphi_b \leq -1.0$	$\varphi_c \geq 1.0$	$\omega_m = e_a / (\lambda_m \times \varphi_a)$
$\varphi_a \geq 1.0$	$\varphi_b \leq -1.0$	-	$\omega_m = e_c / (\lambda_m \times \varphi_c)$
$\varphi_a \geq 1.0$	-	$\varphi_c \leq -1.0$	$\omega_m = e_b / (\lambda_m \times \varphi_b)$
-	$\varphi_b \geq 1.0$	$\varphi_c \leq -1.0$	$\omega_m = e_a / (\lambda_m \times \varphi_a)$
$\varphi_a \leq -1.0$	$\varphi_b \geq 1.0$	-	$\omega_m = e_c / (\lambda_m \times \varphi_c)$
$\varphi_a \leq -1.0$	-	$\varphi_c \geq 1.0$	$\omega_m = e_b / (\lambda_m \times \varphi_b)$
$\varphi_a < 0$	$\varphi_b \leq -1.0$	$\varphi_c \geq 1.0$	$\omega_m = e_a / (\lambda_m \times \varphi_a)$

5.5.2 PMBLDC Motor Speed Estimation for Algorithm 2

In algorithm 2 for sensorless operation of PMBLDC motor for field oriented vector control as shown in Fig. 5.2, different strategy has chosen to determine the motor speed. At first developed electromagnetic torque is estimated by using estimated flux linkage according to Eq. 5.4. Then the well-known power equation for motor is used to determine PMBLDC motor speed as given by Eq. 5.5.

$$T_{em} = K_t(\varphi_a i_{as} + \varphi_b i_{bs} + \varphi_c i_{cs}) \quad (5.4)$$

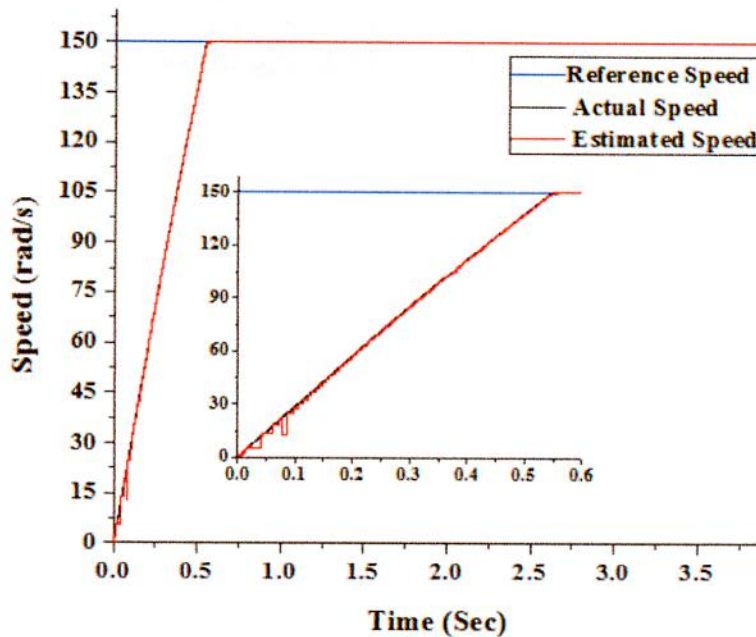
$$\omega_m = (e_a i_{as} + e_b i_{bs} + e_c i_{cs}) / T_{em} \quad (5.5)$$

5.6 Simulation Results and Discussion

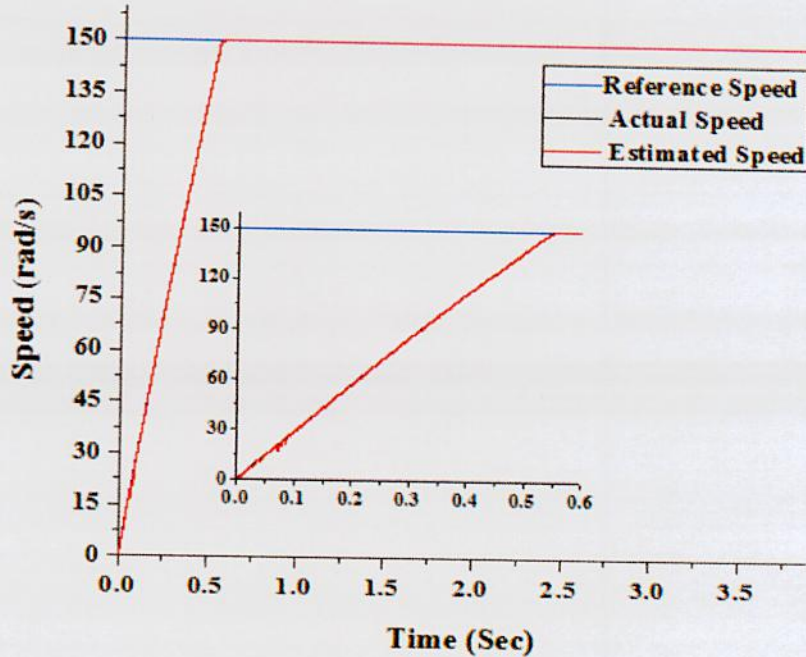
Field oriented controlled current fed PMSM motor drive without rotor position or speed sensors has been simulated in a digital computer with software written in C++ platform. The sampling time used for this simulation is 0.0000025 second. The specifications of the simulated PMSM motor are depicted in Appendix.

5.6.1 Starting Characteristics

The PMSM motor starts with an initial load torque 0.4 Nm. Starting speed characteristics i.e. time taken by the motor to reach its rated speed (150 rad/s) with its initial torque (0.4 Nm) for field oriented controlled PMSM motor drives is shown in Fig. 5.5. From Fig. 5.5, it is seen that, PMSM motor takes 0.55 second for both proposed algorithm 1 and algorithm 2 to gain rated speed. Field oriented controlled sensed PMSM motor drive also takes 0.55 second as shown Fig. 3.6 in chapter III. Comparing Fig. 5.5(a) with Fig. 5.5(b), estimated speed sharply follows actual speed of PMSM motor for proposed algorithm 2. I.e. speed estimation for proposed algorithm 2 is better than the proposed algorithm 1. For both of these two cases, there exists negligible amount of speed deviation between the actual and estimated speed at the initial time of starting. Because at initial transient state (before 0.085 second), there exists deviation between the actual and estimated flux and rotor position as shown in Fig. 5.10 and Fig. 5.11. After 0.085 seconds estimated speed follows actual speed very sharply for both proposed algorithm 1 and algorithm 2. I.e. at steady state there is no error for speed estimation both for proposed algorithm 1 and algorithm 2.



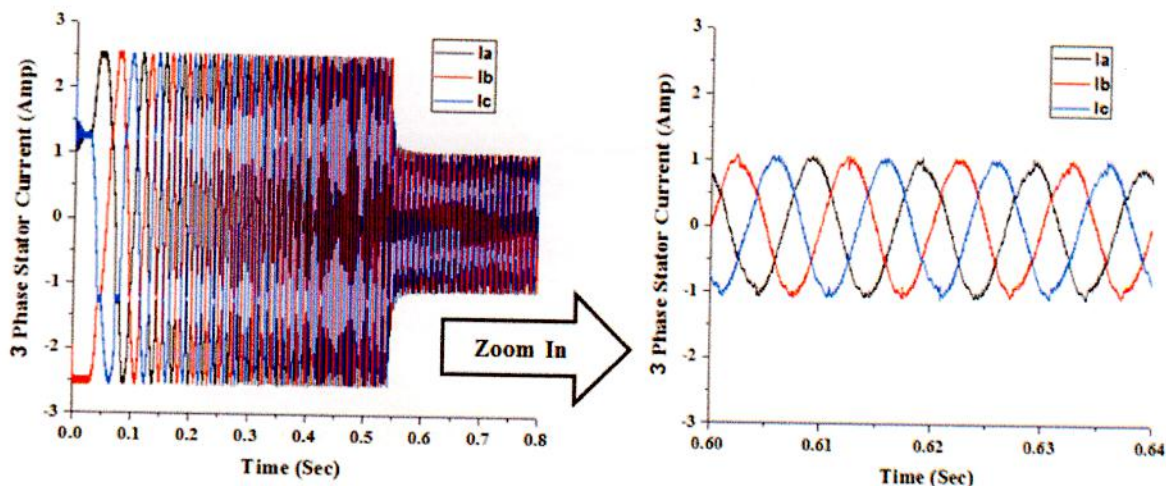
(a) For sensorless field oriented control drive based on proposed algorithm 1



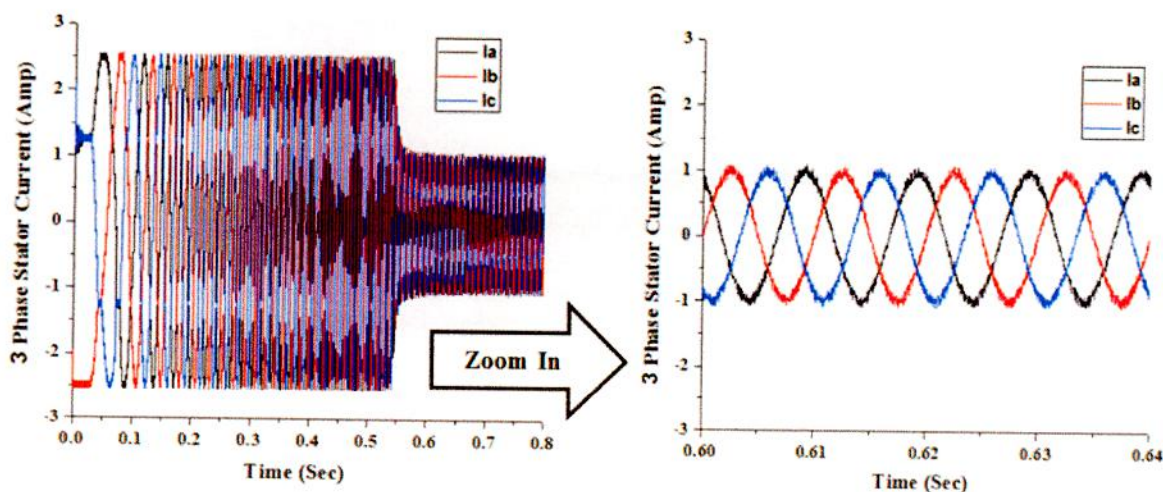
(b) For sensorless field oriented control drive based on proposed algorithm 2

Fig. 5.5: Starting characteristics of PMSM motor drives for field oriented control without position sensor

Phase currents of PMSM motor at the time of starting for field oriented current fed drives both for proposed algorithm 1 and algorithm 2 for sensorless operation are depicted in Fig. 5.6. It shows that the amplitude of 3-phase current is 2.5 Amp (rated current of the motor) at the transient time of starting for these two control drives. Started current is limited using the current limiter. Fig. 5.6 also describes that after gaining rated speed i.e. at steady state motor takes maximum 1.0 Amp current for both field oriented current fed drives for initial torque 0.4 Nm. Same scenario is noticed for position sensed field oriented vector controlled PMSM motor drive as shown in Fig. 3.7(a) in chapter III. Comparing with proposed algorithm 2, there are less oscillation in stator current for proposed algorithm 1 as shown in 3-phase steady state stator current in Fig. 5.6.



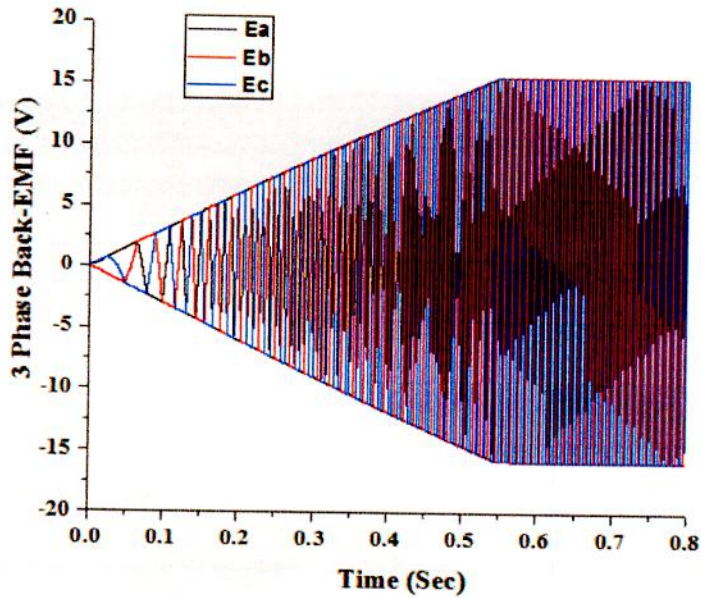
(a) For sensorless field oriented control drive based on proposed algorithm 1



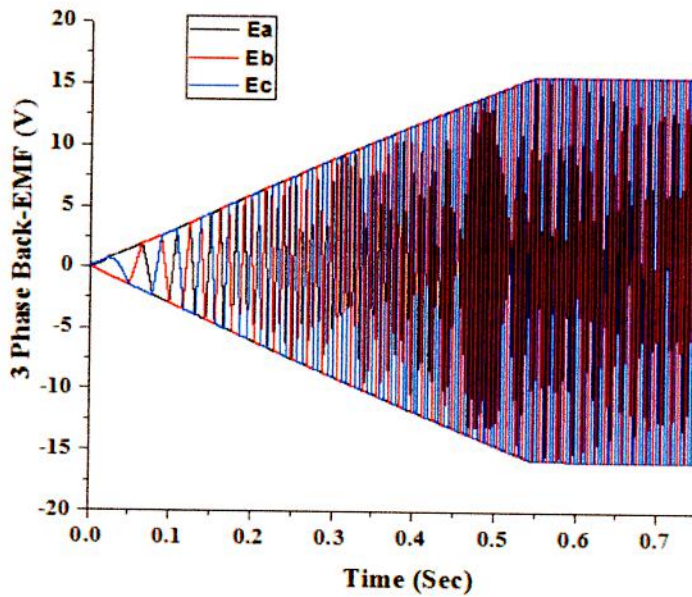
(b) For sensorless field oriented control drive based on proposed algorithm 2

Fig. 5.6: 3-Phase stator current of PMSM motor for field oriented current fed drive without position sensor

3-phase back EMF at the time of starting for field oriented vector controlled current fed PMSM drives for both proposed algorithm 1 and algorithm 2 for sensorless operation are shown in Fig. 5.7. Now the per phase back EMF and corresponding phase current of these two sensorless drives for steady state condition are pictured in Fig. 5.8. In Fig. 5.9, actual back EMF and corresponding calculated back EMF for algorithm 1 and algorithm 2 are depicted for comparison.

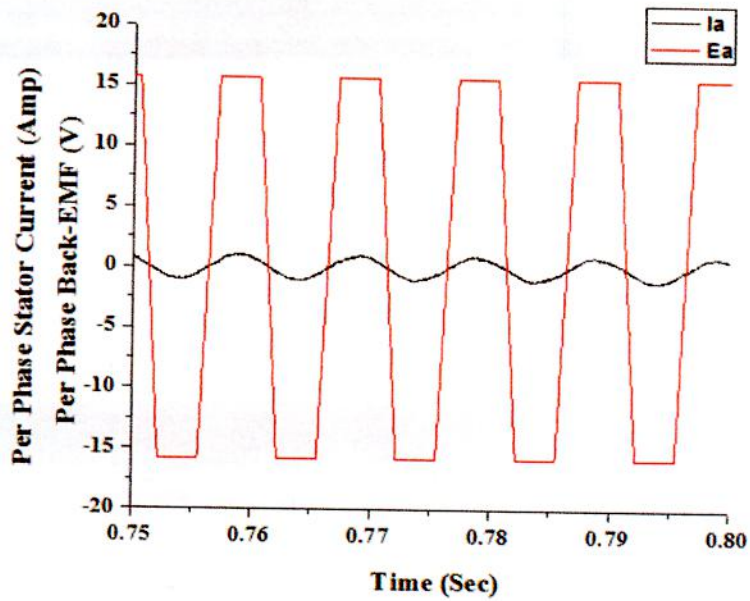


(a) For sensorless field oriented control drive based on proposed algorithm 1

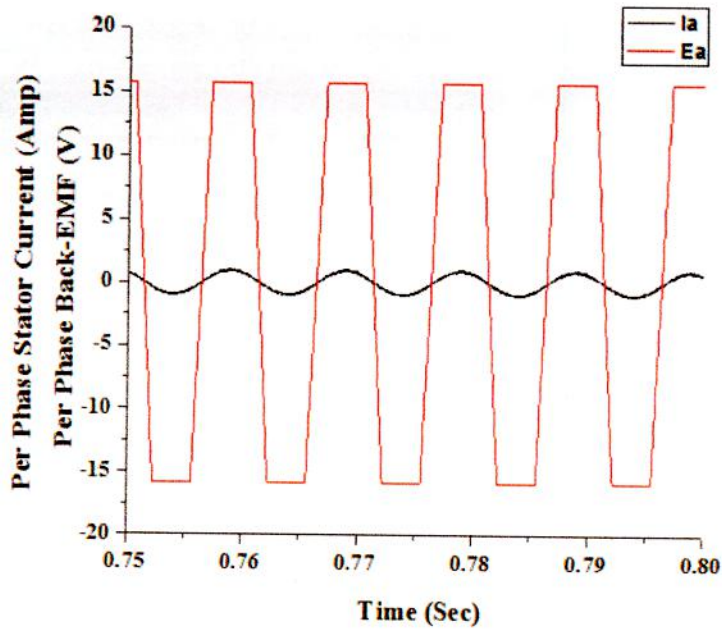


(b) For sensorless field oriented control drive based on proposed algorithm 2

Fig. 5.7: 3-phase back EMF of field oriented controlled PMLDLC motor drive without position sensor

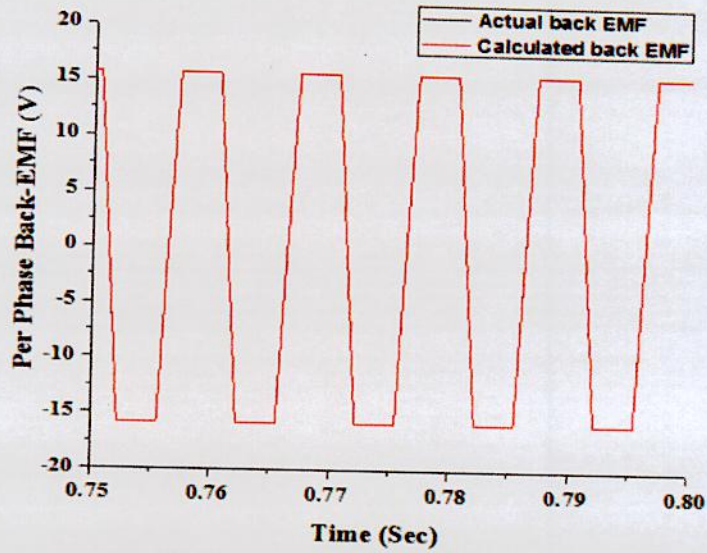


(a) For sensorless field oriented control drive based on proposed algorithm 1

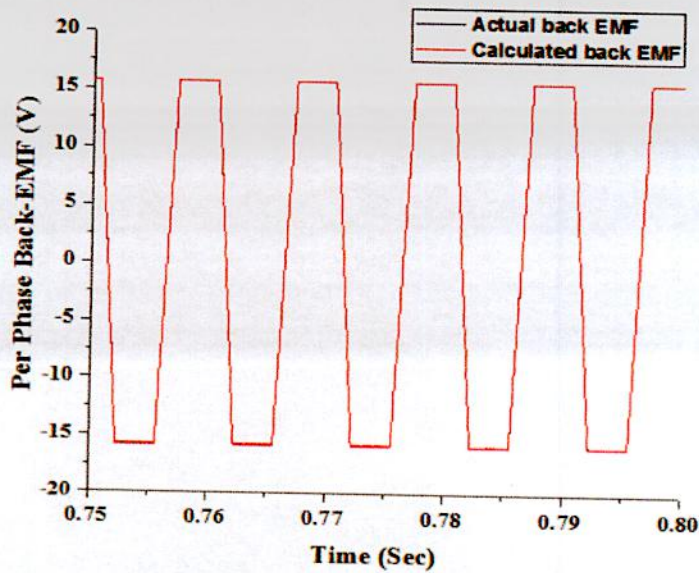


(b) For sensorless field oriented control drive based on proposed algorithm 2

Fig. 5.8: Per phase back EMF and corresponding phase current for field oriented controlled current fed drives without position sensor



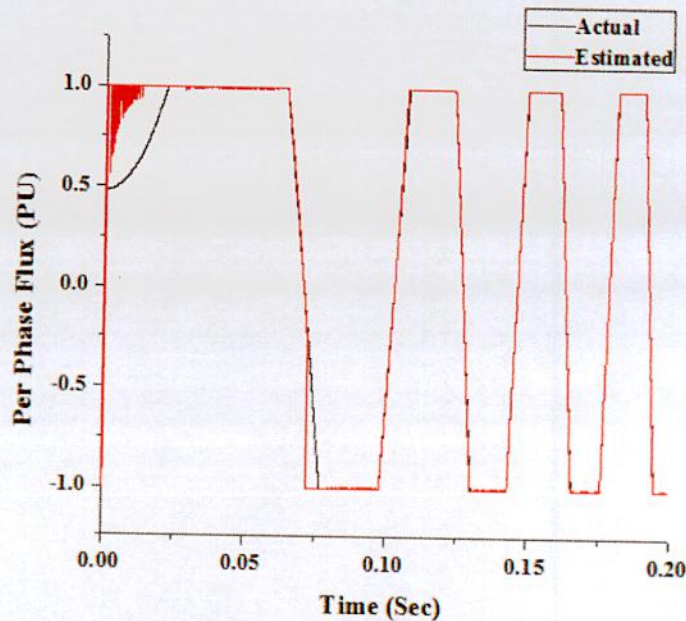
(a) For sensorless field oriented control drive based on proposed algorithm 1



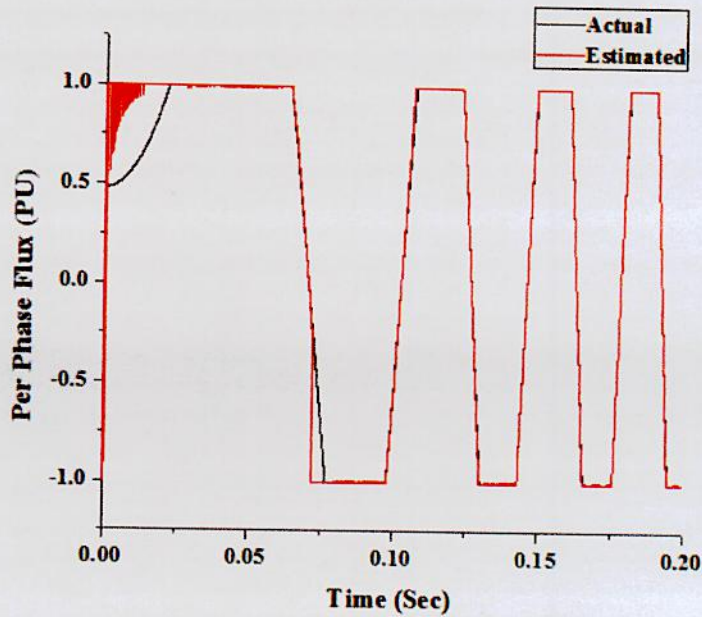
(b) For sensorless field oriented control drive based on proposed algorithm 2

Fig. 5.9: Comparison of per phase actual back EMF with calculated back EMF for field oriented current fed drives without position sensor

Comparison of actual and estimated flux for sensorless field oriented vector controlled PMSM motor drives for both proposed algorithm 1 and algorithm 2 are shown in Fig. 5.10. Fluxes are estimated by using the algorithm shown in Fig. 5.3. From Fig. 5.10, it is seen that, the estimated flux for both algorithm 1 and algorithm 2 is exactly same. Because for these two algorithms, similar flux estimation block is used. From Fig. 5.10 it can be said that, at the initial transient time of starting of PMSM motor (before 0.085 second), there exists little mismatch between the actual flux and estimated flux. Actual and estimated rotor position for sensorless field oriented vector controlled PMSM motor drives for both proposed algorithm 1 and algorithm 2 are shown in Fig.5.11. Since rotor positions are calculated by using the estimated flux. So, there is little misalignment between the actual and estimated rotor position at the initial time of starting as shown in Fig. 5.11. After 0.085 second, estimated flux fully traced actual flux. So, estimated rotor position can be fully matched with actual rotor position. It is one of the novelties of the proposed algorithms.

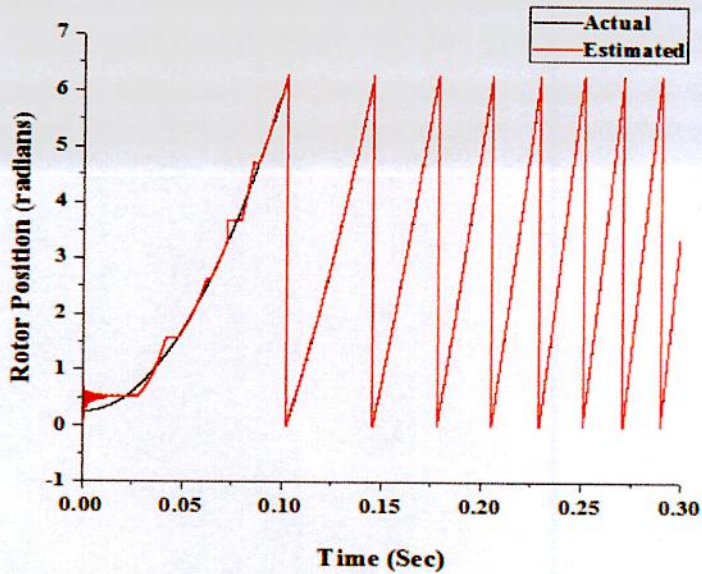


(a) For sensorless field oriented control drive based on proposed algorithm 1

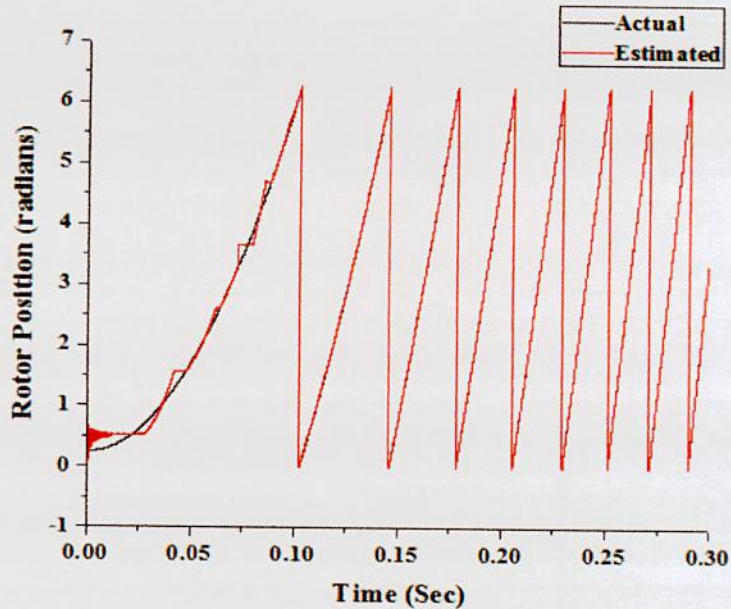


(b) For sensorless field oriented control drive based on proposed algorithm 2

Fig. 5.10: Actual and estimated rotor flux for field oriented control drives without position sensor



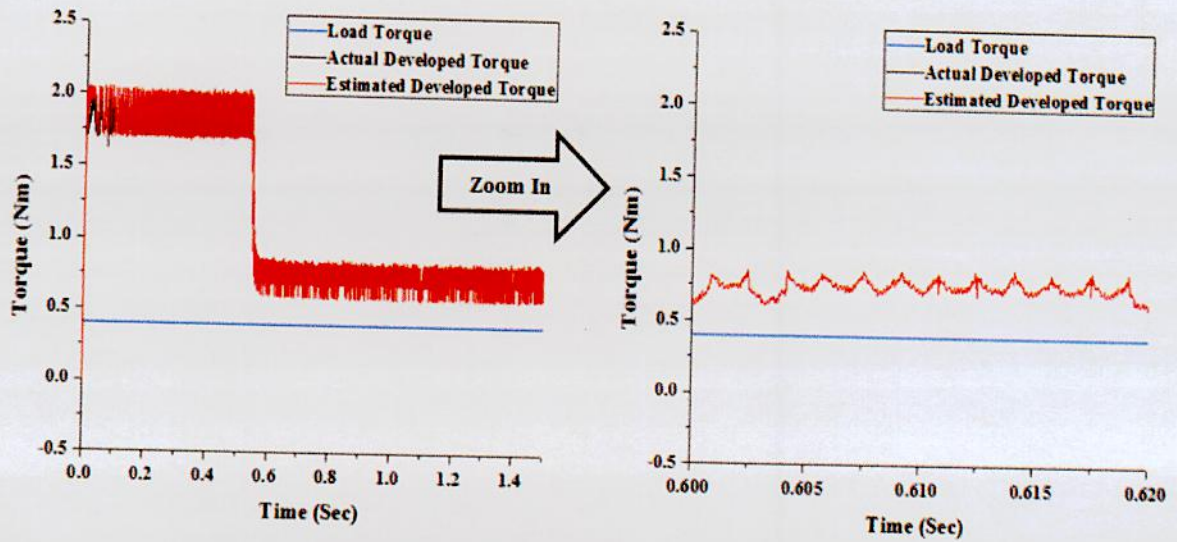
(a) For sensorless field oriented control drive based on proposed algorithm 1



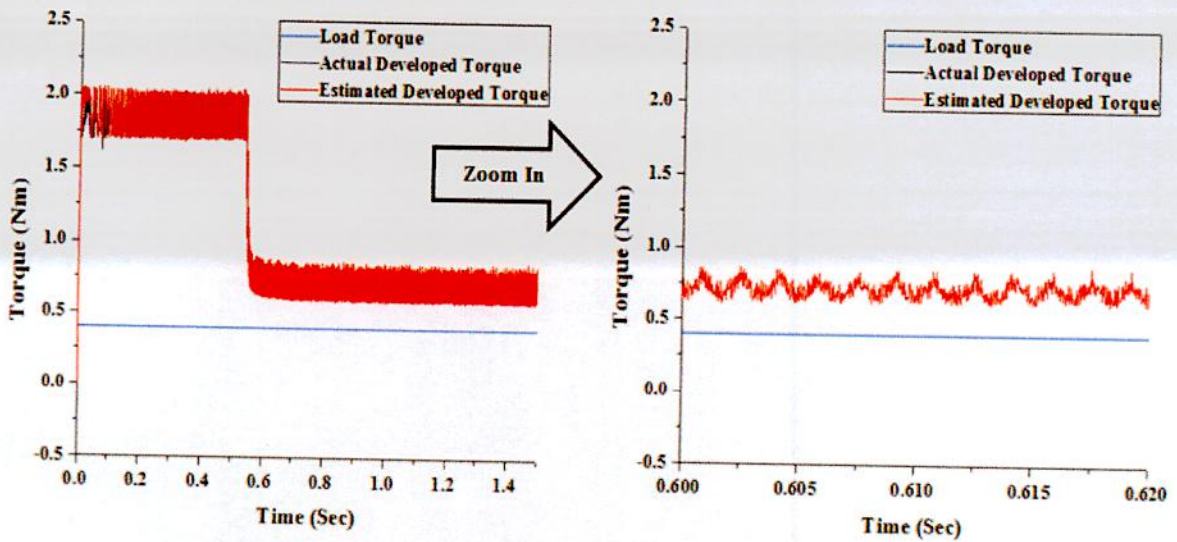
(b) For sensorless field oriented control drive based on proposed algorithm 2

Fig. 5.11: Comparison of actual rotor position with estimated rotor position for field oriented control drives without position sensor

Fig. 5.12 depicts developed electromagnetic torque in PMSM motor according to the load torque 0.4 Nm for sensorless field oriented current fed drives. Fig. 5.12 also represents the comparison between the actual developed torque with the estimated developed torque. Torque estimation is done using estimated flux. This estimated developed torque is used to calculate speed of the PMSM motor for proposed algorithm 2. From Fig. 5.12, it is seen that, developed electromagnetic torque oscillates more for proposed algorithm 2 based field oriented vector controlled PMSM motor drive than algorithm 1 based drive. For both of these proposed algorithms, estimated developed torque exactly follows the actual developed torque in PMSM motor.



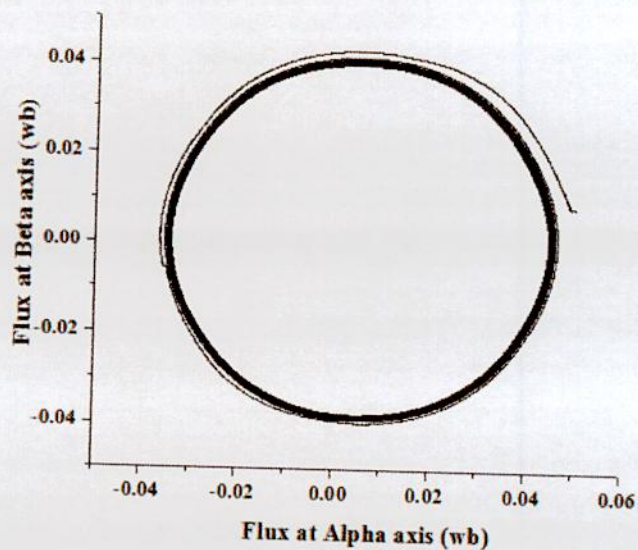
(a) For sensorless field oriented control drive based on proposed algorithm 1



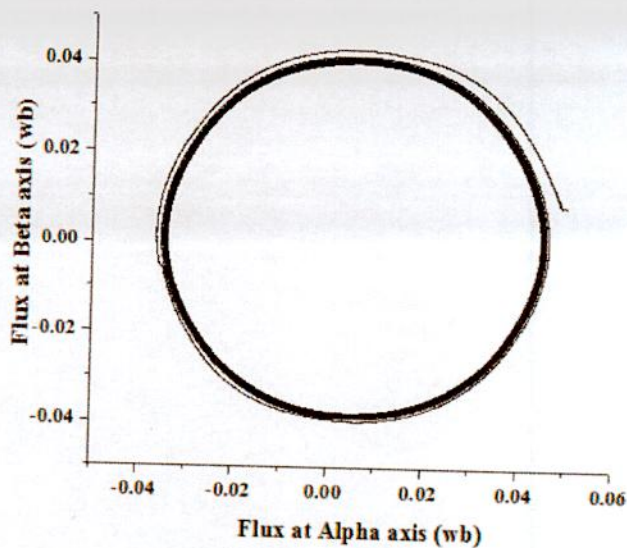
(b) For sensorless field oriented control drive based on proposed algorithm 2

Fig. 5.12: Actual and estimated developed torque according to load torque for sensorless field oriented vector controlled PMSBLDC motor drives

In Fig. 5.13, stator flux linkage trajectories i.e. flux orientation representation in the stationary $\alpha\beta$ axes reference frame for sensorless field oriented vector controlled PMSM motor drives are pictured both for proposed algorithm 1 and algorithm 2.



(a) For sensorless field oriented control drive based on proposed algorithm 1



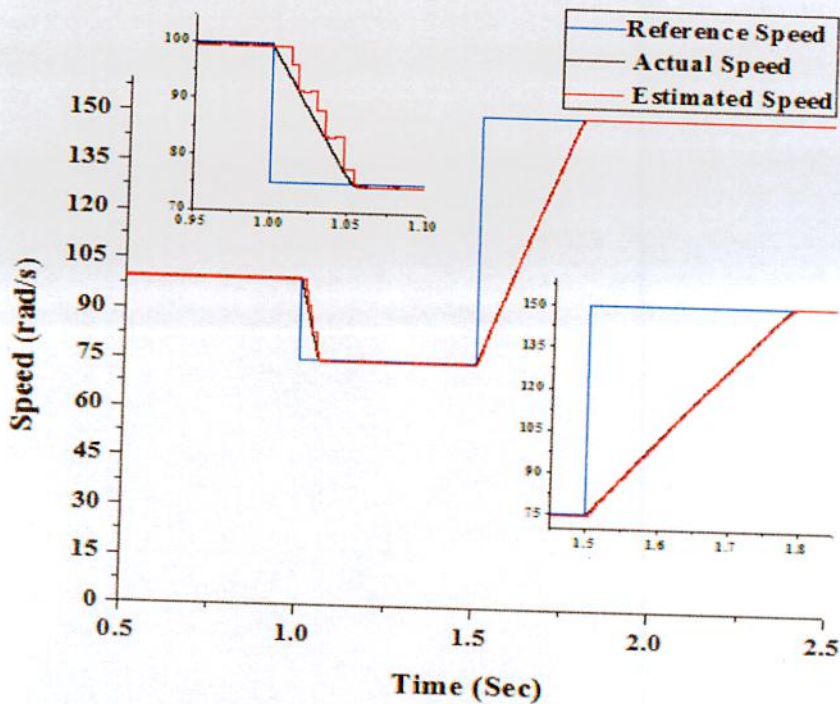
(b) For sensorless field oriented control drive based on proposed algorithm 2

Fig. 5.13: Stator flux linkage trajectories in the stationary $\alpha\beta$ axes reference frame for sensorless field oriented vector controlled PMSM motor drives

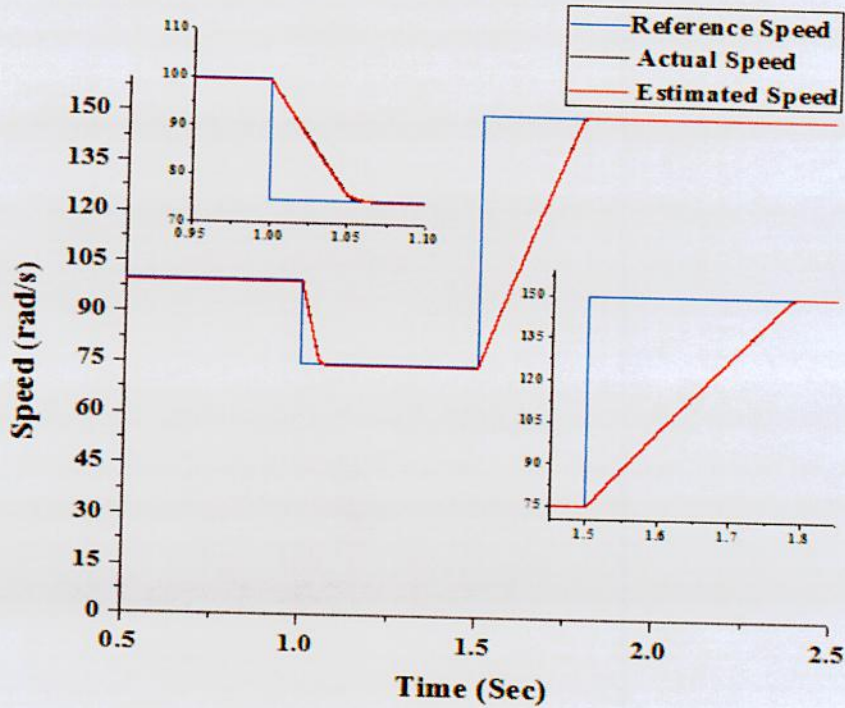
5.6.2 Variable Speed Characteristics

Variable speed command is given to measure the dynamic performance of field oriented vector controlled PMBLDC motor drives based on two different proposed algorithms. Motor runs at speed 100 rad/s. At 1.0 second the speed command is changed to 75 rad/s and finally at 1.5 second speed command is changed to 150 rad/s. Motor speed follows the reference speed for both proposed algorithm 1 and algorithm 2 based vector controlled PMBLDC motor drives as shown in Fig. 5.14.

For dynamic speed changing condition, estimated speed nearly follows the actual speed of PMBLDC motor for both two cases. When speed command is changed to 75 rad/s from 100 rad/s with load torque 0.4 Nm, there is a small amount of mismatch between the actual speed and estimated speed for algorithm 1 at transient time interval 1.0 second to 1.05 second. But during this interval, there is no mismatch between actual and estimated motor speed for proposed algorithm 2 as depicted in subplot of Fig. 5.14. When speed command is changed to 150 rad/s from 75 rad/s at 1.5 second, there is no noticeable error between the estimated and actual motor speed for both algorithm 1 and algorithm 2. At steady state condition, estimated speed exactly traced out the actual speed of the motor for both of these proposed algorithms.



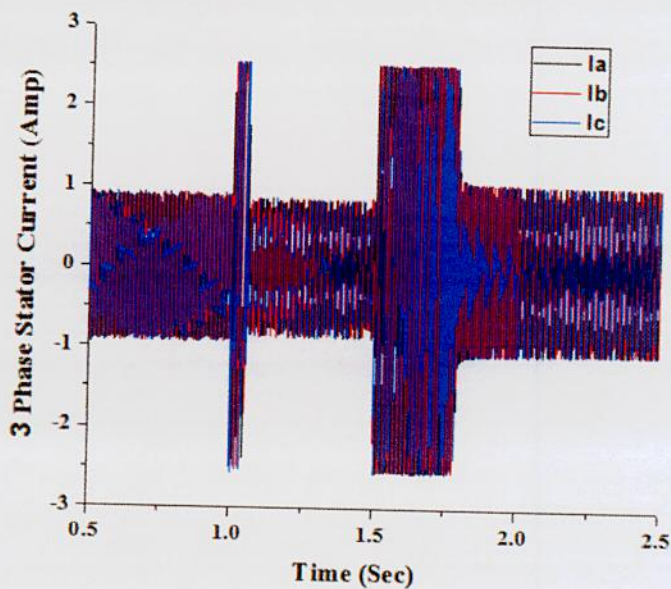
(a) For sensorless field oriented control drive based on proposed algorithm 1



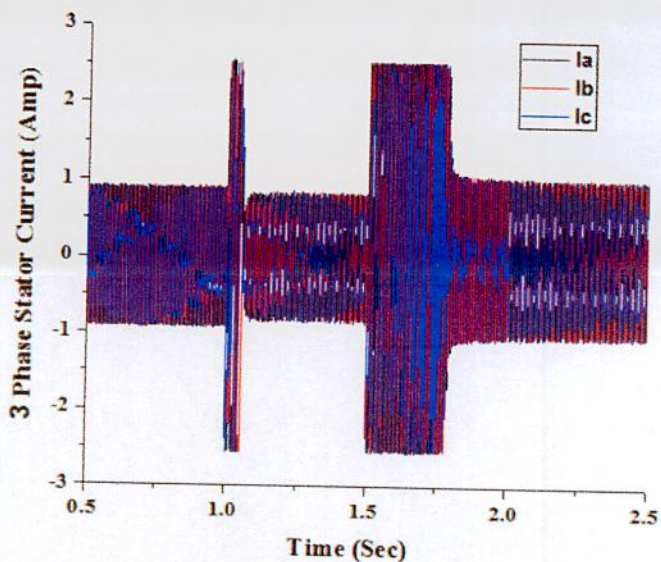
(b) For sensorless field oriented control drive based on proposed algorithm 2

Fig. 5.14: Comparison between speed responses of PMSBLDC motor for sensorless field oriented vector controlled drives at dynamic speed changing condition

From 3-phase stator current for variable speed condition of sensorless field oriented vector controlled PMSBLDC motor drives are shown in Fig. 5.15. It is seen that, at 1.0 second when the reference speed changes from 100 rad/s to 75 rad/s, there exists no high value of transient current beyond the limit of rated current (2.5 Amp) and no undershoot from reference speed for both of these two different algorithm based drives. Besides there is no overshoot at 1.5 second, when the reference speed goes to 150 rad/s from 75 rad/s. Condition of back EMF at the time of variable speed change for sensorless field oriented current fed drives are pictured in Fig. 5.16.

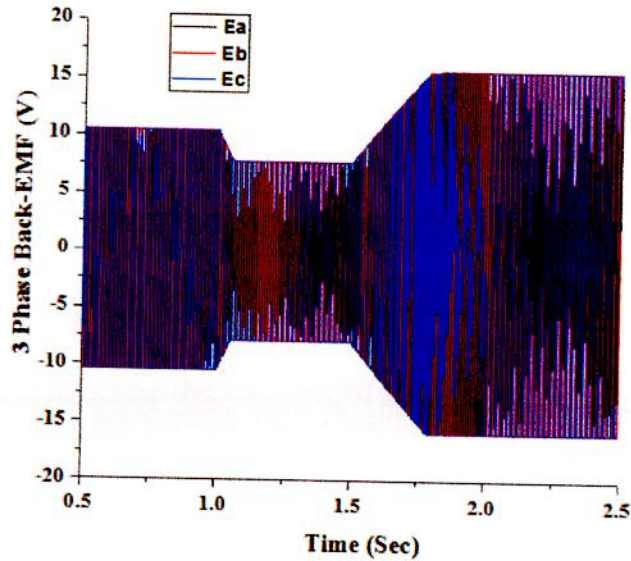


(a) For sensorless field oriented control drive based on proposed algorithm 1

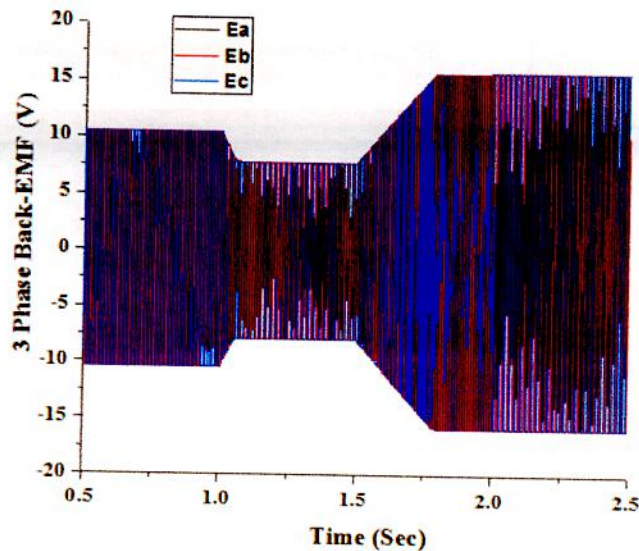


(b) For sensorless field oriented control drive based on proposed algorithm 2

Fig. 5.15: 3-phase current of PMSBLDC motor for sensorless field oriented control drive for variable speed condition considering transient current at the interface of speed changes



(a) For sensorless field oriented control drive based on proposed algorithm 1

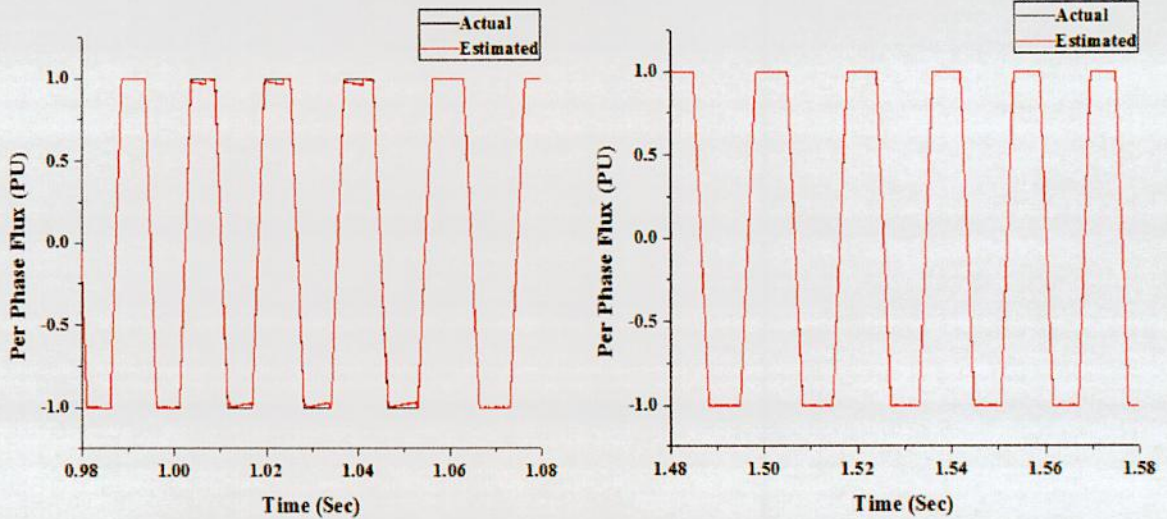


(b) For sensorless field oriented control drive based on proposed algorithm 2

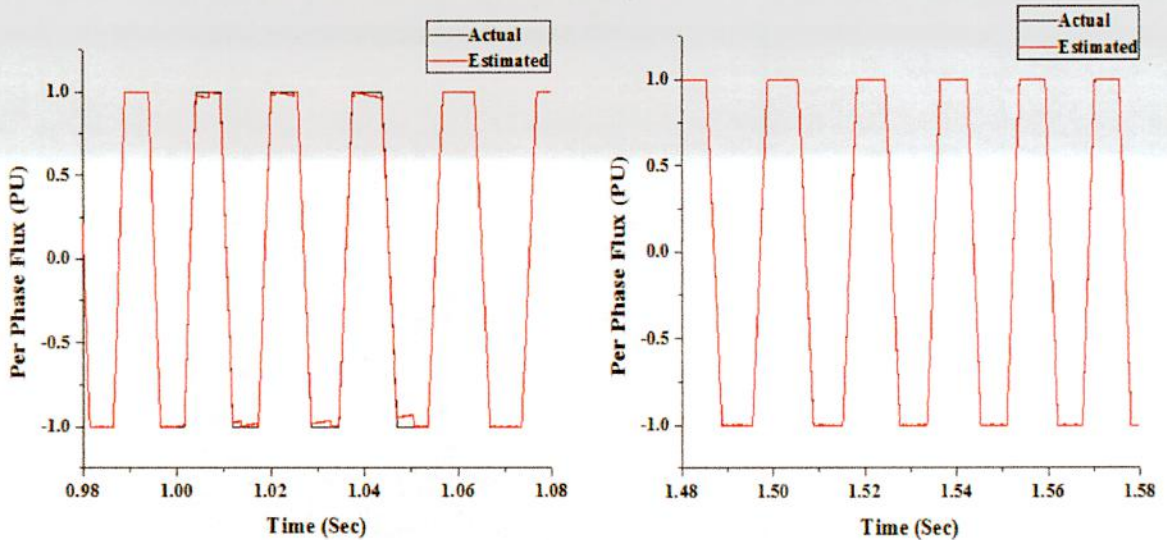
Fig. 5.16: 3-phase back EMF at dynamic speed changing condition for field oriented vector controlled PMSBLDC motor drive without position sensor

Condition of actual and estimated flux at variable speed changing interface for sensorless field oriented current fed drives are shown in Fig. 5.17. When speed command changes from 100 rad/s to 75 rad/s, i.e. for decreasing motor speed transient condition, there is very small mismatch between actual and estimated flux for both of these two proposed algorithms. When speed command changes from 75 rad/s to 150 rad/s, i.e. for increasing motor speed transient condition, there is no mismatch between actual and estimated flux for both of these two proposed

algorithms as shown in Fig. 5.17. In Fig. 5.18, actual and estimated rotor position of the PMLDC motor at variable speed changing interface for sensorless field oriented current fed drives are plotted. Rotor position of the motor is estimated using estimated stator flux linkage. So estimated rotor position shows the similar behavior as described for estimated flux earlier.

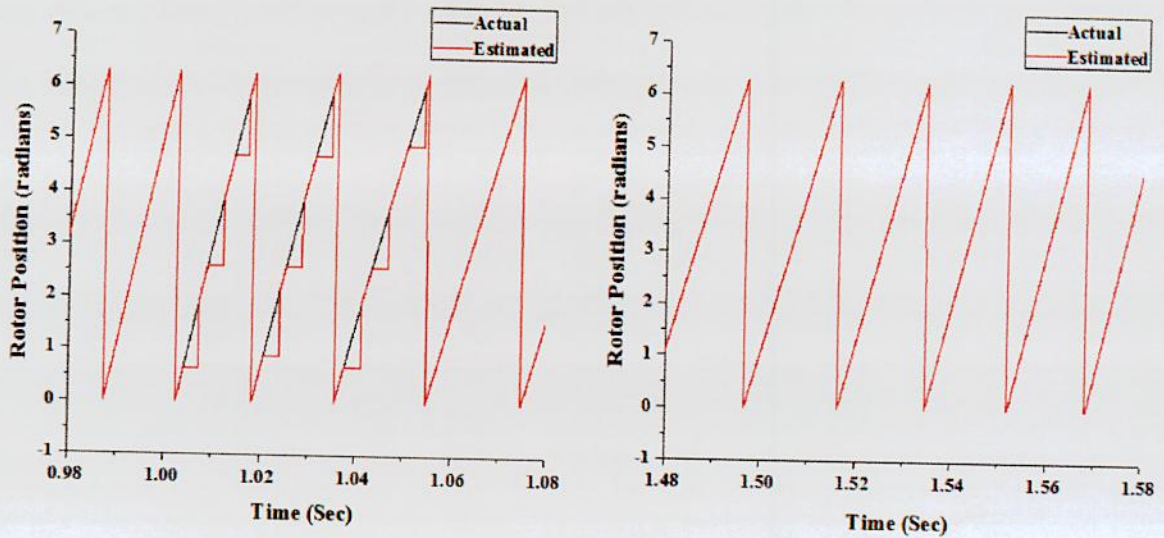


(a) For sensorless field oriented control drive based on proposed algorithm 1

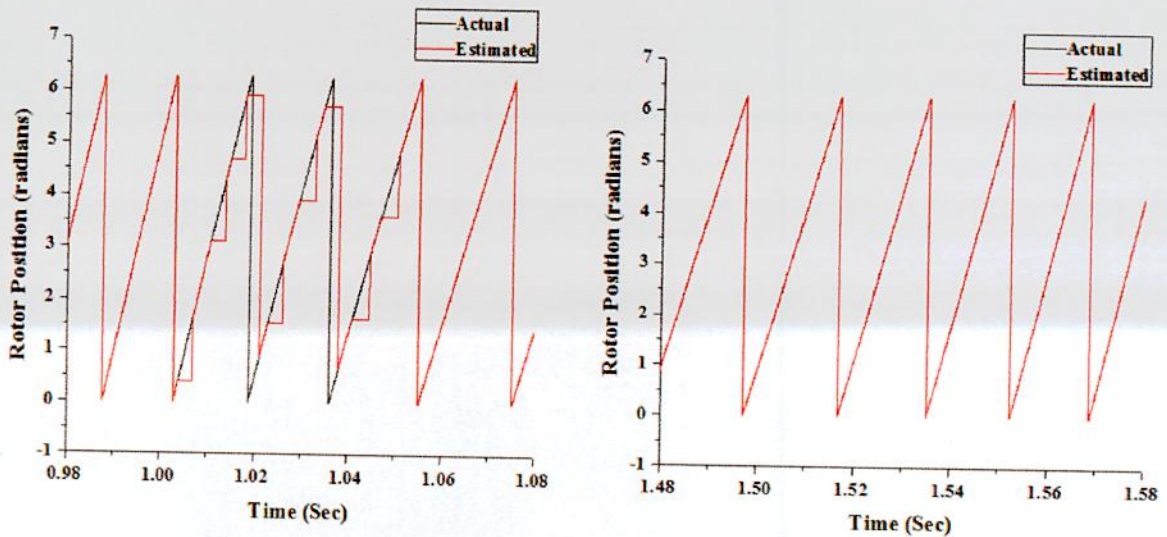


(b) For sensorless field oriented control drive based on proposed algorithm 2

Fig. 5.17: Actual and estimated rotor flux in per unit value at dynamic speed changing condition for field oriented vector controlled PMLDC motor drive without position sensor



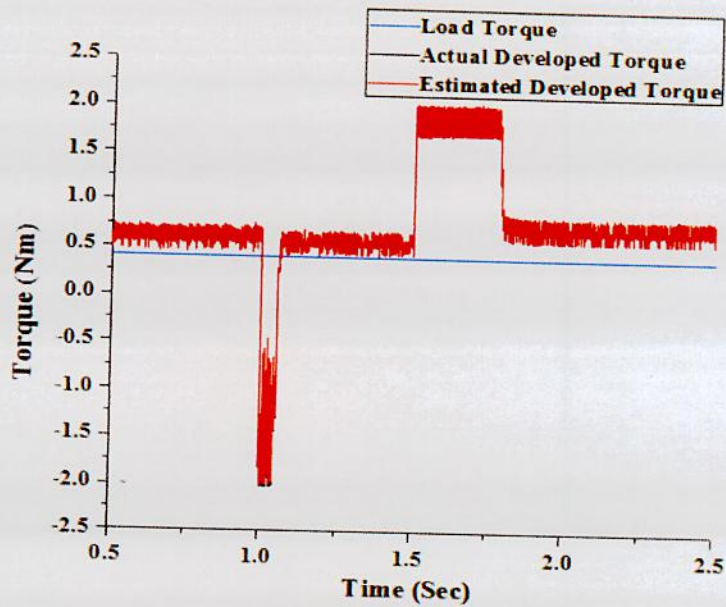
(a) For sensorless field oriented control drive based on proposed algorithm 1



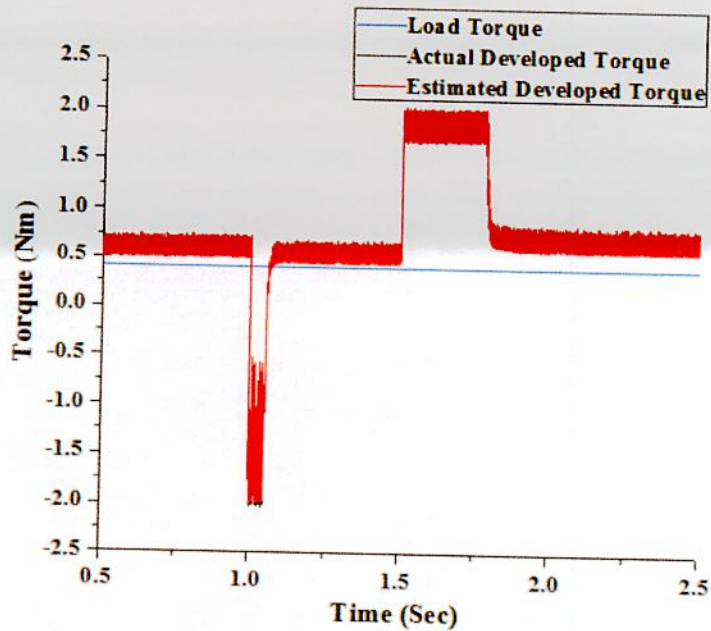
(b) For sensorless field oriented control drive based on proposed algorithm 2

Fig. 5.18: Actual and estimated rotor position at dynamic speed changing condition for field oriented control drive without position sensor

The scenario of actual and estimated developed electromagnetic torque according to the response of constant load torque at dynamic speed changing condition for sensorless operation of field oriented vector controlled PMSM motor drives for both proposed algorithm 1 and algorithm 2 are shown in Fig. 5.19.



(a) For sensorless field oriented control drive based on proposed algorithm 1

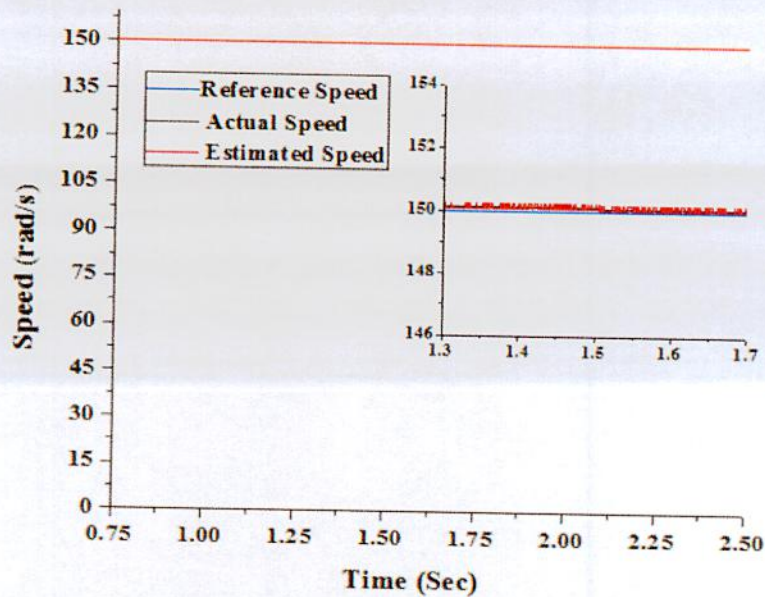


(b) For sensorless field oriented control drive based on proposed algorithm 2

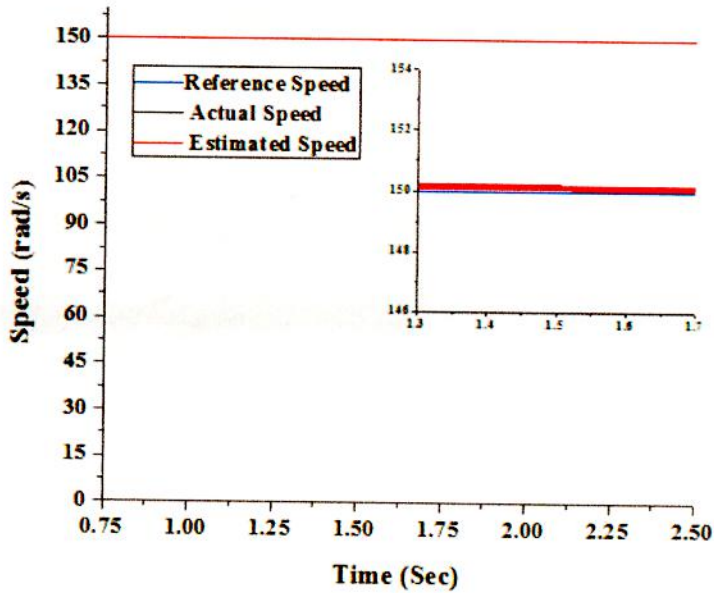
Fig. 5.19: Actual and estimated rotor developed torque according to the response of load torque at dynamic speed changing condition for current fed field oriented controlled PMSBLDC motor drives without position sensor

5.6.3 Motor Characteristics due to Load Torque Change

Now performance of sensorless field oriented vector controlled PMBLDC motor drives are determined under the condition of load torque change. At first motor runs at 150 rad/s rated speed with initial load torque 0.4 Nm. At time 1.5 second motor is loaded with 1.55 Nm load torque. At that condition sensorless field oriented control drives for both the proposed algorithm 1 and algorithm 2 can sustain motor speed to its rated value 150 rad/s as shown in Fig. 5.20. Fig. 5.20 depicts that, there is no change in speed characteristic at the time 1.5 second when the motor is loaded with 1.55 Nm torque. Both actual and estimated motor speed sharply follows the given reference speed command. Maximum load torque have to be applied to a field oriented controlled drive is 1.55 Nm for the specific PMBLDC motor as shown in chapter III for position sensed operation. This statement is also true for these two position sensorless field oriented PMBLDC motor drives. So the maximum load torque have to be given to the sensorless field oriented controlled PMBLDC motor without drive hampering the system stability is 1.55 Nm for both of these two proposed algorithms.



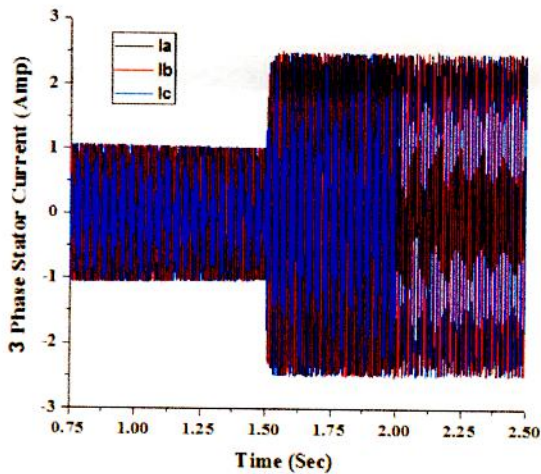
(a) For sensorless field oriented control drive based on proposed algorithm 1



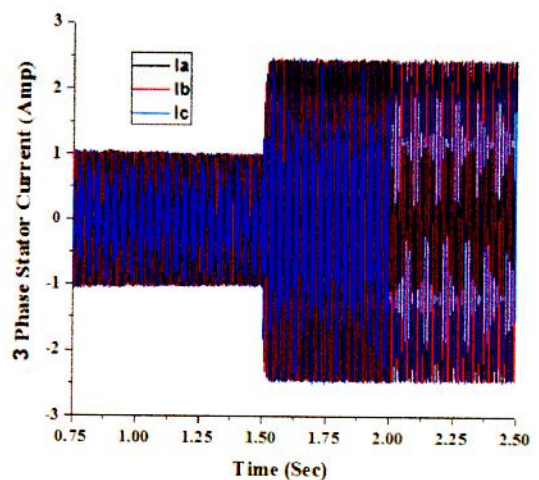
(b) For sensorless field oriented control drive based on proposed algorithm 2

Fig. 5.20: Speed characteristics of PMBLDC motor for sudden load torque change at 1.5 second from initial load torque 0.4 Nm to load torque 1.55 Nm for sensorless field oriented control drives

From graphical representation of 3-phase stator current for sudden load torque change of sensorless field oriented current fed drives as shown in Fig. 5.21, it summaries that, though applying 1.55 Nm load torque, stator current remains within the rated current (2.5 Amp) limit.



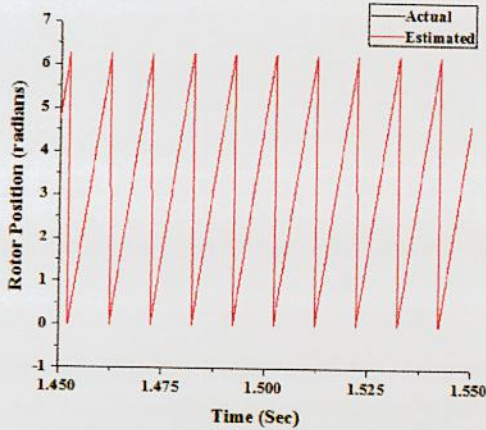
(a) Based on proposed algorithm 1



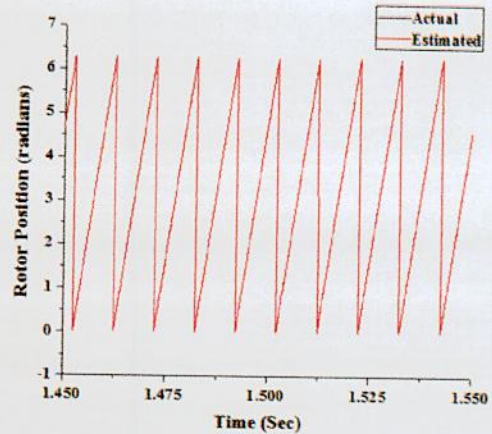
(b) Based on proposed algorithm 2

Fig. 5.21: 3-phase stator current of sensorless field oriented vector controlled PMBLDC motor drives for sudden load torque change at 1.5 second

Rotor position of sensorless current fed field oriented controlled PMSM motor drives for sudden load torque change at 1.5 second are pictured in Fig. 5.22. At the time 1.5 second when the motor is loaded with the rated load torque 1.55 Nm, there is no difference between the actual and estimated rotor position for both proposed algorithm 1 and algorithm 2.



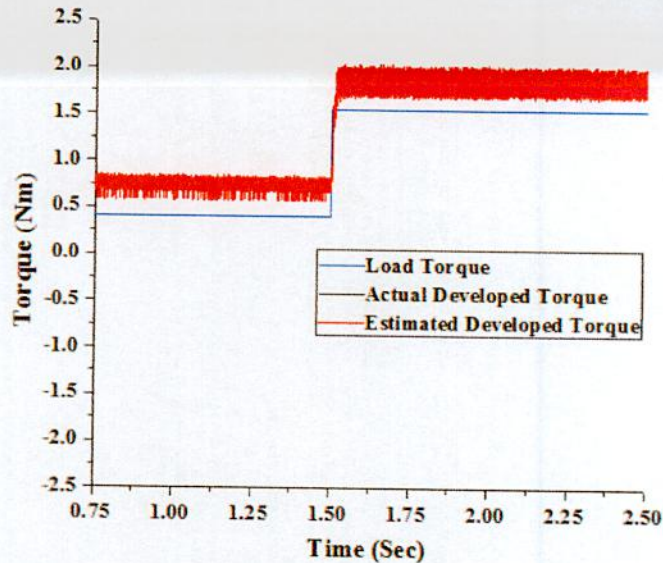
(a) For proposed algorithm 1



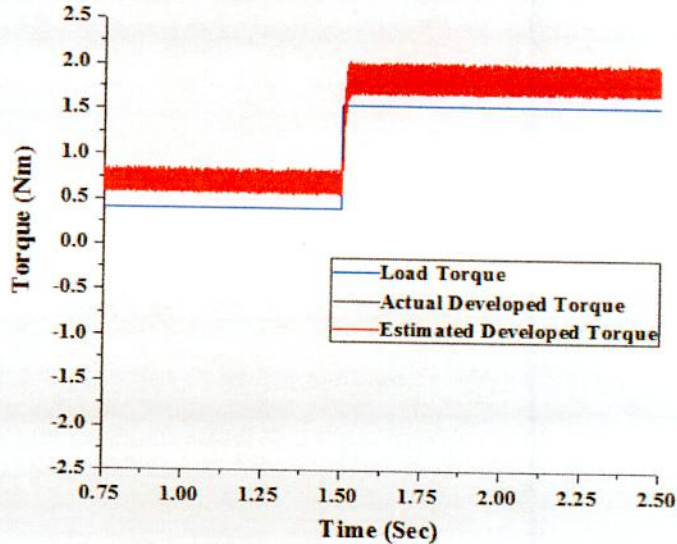
(b) For proposed algorithm 2

Fig. 5.22: Comparison of actual and estimated rotor position of sensorless field oriented vector controlled PMSM motor drives for sudden load torque change at 1.5 second

The scenario of actual and estimated developed electromagnetic torque according to the response of dynamic load torque change for sensorless operation of field oriented vector controlled PMSM motor drives for both proposed algorithm 1 and algorithm 2 are shown in Fig. 5.23.



(a) For sensorless field oriented control drive based on proposed algorithm 1



(a) For sensorless field oriented control drive based on proposed algorithm 2

Fig. 5.23: Actual and estimated rotor developed torque according to the response of dynamic load torque change for field oriented vector controlled PMSM motor drives without position sensor

5.7 Conclusion

Algorithm 1 and algorithm 2 based position sensorless field oriented vector controlled current fed delta modulated PMSM motor drives are designed in this chapter. Except initial starting time error (before 0.085 second), estimated flux exactly traced out the actual flux linkage of the PMSM motor for both algorithm 1 and algorithm 2. That is the performance of flux estimation algorithm is working well. Similar to the estimated flux, there is no mismatch between actual and estimated rotor position excluding the initial starting time error. So, the performance of rotor position estimator is satisfactory. With the speed estimator, there are negligible amount of speed error between the estimated and actual motor speed at the transient time of starting and transient time of dynamic speed decreasing interface for algorithm 1. The performance of algorithm 2 for speed estimation is better than the algorithm 1 for sensorless operation of field oriented control. There are less oscillation in stator phase current currents and developed electromagnetic torque for proposed algorithm 1 than algorithm 2. Considering this point of view, algorithm 1 is better than algorithm 2. By considering starting, dynamic speed and load torque changing characteristics, it is clear that, the performance of these sensorless field oriented vector controlled PMSM motor drives for both algorithm 1 and algorithm 2 are similar to sensed field oriented PMSM motor drive. Instead of using position sensor, two different algorithms are used for sensorless operation of field oriented vector controlled PMSM motor drive. But the performance of this drive remains unchanged.

Chapter VI

High Performance Controlled PMBLDC Motor Drives

Chapter Outlines:

6.1 Introduction

6.2 Proposed Control Scheme

6.3 Simulation Results and Discussion

6.4 Conclusion

6.1 Introduction

In this section, position sensorless trapezoidal current fed field oriented vector controlled PMBLDC motor drives are proposed. Field oriented vector control is used in this proposed PMBLDC motor drive. Because the advantages of field oriented control drive over scalar control drive have been discussed in chapter III. Trapezoidal current fed drive is chosen because the torque handling capacity of a specific PMBLDC motor can be enhanced 25% than the conventional 120° conduction square current fed drive without exceeding the maximum current rating of the motor as shown in chapter IV.

Instead of rotor position encoder and speed sensor, two different algorithms will be used to estimate the rotor position and speed as shown in chapter V. Because in PMBLDC motor, for proper commutation of the phase currents, the conventional PMBLDC motor rotor position information must be obtained by the position sensors such as hall-effect sensors or optical encoders. But there are some constraints to the position sensors including high cost, installation difficulty for misalignments in position sensors, and poor reliability. Therefore, strategy for position sensorless operation is considered for this chapter.

So, in this chapter, position sensorless trapezoidal current fed field oriented vector controlled PMBLDC motor drives are considered. Because all the advantages of field oriented control, trapezoidal current fed drive, sensorless operation are tried to incorporate into a single PMBLDC motor drive. Therefore, this motor drive is called high performance controlled PMBLDC motor drive.

Two different algorithms to estimate rotor position and speed for sensorless operation are used to enhance the torque handling capacity of a PMBLDC motor drive without exceeding the maximum current rating of the motor. For algorithm 1 both rotor position and speed of the motor is determined from the estimated flux linkage. For algorithm 2 only rotor position of the PMBLDC motor is determined from the estimated flux and the speed of the motor is detected by the estimated developed electromagnetic torque and power equation as discussed in chapter V.

The starting and dynamic speed and load torque variation performances of algorithm 1 based sensorless trapezoidal current fed field oriented vector controlled PMBLDC motor drive are compared with algorithm 2 based sensorless drive. The performance of these two different position sensorless trapezoidal current fed field oriented vector controlled PMBLDC motor drives are also verified by comparing with the performance of sensed trapezoidal current fed field oriented vector controlled PMBLDC motor drive as discussed in chapter IV.

6.2 Proposed Control Scheme

Two different PMBLDC motor control drives are proposed in this section. Both of these two control drives are proposed for position sensorless operation. Position sensorless means that, rotor position encoder or speed sensors are absent in these proposed system. In Fig. 6.1, block diagram of high performance trapezoidal current fed field oriented PMBLDC motor drive without rotor position are depicted based on algorithm 1 for sensorless operation. In this control drive, instead of using position sensor, flux estimation block, rotor position and speed estimation block are used to estimate the rotor position and the speed of PMBLDC motor. In this drive both rotor position and speed of the motor is estimated by using the estimated flux linkage as discussed in chapter V. Block diagram of high performance trapezoidal current fed field oriented PMBLDC motor drive without rotor position based on algorithm 2 for sensorless operation are shown in Fig. 6.2. In this drive rotor position is estimated by using the estimated flux linkage and speed of the motor is determined by using the estimated developed torque and power equation. Detail operation of flux estimation algorithm, rotor position and speed estimation blocks are discussed in the section 5.3, 5.4 and 5.5 in chapter V respectively.

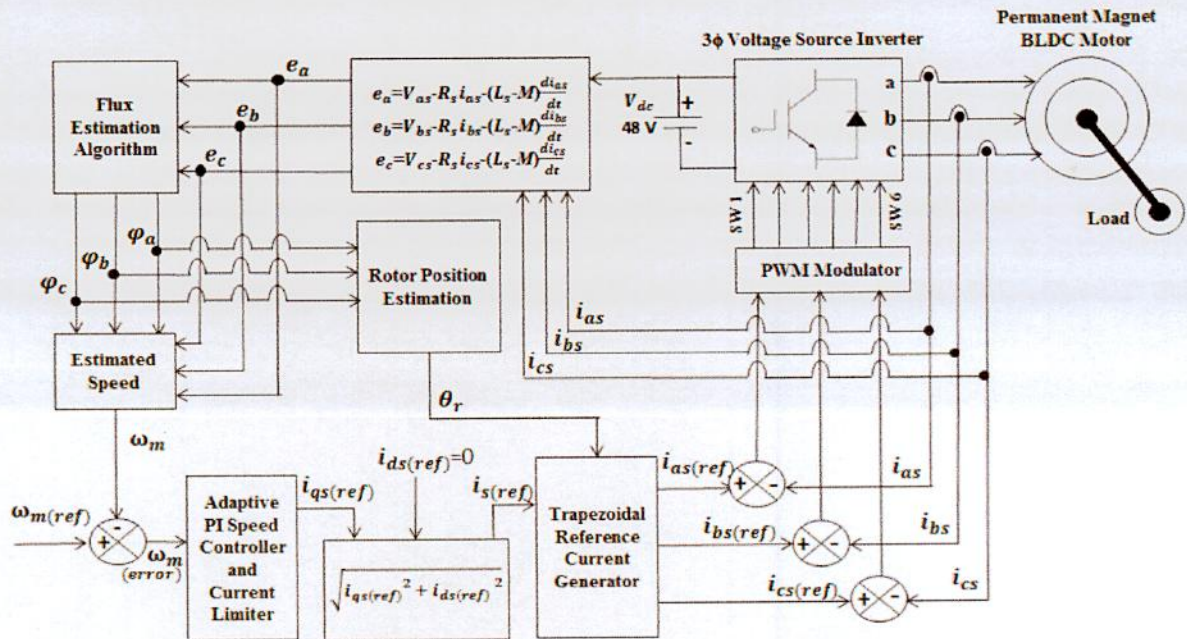


Fig. 6.1: Block diagram of high performance trapezoidal current fed field oriented PMBLDC motor drive without rotor position or speed sensor (Based on Algorithm 1)

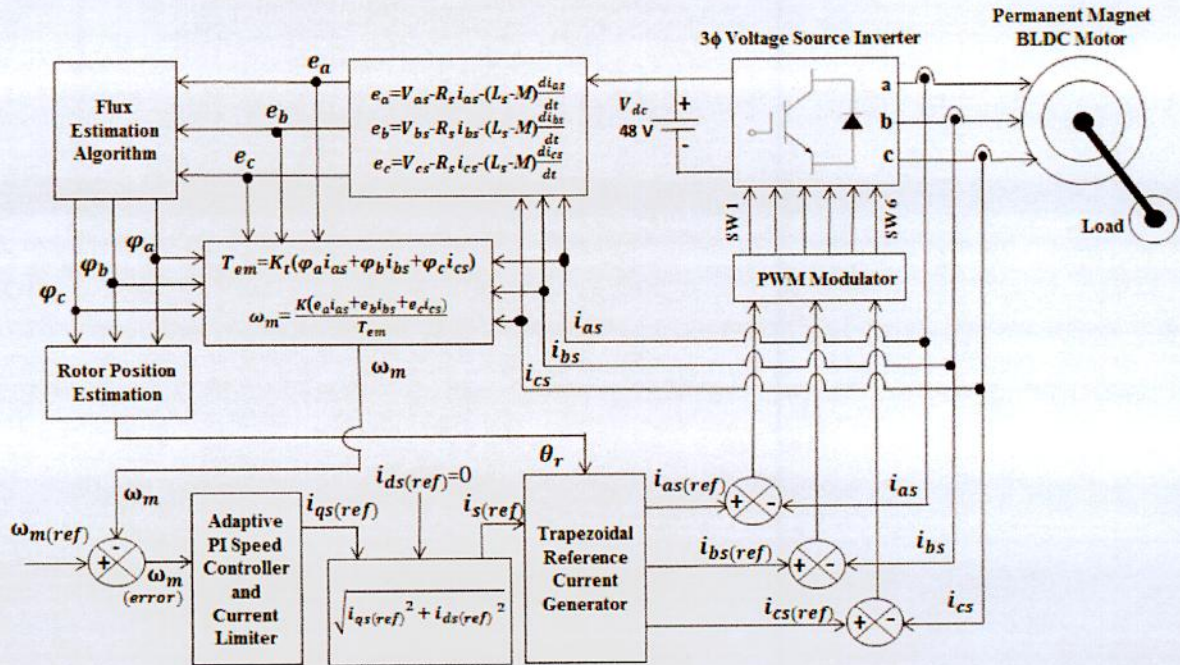


Fig. 6.2: Block diagram of high performance trapezoidal current fed field oriented PMBLDC motor drive without rotor position or speed sensor (Based on Algorithm 2)

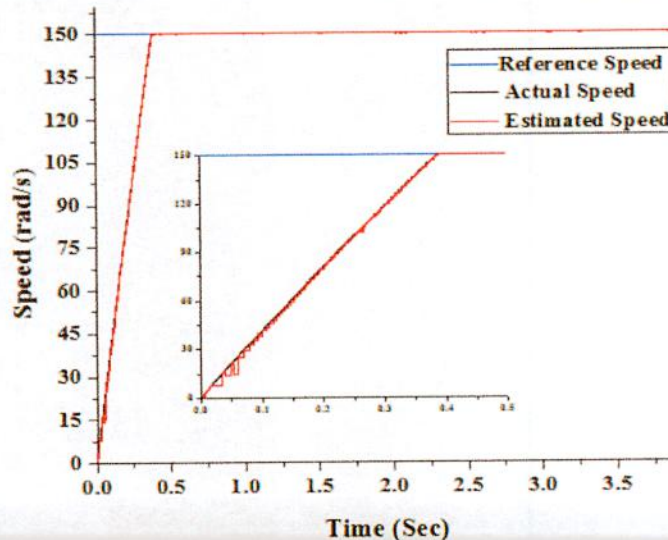
Each of these proposed control drive also consists of an adaptive PI controller, trapezoidal reference current generator, delta modulated PWM current controller, IGBT voltage source inverter, current sensors and PMBLDC motor as shown in Fig. 6.1 and Fig. 6.2. Adaptive PI controller and delta modulated PWM current controller are designed in the section 3.4.1 and 3.4.3 respectively in chapter III for field oriented vector controlled PMBLDC motor drive. Trapezoidal reference current generator block is discussed in the section 4.3.1 in chapter IV by using the Eq. (4.2-4.4).

6.3 Simulation Results and Discussion

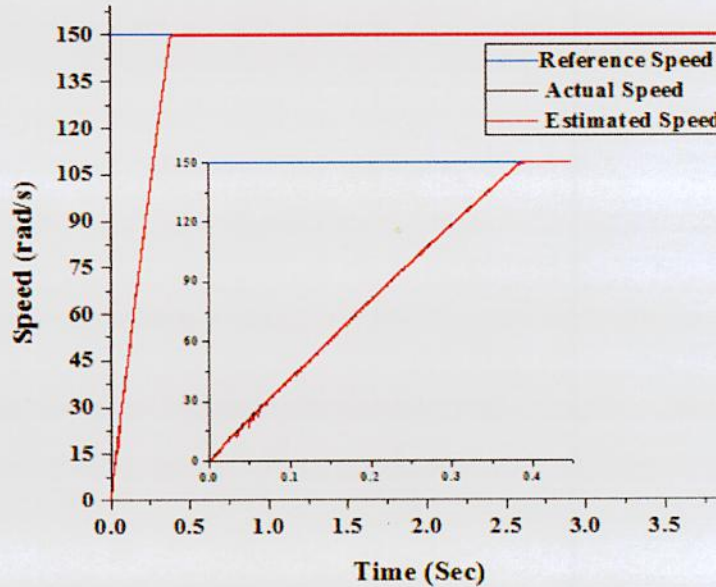
High performance trapezoidal current fed field oriented PMBLDC motor drive has been simulated in a digital computer with software written in C++ environment. The sampling time used for this simulation is 0.0000025 second. The specifications of the simulated PMBLDC motor are given in Appendix.

6.3.1 Starting Characteristics

The PMBLDC motor starts with an initial load torque 0.4 Nm. Starting speed characteristics i.e. time taken by the motor to reach its rated speed (150 rad/s) with its initial torque (0.4 Nm) for proposed algorithm 1 and algorithm 2 for trapezoidal current fed field oriented controlled drives is shown in Fig. 6.3. From Fig. 6.3, it is seen that, PMBLDC motor takes 0.39 second for both proposed algorithm 1 and algorithm 2 to gain rated speed. Trapezoidal current fed field oriented PMBLDC motor drive with position sensor also takes 0.39 second as shown Fig. 4.5 in chapter IV. Comparing Fig. 6.3(a) with Fig. 6.3(b), estimated speed sharply follows actual speed of PMBLDC motor for proposed algorithm 2. I.e. speed estimation for proposed algorithm 2 is better than the proposed algorithm 1. For both of these two cases, there exists negligible amount of speed deviation between the actual and estimated speed at the initial time of starting. Because at initial state (before 0.085 second), there exists deviation between the actual and estimated flux and rotor position as shown in Fig. 6.8 and Fig. 6.9. After 0.085 seconds estimated speed follows actual speed exactly for both proposed algorithm 1 and algorithm 2. Similar scenario is found for position sensorless field oriented PMBLDC motor drive as discussed in chapter V for both of these proposed algorithm 1 and algorithm 2. So by using proposed algorithm 1 and algorithm 2, trapezoidal reference current fed drive without position sensor can takes minimum time to reach its rated speed than square and sinusoidal reference current fed drives, because the torque handling capacity of trapezoidal reference current fed PMBLDC motor drive is greater than the other two reference current fed PMBLDC motor drives as shown in chapter IV.



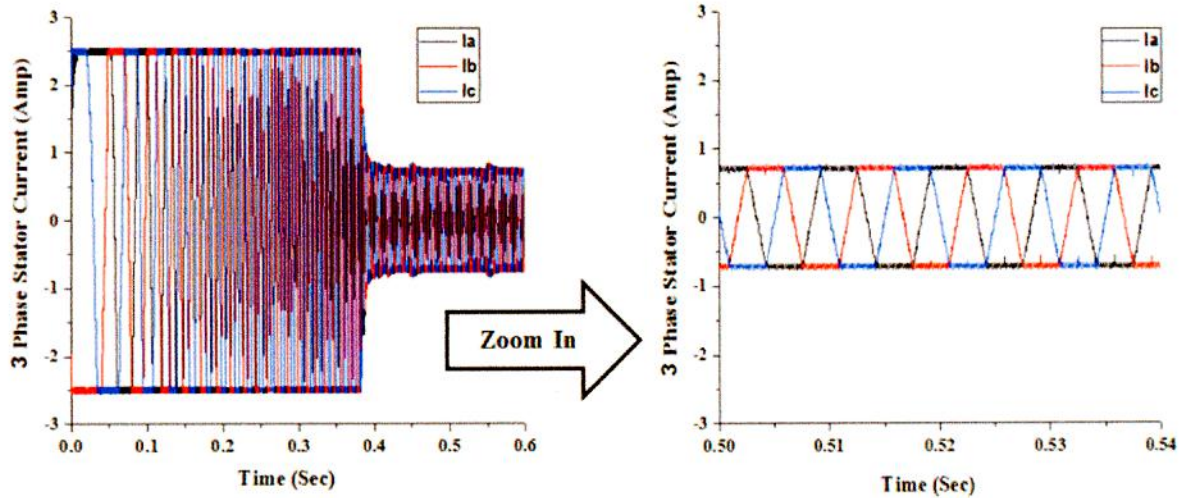
(a) For sensorless trapezoidal current fed FOC drive based on proposed algorithm 1



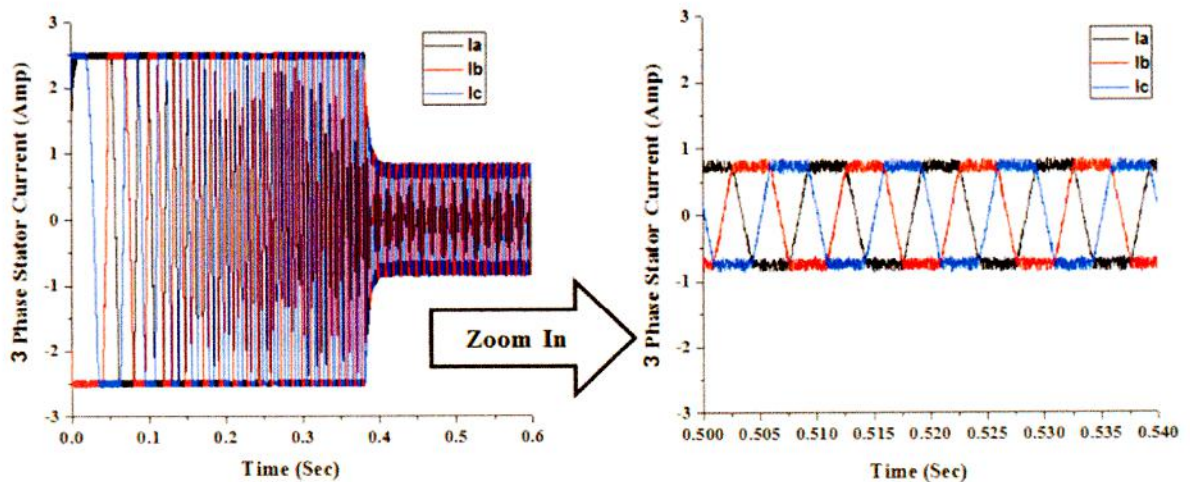
(b) For sensorless trapezoidal current fed FOC drive based on proposed algorithm 2

Fig. 6.3: Starting characteristics of PMBLDC motor drives for trapezoidal current fed field oriented control without position sensor

Phase currents of PMBLDC motor at the time of starting for vector controlled trapezoidal current fed drives both for proposed algorithm 1 and algorithm 2 for sensorless operation are depicted in Fig. 6.4. It shows that the amplitude of 3-phase current is 2.5 Amp (rated current of the motor) at the transient time of starting for these two control drives. Starting current is limited using the current limiter. Fig. 6.4 also describes that after gaining rated speed i.e. at steady state PMBLDC motor takes maximum 0.75 Amp current for both of these two position sensorless trapezoidal current fed drives for initial torque 0.4 Nm. At steady state PMBLDC motor also takes maximum 0.75 Amp current for initial torque 0.4 Nm for position sensed trapezoidal current fed drive as shown in Fig. 4.6(a) in chapter IV. From 3-phase steady state stator current as shown in Fig 6.4, there is less oscillation in stator current for proposed algorithm 1 as compared with proposed algorithm 2.



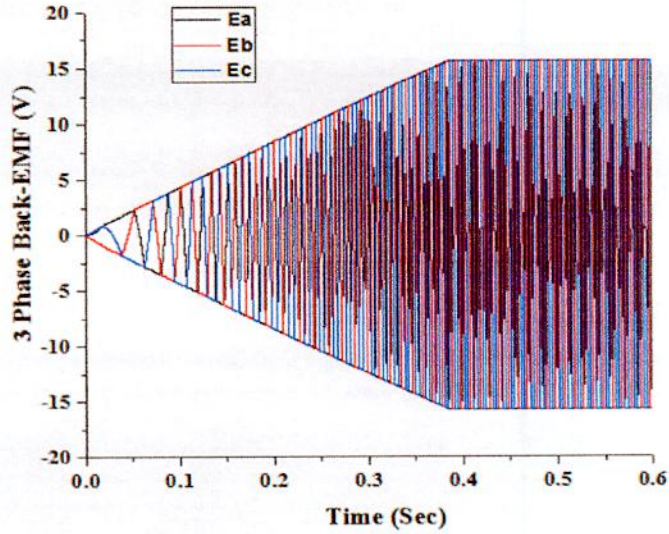
(a) For sensorless trapezoidal current fed FOC drive based on proposed algorithm 1



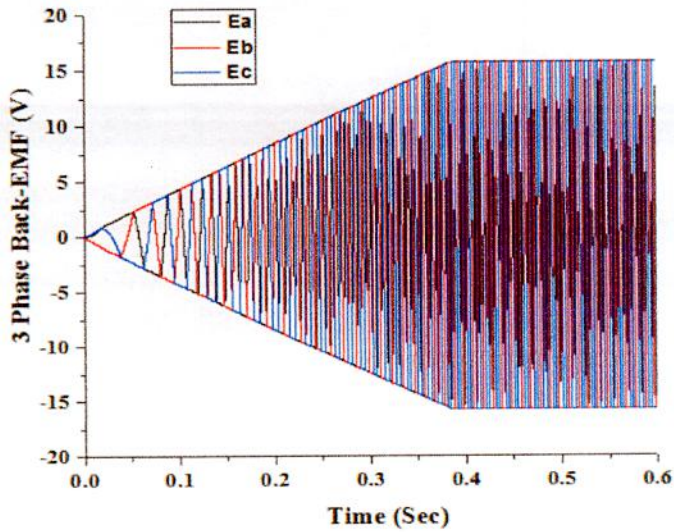
(b) For sensorless trapezoidal current fed FOC drive based on proposed algorithm 2

Fig. 6.4: 3-Phase stator current of PMSBLDC motor for high performance trapezoidal current fed field oriented control drive without position sensor

3-phase back EMF at the time of starting for field oriented trapezoidal current fed PMSBLDC drives for both proposed algorithm 1 and algorithm 2 for sensorless operation are shown in Fig. 6.5. Now the per back EMF and corresponding phase current of these two sensorless drives for steady state condition are pictured in Fig. 6.6. In Fig. 6.7, actual back EMF and corresponding calculated back EMF for algorithm 1 and algorithm 2 are depicted for comparison.

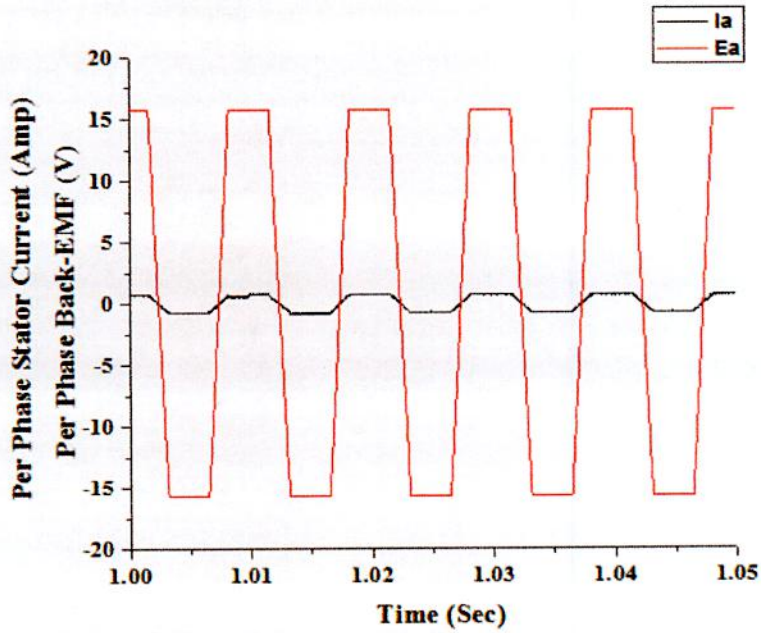


(a) For sensorless trapezoidal current fed FOC drive based on proposed algorithm 1

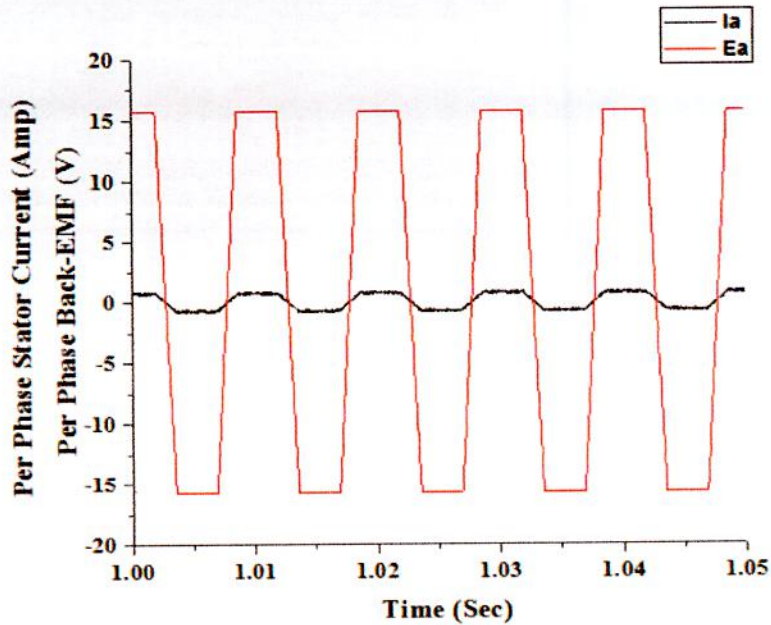


(b) For sensorless trapezoidal current fed FOC drive based on proposed algorithm 2

Fig. 6.5: 3-phase back EMF of trapezoidal current fed field oriented controlled PMSBLDC motor drive without position sensor

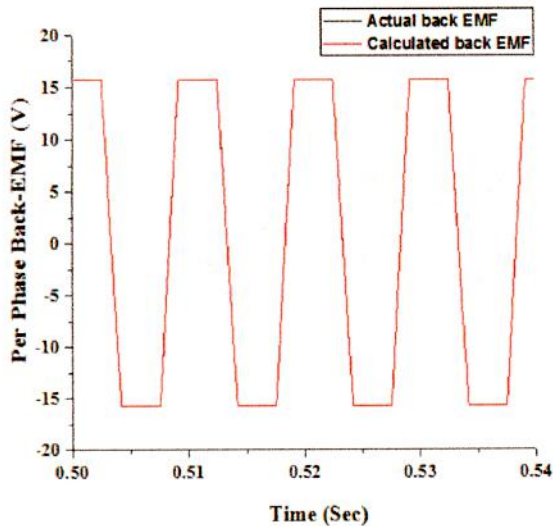


(a) For sensorless trapezoidal current fed FOC drive based on proposed algorithm 1

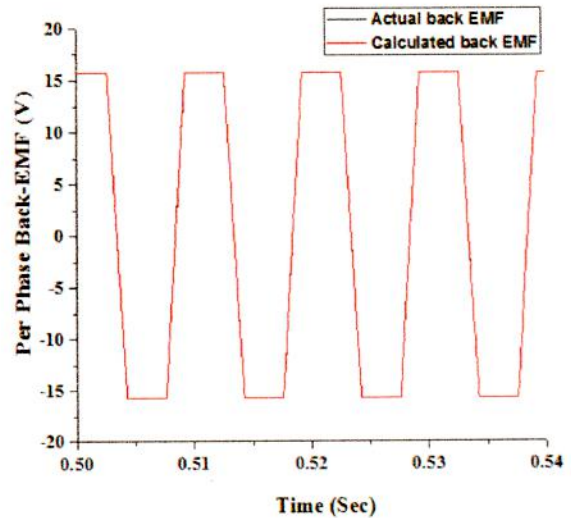


(b) For sensorless trapezoidal current fed FOC drive based on proposed algorithm 2

Fig. 6.6: Per phase back EMF and corresponding phase current for trapezoidal current fed field oriented control drives without position sensor



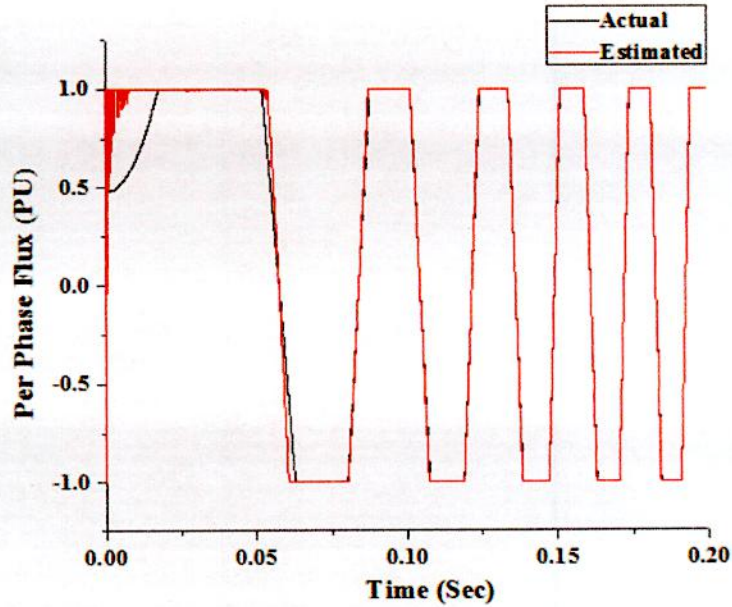
(a) For proposed algorithm 1



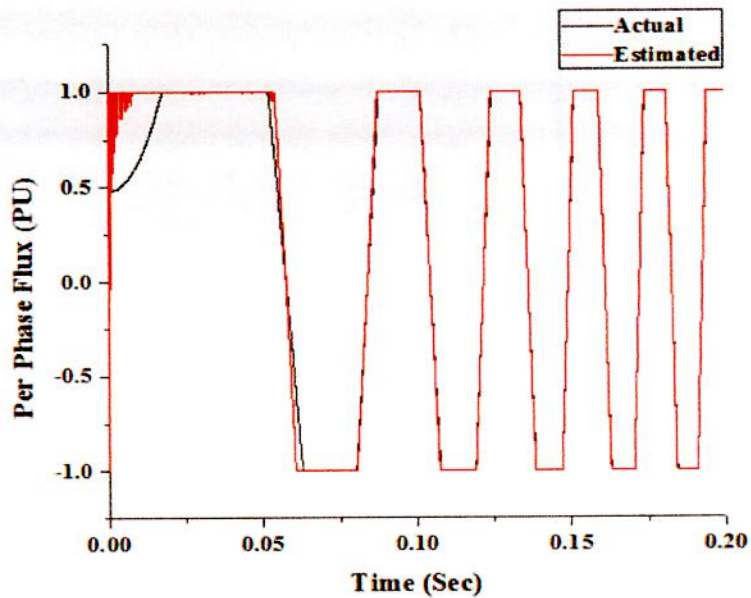
(b) For proposed algorithm 2

Fig. 6.7: Comparison of per phase actual back EMF with calculated back EMF for proposed algorithm 1 and algorithm 2 of trapezoidal current fed FOC drives without position sensor

Comparison of actual and estimated flux for sensorless trapezoidal current fed field oriented PMSM motor drives for both proposed algorithm 1 and algorithm 2 are shown in Fig. 6.8. From Fig. 6.8, it is seen that, the estimated flux for both algorithm 1 and algorithm 2 is exactly same. Because for these two algorithms, similar flux estimation block is used. From Fig. 6.8, it can be said that, at the initial time of starting of PMSM motor (before 0.085 second), there exists little mismatch between the actual flux and estimated flux. Actual and estimated rotor position for sensorless trapezoidal current fed field oriented PMSM motor drives for both proposed algorithm 1 and algorithm 2 are shown in Fig. 6.9. Since rotor positions are calculated by using the estimated flux. So, there is little misalignment between the actual and estimated rotor position at the initial time of starting as shown in Fig. 6.9. After 0.085 second, estimated flux fully traced actual flux. So, estimated rotor position can be fully matched with actual rotor position. It is one of the novelties of the proposed algorithms.

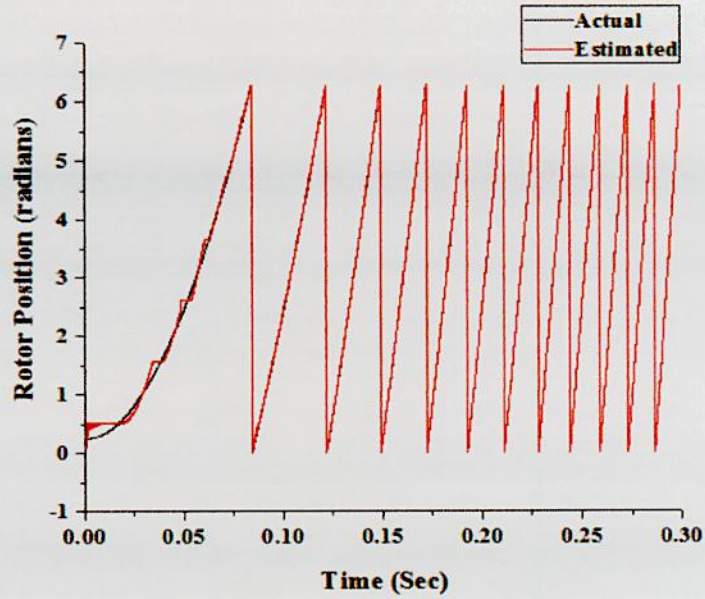


(a) For sensorless trapezoidal current fed FOC drive based on proposed algorithm 1

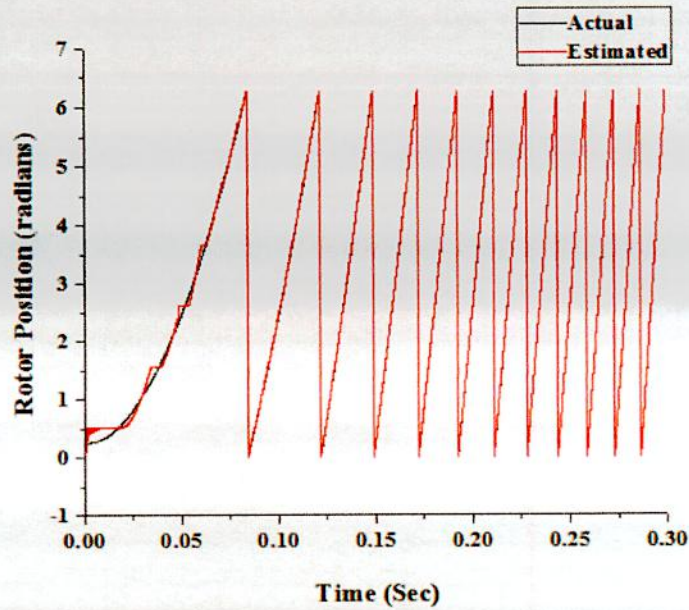


(b) For sensorless trapezoidal current fed FOC drive based on proposed algorithm 2

Fig. 6.8: Actual and estimated rotor flux for trapezoidal current fed field oriented control drives without position sensor



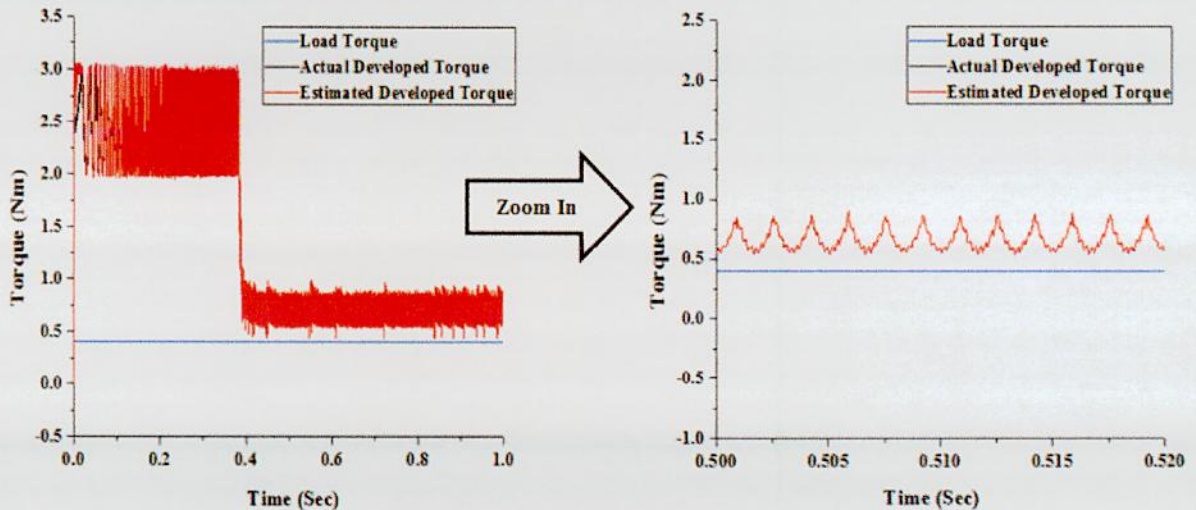
(a) For sensorless trapezoidal current fed FOC drive based on proposed algorithm 1



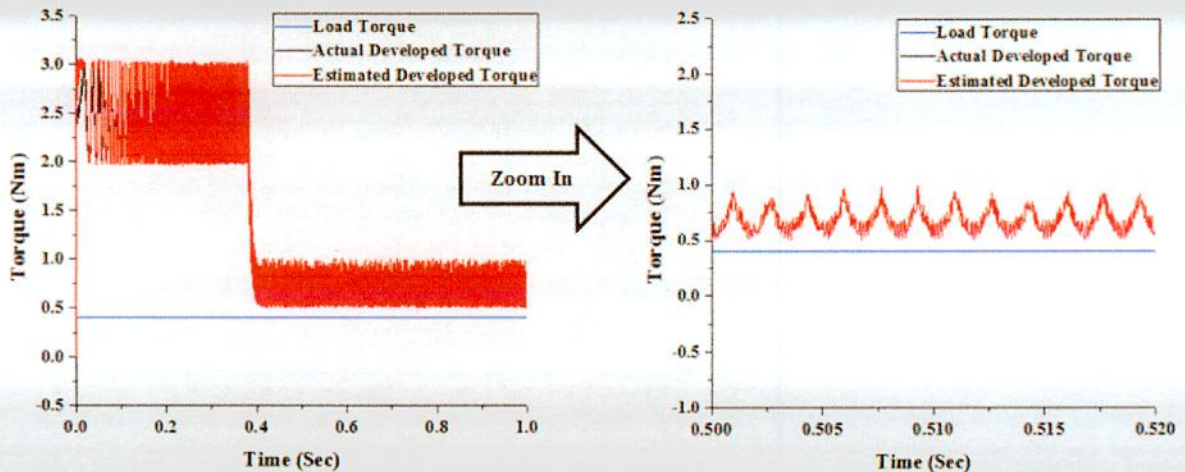
(b) For sensorless trapezoidal current fed FOC drive based on proposed algorithm 2

Fig. 6.9: Actual and estimated rotor position for trapezoidal current fed field oriented control drives without position sensor

Fig. 6.10 depicts developed electromagnetic torque in PMSM motor according to the load torque 0.4 Nm for sensorless trapezoidal current fed field oriented control drives. Fig. 6.10 also represents the comparison between the actual developed torque with the estimated developed torque. Torque estimation is done using estimated flux. This estimated developed torque is used to calculate speed of the PMSM motor for proposed algorithm 2. From Fig. 6.10, it is seen that, developed electromagnetic torque oscillates more for proposed algorithm 2 based trapezoidal current fed field oriented PMSM motor drive than algorithm 1 based drive. For both of these proposed algorithms, estimated developed torque exactly follows the actual developed torque in PMSM motor.



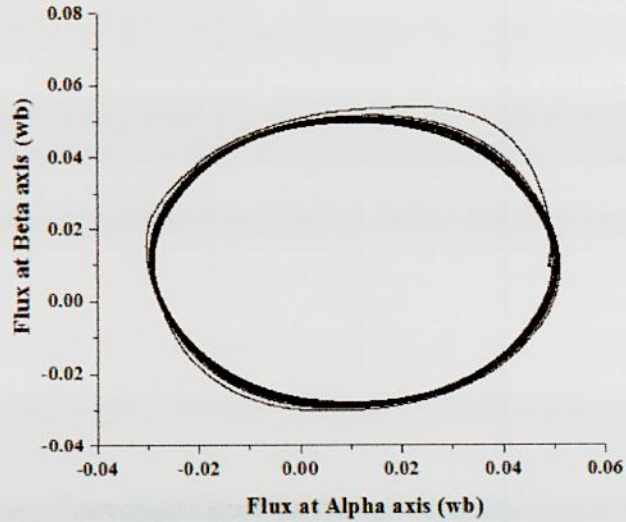
(a) For sensorless trapezoidal current fed FOC drive based on proposed algorithm 1



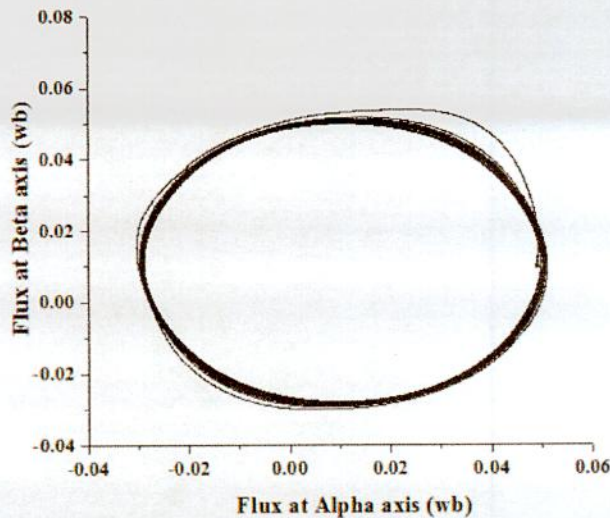
(b) For sensorless trapezoidal current fed FOC drive based on proposed algorithm 2

Fig. 6.10: Actual and estimated developed torque according to load torque for sensorless trapezoidal current fed field oriented controlled drives

In Fig. 6.11, stator flux linkage trajectories i.e. flux orientation representation in the stationary $\alpha\beta$ axes reference frame for sensorless trapezoidal current fed vector controlled PMSM motor drives are pictured both for proposed algorithm 1 and algorithm 2. These stator flux trajectories are same as the stator flux trajectory for position sensed trapezoidal current fed field oriented controlled PMSM motor drive as shown in Fig. 4.10(a) in chapter IV.



(a) For sensorless trapezoidal current fed FOC drive based on proposed algorithm 1

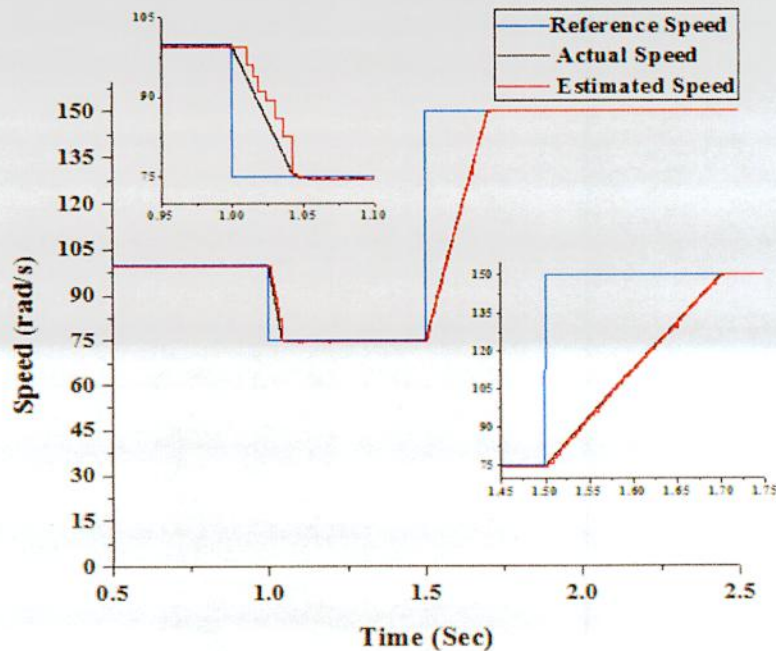


(b) For sensorless trapezoidal current fed FOC drive based on proposed algorithm 2

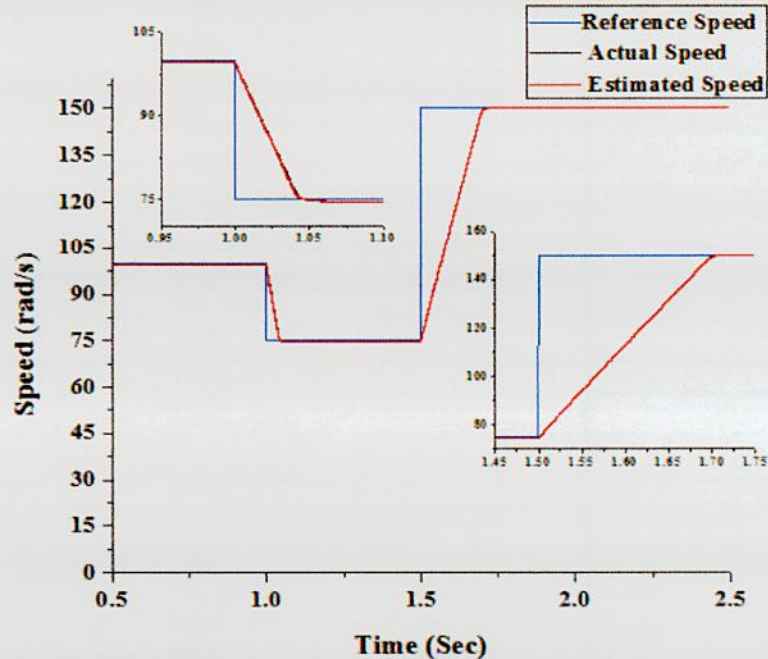
Fig. 6.11: Stator flux linkage trajectories in the stationary $\alpha\beta$ axes reference frame for sensorless trapezoidal current fed vector controlled PMSM motor drive

6.3.2 Variable Speed Characteristics

To measure the dynamic performance for these two different algorithms based high performance trapezoidal current fed field oriented PMBLDC motor drives, variable speed command is given. Motor runs at speed 100 rad/s. At 1.0 second the speed command is changed to 75 rad/s and finally at 1.5 second speed command is changed to 150 rad/s. Motor speed follows the reference speed for both proposed algorithm 1 and algorithm 2 based field oriented PMBLDC motor drive as shown in Fig. 6.12. For dynamic speed changing condition, estimated speed nearly follows the actual speed of PMBLDC motor for both the two cases. When speed command is changed to 75 rad/s from 100 rad/s with load torque 0.4 Nm, there is a small amount of mismatch between the actual speed and estimated speed for algorithm 1 at transient time interval 1.0 second to 1.05 second. When steady state occurs (after 1.05 second), estimated speed exactly traced out the actual speed of the motor as shown in subplot of Fig. 6.12(a). On the other hand, when speed command is changed to 150 rad/s from 75 rad/s, i.e. for increasing speed dynamics, estimated speed follows the actual motor speed without any mismatch. But for proposed algorithm 2 as shown in Fig. 6.12(b), there are no misalignment between the actual motor speed and estimated motor speed for both transient and steady state condition.



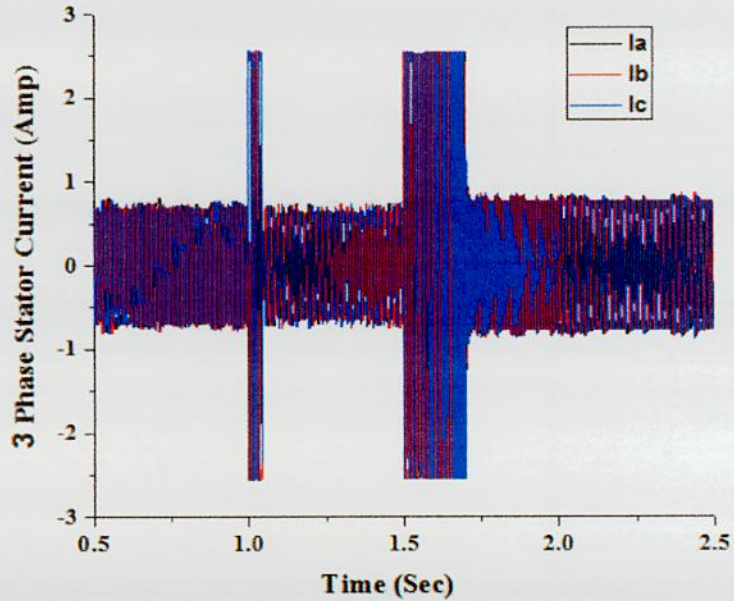
(a) For sensorless trapezoidal current fed FOC drive based on proposed algorithm 1



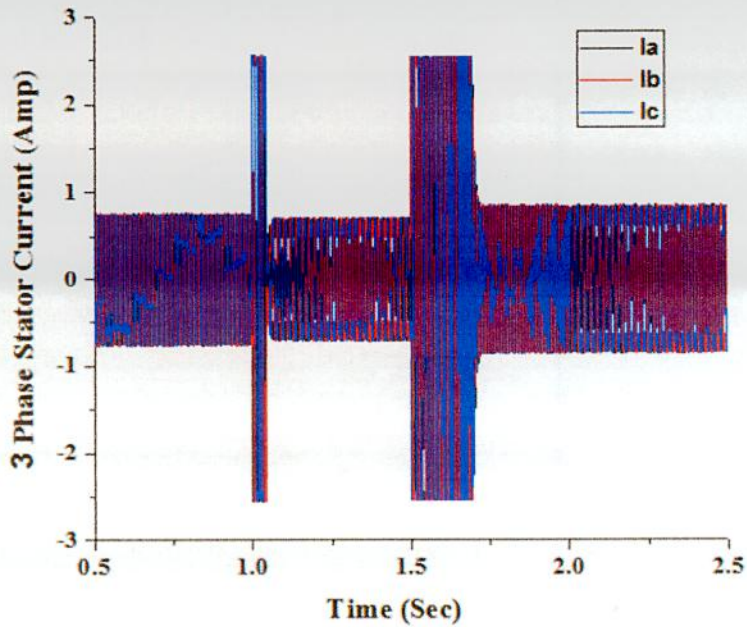
(b) For sensorless trapezoidal current fed FOC drive based on proposed algorithm 2

Fig. 6.12: Comparison between speed responses of PMBLDC motor for sensorless trapezoidal current fed vector controlled drives at dynamic speed changing condition

From 3-phase stator current curve for variable speed condition for two different proposed algorithm as shown in Fig. 6.13, it is seen that, at 1.0 second when the reference speed changes from 100 rad/s to 75 rad/s, there exists no high value of transient current beyond the limit of rated current (2.5 Amp) and no undershoot from reference speed for both algorithm 1 and algorithm 2 for sensorless operation. Besides there is no overshoot at 1.5 second, when the reference speed goes to 150 rad/s from 75 rad/s. Condition of back EMF at the time of variable speed change for sensorless trapezoidal current fed field oriented control drives are shown in Fig. 6.14.



(a) For sensorless trapezoidal current fed FOC drive based on proposed algorithm 1



(b) For sensorless trapezoidal current fed FOC drive based on proposed algorithm 2

Fig. 6.13: 3-phase current of PMBLDC motor for sensorless trapezoidal current fed field oriented controlled drive for variable speed condition considering transient current at the interface of speed changes

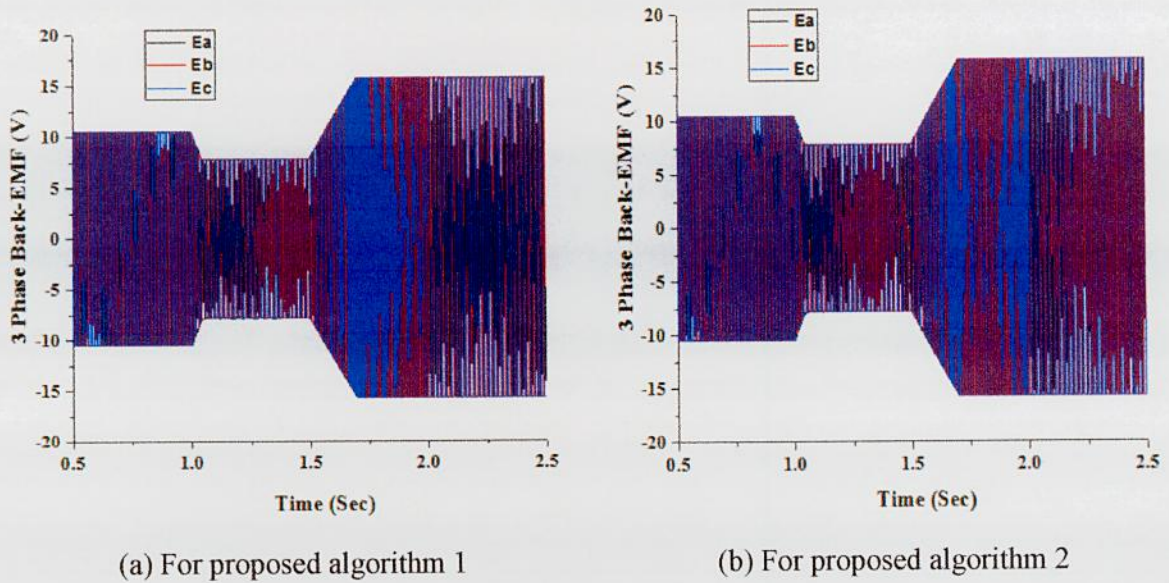
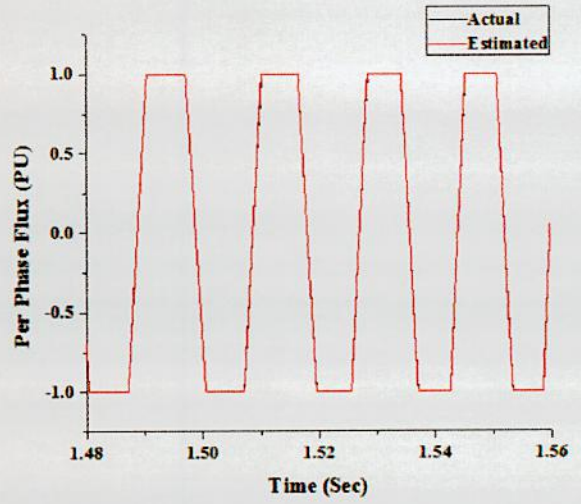
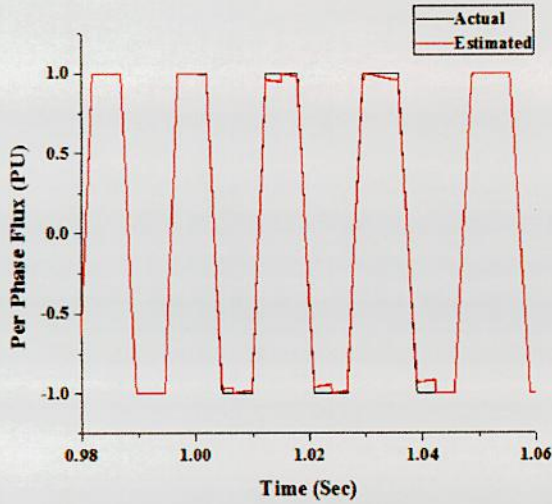
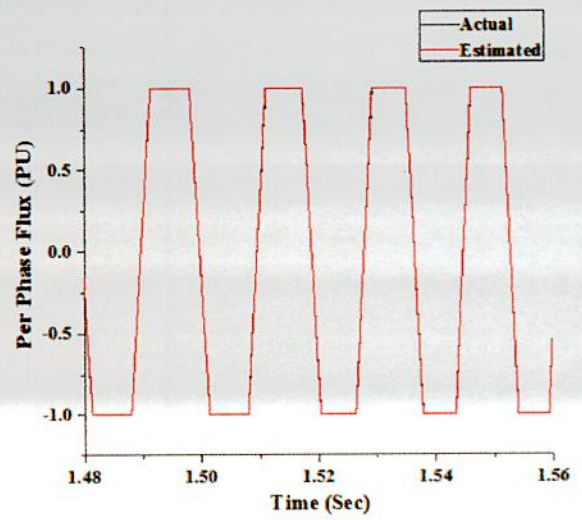
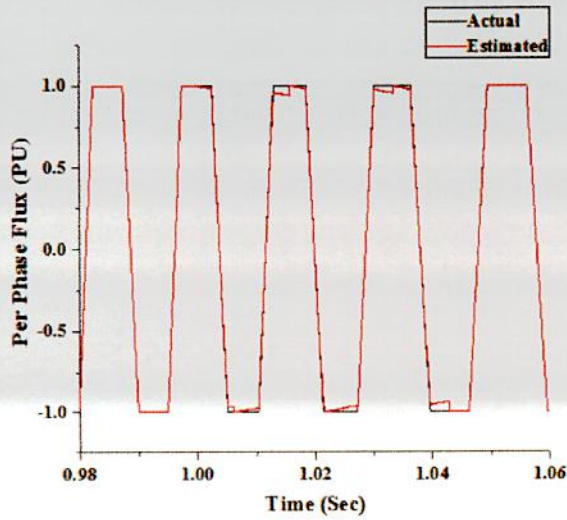


Fig. 6.14: 3-phase back EMF at dynamic speed changing condition for trapezoidal current fed vector controlled PMLDLC motor drive without position sensor

Condition of actual and estimated flux at variable speed changing interface for sensorless trapezoidal current fed drives are shown in Fig. 6.15. When speed command changes from 100 rad/s to 75 rad/s, i.e. for decreasing speed condition, there is very small mismatch between actual and estimated flux for both of these two proposed algorithms. When speed command changes from 75 rad/s to 150 rad/s, i.e. for increasing motor speed transient condition, there is no mismatch between actual and estimated flux for both of these two proposed algorithms as shown in Fig. 6.15. Comparison of actual and estimated rotor position at variable speed changing interface for sensorless trapezoidal current fed drives are illustrated in Fig 6.16. Since rotor position of the motor is estimated using estimated flux linkage. So, estimated rotor position shows the similar behavior as described for estimated flux.

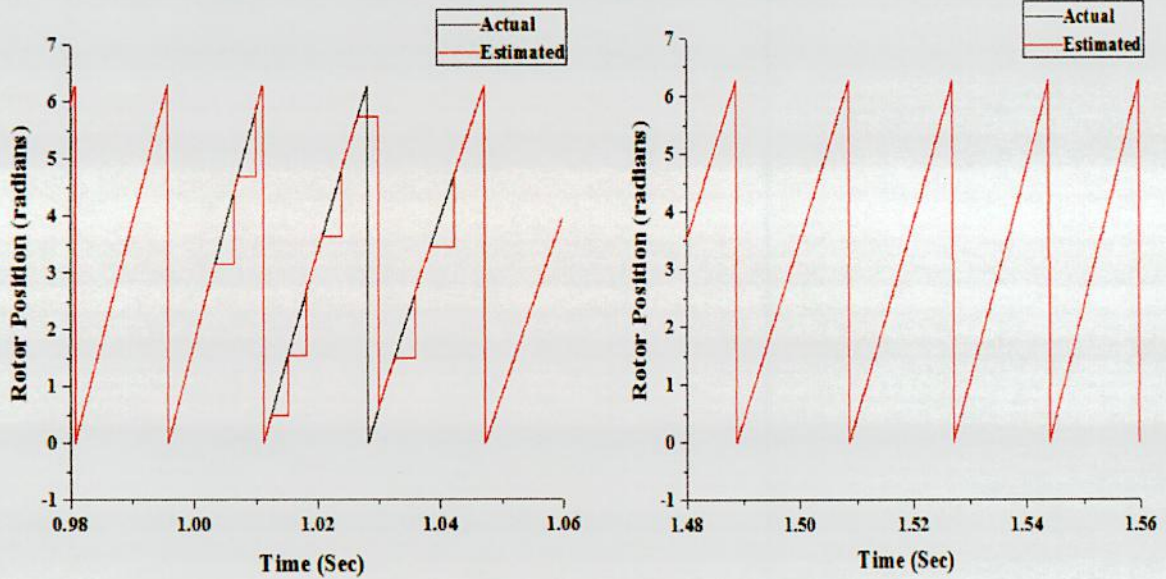


(a) For sensorless trapezoidal current fed FOC drive based on proposed algorithm 1

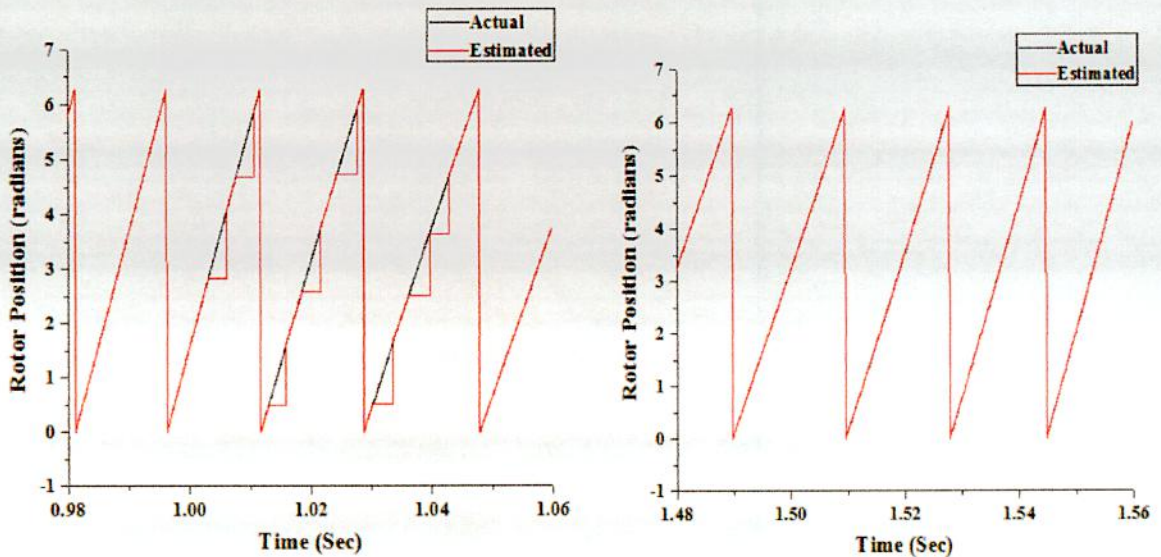


(b) For sensorless trapezoidal current fed FOC drive based on proposed algorithm 2

Fig. 6.15: Actual and estimated rotor flux in per unit value at dynamic speed changing condition for trapezoidal current fed field oriented PMSBLDC motor drive without position sensor



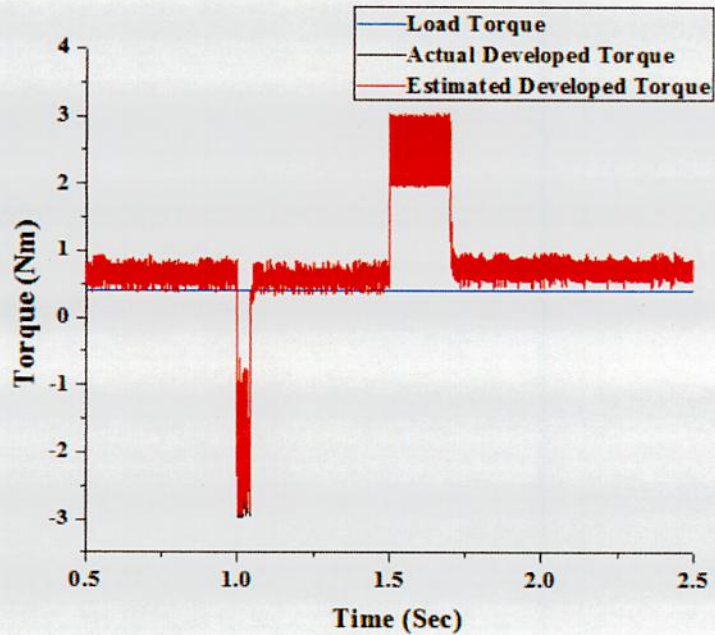
(a) For sensorless trapezoidal current fed FOC drive based on proposed algorithm 1



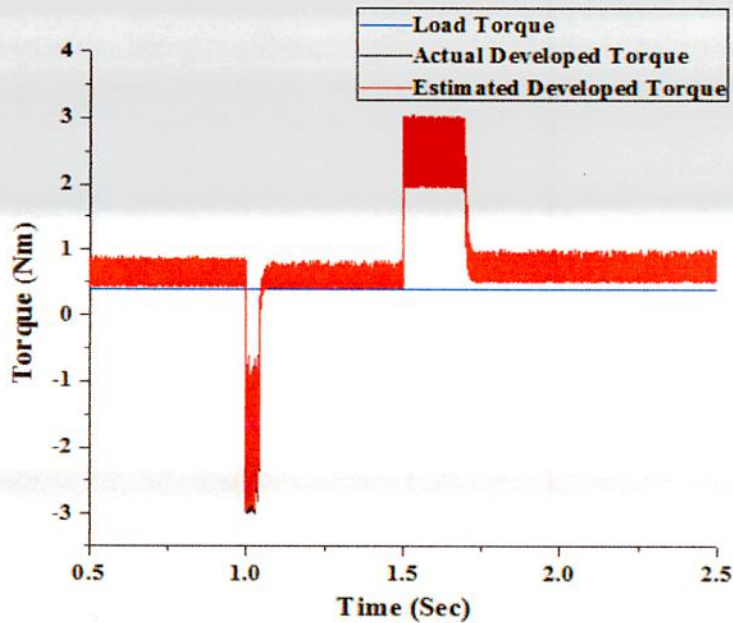
(b) For sensorless trapezoidal current fed FOC drive based on proposed algorithm 2

Fig. 6.16: Actual and estimated rotor position at dynamic speed changing condition for trapezoidal current fed field oriented PMBLDC motor drive without position sensor

The scenario of actual and estimated developed electromagnetic torque according to the response of load torque 0.4 Nm at dynamic speed changing condition for sensorless operation of trapezoidal current fed field oriented PMBLDC motor drives for both proposed algorithm 1 and algorithm 2 are shown in Fig. 6.17.



(a) For sensorless trapezoidal current fed FOC drive based on proposed algorithm 1

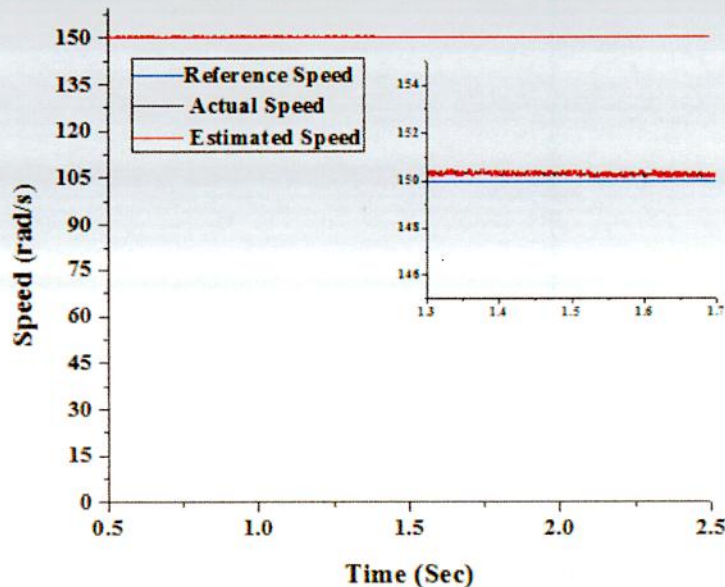


(b) For sensorless trapezoidal current fed FOC drive based on proposed algorithm 2

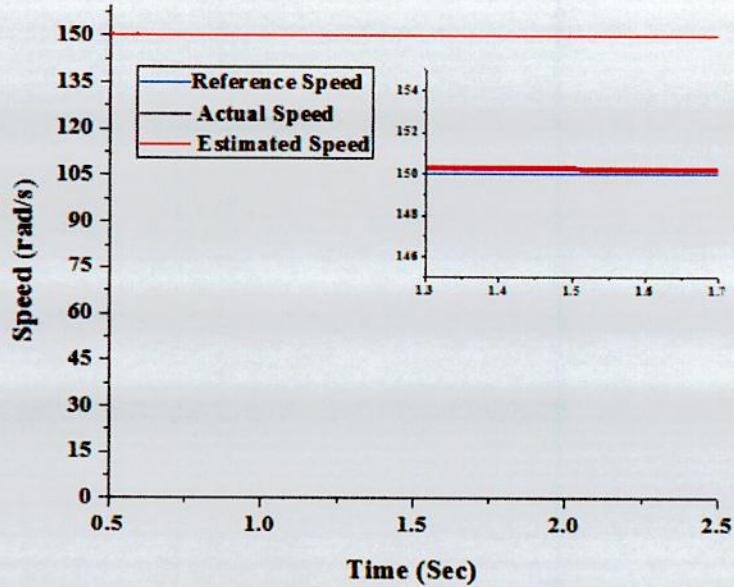
Fig. 6.17: Actual and estimated developed electromagnetic torque according to the response of load torque at dynamic speed changing condition for trapezoidal current fed vector controlled PMBLDC motor drives without position sensor

6.3.3 Motor Characteristics due to Load Torque Change

Now performance of position sensorless trapezoidal current fed vector controlled PMBLDC motor drives are determined under the condition of load torque change. At first motor runs at 150 rad/s rated speed with initial load torque 0.4 Nm. At time 1.5 second motor is loaded with load torque 2.0 Nm. At that condition sensorless trapezoidal current fed drives for both the proposed algorithm 1 and algorithm 2 can sustain motor speed to its rated value 150 rad/s as shown in Fig. 6.18. In chapter IV, it is shown that, by using trapezoidal current fed drive, the maximum load torque handling capacity of a specified PMBLDC motor can be increased 25% than the conventional 120° conduction square current fed drive. From Fig. 6.18, it can be said that, the maximum load torque handling capacity of a specified PMBLDC motor can also be possible to increase 25% using trapezoidal current fed drive without rotor position or speed sensor. Fig. 6.18 depicts that, there is no change in speed characteristic at the time 1.5 second when the motor is loaded with rated load torque 2.0 Nm. Both actual and estimated motor speed sharply follows the given reference speed command. Maximum load torque have to be given to the trapezoidal current fed field oriented PMBLDC motor drive without hampering the system stability is 2.0 Nm for both of these two proposed algorithms. I.e. when trapezoidal current fed drive is used to control the specified PMBLDC motor (From Appendix), the maximum torque generating capacity is increased to 2.0 Nm by keeping the maximum current of the PMBLDC motor to its rated value 2.5 Amp.



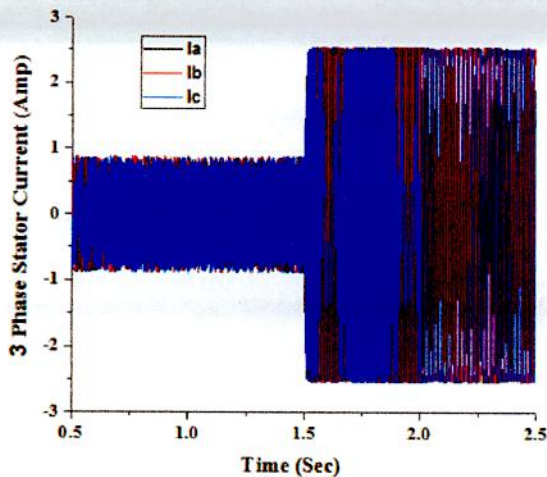
(a) For sensorless trapezoidal current fed FOC drive based on proposed algorithm 1



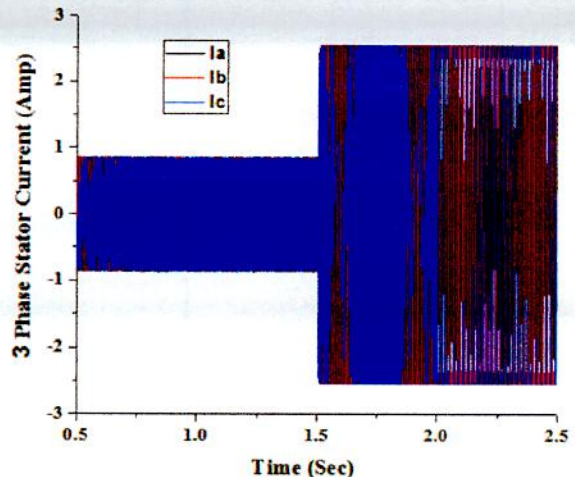
(b) For sensorless trapezoidal current fed FOC drive based on proposed algorithm 2

Fig. 6.18: Speed characteristics of PMLDLC motor for sudden load torque change at 1.5 second from initial load torque 0.4 Nm to rated load torque 2.0 Nm for sensorless trapezoidal current fed field oriented control drives

From graphical representation of 3-phase stator current for sudden load torque change of sensorless trapezoidal current fed field oriented control drives as shown in Fig. 6.19, it summarizes that, though 2.0 Nm load torque is applied, stator current remains within the rated current (2.5 Amp) limit.



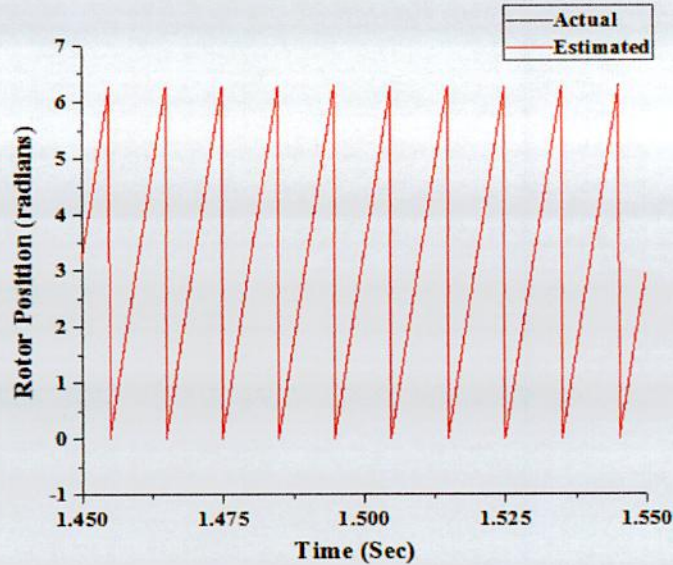
(a) For proposed algorithm 1



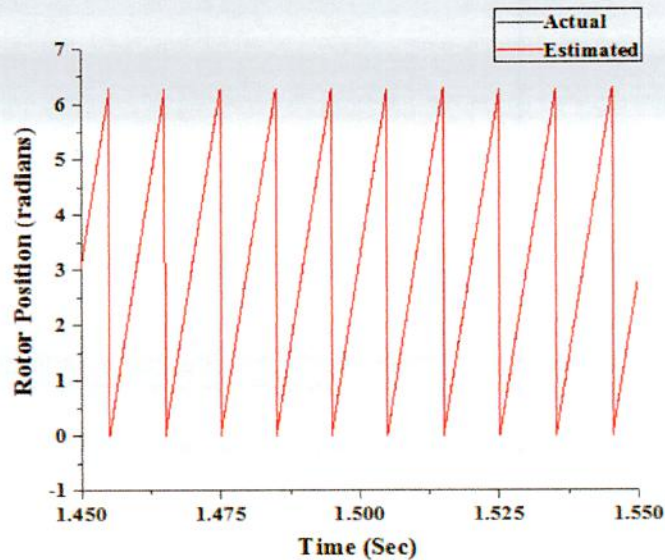
(b) For proposed algorithm 2

Fig. 6.19: 3-phase stator current of sensorless trapezoidal current fed field oriented PMLDLC motor drives for sudden load torque change at 1.5 second

Rotor position of sensorless trapezoidal current fed field oriented PMLDC motor drives for sudden load torque change at 1.5 second are pictured in Fig. 6.20. At the time 1.5 second when the motor is loaded with rated torque 2.0 Nm, there is no difference between the actual and estimated rotor position for both proposed algorithm 1 and algorithm 2.



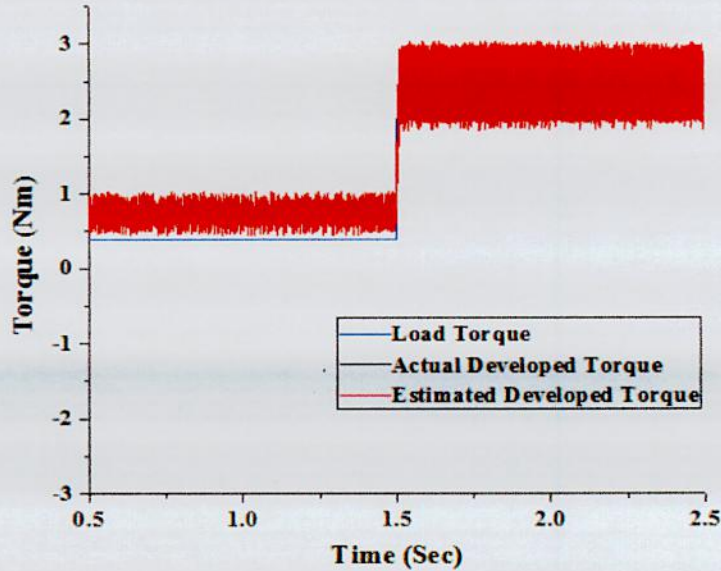
(a) For sensorless trapezoidal current fed FOC drive based on proposed algorithm 1



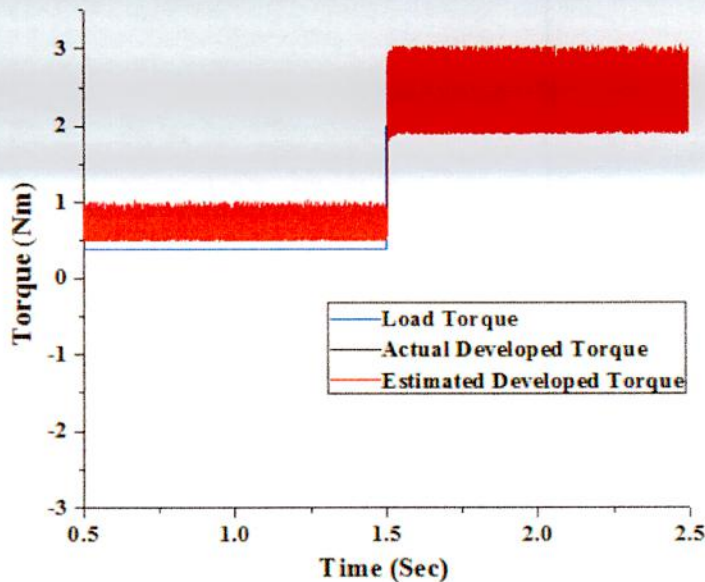
(b) For sensorless trapezoidal current fed FOC drive based on proposed algorithm 2

Fig. 6.20: Comparison of actual and estimated rotor position of sensorless trapezoidal current fed field oriented PMLDC motor drives for sudden load torque change at 1.5 second

The scenario of actual and estimated developed electromagnetic torque according to the response of dynamic load torque change for sensorless operation of trapezoidal current fed field oriented PMBLDC motor drives for both proposed algorithm 1 and algorithm 2 are shown in Fig. 6.21.



(a) For sensorless trapezoidal current fed FOC drive based on proposed algorithm 1



(b) For sensorless trapezoidal current fed FOC drive based on proposed algorithm 2

Fig. 6.21: Actual and estimated developed electromagnetic torque according to the response of dynamic load torque change for trapezoidal current fed field oriented PMBLDC motor drives without position sensor

6.4 Conclusion

High performance trapezoidal current fed field oriented vector controlled delta modulated PMBLDC motor drives based on algorithm 1 and algorithm 2 for sensorless operation are designed in this chapter. Estimated speed sharply follows actual speed of PMBLDC motor for proposed algorithm 2. Speed estimation for proposed algorithm 2 is better than the proposed algorithm 1. For both of these two cases, there exists negligible amount of speed deviation between the actual and estimated speed at the initial time of starting. Because speed of the motor is estimated by using estimated rotor flux linkage and there exists deviation between the actual and estimated flux at initial starting transient time (before 0.085 second). Expect initial starting time error (before 0.085 second), estimated flux exactly traced out the actual flux linkage of the PMBLDC motor for both algorithm 1 and algorithm 2, i.e. the performance of flux estimation algorithm is very good. Similar to the estimated flux, there is no mismatch between actual and estimated rotor position excluding the initial starting time error. So, the performance of rotor position estimator is satisfactory. There is less oscillation in stator phase current currents and developed electromagnetic torque for proposed algorithm 1 than algorithm 2. Considering this point of view, algorithm 1 is better than algorithm 2. This chapter mainly presents how to increase the load torque handling capacity of field oriented PMBLDC motor drives only by changing the reference current of a current fed delta modulated inverter without rotor position sensor. In this chapter approach to enhance the torque handling capacity, approach for position sensorless operation and approach for field oriented control are incorporated in a single PMBLDC motor drive to make a most high performance system. All advantages of these three strategies are present in this high performance PMBLDC motor drive.

By considering both transient and steady state characteristics, it is clear that, the performance of these sensorless trapezoidal current fed field oriented PMBLDC motor drives for both algorithm 1 and algorithm 2 are similar to sensed trapezoidal current fed field oriented PMBLDC motor drive. Instead of using position sensor, two different algorithms are used for sensorless operation of trapezoidal current fed field oriented PMBLDC motor drive to enhance the torque handling capacity of PMBLDC motor without exceeding the maximum current rating of the motor.

Chapter VII

Direct Torque Control of PMBLDC Motor without Position Sensor

Chapter Outlines:

7.1 Introduction

7.2 Conventional DTC Drive Using Two Phase Conduction Mode

7.3 Novel Position Sensorless DTC Drive Using Two Phase Conduction Mode

7.4 Simulation Results and Discussion

7.5 Conclusion

7.2 Conventional DTC Drive Using Two Phase Conduction Mode

The key issue in the conventional DTC of a PMBLDC motor drive in the constant torque region is to estimate the electromagnetic torque correctly. For a PMBLDC motor the back-EMF waveform is trapezoidal, therefore irrelevant to conducting mode (two or three-phase), Eq. 7.1 should be used for the electromagnetic torque calculation in the stationary reference frame.

$$T_{em} = \frac{3P}{2} \left[\frac{d\varphi_{\alpha r}}{d\theta_r} i_{\alpha s} + \frac{d\varphi_{\beta r}}{d\theta_r} i_{\beta s} \right] = \frac{3P}{2} \left[\frac{e_{\alpha}}{\omega_r} i_{\alpha s} + \frac{e_{\beta}}{\omega_r} i_{\beta s} \right] \quad (7.1)$$

where P is the number of poles, θ_r is the electrical rotor angle, ω_r is the electrical rotor speed, and $\varphi_{\alpha r}$, $\varphi_{\beta r}$, e_{α} , e_{β} , $i_{\alpha s}$, $i_{\beta s}$ are the stationary reference frame ($\alpha\beta$ -axes) rotor flux linkages, motor back-EMFs, and stator currents respectively. Eq. 7.2 and Eq. 7.3 describes the machine equations in $\alpha\beta$ -axes. Where $V_{\alpha s}$, $V_{\beta s}$, R_s and L_s are the $\alpha\beta$ -axes stator voltages, per phase resistance and per phase inductance respectively. The rotor flux linkages in $\alpha\beta$ -axes $\varphi_{\alpha r}$ and $\varphi_{\beta r}$ can be obtained by taking the integral of both sides of Eq. 7.2 and Eq. 7.3 as follows by Eq. 7.4 and Eq. 7.5.

$$V_{\alpha s} = R_s i_{\alpha s} + L_s \frac{di_{\alpha s}}{dt} + \frac{d\varphi_{\alpha r}}{dt} \quad (7.2)$$

$$V_{\beta s} = R_s i_{\beta s} + L_s \frac{di_{\beta s}}{dt} + \frac{d\varphi_{\beta r}}{dt} \quad (7.3)$$

$$\varphi_{\alpha r} = \varphi_{\alpha s} - L_s i_{\alpha s} \quad (7.4)$$

$$\varphi_{\beta r} = \varphi_{\beta s} - L_s i_{\beta s} \quad (7.5)$$

In which, $\varphi_{\alpha s}$ and $\varphi_{\beta s}$ are the α and β axis stator flux linkages respectively. A PMBLDC motor is operated ideally when the phase current is injected at the flat top portion of the phase-to-neutral back-EMF. The back-EMF is usually flat for 120 electrical degrees and in transition for 60 electrical degrees during each half cycle. In the constant torque region (below base speed) when the phase-to-phase back-EMF voltage is smaller than the dc bus voltage there is no reason to change the amplitude of stator flux linkage. Above base speed, however, the motor performance will significantly deteriorate because the back-EMF exceeds the dc bus voltage, and the stator inductance X_s will not allow the phase current to develop quickly enough to catch up to the flat top of the trapezoidal back-EMF. Beyond the base speed, the desired torque cannot be achieved unless other techniques such as phase advancing, 180 degree conduction etc. are used. Operation of the DTC of a BLDC motor above the base speed is not in the scope of this chapter.

Conventional two-phase conduction quasi-square wave current control causes the locus of the stator flux linkage to be unintentionally kept in hexagonal shape if the unexcited open phase back-EMF effect and the free-wheeling diodes are neglected, as shown in Fig. 7.1 with dashed lines. If the freewheeling diode effect which is caused by commutation is ignored, more circular flux trajectory can be obtained similar to a PMSM drive.

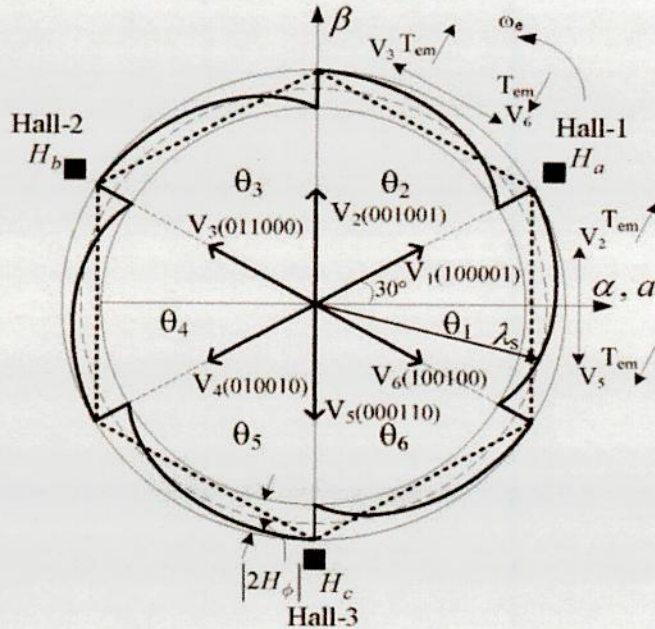


Fig. 7.1: Actual (solid-line) and ideal (dashed-line) stator flux linkage trajectories, representation of two-phase voltage space vectors, and placement of the three hall-effect sensors in the stationary $\alpha\beta$ -axes reference frame [46]

When conventional two-phase PWM current control is used, sharp dips occur at every 60 electrical degrees in the stator flux linkage trajectory. This is due to the operation of the freewheeling diodes. The same phenomenon has been noticed when the DTC scheme for a PMLDLC motor is used, as shown in Fig. 7.1 with solid lines. Due to the sharp dips in the stator flux linkage space vector at every commutation and the tendency of the currents to match with the flat top part of the phase back-EMF for smooth torque generation, there is no easy way to control the stator flux linkage amplitude. On the other hand, rotational speed of the stator flux linkage can be easily controlled and therefore fast torque response is obtained. The size of the sharp dips is quite unpredictable. The best way to control the stator flux linkage amplitude is to know the exact shape of it, but it is considered too cumbersome in the constant torque region. Therefore, in the DTC of a PMLDLC motor drive with two-phase conduction scheme, the flux error, φ_{error} in the voltage vector selection look-up table is always selected as zero and only the torque error, τ is used depending on the error level of the actual torque from the reference torque. If the reference torque is bigger than the actual torque, within the hysteresis bandwidth, the torque error τ is defined as "1", otherwise it is "-1", as shown in Table 7.1.

Table 7.1: Two-phase voltage vector selection for PMBLDC motor

τ	θ_r					
	θ_1	θ_2	θ_3	θ_4	θ_5	θ_6
1	V_2 (001001)	V_3 (011000)	V_4 (010010)	V_5 (000110)	V_6 (100100)	V_1 (100001)
-1	V_5 (000110)	V_6 (100100)	V_1 (100001)	V_2 (001001)	V_3 (011000)	V_4 (010010)

A change in the torque can be achieved by keeping the amplitude of the stator flux linkage constant and increasing the rotational speed of the stator flux linkage as fast as possible. This allows a fast torque response to be achieved. It is shown in this section that the rotational speed of the stator flux linkage can be controlled by selecting the proper voltage vectors while keeping the flux amplitude almost constant, in other words eliminating the flux control.

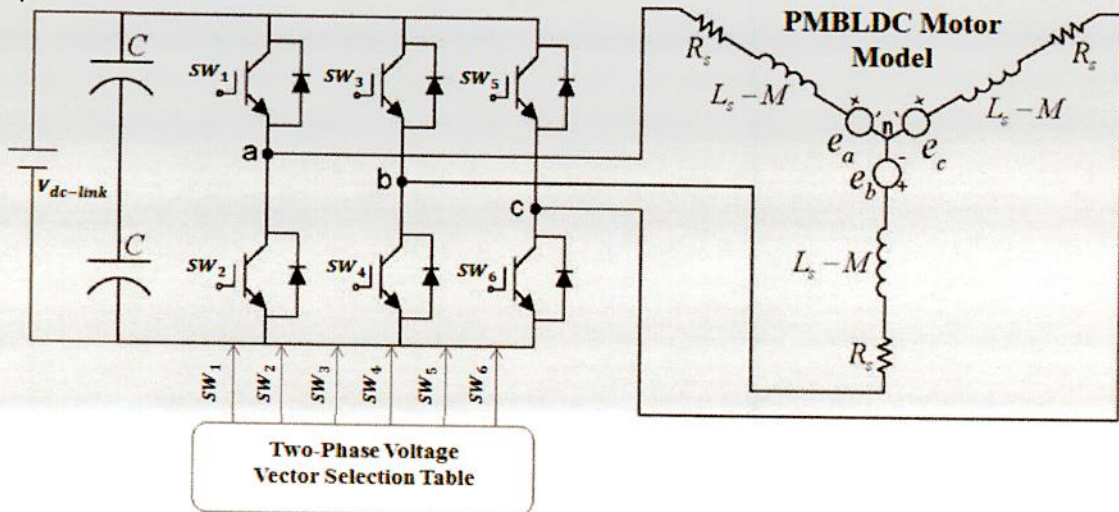


Fig. 7.2: Two-phase switching states of the inverter voltage space vectors for a PMBLDC motor

When the primary symmetric windings are fed by an inverter using two-phase conduction mode, as shown in Fig. 7.2, the primary phase voltages V_{an} , V_{bn} and V_{cn} are determined by the status of the six switches SW_1 , SW_2 , SW_3 , SW_4 , SW_5 and SW_6 . Since the upper and lower switches in a phase leg may both be simultaneously off, irrespective of the state of the associated freewheeling diodes in two-phase conduction mode, six digits are required for the inverter operation, one digit for each switch. Therefore, there is a total of six non-zero voltage vectors and a zero voltage vector for the two-phase conduction mode which can be represented as $V_{0,1,2,\dots,6}$ (SW_1 , SW_2, \dots, SW_6), as shown in Fig. 7.1. The six nonzero vectors are 60 degrees electrically apart from each other, as depicted in Fig. 7.1, but 30 electrical degrees phase shifted from the corresponding three-phase voltage vectors which are used in DTC of a PMSM drive. The overall

block diagram of the closed-loop DTC scheme of a PMBLDC motor drive in the constant torque region is represented in Fig. 7.3.

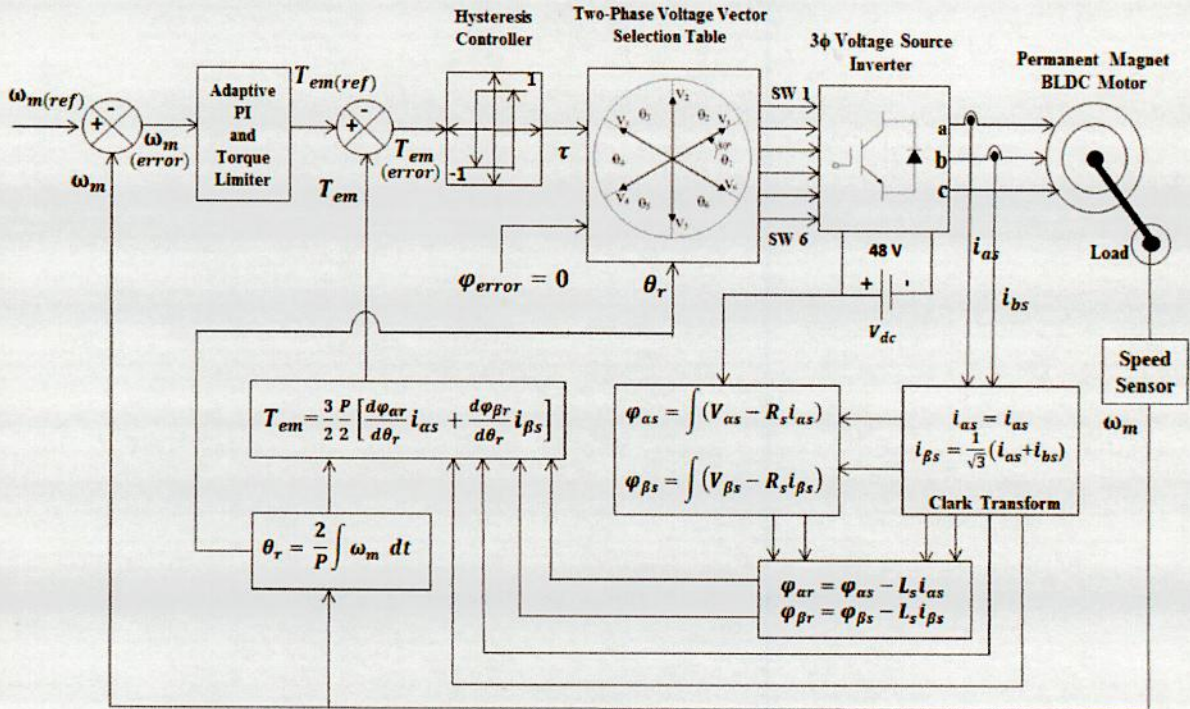


Fig. 7.3: Block diagram of conventional two phase conduction direct torque controlled PMBLDC motor drive

In the two-phase conduction mode the shape of stator flux linkage trajectory is ideally expected to be hexagonal, as illustrated with dashed-lines in Fig. 7.1. However, the influence of the unexcited open-phase back-EMF causes each straight side of the ideal hexagonal shape of the stator flux linkage locus to be curved and the actual stator flux linkage trajectory tends to be more circular in shape, as shown in Fig. 7.1 with solid lines. In addition to the sharp changes, curved shape in the flux locus between two consecutive commutations complicates the control of the stator flux linkage amplitude because it depends on the size of the sharp dips and the depth of the change may vary with sampling time, dc-link voltage, hysteresis bandwidth, motor parameters especially the phase inductance, motor speed, snubber circuit, and the amount of load torque. Generally, to achieve torque estimation for trapezoidal PMBLDC motor, Eq. 7.1 is used.

Hall-effect position sensors or speed sensors are most important components of this two phase conduction DTC drive. But misalignments in position sensors, running in extreme ambient conditions, or electromagnetic interference introduce error in the position information. Moreover, there are some constraints to the position sensors including high cost, installation difficulty of mechanics, and poor reliability. On the other hand, the derivative of the rotor $\alpha\beta$ axes fluxes over electrical rotor position θ_r , which is described in Eq. 7.1, will cause problems mainly due to sharp dips at every commutation point. Besides the accurate value of estimated torque greatly

depends on the resolution of the position sensor, when torque is calculated by using the $\alpha\beta$ axes motor back EMFs e_α, e_β and electrical rotor speed ω_r according to Eq. 7.1. So position or speed sensorless two phase conduction DTC scheme for PMBLDC motor is proposed in the next section.

7.3 Novel Position Sensorless DTC Drive Using Two Phase Conduction Mode

Two phase conduction direct torque control (DTC) of a PMBLDC motor drive in the constant torque region, with novel electromagnetic torque and rotor position estimator, without considering flux control is proposed as shown in Fig. 7.4. Sensorless means that, rotor position encoder or speed sensors are absent in this proposed system. No Hall sensors or optical encoders are used to detect the rotor position. The proposed control drive consists of an adaptive PI controller, Hysteresis controller, two phase voltage vector selection table, IGBT voltage source inverter, current sensors and PMBLDC motor as shown in block diagram in Fig. 7.4. There is no speed sensor or rotor position encoder and electromagnetic torque calculation blocks as needed in conventional two phase conduction DTC drive as shown Fig. 7.3. Instead of position sensors, rotor position estimation algorithm is used for the detection of rotor position information. Developed electromagnetic torque is also estimated using estimated rotor flux. Thus complicated electromagnetic torque calculation blocks as used in conventional DTC drive can be avoided for this proposed sensorless two phase conduction DTC scheme.

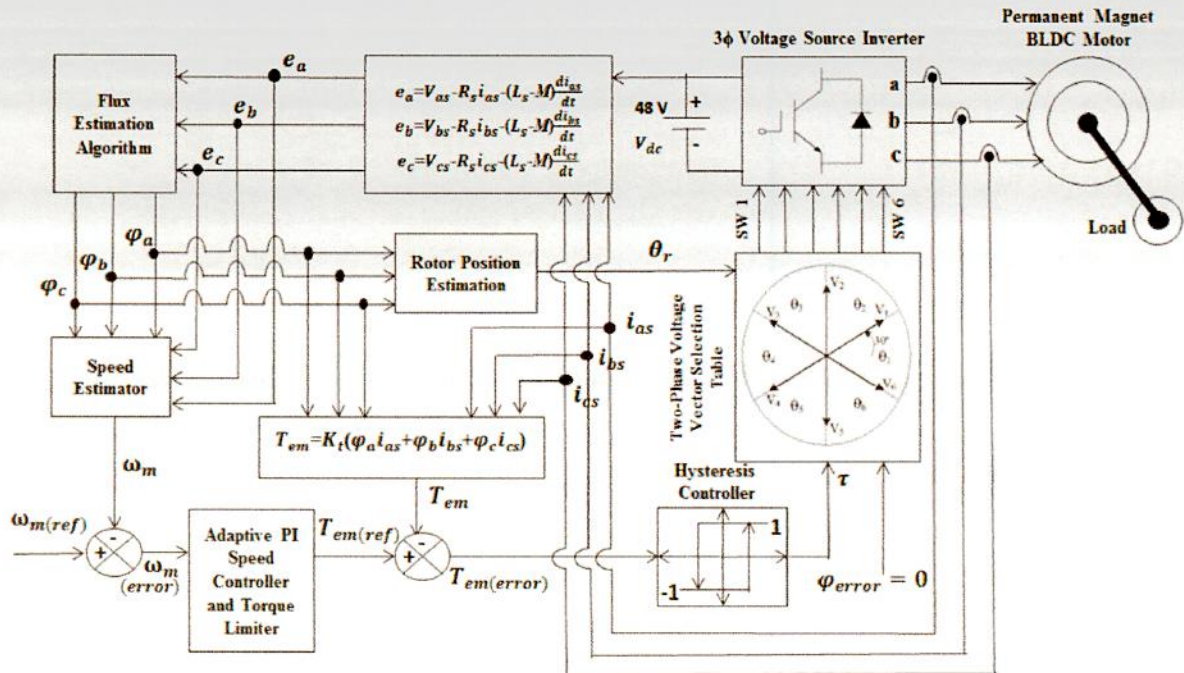


Fig. 7.4: Block diagram of two phase conduction direct torque controlled PMBLDC motor drive without rotor position or speed sensor

Novel flux estimation algorithm used in Fig. 7.4 has been discussed in the section 3.5 in chapter V. Three phase back EMF e_a , e_b , e_c have to be calculated for the flux estimation algorithm by using Eq. (7.6-7.8). Three phase flux linkage φ_a , φ_b , φ_c can be estimated by using three phase back EMF e_a , e_b , e_c according to the following algorithm as shown in Fig 5.3.

$$e_a = V_{as} - R_s i_{as} - (L_s - M) \frac{di_{as}}{dt} \quad (7.6)$$

$$e_b = V_{bs} - R_s i_{bs} - (L_s - M) \frac{di_{bs}}{dt} \quad (7.7)$$

$$e_c = V_{cs} - R_s i_{cs} - (L_s - M) \frac{di_{cs}}{dt} \quad (7.8)$$

Rotor position θ_r is estimated by using estimated flux φ_a , φ_b and φ_c according to the Table 5.1 as discussed in chapter V. At a specific time, rotor position is determined only by using estimated flux of a single phase as tabulated in Table 5.1. This phase is selected on the basis of a simple rule. At every instant flux of any two phases have constant value and flux of other phase changes with rotor position. This phase have to be chosen to determine the rotor position according to the value of flux of that phase.

Generally motor speed can be determined by the differentiation of the rotor position of a motor. But this conventional approach is not applicable for estimated rotor position of a PMBLDC motor for two phase conduction DTC drive. Because there exist oscillation in the estimated rotor position which is incorporated from oscillated stator phase currents due to the oscillation of developed electromagnetic torque. So new approach to determine motor speed has to be found out. PMBLDC motor speed can be estimated by using the estimated flux linkage φ_a , φ_b , φ_c and calculated three phase back EMF e_a , e_b , e_c according to the Table 5.2 as tabulated in chapter V. Flux of one phase and the calculated back EMF of that phase are used to determine the motor speed. Similar to the rotor position estimation, the phase has to be selected to determine the motor speed according to a rule that, the value of flux of selected phase changes with rotor position and other two phases have constant value of flux. Developed electromagnetic torque can be estimated by using estimated rotor flux φ_a , φ_b , φ_c according to Eq. 7.9.

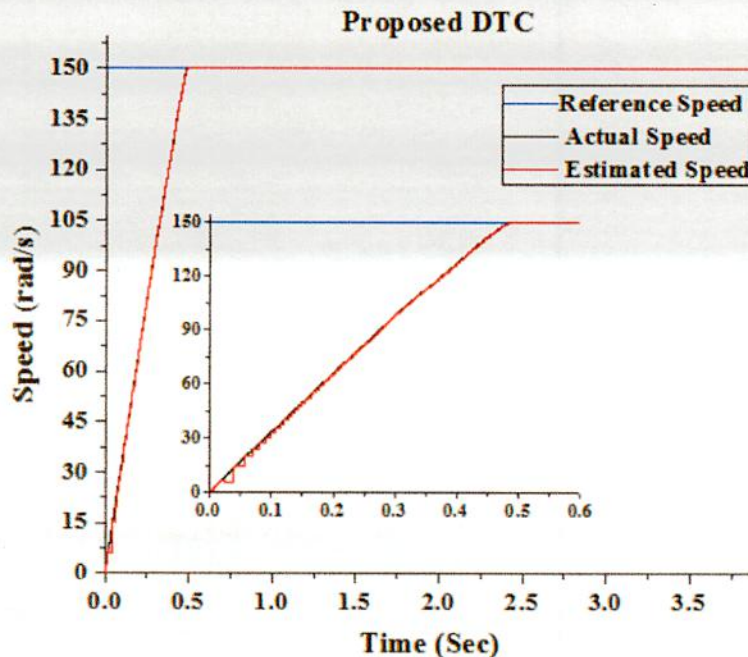
$$T_{em} = K_t(\varphi_a i_{as} + \varphi_b i_{bs} + \varphi_c i_{cs}) \quad (7.9)$$

7.4 Simulation Results and Discussion

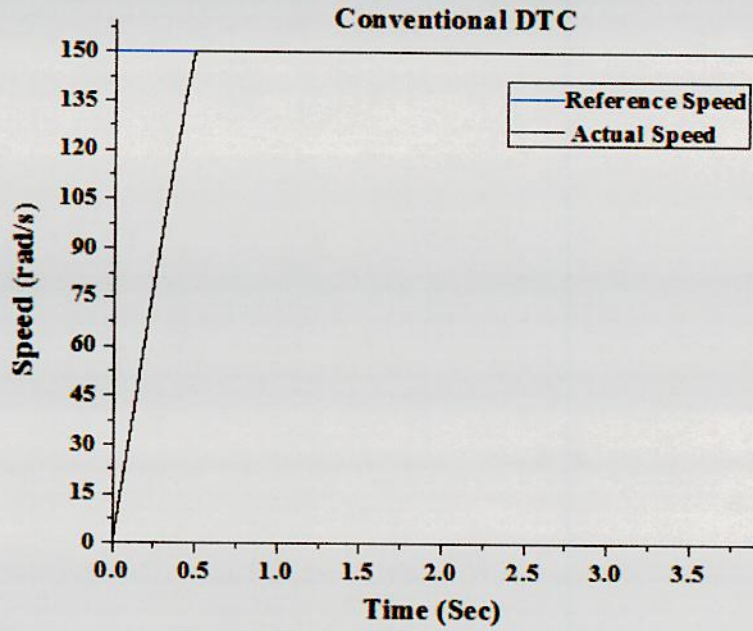
Two phase conduction DTC scheme for PMBLDC motor drive without rotor position or speed sensors in the constant torque region has been simulated in a digital computer with software written in C++ environment. The sampling time used for this simulation is 0.0000025 second. The specifications of the simulated PMBLDC motor are depicted in Appendix.

7.4.1 Starting Characteristics

The PMBLDC motor starts with an initial load torque 0.4 Nm. Starting speed characteristics i.e. time taken by the motor to reach its rated speed (150 rad/s) with its initial torque (0.4 Nm) for direct torque controlled PMBLDC motor drives is shown in Fig. 7.5. From Fig. 7.5(a), it is seen that, PMBLDC motor takes 0.48 second for proposed sensorless DTC drive to gain rated speed. Conventional sensed DTC PMBLDC motor drive also takes 0.48 second as shown Fig. 7.5(b). Phase currents are limited to its rated value by implementing torque limiter. There exists negligible amount of speed deviation between the actual and estimated speed at the initial time of starting for proposed sensorless two phase conduction DTC drive. Because at initial transient state (before 0.08 second), there exists little deviation between the actual and estimated rotor flux and rotor position as shown in Fig. 7.8 and Fig. 7.9. After 0.08 seconds estimated speed follows actual speed accurately. That is, at steady state there is no error for speed estimation for proposed sensorless DTC drive.



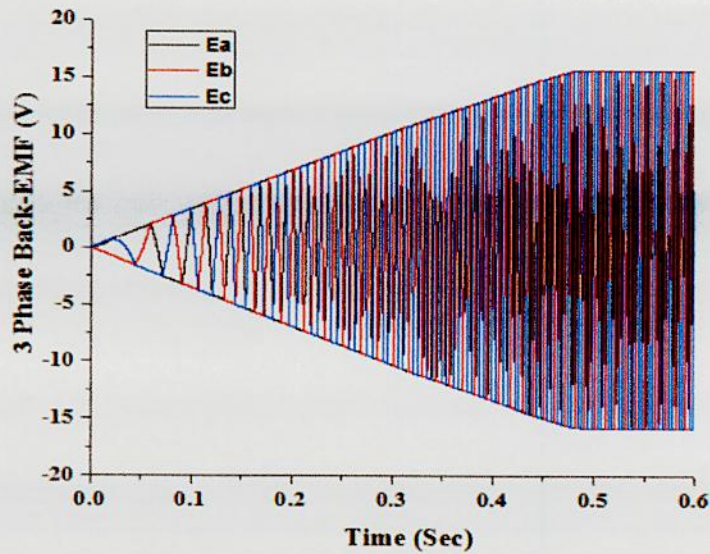
(a) For proposed position sensorless two phase conduction DTC PMBLDC motor drive



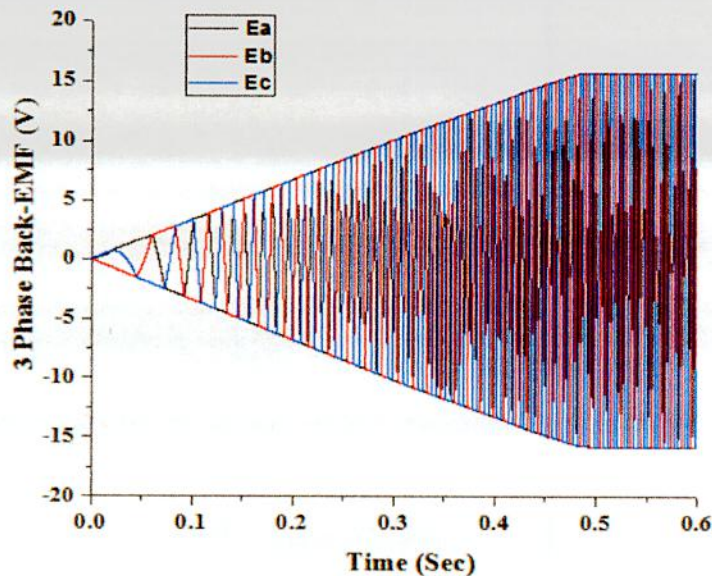
(b) For conventional two phase conduction DTC PMBLDC motor drive

Fig. 7.5: Starting characteristics of PMBLDC motor drives for two phase conduction direct torque control

3-phase back EMF at the time of starting for direct torque controlled PMLBDC drives for both proposed sensorless DTC and conventional sensed DTC are shown in Fig. 7.6. In Fig. 7.7, actual back EMF and corresponding calculated back EMF for proposed sensorless two phase conduction DTC drive is depicted. It is seen that, calculated back EMF fully matched with actual back EMF.



(a) For proposed position sensorless two phase conduction DTC PMLBDC motor drive



(b) For conventional two phase conduction DTC PMLBDC motor drive

Fig. 7.6: 3-phase back EMF of two phase conduction direct torque controlled PMLBDC motor drive

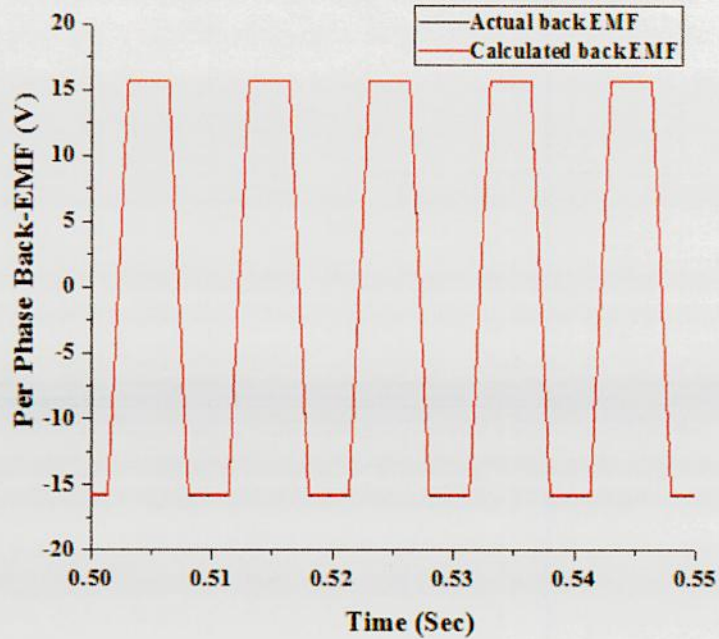
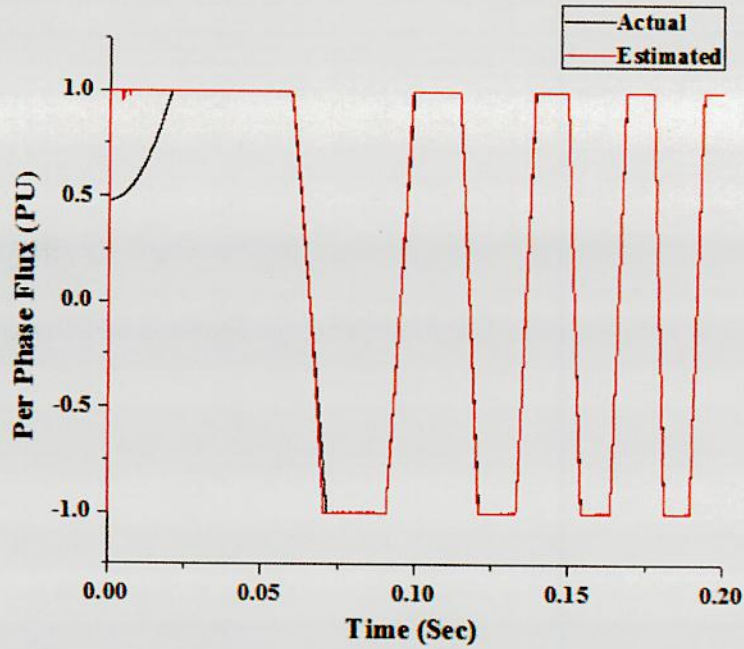
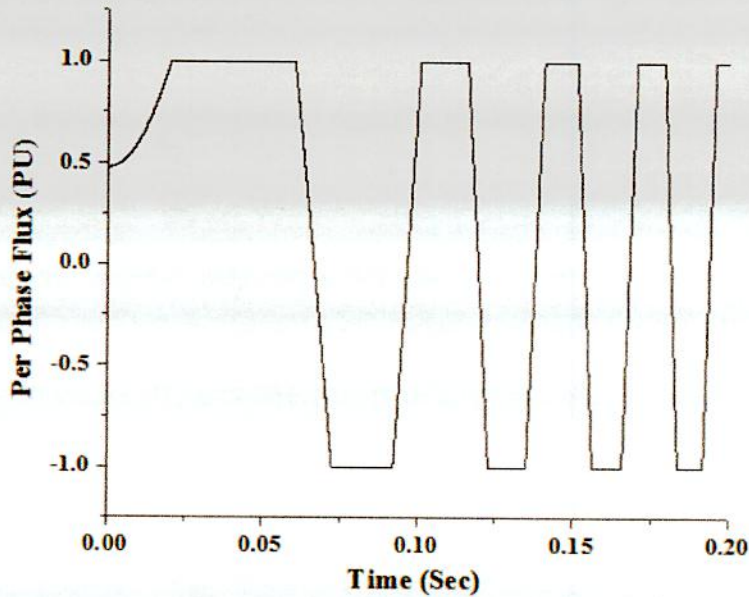


Fig. 7.7: Comparison of per phase actual back EMF with calculated back EMF for two phase conduction DTC drive without position sensor

A comparison of actual and estimated flux for sensorless direct torque controlled PMBLDC motor drive is shown in Fig. 7.8(a). From Fig. 7.8(a) it can be said that, at the initial transient time of starting of PMBLDC motor (before 0.08 second), there exists little mismatch between the actual flux and estimated flux. Actual and estimated rotor position for sensorless direct torque controlled PMBLDC motor drive is pictured in Fig. 7.9(a). Since rotor positions are calculated by using the estimated flux. So, there is little misalignment between the actual and estimated rotor position at the initial time of starting as shown in Fig. 7.9(a). After 0.08 second, estimated flux fully traced actual flux. So, estimated rotor position can be fully matched with actual rotor position. Rotor per phase flux linkage and rotor position for conventional sensed direct torque controlled PMBLDC motor drive are illustrated in Fig. 7.8(b) and Fig. 7.9(b) respectively.

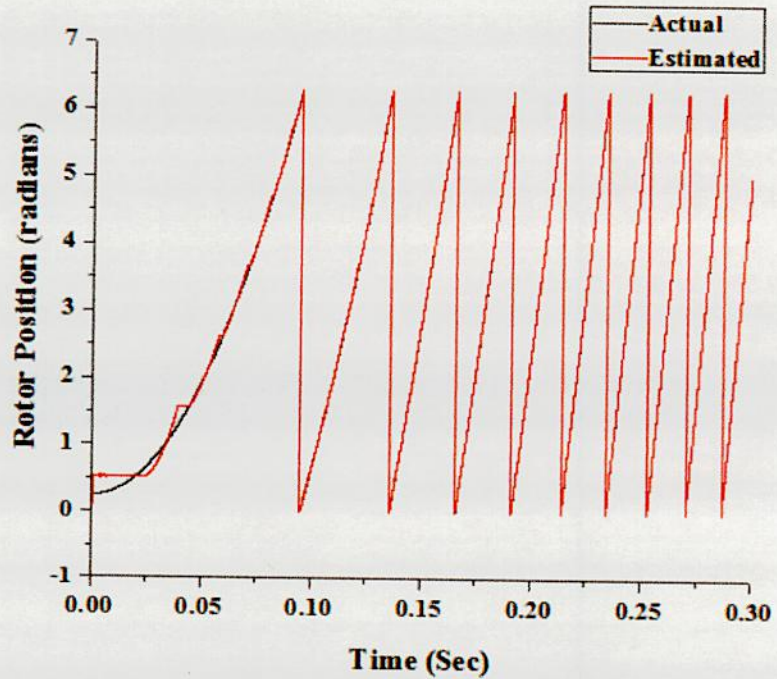


(a) For proposed position sensorless two phase conduction DTC PMBLDC motor drive

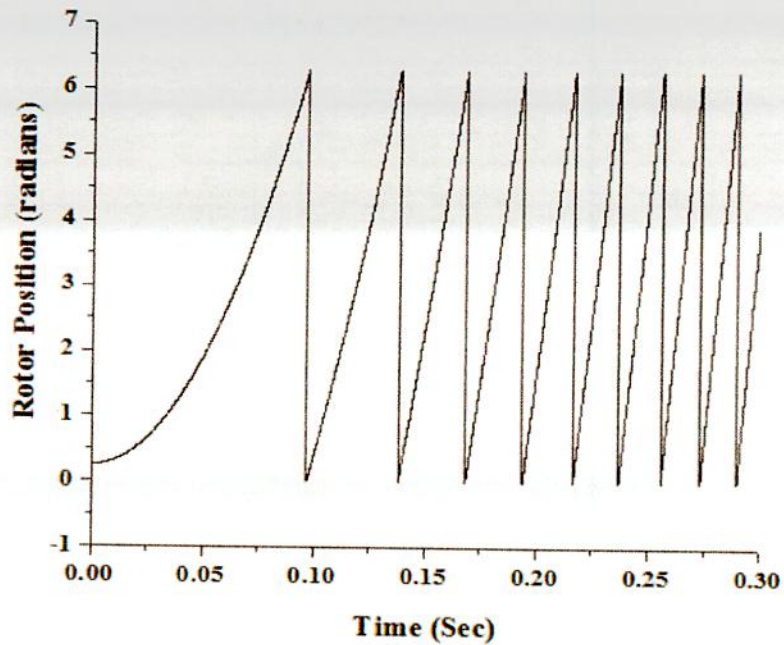


(b) For conventional two phase conduction DTC PMBLDC motor drive

Fig. 7.8: Per phase rotor flux for two phase conduction direct torque controlled PMBLDC motor drives with and without position sensor



(a) For proposed position sensorless two phase conduction DTC PMBLDC motor drive



(b) For conventional two phase conduction DTC PMBLDC motor drive

Fig. 7.9: Rotor position for two phase conduction direct torque controlled PMBLDC motor drives

Fig. 7.10 depicts developed electromagnetic torque in PMBLDC motor according to the load torque 0.4 Nm for sensorless two phase conduction direct torque controlled PMBLDC motor drive. Fig. 7.10 also represents the comparison between the actual developed torque with the estimated developed torque. Torque estimation is done using estimated rotor flux. This estimated developed torque is compared to the reference torque to select the proper voltage vectors while keeping the stator flux linkage amplitude almost constant by using two phase voltage vector selection Table 7.1. For the proposed sensorless DTC drive, there exist little mismatch between estimated torque and actual torque at the starting transient time. But at steady state, estimated developed torque exactly follows the actual developed torque in PMBLDC motor. It is the novelty of this proposed torque estimation algorithm. Fig. 7.11 depicts the developed electromagnetic torque according to the load torque 0.4 Nm for conventional sensed DTC drive of PMBLDC motor. Comparing Fig. 7.10 with Fig. 7.11, it can be said that, oscillation ripple in the developed electromagnetic torque for proposed sensorless DTC drive is same to the conventional sensed DTC drive. That is, the performance of the proposed sensorless DTC drive meets with the performance of conventional sensed DTC drive. The extra benefit for the proposed drive is that, no high cost high resolution position sensors or speed sensors are used as compared to the conventional sensed DTC drive.

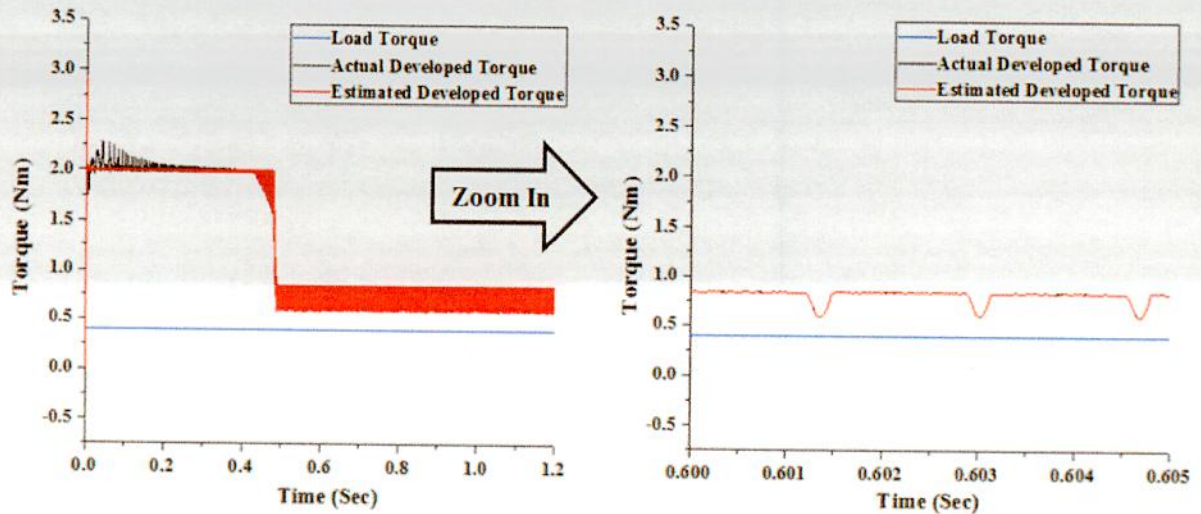


Fig. 7.10: Actual and estimated developed torque according to load torque for proposed position sensorless two phase conduction DTC PMBLDC motor drive

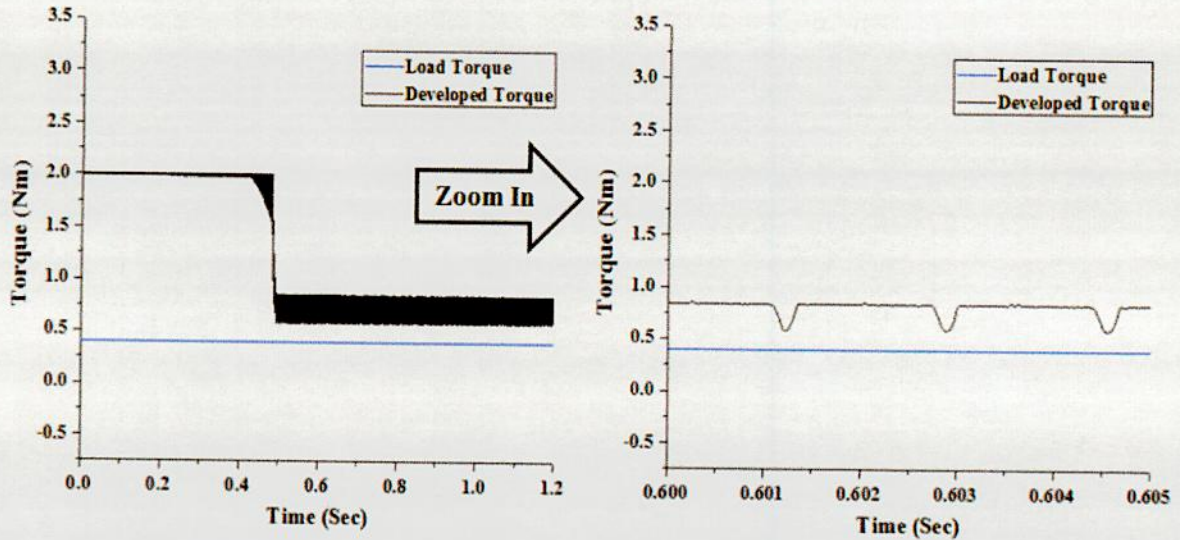
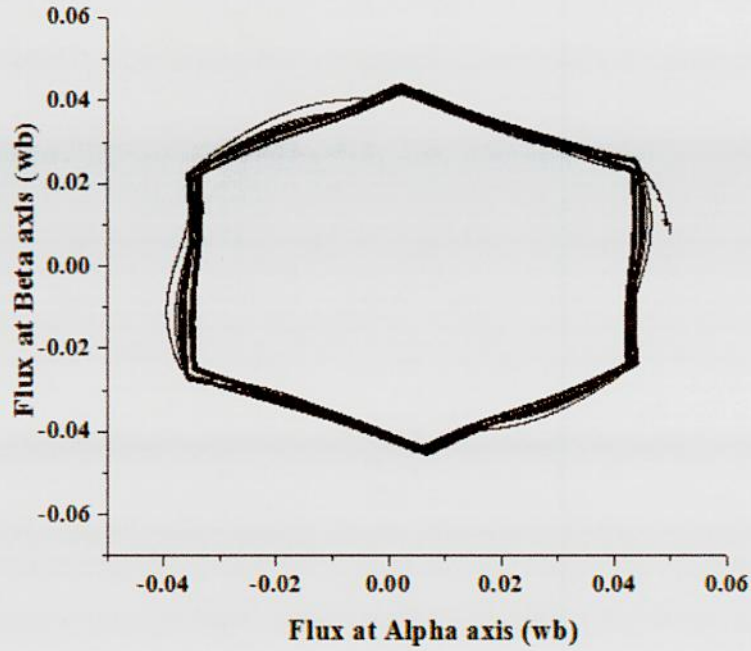
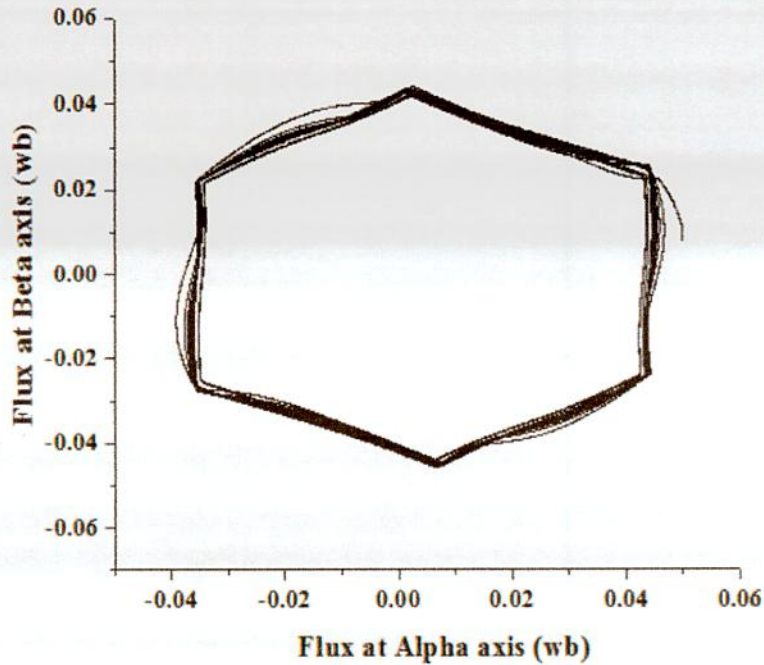


Fig. 7.11: Developed electromagnetic torque according to load torque for conventional sensed two phase conduction DTC PMLBDC motor drive

In Fig. 7.12, stator flux linkage trajectories i.e. flux orientation representation in the stationary $\alpha\beta$ axes reference frame for PMLBDC motor drives are pictured both for proposed position sensorless DTC drive and conventional position sensed DTC drive of PMLBDC motor. Similar stator flux linkage trajectories are obtained from both the proposed and conventional DTC drives. Ideally, conventional two-phase conduction direct torque control causes the locus of the stator flux linkage to be kept in hexagonal shape if the unexcited open phase back-EMF effect and the free-wheeling diodes are neglected, as shown in Fig. 7.1 with dashed lines. Though the PMLBDC motor is loaded with 0.4 Nm load torque, for both of the proposed and conventional DTC drives, stator flux linkage trajectories are nearly hexagonal shape and there are no noticeable sharp dips in stator flux linkage trajectories.



(a) For proposed position sensorless two phase conduction DTC PMLDC motor drive

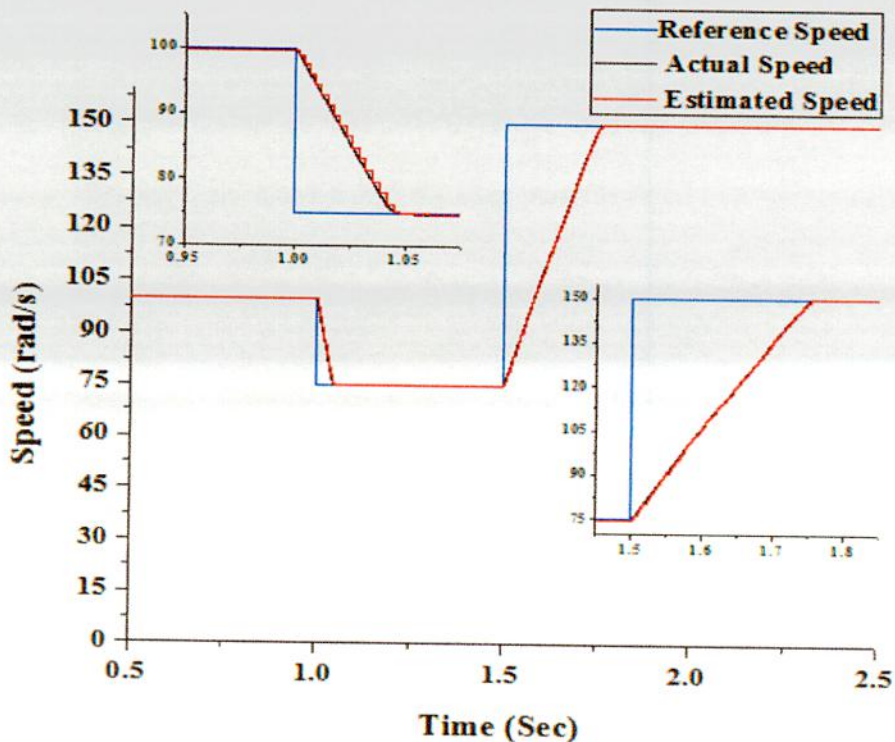


(b) For conventional two phase conduction DTC PMLDC motor drive

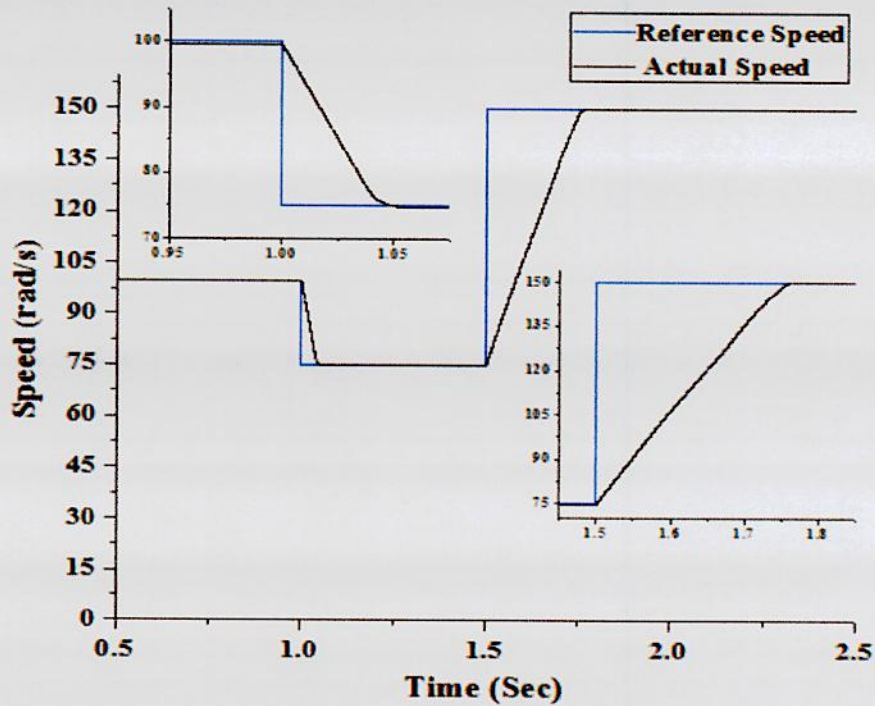
Fig. 7.12: Stator flux linkage trajectories in the stationary $\alpha\beta$ axes reference frame for two phase conduction direct torque controlled PMLDC motor drives

7.4.2 Variable Speed Characteristics

Variable speed command is given to measure the dynamic performance of two phase conduction direct torque controlled PMBLDC motor drives. Motor runs at speed 100 rad/s. At 1.0 second the speed command is changed to 75 rad/s and finally at 1.5 second speed command is changed to 150 rad/s. Motor speed follows the reference speed for both proposed and conventional DTC drives as shown in Fig. 7.13. For dynamic speed changing condition, estimated speed nearly follows the actual speed of PMBLDC motor for proposed position sensorless DTC drive. When speed command is changed to 75 rad/s from 100 rad/s with load torque 0.4 Nm, there is a small amount of mismatch between the actual speed and estimated speed for proposed DTC drive at transient time interval 1.0 second to 1.05 second. During this interval, estimated speed traces the actual speed like staircase as depicted in subplot of Fig. 7.13(a). When speed command is changed to 150 rad/s from 75 rad/s at 1.5 second, there is no noticeable error between the estimated and actual motor speed for proposed DTC drive. At steady state condition, estimated speed exactly traced out the actual speed of the motor. Proposed position sensorless DTC drive shows similar performance to the conventional position sensed DTC drive for dynamic speed changing condition.



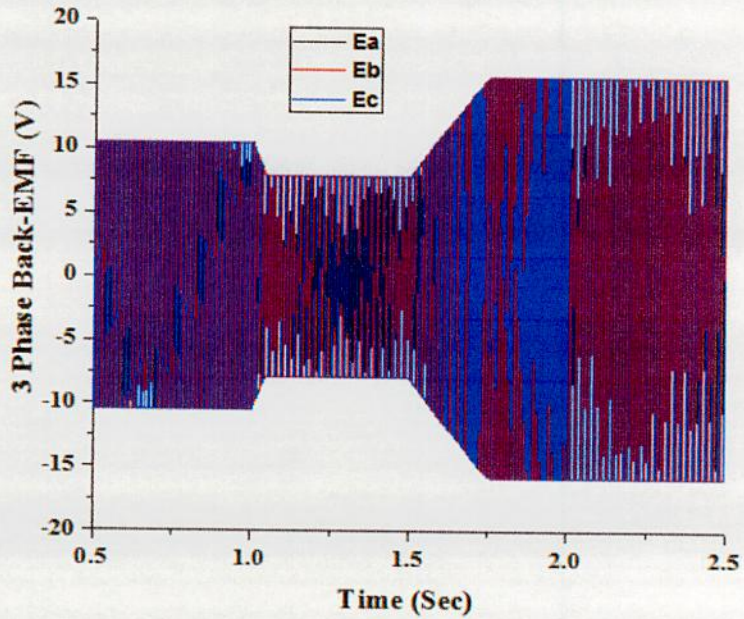
(a) For proposed position sensorless two phase conduction DTC PMBLDC motor drive



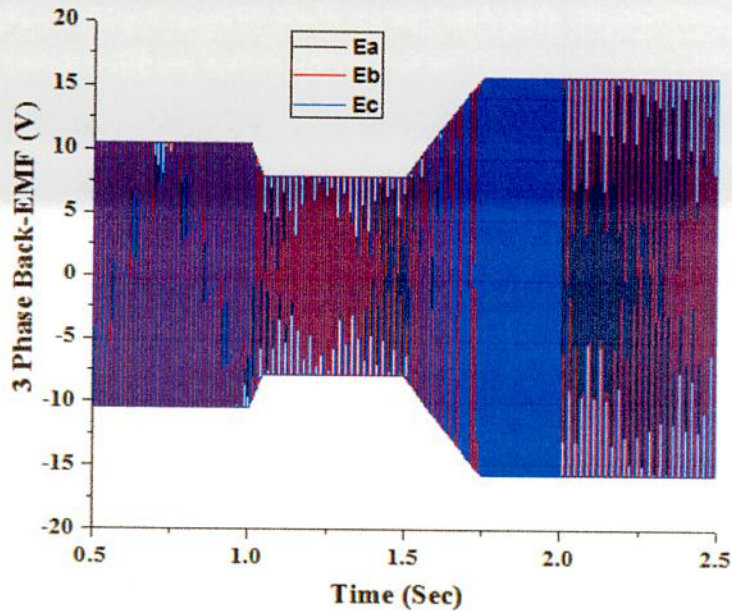
(b) For conventional two phase conduction DTC PMLDLC motor drive

Fig. 7.13: Comparison between speed responses of PMLDLC motor for proposed position sensorless DTC drive and conventional position sensed DTC drive at dynamic speed changing condition

Condition of back EMF at the time of variable speed change for both proposed position sensorless and conventional sensed DTC drives are pictured in Fig. 7.14.



(a) For proposed position sensorless two phase conduction DTC PMBLDC motor drive



(b) For conventional two phase conduction DTC PMBLDC motor drive

Fig. 7.14: 3-phase back EMF at dynamic speed changing condition for two phase conduction direct torque controlled PMBLDC motor drives

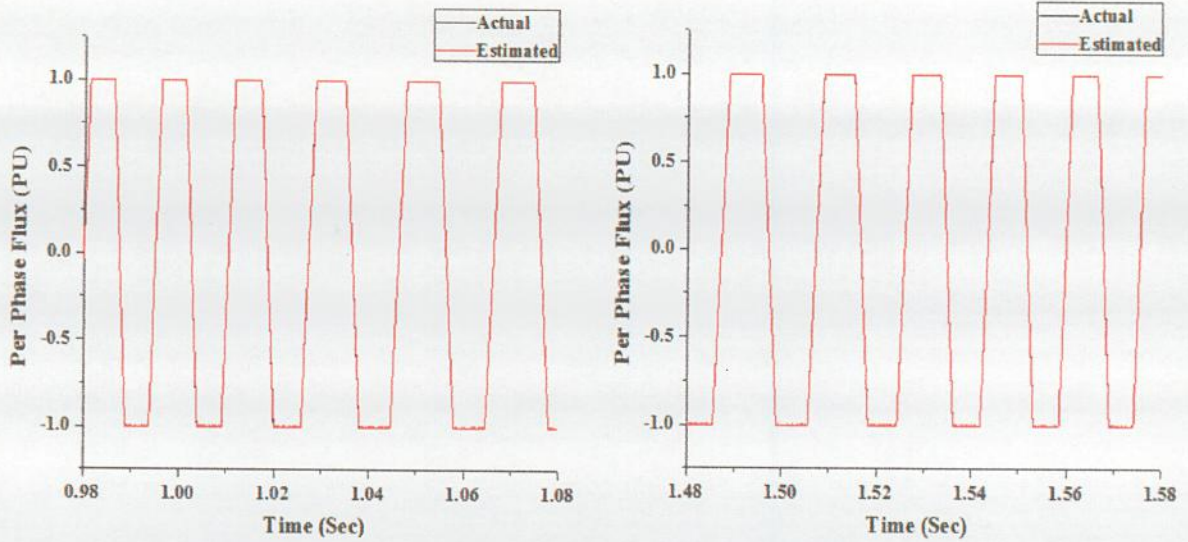


Fig. 7.15: Per phase actual and estimated rotor flux (in PU) at dynamic speed changing condition for proposed position sensorless two phase conduction DTC drive of PMBLDC motor

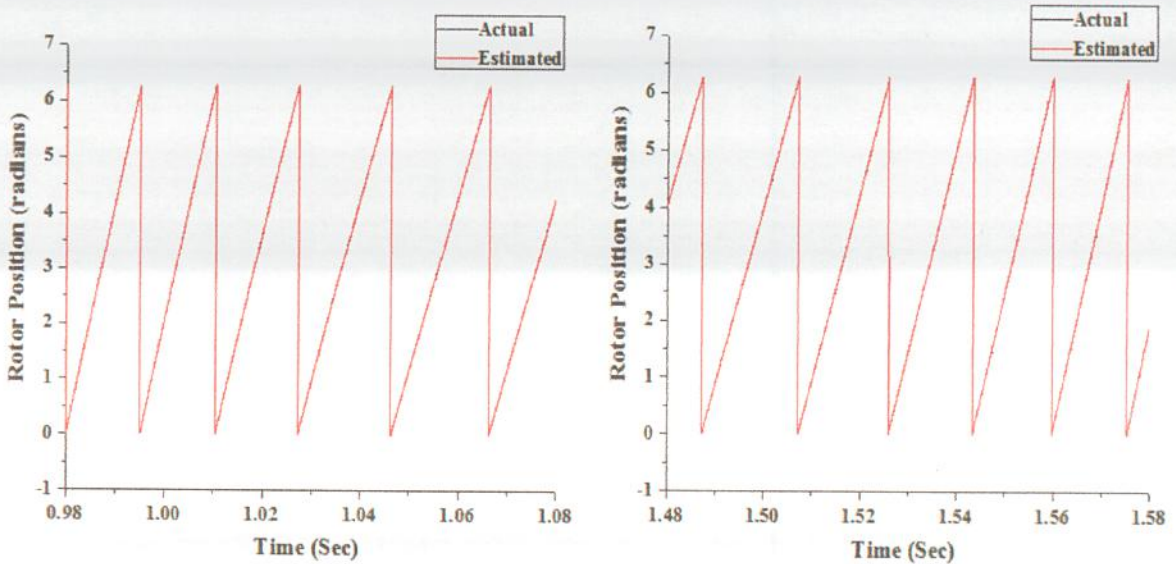


Fig. 7.16: Actual and estimated rotor position at dynamic speed changing condition for proposed position sensorless two phase conduction DTC drive of PMBLDC motor

Condition of actual and estimated per phase rotor flux at variable speed changing interface for proposed sensorless DTC drive is shown in Fig. 7.15. When speed command changes from 100 rad/s to 75 rad/s, i.e. for decreasing motor speed transient condition, there is no mismatch between actual and estimated rotor flux. When speed command changes from 75 rad/s to 150 rad/s, i.e. for increasing motor speed transient condition, there is also no mismatch between actual and estimated rotor flux for as shown in Fig. 7.15. In Fig. 7.16, actual and estimated rotor position of the PMBLDC motor at variable speed changing interfaces for proposed sensorless two phase conduction DTC drive are plotted. Rotor position of the motor is estimated using estimated stator flux linkage. So estimated rotor position shows the similar behavior as depicted for estimated rotor flux.

The scenario of actual and estimated developed electromagnetic torque according to the response of constant load torque at dynamic speed changing condition for proposed position sensorless two phase conduction direct torque controlled PMBLDC motor drive is shown in Fig. 7.17. Estimated developed torque exactly traced out the actual developed torque. Developed electromagnetic torque for conventional sensed two phase conduction direct torque controlled PMBLDC motor drive is illustrated in Fig. 7.18 for the comparison with the proposed DTC drive.

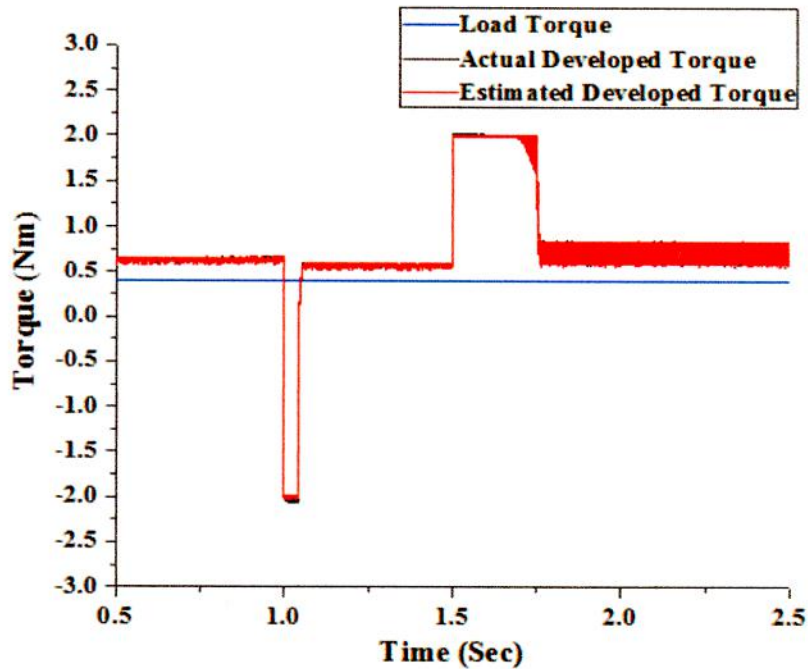


Fig. 7.17: Actual and estimated rotor developed torque according to the response of load torque at dynamic speed changing condition for proposed position sensorless two phase conduction DTC PMLDC motor drive

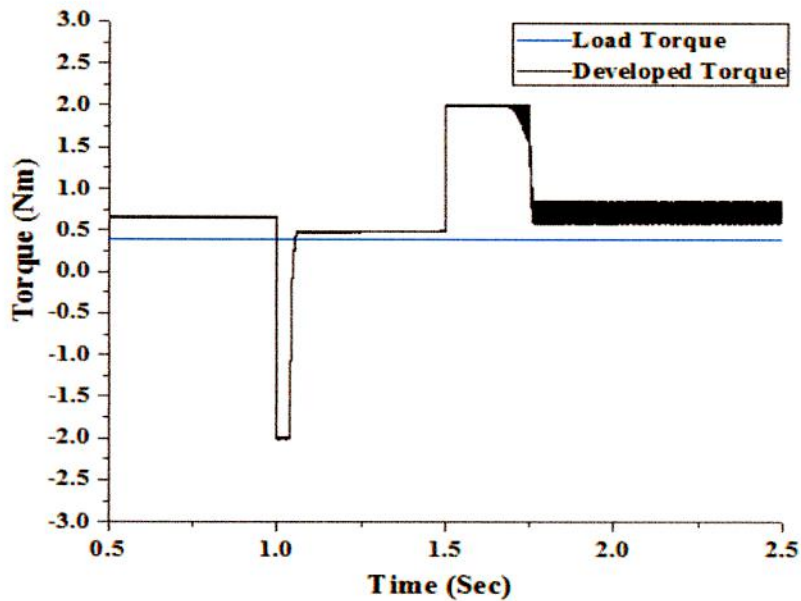
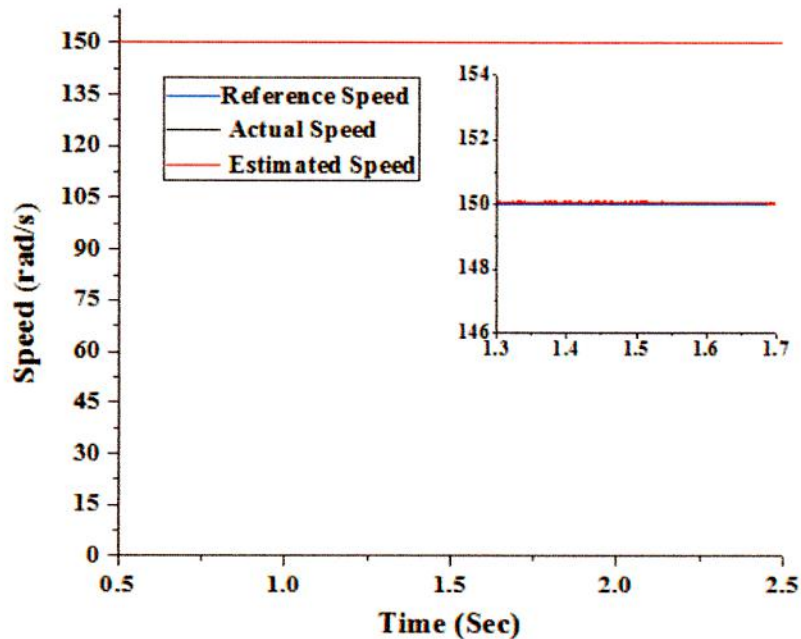


Fig. 7.18: Developed electromagnetic torque according to the response of load torque at dynamic speed changing condition for conventional position sensed two phase conduction DTC drive of PMLDC motor

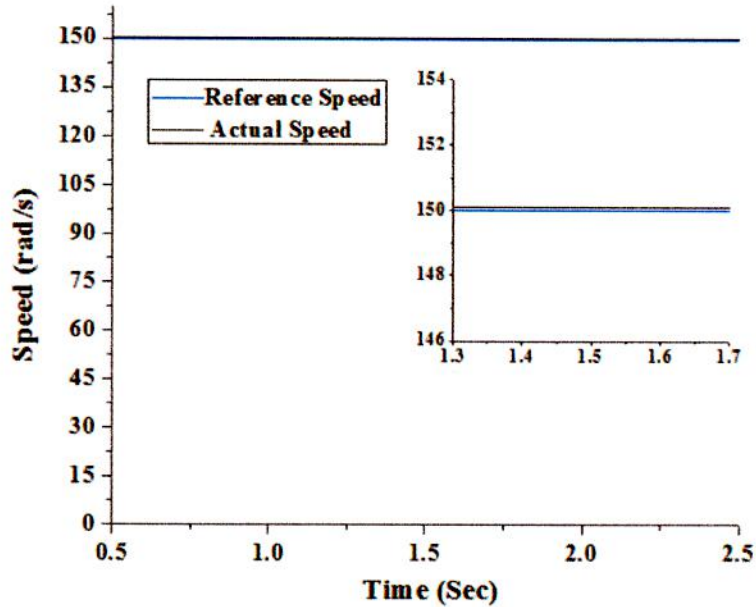
7.4.3 Motor Characteristics due to Load Torque Change

Now the performance of proposed and conventional DTC drives is determined under the condition of load torque change. At first motor runs at 150 rad/s rated speed with initial load torque 0.4 Nm. At time 1.5 second motor is loaded with its load torque 1.55 Nm. At that condition two phase conduction DTC drives for both proposed position sensorless and conventional sensed schemes can sustain motor speed to its rated value 150 rad/s as shown in Fig. 7.19. Fig. 7.19 depicts that, there is no change in speed characteristic at the time 1.5 second when the motor is loaded with torque 1.55 Nm. Both actual and estimated motor speed sharply follows the given reference speed command for proposed DTC drive. Maximum load torque have to be given to these two phase conduction direct torque controlled PMBLDC motor drives without hampering the system stability is 1.55 Nm for both proposed and conventional DTC drives.

Rotor position of proposed position sensorless direct torque controlled PMBLDC motor drive for sudden load torque change at 1.5 second is pictured in Fig. 7.20. At the time 1.5 second when the motor is loaded with the rated load torque 1.55 Nm, there is no difference between the actual and estimated rotor position.



(a) For proposed position sensorless two phase conduction DTC drive of PMBLDC motor



(b) For conventional two phase conduction DTC drive of PMBLDC motor

Fig. 7.19: Speed characteristics of PMBLDC motor for sudden load torque change at 1.5 second from initial load torque 0.4 Nm to load torque 1.55 Nm for proposed and conventional DTC drives

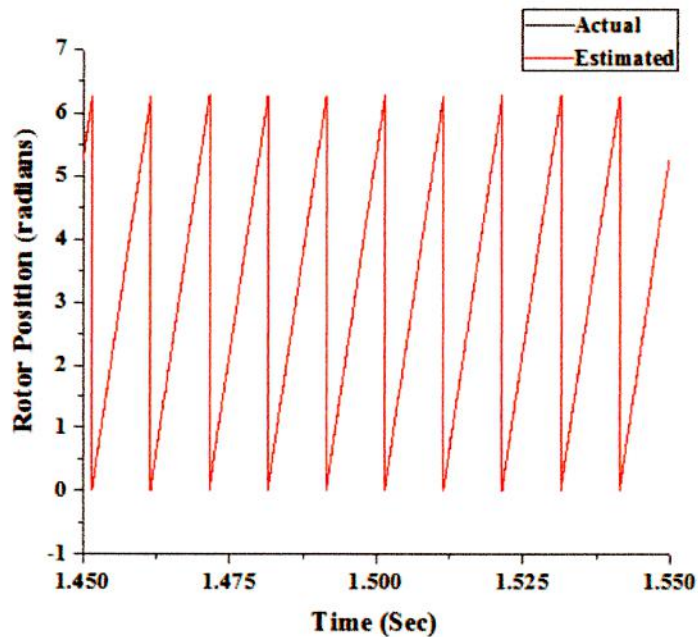


Fig. 7.20: Comparison of actual and estimated rotor position of proposed position sensorless two phase conduction DTC drive for sudden load torque change at 1.5 second

The scenario of actual and estimated developed electromagnetic torque according to the response of dynamic load torque change for proposed position sensorless direct torque controlled PMSM motor drive is shown in Fig. 7.21. The developed electromagnetic torque according to the response of dynamic load torque change for conventional direct torque controlled PMSM motor drive as shown in Fig. 7.22, shows similar behavior like the proposed DTC drive.

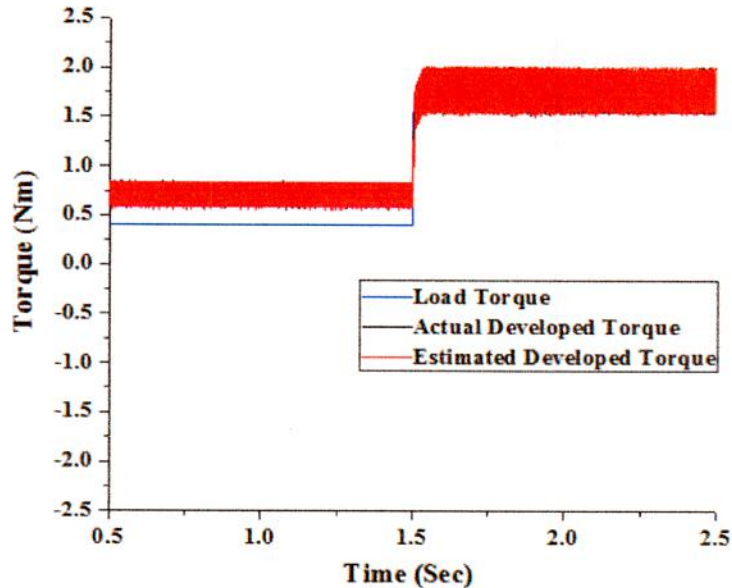


Fig. 7.21: Actual and estimated developed torque according to the response of dynamic load torque change for proposed two phase conduction direct torque controlled PMSM motor drive without position sensor

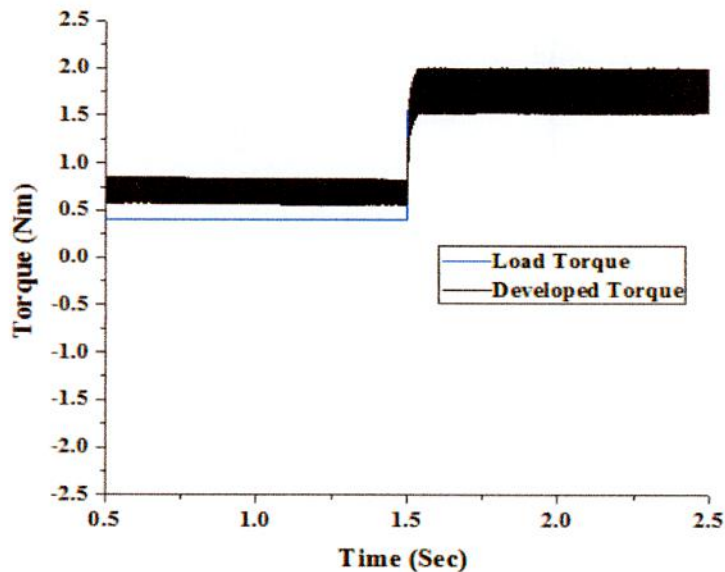


Fig. 7.22: Developed torque according to the response of dynamic load torque change for conventional position sensed direct torque controlled PMSM motor drive

7.5 Conclusion

Conventional two phase conduction direct torque technique for PMBLDC motor operating in the constant torque region is presented due to the higher power/weight and torque/current ratios. Voltage space vectors are directly controlled while the stator flux linkage amplitude is kept almost constant by ignoring the flux control in the constant torque region because of achieving faster torque response. A novel position sensorless DTC drive is proposed, which has the all benefits of conventional two phase conduction DTC scheme. Moreover, in this proposed DTC drive, the necessity of high cost and high resolution speed sensors or position encoders are totally eliminated. These sensors are mandatory for conventional two phase conduction DTC drive.

There are negligible amount of speed error between the estimated and actual motor speed at the transient time of starting and transient time of dynamic speed decreasing interface for proposed sensorless DTC drive. After initial transient time 0.08 second, estimated motor speed, estimated rotor flux and estimated rotor position sharply follows actual motor speed, actual rotor flux and actual rotor position respectively. So, there is no error for speed estimation, flux estimation and rotor position estimation algorithms for proposed position sensorless DTC drive.

For the proposed sensorless DTC drive, there exist little mismatch between estimated torque and actual torque at the starting transient time. But at steady state, estimated developed torque exactly follows the actual developed torque in PMBLDC motor. Oscillation of developed electromagnetic torque for proposed sensorless DTC drive is same to the conventional sensed DTC drive. In spite of using no position sensors or speed sensors, the performance of torque estimation of the proposed sensorless DTC drive is exactly similar with the performance of conventional sensed DTC drive. It is the novelty of this proposed torque estimation algorithm.

Exactly same stator flux linkage trajectories are obtained for both proposed position sensorless DTC drive and conventional position sensed DTC drive of PMBLDC motor. The obtained stator flux linkage trajectories are nearly hexagonal shaped there are no noticeable sharp dips in stator flux linkage trajectories. These criteria are nearly matched with the ideal condition. By considering starting, dynamic speed and load torque changing characteristics, it is clear that, the performances of proposed position sensorless direct torque controlled PMBLDC motor drive is fully matched with the performances of conventional position sensed direct torque controlled PMBLDC motor drive.

Chapter VIII

Conclusion

Chapter Outlines:

8.1 Conclusion

8.2 Recommendation for Future Work

8.1 Conclusion

High performance position sensorless adaptive PI controller based vector controlled current fed delta modulated PMBLDC motor drives are designed tested in this study. Field oriented vector controlled PMBLDC motor drive is proposed and compared with the scalar controlled PMBLDC motor drive. The performance of field oriented control drive ($i_d = 0.0$) is compared with the scalar controlled PMBLDC motor drive at $i_d=1.0$ and $i_d=i_q$ through the simulation results. By considering starting condition, dynamic speed and load torque changing characteristics, it is clear that, the performance of vector control PMBLDC drive is superior to scalar control drives. Keeping maximum rated current of the PMBLDC motor constant, the performance of scalar controlled drives degrades with the increasing of i_d . Load torque handling capacity of scalar controlled PMBLDC motor drives decreases with increasing the value of direct axis current component in scalar control drives. Both the transient and steady state characteristics of vector control current fed PMBLDC motor drive are outstanding. Performance of the field oriented vector controlled and scalar controlled PMBLDC motor drives are tested due to the change of PMBLDC motor parameters. There are no effects of 25% increase or decrease of motor inertia, damping constant, stator resistance per phase, self-inductance, and mutual inductance from its rated value on the performance of PMBLDC motor drives for both vector and scalar control.

A novel approach to enhance the torque handling capacity of a PMBLDC motor without exceeding the maximum rated current of the motor is proposed in this thesis. An adaptive PI speed controller based high performance vector controlled three different trapezoidal, square and sinusoidal reference current fed delta modulated PMBLDC motor drives are designed. Torque handling capacity of a PMBLDC motor can be increased up to 25% from the conventional 120° conduction square wave current fed drive by only using the novel trapezoidal current fed field oriented control drive. Load torque handling capacity of square current fed PMBLDC motor drive (1.60 Nm) is higher than the sinusoidal current fed drive (1.55 Nm). Performance of trapezoidal current fed vector controlled drive is superior to the square and sinusoidal vector controlled drives considering response time, load torque handling capacity, dynamic speed and load torque changing condition, settling time of the system. For trapezoidal current fed drive, the developed electromagnetic torque is periodic in nature and has constant average value.

Instead of using rotor position or speed sensor, two novel algorithms have been proposed to estimate the rotor position and speed to perform the operation of position sensorless field oriented vector control of PMBLDC motor. Novel rotor flux estimation and rotor position estimation algorithms are proposed for position sensorless operation. Two different approaches to estimate the speed of PMBLDC motor have been illustrated for speed sensorless operation. Algorithm 1 and algorithm 2 based position sensorless field oriented vector controlled current fed delta modulated PMBLDC motor drives is designed. Excluding initial starting time negligible error, estimated flux exactly traced out the actual flux linkage of the PMBLDC motor for both algorithm 1 and algorithm 2. That is, the performance of flux estimation algorithm is outstanding. Similar to the estimated flux, there is no mismatch between actual and estimated rotor position excluding the initial starting time error. So, the performance of rotor position estimator is satisfactory. The performance of algorithm 2 for speed estimation is better than the

algorithm 1 for sensorless operation of field oriented control. But there are less oscillation in stator phase current currents for proposed algorithm 1 than algorithm 2. These oscillations of stator phase current incorporate in the developed electromagnetic torque. Therefore, developed electromagnetic torque for proposed algorithm 2 oscillates more than the algorithm 1. Considering this point of view, algorithm 1 is better than algorithm 2. Performances of these sensorless field oriented vector controlled PMLBDC motor drives for both algorithm 1 and algorithm 2 are similar to sensed field oriented PMLBDC motor drive. Instead of using position sensors, two different algorithms are used for sensorless operation of field oriented vector controlled PMLBDC motor drive. But the performance of this drive remains unchanged.

High performance trapezoidal current fed field oriented controlled PMLBDC motor drive without position sensor has been also proposed in this thesis work. This drive is proposed to increase the torque handling capacity of a PMLBDC motor drive without exceeding the maximum current rating of the motor and without high cost and high resolution speed sensor or rotor position encoder. In this proposed drive, approaches of the torque handling capacity enhancement, position sensorless operation and field oriented control are incorporated in a single PMLBDC motor drive to make a high performance system. All advantages of these three strategies are present in this high performance PMLBDC motor drive. Torque handling capacity of this high performance field oriented vector controlled PMLBDC motor is 25% more than the conventional 120° conduction square wave current fed drive without using position or speed sensors. Similar to the position sensorless field oriented controlled PMLBDC motor drives, speed estimation for proposed algorithm 2 is better than the proposed algorithm 1 for this high performance controlled PMLBDC motor drive and there exists less oscillation in stator phase current currents and developed electromagnetic torque for proposed algorithm 1 than algorithm 2. Because of similar flux, rotor position and speed estimation algorithms are used in this high performance control drive as used in field oriented controlled PMLBDC motor drives for position sensorless operation. By considering both transient and steady state characteristics, the performance of this position sensorless trapezoidal current fed field oriented PMLBDC motor drives for both algorithm 1 and algorithm 2 are similar to sensed trapezoidal current fed field oriented PMLBDC motor drive. Instead of using position sensor, two different algorithm is used for position sensorless operation of trapezoidal current fed field oriented PMLBDC motor drive to enhance the torque handling capacity of PMLBDC motor without exceeding the maximum current rating of the motor.

A novel position sensorless two phase conduction DTC drive has also been proposed, which has the all benefits of conventional two phase conduction DTC scheme. Moreover, in this proposed DTC drive, the necessity of high cost and high resolution speed sensors or position encoders are totally eliminated. These sensors are mandatory for conventional two phase conduction DTC drive. For the proposed sensorless DTC drive, there exist negligible amount of mismatch between estimated torque and actual torque at the starting transient time. But at steady state, estimated developed torque exactly follows the actual developed torque in PMLBDC motor. Oscillation of developed electromagnetic torque for proposed sensorless DTC drive is same to the conventional sensed DTC drive. In spite of using no position sensors or speed sensors, the performance of torque estimation of the proposed sensorless DTC drive is exactly similar with

the performance of conventional sensed DTC drive. It is the novelty of this proposed torque estimation algorithm. The stator flux linkage trajectory is nearly hexagonal shaped and there are no noticeable sharp dips in stator flux linkage trajectories for proposed position sensorless DTC drive. Performances of proposed position sensorless direct torque controlled PMBLDC motor drive is fully matched with the performances of conventional position sensed direct torque controlled PMBLDC motor drive. Both of these drives, flux control are ignored by keeping stator flux linkage amplitude almost constant in the constant torque region due to achieve faster torque response.

8.2 Recommendation for Future Work

Here it is focused on the performance enhancement of PMBLDC motor drives. Performance of field oriented vector controlled PMBLDC motor drive is compared with scalar control drives. A novel approach to enhance the torque handling capacity of a field oriented vector controlled PMBLDC motor drive is proposed in this thesis. Two different novel algorithms are proposed to estimate rotor position and speed of PMBLDC motor for position sensorless operation of PMBLDC motor drives. Unique position sensorless direct torque controlled PMBLDC motor drive is also proposed in this thesis and compared with the conventional DTC drive.

Simulation work has been done for the analysis of these high performance PMBLDC motor drives. However, due to equipment limitations these control methods could not tested practically. So in the future work, the results obtained for proposed control techniques from simulation environment will be validated with experimental results. In addition to that, these high performance PMBLDC motor drives can be analyzed by implementing further advanced and intelligent controller like adaptive Fuzzy controller, ANN based controller and ANN-Fuzzy controller in both speed and current loop.

References

- [1] Mourad Masmoudi, Bassem El Badsy, and Ahmed Masmoudi, "Direct Torque Control of Brushless DC Motor Drives with Improved Reliability," *IEEE Transactions on Industry Applications*, vol. 5, no. 6, pp. 3744-3753, November-December 2014.
- [2] Salih Baris Ozturk, William C. Alexander, and Hamid A. Toliyat, "Direct Torque Control of Four-Switch Brushless DC Motor with Non-Sinusoidal Back EMF," *IEEE Transactions on Power Electronics*, vol. 25, no. 2, pp. 263-271, February 2010.
- [3] Changliang Xia, Guokai Jiang, Wei Chen, and Tingna Shi, "Switching-Gain Adaptation Current Control for Brushless DC Motors," *IEEE Transactions on Industrial Electronics*, vol. 63, pp. 2044-2052, April 2016.
- [4] An-Chen Lee, Samuel Wang, and Chia-Juei Fan, "A Current Index Approach to Compensate Commutation Phase Error for Sensorless Brushless DC Motors With Nonideal Back EMF," *IEEE Transactions on Power Electronics*, vol. 31, no. 6, June 2016.
- [5] Cheng-Tsung Lin, Chung-Wen Hung, and Chih-Wen Liu, "Position Sensorless Control for Four-Switch Three-Phase Brushless DC Motor Drives," *IEEE Transactions on Power Electronics*, vol. 23, no. 1, pp. 438-444, January 2008.
- [6] Kuang-Yao Cheng, and Ying-Yu Tzou, "Design of a Sensorless Commutation IC for BLDC Motors," *IEEE Transactions on Power Electronics*, vol. 18, no. 6, pp. 1365-1375, November 2003.
- [7] P. Pillay and R. Krishnan, "Application characteristics of permanent magnet synchronous and brushless dc motors for servo drives," *IEEE Transactions on Industry Applications*, vol. 27, no. 5, pp. 986-996, Sep./Oct. 1991.
- [8] Sang-Yong Jung, Yong-Jae Kim, Jungmoon Jae, and Jaehong Kim, "Commutation Control for the Low-Commutation Torque Ripple in the Position Sensorless Drive of the Low-Voltage Brushless DC Motor," *IEEE Transactions on Power Electronics*, vol. 29, no. 11, pp. 5983-5994, November 2014.
- [9] Jianwen Shao, "An Improved Microcontroller-Based Sensorless Brushless DC (BLDC) Motor Drive for Automotive Applications," *IEEE Transactions on Industry Applications*, vol. 42, no. 5, pp. 1216-1221, September/ October 2006.
- [10] Kwang-Woon Lee, Dae-Kyong Kim, Byung-Taek Kim, and Byung-Il Kwon, "A Novel Starting Method of the Surface Permanent-Magnet BLDC Motors Without Position Sensor for Reciprocating Compressor," *IEEE Transactions on Industry Applications*, vol. 44, no. 1, pp. 85-92, January/ February 2008.

- [11] Liviu Ioan Iepure, Ion Boldea, and Frede Blaabjerg, "Hybrid I-f Starting and Observer-Based Sensorless Control of Single-Phase BLDC-PM Motor Drives," *IEEE Transactions on Industrial Electronics*, vol. 59, no. 2, pp. 3436-3444, September 2012.
- [12] Hrushikesh Meher, "Performance Analysis of Interior Permanent Magnet Synchronous Motor (IPMSM) Drive System using different Speed Controllers," M. Tech. Thesis, Department of Electrical Engineering National Institute of Technology Rourkela, India.
- [13] Savvas Tsotoulidis, and Athanasios N. Safacas, "Deployment of an Adaptable Sensorless Commutation Technique on BLDC Motor Drives Exploiting Zero Sequence Voltage," *IEEE Transactions on Industrial Electronics*, vol. 62, no. 2, February 2015.
- [14] P. Sreekala, A. Sivasubramanian, "Speed Control of Brushless DC Motor with PI and FUZZY Logic Controller using Resonant Pole Inverter," *IEEE PES Innovative Smart Grid Technologies-India*, 2011.
- [15] H. K. Samitha Ransara and Udaya K. Madawala, "A Torque Ripple Compensation Technique for a Low Cost Brushless DC Motor Drive," *IEEE Transactions on Industrial Electronics*, vol. 62, no.10, pp. 6171 – 6182, October 2015.
- [16] M.V. Ramesh, J. Amarnath, S. Kamakshaiah, and G. S. Rao, "Speed Control of Brushless DC Motor by using Fuzzy Logic PI Controller," *ARNP Journal of Engineering and Applied Sciences*, vol. 6, no. 9, pp. 55-62, September 2011.
- [17] S. Rambabu, "Modeling and Control of a Brushless DC Motor," M Tech Thesis, Department of Electrical Engineering, National Institute of Technology Rourkela, 2007.
- [18] M.V.Ramesh, J.Amarnath, S.Kamakshaiah, and M.Balakrishna, "Field Oriented Control for Space Vector Modulation based Brushless DC Motor Drive," *International Journal of Advanced Research in Electrical, Electronics and Instrumentation Engineering* , Vol. 2, no. 9, pp.4231-4238, September 2013.
- [19] Abhisek Jain, P R Sarkar and Mohd Kursheed Siddique, " Modeling and Performance Analysis of a Permanent Magnet Brushless DC Motor using Instrumentation Technique," *International Journal of Engineering Research and Control Science*, vol. 5, no. 1, pp814-820, Jan/Feb 2015.
- [20] Marek Lazor, and Marek Stulrajter, "Modified Field Oriented Control for Smooth Torque Operation of a BLDC Motor," *Technically IEEE sponsored ELEKTRO conference*, Rajecke Teplice, 19-20 May, 2014.
- [21] Junhwi Park, Yunchang Kwak, Yeongjun Jo, Jongnam Bae, and Dong-Hee Lee, "Torque Ripple Reduction of BLDC motor using Predicted Current Control," *IEEE Transportation Electrification Conference and Expo, Asia- Pacific (ITEC)*, Busan, Korea, 1-4 June, 2016.
- [22] B. Pavan Kumar, and Krishnan C.M.C, "Comparative Study of Different Control Algorithms on Brushless DC Motors," *Biennial International Conference on Power and Energy Systems: Towards Sustainable Energy (PESTSE)*, Bangalore, 21-23 January, 2016.

- [23] Sung Jun Park, Han Woong Park, Man Hyung Lee, and Fumio Harashima, "A New Approach for Minimum-Torque-Ripple Maximum-Efficiency Control of BLDC Motor," *IEEE Transactions on Industrial Electronics*, vol. 47, no. 1, pp. 109–114, February 2000.
- [24] Virginia Manzolini, Araz Darba and Frederik De Belie, "Improving the Torque Generation in Self-Sensing BLDC Drives by Shaping the Current Waveform," 2016 International Symposium on Power Electronics, Electrical Drives, Automation and Motion, pp. 510 – 515, June 2016.
- [25] Chenjun Cui, Gang Liu and Kun Wang, "A Novel Drive Method for High-Speed Brushless DC Motor Operating in a Wide Range," *IEEE Transactions on Power Electronics*, vol. 30, no. 9, pp. 4998 – 5008, September 2015.
- [26] Y. Wang, X. Zhang, X. Yuan, and G. Liu, "Position-sensorless hybrid sliding-mode control of electric vehicles with brushless DC motor," *IEEE Transactions on Vehicular Technology*, vol. 60, no. 2, pp. 421–432, February 2011.
- [27] J. Fang, W. Li, and H. Li, "Self-compensation of the commutation angle based on dc-link current for high-speed brushless dc motors with low inductance," *IEEE Transactions on Power Electronics*, vol. 29, no. 1, pp. 428–439, January 2014.
- [28] Gang Liu, Chenjun Cui, Kun Wang, Bangcheng Han, and Shiqiang Zheng, "Sensorless Control for High-Speed Brushless DC Motor Based on the Line-to-Line Back EMF," *IEEE Transactions on Power Electronics*, vol. 31, no. 7, July 2016.
- [29] Haitao Li, Shiqiang Zheng, and Hongliang Ren, "Self-Correction of Commutation Point for High-Speed Sensorless BLDC Motor with Low Inductance and Nonideal Back EMF," *IEEE Transactions on Industrial Electronics*, vol. 32, no. 1, pp. 642-651, January 2017.
- [30] Wenzhuo Li, Jiancheng Fang, Haitao Li, and Jiqiang Tang, "Position Sensorless Control Without Phase Shifter for High-Speed BLDC Motors With Low Inductance and Nonideal Back EMF," *IEEE Transactions on Power Electronics*, vol. 31, no. 2, February 2016.
- [31] J. C. Gamazo-Real, E. Vazquez-Sanchez, and J. Gomez-Gil, "Position and speed control of brushless dc motors using sensorless techniques and application trends," *Sensors*, vol. 10, pp. 6901–6947, 2010.
- [32] Tae-Hyung Kim, and Mehrdad Ehsani, "Sensorless Control of the BLDC Motors From Near-Zero to High Speeds," *IEEE Transactions on Power Electronics*, vol. 19, no. 6, pp. 1635-1645, November 2004.
- [33] Wook-Jin Lee, and Seung-Ki Sul, "A New Starting Method of BLDC Motors Without Position Sensor," *IEEE Transactions on Industry Applications*, vol. 42, no. 6, pp. 1532-1538, November/ December 2006.

- [34] Tae-Won Chun, Quang-Vinh Tran, Hong-Hee Lee, and Heung-Geun Kim, "Sensorless Control of BLDC Motor Drive for an Automotive Fuel Pump Using a Hysteresis Comparator," *IEEE Transactions on Power Electronics*, vol. 29, no. 3, March 2014.
- [35] P. Damodharan and Krishna Vasudevan, "Sensorless Brushless DC Motor Drive Based on the Zero-Crossing Detection of Back Electromotive Force (EMF) From the Line Voltage Difference," *IEEE Transactions on Energy Conversion*, vol. 25, no. 3, pp. 661-668, September 2010.
- [36] Abolfazl Halvaei Niasar, Abolfazl Vahedi, and Hassan Moghbelli, "A Novel Position Sensorless Control of a Four-Switch, Brushless DC Motor Drive Without Phase Shifter," *IEEE Transactions on Power Electronics*, vol. 23, no. 6, November 2008.
- [37] Chenjun Cui, Gang Liu, Kun Wang, and Xinda Song, "Sensorless Drive for High-Speed Brushless DC Motor Based on the Virtual Neutral Voltage," *IEEE Transactions on Power Electronics*, vol. 30, no. 6, June 2015.
- [38] Alin Stirban, Ion Boldea, and Gheorghe-Daniel Andreescu, "Motion-Sensorless Control of BLDC-PM Motor with Offline FEM-Information-Assisted Position and Speed Observer," *IEEE Transactions on Power Electronics*, vol. 48, no. 6, December 2012.
- [39] Samuel Wang and An-Chen Lee, "A 12-Step Sensorless Drive for Brushless DC Motors Based on Back-EMF Differences," *IEEE Transactions on Energy Conversion*, vol. 30, no. 2, June 2015.
- [40] Yuanyuan Wu, Zhiquan Deng, Xiaolin Wang, Xing Ling, and Xin Cao, "Position Sensorless Control Based on Coordinate Transformation for Brushless DC Motor Drives," *IEEE Transactions on Power Electronics*, vol. 25, no. 9, September 2010.
- [41] Prasit Champa, Pakasit Somsiri, Pongpit Wipasuramonton, and Paiboon Nakhachalasint, "Initial Rotor Position Estimation for Sensorless Brushless DC Drives," *IEEE Transactions on Industry Applications*, vol. 45, no. 4, August 2009.
- [42] J. X. Shen, and S. Iwasaki, "Sensorless Control of Ultrahigh-Speed PM Brushless Motor Using PLL and Third Harmonic Back EMF," *IEEE Transactions on Industrial Electronics*, vol. 53, no. 2, April 2006.
- [43] I. Takahashi and T. Noguchi, "A New Quick-Response and High-Efficiency Control Strategy of an Induction Motor," *IEEE Transactions on Industry Applications*, vol. 22, no. 5, pp. 820-827, 1986.
- [44] Z. Q. Zhu and J. H. Leong, "Analysis and Mitigation of Torsional Vibration of PM Brushless AC/DC Drives with Direct Torque Controller," *IEEE Transactions on Industry Applications*, vol. 48, no. 4, pp. 1296-1306, 2012.

[45] Yong Liu, Z. Q. Zhu, and David Howe, "Direct Torque Control of Brushless DC Drives With Reduced Torque Ripple," *IEEE Transactions on Industry Applications*, vol. 41, no. 2, April 2005.

[46] Salih Baris Ozturk, and Hamid A. Toliyat, "Direct Torque Control of Brushless DC Motor with Non-sinusoidal Back-EMF," *IEEE International Electric Machines & Drives Conference 2007*, vol. 2, pp. 165 - 171, 2007.

[47] Sajana Kunjumon and Johnson Mathew, "Direct Torque Controlled Brushless DC Motor Drive with Rotor Position Estimation using LabVIEW," *International Journal of Advanced Research in Electrical, Electronics and Instrumentation Engineering*, Vol. 2, Special Issue 1, pp. 148-156, December 2013.

[48] Salih Ozturk, and Hamid A. Toliyat, "Sensorless Direct Torque and Indirect Flux Control of Brushless DC Motor with Non-sinusoidal Back-EMF," *34th Annual Conference of IEEE Industrial Electronics, IECON 2008*, 10-13 November 2008.

[49] Anders Kronberg, "Design and Simulation of Field Oriented Control and Direct Torque Control for a Permanent Magnet Synchronous Motor with Positive Saliency," *Uppsala Universitet*, 12-20, 2012.

Available: <http://www.divaportal.org/smash/get/diva2:534947/fulltext01.pdf>.

[50] R.D. Doncker, D.W.J. Pille, and A. Veltman. *Advanced Electrical Drives: Analysis, Modeling, Control. Power Systems*. Springer, 2011. ISBN 9789400701793.

URL <http://books.google.se/books?id=/sEDx2IAKboC>.

[51] "Optimum Vector Control for Brushless Motors," Toshiba.

Available:<http://www.newelectronics.co.uk/articleimages/25930%5CMotor%20Control%20Solutions.pdf>. [Accessed Oct. 10, 2016]

Appendix

Table App. 1: PMBLDC Motor Specifications

Sl. No.	Specifications	Quantity
01	No. of Poles	8
02	Rated Voltage	48 V
03	Peak Value of Rated Current	2.5 Amp
04	Rated Speed	150 rad/s
05	Rated Torque	2.0 Nm
06	Initial Torque	0.4 Nm
07	Per Phase Resistance	0.36 Ω
08	Per Phase Self-Inductance	2.1 mH
09	Mutual inductance	1.5 mH
10	Flux linkages constant	0.105
11	Moment of Inertia	0.0048 kg-m ²
12	Damping constant	0.002 N-m/rad/sec

Achievement

International Journals:

[1] **Protik Chandra Biswas**, and Bashudeb Chandra Ghosh, "A New Approach to Enhance the Torque Handling Capacity of a PMBLDC Motor Drive," *American Journal of Electrical and Electronic Engineering (AJEEE)*, vol. 4, no. 6, pp. 164-176, Dec. 2016, DOI: 10.12691/ajeee-4-6-3.

[2] **Protik Chandra Biswas**, Bashudeb Chandra Ghosh, and Md. Ashrafur Islam, "Field Oriented Control of a Current Fed PMBLDC Motor and Its Comparison to Scalar Control Drive," *AIUB Journal of Science and Engineering (AJSE)*, vol. 15, no. 1, pp. 15-24, Aug. 2016, ISSN: 1608-3679.